

***DNAJC6*-related Parkinsonism: Disease
Characterisation and Development of a
Patient-Derived Dopaminergic Neuronal
Cell Model**

A thesis submitted to University College London for the
degree of Doctor of Philosophy

Lucia Abela-Arnold

UCL Great Ormond Street Institute of Child Health




June 2024

Declaration of work

I, Lucia Abela-Arnold declare that this PhD Thesis has been written by myself. The work presented herein has been conducted by myself, unless otherwise stated. Due to the closure of the GOSH Institute of Child Health in March 2020 (Covid-19 pandemic) and my return to part-time clinical duties at the end of 2020, I have been supported by Lorita Gianfrancesco (Research Assistant in the Kurian lab) for the last part of my PhD, in particular for tissue culture and lentivirus production/transduction. Due to their specific expertise, I have also collaborated with Dr. Erica Tagliatti (Postdoctoral research associate at the Department of Clinical and Experimental Epilepsy, UCL Queen Square Institute of Neurology, University College London) for electron microscopy analysis, and also with Clara Zourray (PhD student in the Barral, Kurian and Lignani laboratory) and Prof. Gabriele Lignani (PI at the Department of Clinical and Experimental Epilepsy, UCL Queen Square Institute of Neurology, University College London) for patch clamp analysis. Giada Rossignoli (Postdoctoral research associate in the Kurian lab) also guided me for RNA sequencing analysis. A detailed description of all experimental contributions are listed in the table below:

Experimental contribution	
Characterisation of <i>DNAJC6</i> patient cohort	
Clinical characterisation	Lucia Abela-Arnold, Jo Ng, Manju Kurian
Genetic analysis	Elisenda Cortès-Saladelafont
Biochemical investigation	Jo Ng
iPSC reprogramming and characterisation	
iPSC reprogramming	Lucia Abela-Arnold (Patient 1&2, Patient 3&4 from Passage 6), Serena Barral (Patient 3&4 until Passage 6)
iPSC characterisation	Lucia Abela-Arnold
Dopaminergic neuronal differentiation	
Batches 2017-2020 (5)	Lucia Abela-Arnold
Last batch 2020/2021	Lorita Gianfrancesco
Phenotype analysis	
Immunoblotting	Lucia Abela-Arnold
FM-43 uptake assay design and analysis	Lucia Abela-Arnold
FM-43 uptake assay and imaging	Lorita Gianfrancesco
Differentiations for EM analysis (Patient 1/2)	Lucia Abela-Arnold
Differentiations for EM analysis (Patient 3)	Lorita Gianfrancesco
EM imaging and analysis	Erica Tagliatti
Differentiations for patch clamp analysis	Lucia Abela-Arnold
Patch clamp analysis	Clara Zourray
Differentiations for RNA Seq analysis	Lucia Abela-Arnold
RNA Seq analysis	Lucia Abela-Arnold (technical guidance Giada Rossignoli)
Lentivirus work	
Design <i>DNAJC6</i> Lentivirus	Lucia Abela-Arnold (technical guidance John Counsell)
Cloning, plasmid preparation	Lucia Abela-Arnold
Lentivirus titration, production and transduction	Lorita Gianfrancesco
Imaging FM-43 uptake assay	Lorita Gianfrancesco
Immunoblotting auxilin	Lorita Gianfrancesco
FM-43 uptake assay analysis	Lucia Abela-Arnold

I confirm that this Thesis (page 1 - 216 excluding references) has been submitted to Turnitin and as a result shows 6 % similarity to other work.

Submission Title	Turnitin Paper ID	Submitted	Similarity	Grade
View Digital Receipt PhD Thesis Lucia Abela_Without Refs	235180051	28/05/24, 12:27	6% 	-- Submit Paper   --

Abstract

Introduction: Biallelic loss-of-function mutations in *DNAJC6* cause a complex early-onset neurodegenerative condition characterised by juvenile-onset parkinsonism-dystonia with additional neurological, neurodevelopmental and neuropsychiatric features. The disease course is rapidly progressive and usually leads to loss of ambulation in mid-adolescence. *DNAJC6* encodes auxilin, a neuron-specific co-chaperone protein involved in clathrin-mediated endocytosis at presynaptic terminals. To date, the underlying disease mechanisms have not yet been fully elucidated and there are no disease-modifying treatments.

Aim: The aim of this PhD project is to (i) provide comprehensive clinical characterisation of a *DNAJC6* patient cohort and (ii) develop a patient-derived midbrain dopaminergic (mDA) neuronal cell model to investigate molecular disease mechanisms and develop a proof-of-concept gene therapy approach.

Methods: I generated induced pluripotent stem cells (iPSC) from four patients with pathogenic recessive mutations in *DNAJC6* and then differentiated them into mDA neurons along with two age-matched controls and one CRISPR-corrected isogenic control. Using this humanised neuronal cell model, I performed a number of cellular, molecular and transcriptomic assays to further elucidate the role of auxilin deficiency in *DNAJC6*-related disease.

Results: Loss of auxilin expression with impairment of clathrin-mediated endocytosis and disturbance of synaptic vesicle homeostasis are key disease-specific phenotypic findings in the mDA neuronal cell model. Disease-specific defects in ventral midbrain patterning were observed, with reduced LMX1A/FOXA2 co-expression at early stages of dopaminergic differentiation. Terminally differentiated mDA neurons showed decreased staining of the late neuronal marker NeuN and reduced primary neurite outgrowth, suggesting disturbances in neuronal maturation. Transcriptomic analysis using bulk RNA-seq analysis showed disturbance of presynaptic membrane processes and synaptic vesicle cycling as well as dysregulation of numerous neurodevelopmental processes. Transfection of mDA neurons with a lentiviral vector containing the wild-type *DNAJC6* gene restored auxilin protein levels and improved clathrin-mediated endocytosis and thus provides initial proof-of-concept for a gene therapy approach for this condition.

Impact statement

DNAJC6 parkinsonism-dystonia is an ultra-rare early-onset neurodegenerative condition with additional neurological, neurodevelopmental and neuropsychiatric features. Patients harbouring biallelic *DNAJC6* mutations develop complex, rapidly progressive parkinsonism, typically at the end of the first decade, associated with significant morbidity and premature mortality. The movement disorder responds poorly to standard medications and treatment is often associated with intolerable side effects. Hence, there is clear unmet clinical need for developing novel disease-modifying drugs to improve clinical outcome and quality of life.

In this thesis, I have contributed to our understanding of the disease phenotype, through clinical and biochemical characterisation of a new cohort of patients with *DNAJC6* mutations. I have subsequently generated an iPSC-derived midbrain dopaminergic neuronal model for *DNAJC6* parkinsonism-dystonia using patient fibroblasts. Although a *DNAJC6* disease model has been previously generated using a CRISPR-Cas9-based knock-in approach in human embryonic stem cells, my work represents the first patient-derived humanised cell model of disease. This patient-derived neuronal cell model has allowed me to study the effects of three different deleterious *DNAJC6* mutations. Analysis of this model has identified disease-specific features in patient lines, when compared to isogenic and age-matched controls. Whilst some of these cellular phenotypes confirm previous findings in animal models of *DNAJC6* parkinsonism, I have also identified novel disease mechanisms and defective pathways, which provide greater understanding of the complex neurodevelopmental disease phenotype. My findings have shown that auxilin deficiency leads to synaptic and neurodevelopmental abnormalities, highlighting the role of auxilin and clathrin-mediated endocytosis in key neurodevelopmental processes. This neuronal cell model has further served as a suitable platform to test a gene therapy approach; the feasibility of this strategy and promising preliminary results will support further work, ultimately towards clinical translation.

In summary, to my knowledge, I have developed the first patient-derived dopaminergic neuronal cell model for *DNAJC6* parkinsonism-dystonia, which has provided novel insights into disease. Using this model, I have laid the foundations for the development and clinical translation of a gene therapy approach for this progressive, life-limiting and drug-resistant condition.

Research paper declaration form

1. Referencing the doctoral candidate's own published work(s)

1. For a research manuscript that has already been published:

(a) What is the title of the manuscript? **“DNAJC6 Mutations Disrupt Dopamine Homeostasis in Juvenile Parkinsonism-Dystonia”**

(b) Please include a link to or doi for the work: <https://doi.org/10.1002/mds.28063>

(c) Where was the work published? **Movement Disorders**

(d) Who published the work? **Wiley Online Library**

(e) When was the work published? **August 2020 issue**

(f) List the manuscript's authors in the order they appear on the publication: **Joanne Ng, Elisenda Cortès-SaladelaFont, Lucia Abela, Pichet Termsarasab, Kshitij Mankad, Sniya Sudhakar, Kathleen M Gorman, Simon J R Heales, Simon Pope, Lorenzo Biassoni, Barbara Csányi, John Cain, Karl Rakshi, Helen Coutts, Sandeep Jayawant, Rosalind Jefferson, Deborah Hughes, Àngels García-Cazorla, Detelina Grozeva, F Lucy Raymond, Belén Pérez-Dueñas, Christian De Goede, Toni S Pearson, Esther Meyer, Manju A Kurian**

(g) Was the work peer reviewed? **Yes**

(h) Have you retained the copyright? **Yes**

(i) Was an earlier form of the manuscript uploaded to a preprint server (e.g. medRxiv)? If 'Yes', please give a link or doi. If 'No', please seek permission from the relevant publisher and check the box next to the below statement:

☒ I acknowledge permission of the publisher named under 1d to include in this thesis portions of the publication named as included in 1c.

2. For multi-authored work, please give a statement of contribution covering all authors (if single author, please skip to section 3): **LA reviewed all clinical data and wrote the draft of**

the manuscript. JN reviewed clinical data, contributed to the draft of the manuscript and performed fibroblast and CSF immunoblotting and statistical analysis of CSF neurotransmitter analysis. ECS reviewed clinical data and performed molecular genetic analysis. EM provided technical supervision for molecular genetic analysis. KT and SS performed MR imaging analysis and provided imaging figures. LB performed DAT scan analysis and provided imaging figures. SP performed CSF neurotransmitter analysis. SJRH supervised neurotransmitter analysis. PT, KMG, BC, JC, KR, HC, SJ, RJ, DH, AGC, DG, FLR, BPD CDG and TSP contributed clinical patient data. MAK conceptualised and supervised the study and revised the first draft of the manuscript. All authors reviewed the final draft and contributed to the final version of the manuscript.

3. In which chapter(s) of your thesis can this material be found? **Chapter 3 and Discussion**

e-Signatures confirming that the information above is accurate (this form should be co-signed by the supervisor/ senior author unless this is not appropriate, e.g. if the paper was a single-author work):

Candidate: Lucia Abela Arnold



Date: 30th of May 2024

Supervisor/Senior Author signature (where appropriate): Manju A. Kurian Date: 30th of May 2024



2. Referencing the doctoral candidate's own published work(s)

1. For a research manuscript that has already been published:

(a) What is the title of the manuscript? **“Neurodevelopmental and synaptic defects in *DNAJC6* parkinsonism, amenable to gene therapy”**

(b) Please include a link to or doi for the work: <https://doi.org/10.1093/brain/awae020>

(c) Where was the work published? **Brain**

(d) Who published the work? **Oxford University Press**

(e) When was the work published? **June 2024 issue**

(f) List the manuscript's authors in the order they appear on the publication: **Lucia Abela, Lorita Gianfrancesco, Erica Tagliatti, Giada Rossignoli, Katy Barwick, Clara Zourray, Kimberley M Reid, Dimitri Budinger, Joanne Ng, John Counsell, Arlo Simpson, Toni S Pearson, Simon Edvardson, Orly Elpeleg, Frances M Brodsky, Gabriele Lignani, Serena Barral, Manju A Kurian**

(g) Was the work peer reviewed? **Yes**

(h) Have you retained the copyright? **Yes**

(i) Was an earlier form of the manuscript uploaded to a preprint server (e.g. medRxiv)? If 'Yes', please give a link or doi. If 'No', please seek permission from the relevant publisher and check the box next to the below statement:

☒ I acknowledge permission of the publisher named under 1d to include in this thesis portions of the publication named as included in 1c.

2. For multi-authored work, please give a statement of contribution covering all authors (if single author, please skip to section 3): **LA designed and performed most of the experiments and data analysis including iPSC reprogramming and characterisation, neuronal differentiation, immunoblotting (auxilin, clathrin), design and analysis FM-43 uptake assay, RNA seq analysis and lentivirus design and cloning. LG assisted in neuronal differentiation and performed FM-43 uptake assay, immunoblotting experiments**

(lentivirus auxilin) and lentiviral production and transduction. ET performed EM analysis. GR assisted in RNA seq analysis and provided guidance in lentiviral vector production. KB performed Sanger sequencing of iPSC lines. KMR assisted in immunoblot experiments. DB contributed to control iPSC characterisation. JN designed and provided the lentiviral backbone. JC assisted in the design of the lentiviral *DNAJC6* construct. AS contributed to figure design. CZ performed and analysed electrophysiological recordings. GL designed and analysed electrophysiological recordings. SB contributed to iPSC generation and supervised experiments. TSP, SE and OE donated patient fibroblasts and provided intellectual input to the manuscript. FMB provided intellectual input to the manuscript. LA drafted the first manuscript and MAK revised the first manuscript. MAK conceptualised the study, supervised all experiments and provided funding. LG and GR contributed to written sections (Material and Methods) of the manuscript. All authors reviewed the final draft and contributed to the final version of the manuscript.

3. In which chapter(s) of your thesis can this material be found? **Chapter 5, Chapter 6, Chapter 7, Chapter 8 and Discussion**

e-Signatures confirming that the information above is accurate (this form should be co-signed by the supervisor/ senior author unless this is not appropriate, e.g. if the paper was a single-author work):

Candidate: Lucia Abela Arnold



Date: 24th of March 2024

Supervisor/Senior Author signature (where appropriate): Manju A. Kurian Date: 24th of March 2024



Acknowledgements

First of all, I would like to express my deepest gratitude to my primary PhD supervisor, Prof. Manju Kurian. Manju, I joined your lab as a clinician with the intention of learning basic wet lab techniques and I am very grateful to you for encouraging me to pursue a PhD. It has truly been a wonderful, challenging and rewarding journey and I have learnt an incredible amount for both my professional and personal life. I could not have undertaken this journey without your dedicated support, your invaluable guidance and your inspiring example, and in particular your understanding during the challenging times of juggling childcare and clinical responsibilities. I am deeply grateful for the trust you have placed in me.

Second, I would like to thank my secondary supervisors Dr. Serena Barral and Prof. Rick Livesey for their guidance and support throughout my PhD. Serena, I could not have imagined a better teacher in the laboratory than you, and your humour and optimism always cheered me up. The skills I have acquired under your supervision are invaluable assets for my scientific career. Most importantly, I have found a person who has become very dear to my heart.

I would also like to thank other members of the Kurian laboratory, past and present. You have all supported me in so many ways, with technical support, with valuable discussions about experiments, and with wonderful moments of friendship. In particular, I would like to thank Lorita Gianfrancesco for her help and company; Katy, Dimitri, Giada and Clara for their contribution to this work and their much-appreciated input and advice.

I would also like to thank my collaborators Dr. Erica Tagliatti and Prof. Gabriele Lignani from the Department of Clinical and Experimental Epilepsy (UCL Queen Square Institute of Neurology London) for their support with electron microscopy and electrophysiology. I would also like to thank Dr. Dale Moulding from the GOS-ICH microscopy facility for his guidance with imaging assays.

A special thanks goes to my former mentor and friend Prof. Barbara Plecko for all her emotional support during this time and for her constant encouragement, which helped me to grow as a person, physician and scientist.

I am very grateful to the Swiss National Science Foundation, the Anna Müller Grocholski Foundation and the Rosetrees Trust for co-funding this PhD. Most importantly, I would like to thank all the patients and families who were willing to participate in this study and who have made a tremendous contribution to this work.

I would like to express my deepest gratitude to my family, especially my mother and my parents-in-law, but also my brothers, and my sisters- and brothers-in-law, for all their constant support, love and encouragement throughout my PhD. This work is a tribute to my father, who was taken from us too soon.

Finally, I would like to thank my husband Eugenio for his unconditional love. Your belief in me and your tremendous understanding have helped me to carry on regardless of the challenges I have faced. You are my soul mate and my rock, and I am deeply grateful to have you and our three beautiful little girls, Frieda, Hanna and Josefina, by my side.

Table of content

Declaration of work.....	2
Abstract.....	4
Impact statement.....	5
Research paper declaration form	6
Acknowledgements.....	10
Table of content	12
Abbreviations.....	18
CHAPTER 1 Introduction.....	22
1. 1. Parkinson’s Disease.....	23
1. 1. 1. Historical background	23
1. 1. 2. Motor control and basal ganglia circuits	24
1. 1. 2. 1. Motor circuit pathology in Parkinson’s Disease.....	26
1. 1. 3. Aetiology	27
1. 1. 4. Monogenic forms of PD	28
1. 1. 4. 1. Juvenile-onset forms of PD.....	29
1. 1. 5. Molecular disease pathways in monogenic forms of PD	31
1. 1. 5. 1. Protein aggregation and lysosomal dysfunction	32
1. 1. 5. 2. Mitochondrial dysfunction.....	33
1. 1. 5. 3. Dysfunction of intracellular and synaptic trafficking pathways.....	34
1. 1. 6. Dopaminergic dyshomeostasis	37
1. 1. 7. Selective dopaminergic vulnerability	38
1. 1. 8. Synaptic and axonal degeneration in PD.....	39
1. 1. 9. Therapeutic approaches in PD.....	40
1. 2. <i>DNAJC6</i>-related disease: key clinical and molecular features.....	42
1. 2. 1. Gene discovery and key clinical features	42
1. 2. 2. <i>DNAJC6</i> : gene and protein expression	43
1. 2. 3. Auxilin 1 – structure and function.....	44
1. 2. 4. Role of auxilin in clathrin-mediated endocytosis.....	45
1. 2. 5. Role of Auxilin in other intracellular trafficking pathways and signalling.....	46
1. 2. 6. Clathrin-mediated endocytosis in physiological and pathological conditions	48
1. 2. 7. Animal and cellular models of <i>DNAJC6</i> -related parkinsonism	50
1. 3. Induced pluripotent stem cell technology	53

1. 3. 1. Introduction	53
1. 3. 2. Limitations and challenges of iPSC-based research.....	54
1. 3. 3. iPSC reprogramming technologies.....	55
1. 3. 4. Embryonic development of the brain as the basis for iPSC-based neuronal differentiation strategies	55
1. 3. 5. Neuronal iPSC-based differentiation strategies.....	60
1. 3. 5. 1. Established dopaminergic differentiation protocols	62
1. 3. 6. Modelling neurodevelopmental disorders with induced pluripotent stem cells.....	63
1. 3. 7. Modelling neurodegenerative disorders with induced pluripotent stem cells	65
1. 4. Research Hypothesis and Aims	67
1. 4. 1. Background.....	67
1. 4. 2. Hypothesis	68
1. 4. 3. Research aims and methodology	68
CHAPTER 2 Materials and methods	71
2. 1. Introduction	72
2. 2. <i>DNAJC6</i> patient cohort characterisation	72
2. 2. 1. Patient cohort recruitment for study	72
2. 2. 2. Molecular genetic investigations	72
2. 2. 2. 1. Autozygosity mapping and whole-exome sequencing	72
2. 2. 2. 2. Sanger sequencing	73
2. 2. 3. Cerebrospinal fluid neurotransmitter analysis.....	73
2. 2. 4. Patient fibroblast immunoblotting.....	73
2. 2. 5. Patient CSF immunoblotting	73
2. 3. Fibroblast culture.....	74
2. 4. Generation and maintenance of hiPSC lines	74
2. 4. 1. Reprogramming human dermal fibroblasts using CytoTune Kit	74
2. 4. 2. iPSC culture.....	75
2. 4. 3. Generation of CRISPR-Cas9-corrected iPSC line	75
2. 5. Characterisation of patient-derived iPSC.....	76
2. 5. 1. Assessment of genomic integrity of iPSC lines	76
2. 5. 2. Confirmation of patient mutations in HDF and iPSC lines.....	76
2. 5. 3. RNA purification and cDNA production.....	77
2. 5. 4. Sendai Virus clearance	77
2. 5. 5. PluriTest	78

2. 5. 6. PCR analysis of pluripotency markers	78
2. 5. 7. Immunocytochemistry for pluripotency markers	79
2. 5. 8. Spontaneous <i>in vitro</i> differentiation assay	79
2. 6. Midbrain dopaminergic differentiation of control and <i>DNAJC6</i> patient lines	80
2. 6. 1. mDA neuron differentiation protocol	80
2. 6. 2. Day 11 immunocytochemistry for midbrain progenitor markers	81
2. 6. 3. Real-Time Quantitative Reverse Transcription Polymerase Chain Reaction (qRT-PCR) at day 11 and day 65 of differentiation	82
2. 6. 4. Day 65 immunocytochemistry for mature midbrain markers	83
2. 7. Immunoblotting	83
2. 7. 1. Protein extraction and determination of concentration	83
2. 7. 2. Immunoblotting	84
2. 8. FMTM1-43 dye uptake assay	84
2. 9. Electron microscopy analysis	85
2. 10. Bulk RNA seq analysis	85
2. 10. Generation and transfection of a <i>DNAJC6</i> lentiviral vector	86
2. 10. 1. Generation of a lentiviral <i>DNAJC6</i> expression plasmid	86
2. 10. 1. 1. DAT plasmid verification	86
2. 10. 1. 2. Removal of the <i>DAT</i> gene from the DAT plasmid	87
2. 10. 1. 3. Cloning of the <i>DNAJC6</i> gene into the DAT plasmid	88
2. 10. 1. 4. Sequencing of the <i>DNAJC6</i> plasmid	88
2. 10. 2. Lentivirus Production	90
2. 10. 2. 1. Lentiviral Vector Titration by qRT-PCR	90
2. 10. 2. Lentivirus transfection of mDA neurons	94
2. 10. 3. Immunoblotting of lentivirus-transfected mDA neurons	94
2. 10. 4. FM TM 1-43 dye uptake assay analysis in lentivirus-transfected mDA neurons	94
CHAPTER 3 Clinical and molecular genetic features of patients with <i>DNAJC6</i>-related parkinsonism	95
3. 1. Introduction	96
3. 2. Results	96
3. 2. 1. Molecular genetic analysis	96
3. 3. Detailed endophenotyping of the <i>DNAJC6</i> study cohort	97
3. 3. 1. Family history	97
3. 3. 2. Early development and cognition	97

3. 3. 3. Movement disorder and treatment	99
3. 3. 4. Additional neurological, neuropsychiatric and systemic features	100
3. 3. 5. Disease course over time	101
3. 3. 6. Features on Neuroimaging	101
3. 3. 7. Molecular studies	102
3. 4. Literature review on <i>DNAJC6</i>-related disease	104
3. 4. 1. Reported patients with biallelic <i>DNAJC6</i> mutations	104
3. 5. Synopsis of clinical findings in recessive <i>DNAJC6</i> disease	111
3. 5. 1. Patients with heterozygous <i>DNAJC6</i> mutations	113
3. 5. 2. Overview of molecular genetic features in recessive <i>DNAJC6</i> -related disease	114
3. 5. 3. Diagnostic investigation in <i>DNAJC6</i> patients	115
3. 6. Discussion	115
CHAPTER 4 Human induced pluripotent stem cell reprogramming and	
characterisation	117
4. 1. Introduction	118
4. 2. Reprogramming of patient's dermal fibroblasts into iPSC	118
4. 2. 1. Patient lines	118
4. 2. 2. Control lines	119
4. 2. 3. Generation of a CRISPR-Cas9 corrected line for Patient 2-1	119
4. 2. 4. Sendai-Virus reprogramming	120
4. 3. Characterisation of genomic integrity	121
4. 3. 1. Confirmation of a normal karyotype following reprogramming	121
4. 3. 2. Retention of patient-specific mutations following reprogramming	123
4. 4. Characterisation of pluripotent identity	125
4. 4. 1. Sendai Virus clearance of patient and control iPSC lines	125
4. 4. 2. Typical cellular morphology of patient and control iPSC lines	125
4. 4. 3. Expression of pluripotency markers in patient and control iPSC lines	126
4. 4. 4. Pluripotent gene expression profiling in patient and control iPSC lines	129
4. 4. 5. <i>In vitro</i> spontaneous differentiation assay in patient and control iPSC lines	129
4. 5. Discussion	132
CHAPTER 5 Generation and characterisation of a midbrain dopaminergic neuronal	
cell model for <i>DNAJC6</i> parkinsonism-dystonia	134
5. 1. Introduction	135
5. 2. Results	135

5. 2. 1. Midbrain dopaminergic neuron differentiation	135
5. 2. 2. Characterisation of midbrain dopaminergic progenitors	136
5. 2. 2. 1. Patient lines show alterations in early ventral midbrain patterning.....	137
5. 2. 3. Characterisation of mature midbrain dopaminergic neurons	139
5. 2. 3. 1. Patient and control lines differentiate into midbrain dopaminergic neurons	139
5. 2. 3. 2. Patient and control lines show upregulation of mature midbrain markers ...	142
5. 2. 3. 3. Patient lines show absence of neurodegeneration at day 65 of differentiation	143
5. 2. 3. 4. Patient lines show neuronal maturation defects at day 65 of differentiation	144
5. 2. 3. 5. Patient lines show impaired primary neurite outgrowth.....	145
5. 3. Discussion	146
CHAPTER 6 Investigation of disease-specific phenotypes in the <i>DNAJC6</i> dopaminergic neuronal cell model	149
6. 1. Introduction	150
6. 2. Results	150
6. 2. 1. Patient lines show absent auxilin protein expression	150
6. 2. 2. Patient lines show impaired clathrin-mediated endocytosis.....	152
6. 2. 3. Patient lines show synaptic vesicle dyshomeostasis	154
6. 2. 4. Patch clamp analysis in Patient 2-1 shows decreased amplitude of events.....	156
6. 3. Discussion	157
CHAPTER 7 Transcriptome profiling of patient-derived midbrain dopaminergic neurons	159
7. 1. Introduction	160
7. 2. Results	160
7. 2. 1. Patient lines show differential gene expression profiles compared to control lines	161
7. 2. 1. 1. Patient 2-1 compared to its corresponding isogenic CRISPR 2-1 line	161
7. 2. 1. 2. Patient 2-1 compared to Control 03	163
7. 2. 1. 3. All Patients compared to Control 03.....	164
7. 2. 1. 4. CRISPR 2-1 compared to Control 03	165
7. 2. 3. GO term enrichment analysis for biological processes in patient lines compared to control lines reveals dysregulation of developmental processes	167
7. 2. 4. GO term enrichment analysis for cellular compartments in patient lines compared to control lines highlights vesicle membrane compartments.....	167

7. 2. 5. GO term enrichment analysis in CRISPR 2-1 compared to Control 03 allows differentiation of disease-associated and non-disease-associated gene expression patterns	168
7. 2. 6. Analysis of genes associated with Nervous System Development, Dopaminergic Neurogenesis and Clathrin-mediated Endocytosis	169
7. 2. 6. 1. Clathrin-Mediated Endocytosis	174
7. 2. 6. 2. Dopaminergic Neurogenesis	174
7. 2. 6. 3. Nervous System Development.....	176
7. 2. 7. GO enrichment analysis for synaptic location highlights presynaptic locations linked to synaptic vesicle cycling in patient lines compared to control lines.....	180
7. 2. 8. Gene enrichment analysis for synaptic function reveals dysregulation of synaptic signalling and synaptic organization in patient lines compared to control lines	186
7. 3. Discussion	191
CHAPTER 8 An <i>in vitro</i> proof-of-concept gene therapy approach for <i>DNAJC6</i> parkinsonism-dystonia.....	194
8. 1. Introduction	195
8. 2. Results	195
8. 2. 1. Generation of lentivirus construct for <i>DNAJC6</i> gene delivery.....	195
8. 2. 1. 1. Cloning of <i>DNAJC6</i> into a DAT lentivirus vector	195
8. 2. 1. 2. Lentivirus production in HEK-293T cells	197
8. 2. 2. Transduction of patient-derived mDA neurons and validation of gene transfer ...	198
8. 2. 3. Improvement of clathrin-mediated endocytosis in <i>DNAJC6</i> lentivirus-treated patient-derived mDA neurons	199
8. 3. Discussion	201
CHAPTER 9 Discussion	202
References	217

Abbreviations

¹²³I-FP-CIT	I-N-ω-fluoropropyl-2β-carbomethoxy-3β-(4-iodophenyl) nortropane
2D/3D	2/3 dimensions
AA	Ascorbic acid
AADC	Aromatic L-amino acid decarboxylase
AAV	Adeno-associated virus
ADRA2A	Adrenoceptor Alpha 2A
ATP13A2	ATPase Cation Transporting 13A2
AZ	Active zone
BDNF	Brain-derived neurotrophic factor
BHL	Basic helix-loop-helix
BMP	Bone morphogenetic protein
bp	Base pair
CALM	Clathrin assembly lymphoid myeloid leukaemia protein family
cCASP3	Cleaved Caspase 3
CCV	Clathrin-coated vesicle
cDNA	Complementary DNA
CBLN2	Cerebellin 2 precursor
CME	Clathrin-mediated endocytosis
CN	Caudate nucleus
CNV	Copy number variant
COPI/II	Coat protein complex I/ II
CRISPR	Clustered regularly interspaced short palindromic repeats
CSF	Cerebrospinal fluid
CTNNB	Catenin Beta 1
C1QL1	Complement C1q Like 1
DA	Dopamine
DA-Q	DA-o-quinone
DAT	Dopamine transporter
DaTSCAN	Dopamine transporter scan
db-cAMP	N6,2'-O-Dibutyryl adenosine 3',5'-cyclic monophosphate sodium salt
DBS	Deep brain stimulation
DEG	Differentially expressed genes
DNA	Deoxyribonucleic acid
DNAJC5	DnaJ Heat Shock Protein Family (Hsp40) Member C5
DNAJC6	DnaJ Heat Shock Protein Family (Hsp40) Member C6
DNAJC13	DnaJ Heat Shock Protein Family (Hsp40) Member C13
DNM1	Dynamin 1
dNTP	Deoxynucleoside triphosphate
DOPAL	3,4-dihydroxyphenylacetaldehyde
DTDS	Dopamine transporter deficiency syndrome
DTT	Dithiothreitol
DRD1	D1-type dopamine receptor
DRD2	D2-type dopamine receptor
EB	Embryoid body
E-L	Endo-lysosomal system
EN1/2	Homeobox genes engrailed 1

EPHA5/6	EPH Receptor A5/A6
ER	Endoplasmic reticulum
FBXO7	F-Box Protein 7
FDR	False discovery rate
FERD31	Fer3 Like BHLH Transcription Factor
FGF8	Fibroblast growth factor 8
FM1-43	N-(3-Triethylammoniumpropyl)-4-(4-(Dibutylamino) Styryl) Pyridinium dibromide
FN	Fibronectin
FOXA2	Forkhead box protein 2
FOXP1	Forkhead Box P1
GABA	Gamma-aminobutyric acid
GAD	Glutamate decarboxylase
GAK	cyclin-G-associated-kinase
GBX2	Gastrulation brain homeobox 2
GLI	GLI Family Zinc Finger 1
GRM3	Glutamate metabotropic receptor 3
GRM7	Glutamate metabotropic receptor 7
Hsc70	Heat shock cognate protein 70
gDNA	Genomic DNA
GABRB2	Gamma-Aminobutyric Acid Type A Receptor Subunit Rho2
GABRR1	Gamma-Aminobutyric Acid Type A Receptor Subunit Rho1
GBA	Glucosylceramidase Beta 1
GDNF	Glial cell-line derived neurotrophic factor
GFP	Green fluorescent protein
GO	Gene ontology
GPI	Globus pallidus interna
GPe	Globus pallidus externa
GSK3	Glycogen synthase kinase 3
GRM8	Glutamate metabotropic receptor 8
GWAS	Genome-wide association studies
HBSS	Hanks' balanced salt solution
HDF	Human dermal fibroblast
HES	Human embryonic stem cell
HEY2	Hes Related Family BHLH Transcription Factor With YRPW Motif 2
5-HIAA	5-hydroxyindolacetic acid
HPLC	High-pressure liquid chromatography
HVA	Homovanillic acid
iPSC	Induced pluripotent stem cell
iN	Induced neuron
IsO	Isthmic organiser
IRES	Internal ribosome entry site
IZ	Intermediate zone
KCNA4	Potassium Voltage-Gated Channel Subfamily A Member 4
KCNJ11	Potassium Inwardly Rectifying Channel Subfamily J Member 1
LAS	Lysosomal-autophagy system
L-DOPA	L-dihydroxy-phenylalanine
LN	Laminin
LogFC	Logarithmic fold change
LMX1A/B	LIM Homeobox Transcription Factor 1 A/B

LOH	Loss of heterozygosity
LP	Lumbar puncture
LRRK2	Leucine Rich Repeat Kinase 2
LXRα/β	liver X receptors α and β
M	Midbrain
MAP2	Microtubule associated protein 2
MASH1	Mouse achaete-schute homolog 1
Mb	Megabases
mDA	Midbrain dopaminergic neuron
MDS	Movement disorder society
MEIS1	Meis Homeobox 1
mFP	Midbrain floor plate
MEF	Mouse embryonic fibroblasts
MHB	Midbrain-hindbrain boundary
MIBG	Metaiodobenzylguanidine
hMLO	Human midbrain-like organoid
MOI	Multiplicity of infection
MPTP	1-methyl-4-phenyl-1,2,3,6-tetrahydropyridine
MRC	Mitochondrial respiratory chain
MRI	Magnetic resonance imaging
MSN	Medium spiny neuron
MSX1	Muscle segment homeobox homolog 1
mRNA	Messenger RNA
MZ	Marginal zone
NeuN	Neuronal nuclear protein
NDD	Neurodevelopmental disorders
NEUROD1	Neuronal Differentiation 1
NGN2	Neurogenin 2
NGS	Next-generation sequencing
NKX6-1	NK6 Homeobox 1
NTNG1	Netrin G1
NTRK3	Neurotrophic Receptor Tyrosine Kinase 3
NURR1	Nuclear receptor-related factor 1
OTX2	Orthodenticle homolog 2
PAX6	Paired box protein Pax-6
PD	Parkinson's disease
PEI	Polyethylenimine
PES	Polyethersulfone
PFA	Paraformaldehyde
PINK1	PTEN-induced kinase 1
PITX33	Paired- like homeodomain transcription factor 3
PLA2G6	Phospholipase A2 Group VI
PO	Poly-L-ornithine
PRKN	Parkin
PTEN	Phosphatase and tensin-like
RET	C-ret proto-oncogene
RGMA	Repulsive Guidance Molecule BMP Co-Receptor A
RNA	Ribonucleic acid
RNA-seq	RNA sequencing
ROBO	Roundabout homolog 1
ROI	Regions of interest

ROS	Reactive oxygen species
RrF	Retrorubral field
RT	Room temperature
RTK	Receptor tyrosine kinases
SALL4	Sal-like protein 4
scRNAseq	Single cell RNA-sequencing
SEM	Standard error mean
SeV	Sendai virus
sgRNA	Single guide RNA
SHH	Sonic hedgehog
SLC6A3/DAT	Solute Carrier Family 6 Member A3/Dopamine transporter
SLC17A6	Solute Carrier Family 17 Member 6
SLC17A7	Solute Carrier Family 17 Member 7
SLC17A8	Solute Carrier Family 17 Member 8
SLC18A2/VMAT2	Solute carrier family-18 member-2/vesicular monoamine transporter-2
SLIT1	Slit Guidance Ligand 1
SH3GL2	SH3 Domain Containing GRB2 Like 2, Endophilin A1
SN	Substantia nigra
SNc	Substantia nigra pars compacta
SNr	Substantia nigra pars reticulata
SNCA	α-Synuclein
SNV	Single nucleotide variant
SPECT	Single photon emission computed tomography
SPG11	Spastic paraplegia 11
STN	Subthalamic nucleus
SV	Synaptic vesicle
SYP	Synaptophysin
SYNJ1	Synaptojanin 1
SYT	Synaptotagmin
TACR1	Tachykinin Receptor 1
TALNs	Transcription activator-like effector nucleases
TBS	Tris Buffered Saline
TENM1	Teneurin Transmembrane Protein 1
TGFb3	Transforming growth factor-β3
TH	Tyrosine hydroxylase
TGN	Trans-Golgi network
VAV3	Vav Guanine Nucleotide Exchange Factor 3
VCN	Vector copy number
VP	Ventral pallidum
VPS35	Vacuolar protein sorting ortholog 35
VTa	Ventral tegmental area
VZ	Ventricular zone
WES	Whole exome sequencing
WGS	Whole genome sequencing
WLS	Wnt Ligand Secretion Mediator
WNT1	Wnt Family Member 1
WNT5A	Wnt Family Member 5A
ZIC3	Zic Family Member 3

CHAPTER 1

Introduction

1. 1. Parkinson's Disease

1. 1. 1. Historical background

Parkinson's Disease (PD) is the second most common movement disorder after essential tremor¹ and the second most common neurodegenerative disorder after Alzheimer's Disease², with an estimated worldwide incidence of 40/100,000 at 40-49 years and up to almost 2,000/100,000 beyond 80 years of age³. PD is the fastest growing neurological disorder with a projected increase of about 7 million patients in 2015 to an estimated 13 million patients in 2040 and thus poses a significant global socioeconomic burden⁴.

The selective degeneration of midbrain dopaminergic (mDA) neurons in the substantia nigra pars compacta (SNc) and accumulation and aggregation of α -synuclein cytoplasmic Lewy Bodies are neuropathological hallmarks of PD⁵. In 1817, the British physician James Parkinson first described the cardinal clinical symptoms of resting tremor, bradykinesia, rigidity and postural instability in his "Essay on the shaking palsy"⁶. PD is usually accompanied by a variety of non-motor symptoms such as rapid eye movement sleep behaviour disorder, depression, hyposmia, constipation and autonomic dysfunction that arise in an early prodromal phase around 15-20 years before the onset of motor symptoms. At this time, neurodegeneration has already started and progressed, however, typical motor symptoms only arise when about 60-70% of DA neurons have been lost⁷. It is now well established that loss of neurons in PD is not only restricted to the SNc, but also involves other neuronal populations. Accumulation of Lewy bodies and cell loss has been described in the locus coeruleus containing noradrenergic neurons as well as in the pedunculopontine nucleus, the dorsal raphe nucleus and the dorsal motor nucleus of the vagus containing cholinergic neurons⁸. It is most likely that loss of these cell population contribute to the non-motor symptoms reported in PD. The link between severe dopamine deficiency in the dorsal striatum and PD was established in 1957 by Oleh Hornykiewicz and Arvid Carlsson, who was awarded the Nobel Prize in Physiology and Medicine in 2000 for his discovery that dopamine is a neurotransmitter in the brain. The concept of dopamine deficiency was proven later on by rescue of clinical symptoms through administration of levodopa in PD patients in 1961⁹. In 1967, George Cotzias established high-dose levodopa therapy¹⁰. In 1982, William Langston, an American neurologist, described the onset of parkinsonian features in patients that consumed "synthetic heroin"¹¹. The substance 1-methyl-4-phenyl-1,2,3,6-tetrahydropyridine (MPTP), which is neurotoxic to the SNc DA neurons, was later identified as the cause of this drug-induced parkinsonism¹¹. The MPTP

discovery was the beginning of extensive research era into the etiology and pathogenesis of PD and MPTP was used to generate animal models of disease.

The current clinical criteria for parkinsonism as deemed by the International Parkinson's and Movement Disorder Society (MDS) require the presence of three cardinal motor symptoms including bradykinesia, with either rest tremor or rigidity or both¹². Clinical assessment may be carried out using the MDS–Unified Parkinson Disease Rating Scale. Once parkinsonism is confirmed, the clinical diagnosis of PD requires the presence of at least two supportive criteria and the absence of absolute exclusion criteria and red flags¹². Supportive criteria include (i) clear and strong response to dopaminergic medication, (ii) presence of levodopa-induced dyskinesia, (iii) documentation of rest tremor of a limb and (iv) olfactory loss or cardiac sympathetic denervation on metaiodobenzylguanidine (MIBG) scintigraphy. Absolute exclusion criteria include a variety of clinical symptoms indicative of other neurodegenerative disorders (e.g. frontotemporal dementia, progressive aphasia), drug-induced parkinsonism and other conditions known to induce parkinsonism, as well as normal functional neuroimaging of the presynaptic dopaminergic system. Red flags include rapid progression of gait impairment (<3 years of onset) and recurrent falls (<5 years of onset), early bulbar dysfunction, severe autonomic failure and inspiratory respiratory dysfunction (<5 years of onset), unexplained pyramidal tract signs, disproportionate anterocollis (dystonic) or contractures of hand or feet (<10 years of onset), bilateral symmetric parkinsonism as well as absence of progression of motor symptoms and common nonmotor symptoms within 5 years of disease.

1. 1. 2. Motor control and basal ganglia circuits

Movements are characterised by distinct patterns of spatial and temporal muscle activation¹³. Intentional movements are generated in the cerebral motor cortex that projects to the brain stem and spinal cord and from there to peripheral muscles. The coordination, fine-tuning and exact timing of movements require a coordinated interplay of cortical and subcortical centers including the cortex, thalamus, basal ganglia and cerebellum. These structures are organised in complex functional networks, so-called motor circuits. The basal ganglia are a group of subcortical nuclei composed of the putamen and caudate nucleus (CN), which together form the striatum, as well as the globus pallidus interna (GPi) and externa (GPe), ventral pallidum (VP), subthalamic nucleus (STN), substantia nigra pars compacta (SNc) and pars reticulata (SNr) (**Figure 1**). Each of these basal ganglia nuclei is a complex somatotopic and neurochemical structure with distinct network connections.

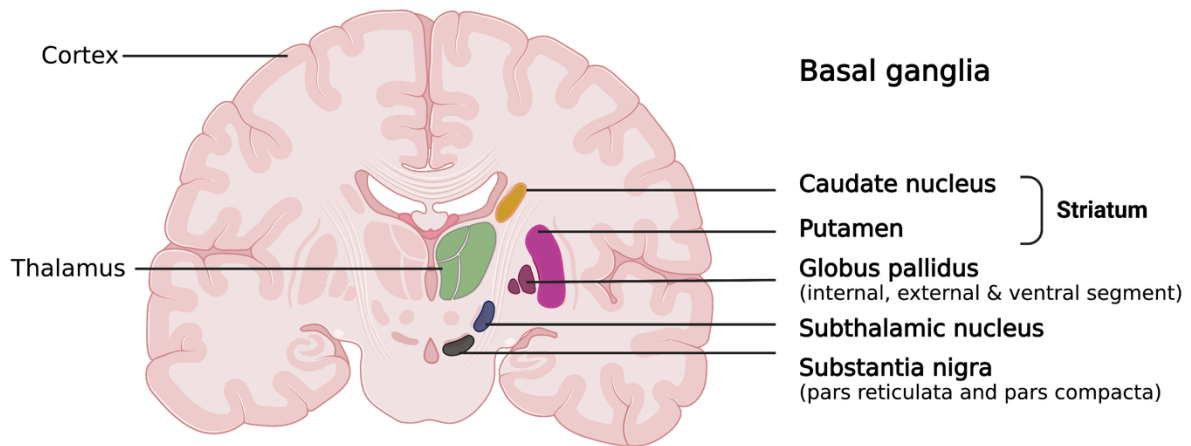


Figure 1. Basal ganglia anatomy. Coronal section of the human brain demonstrating the anatomical localisation of the basal ganglia nuclei. Figure created with Biorender.

The striatum represents the main input station of the basal ganglia and receives information from the cerebral cortex and thalamus, whereas the GPi, VP and the SNr provide output information to the thalamus and the mesencephalic motor regions¹³. In addition to their topographical organisation, basal ganglia nuclei contain distinct neural subpopulations. The striatum is mainly composed of medium spiny neurons (MSNs), which receive excitatory glutamatergic input from the cortex and the thalamus and modulatory dopaminergic input from the midbrain, in particular from the SNc¹⁴. The striatal output projections can be divided into two distinct pathways: the “direct” and “indirect” pathway. According to their type of dopamine receptor expression, D1-type dopamine receptor (DRD1)-expressing MSNs give rise to monosynaptic, **direct**, inhibitory (GABAergic) projections to the GPi, while D2-type dopamine receptor (DRD2)-expressing MSNs project polysynaptic, **indirect**, excitatory (glutamatergic) fibers to the GPi and SNr via the GPe and STN¹⁵. Activation of DRD1-expressing MSNs activates the direct, striatopallidal pathway resulting in thalamocortical excitation and thus facilitation of movements. Activation of DRD2-expressing MSNs in the indirect, striatonigral pathway leads to net thalamocortical inhibition and suppression of movements¹⁶ (**Figure 2**). The classical basal ganglia model has been adapted over time, and it is now believed that the basal ganglia are organised into a complex neural network system with several internal re-entry loops referred to as the Center-Surround model¹⁷. This model relies not only on action initiation but also on action selection and hypothesises simultaneous activation and inhibition of basal ganglia pathways upon distinct signals^{17,18}.

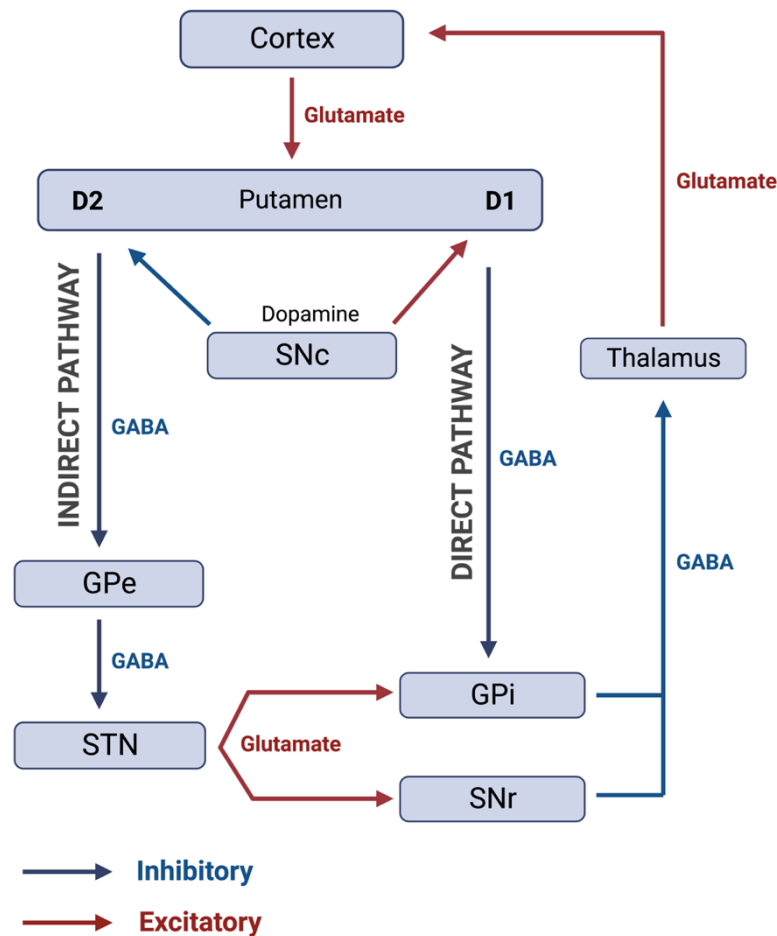


Figure 2. Classical basal ganglia model. DA neurons in the SNc release the neurotransmitter dopamine that activates D1-type dopamine-receptor MSNs and inhibits D2-type dopamine-receptor expressing MSNs in the striatum. Activation of the direct pathway promotes movement, while activation of the indirect pathway suppresses movement (Figure adapted from McGregor 2019¹⁷). Figure created with Biorender.

1. 1. 2. 1. Motor circuit pathology in Parkinson's Disease

Dysfunction of basal ganglia circuits is associated with different movement disorders. In PD, the classical motor features include bradykinesia, tremor and rigidity. The clinical picture of PD patients includes paucity (hypokinesia) and slowness (bradykinesia) of movements but also difficulty in initiating voluntary movement. On a pathophysiological level, PD is characterised by dopamine depletion in the SNc. Dopamine deficiency results in opposing effects on the basal ganglia output pathways⁵. Decreased activation of DRD1-MSNs results in hypoactivation of the direct pathway, while reduced inhibition of DRD2-MSNs leads to increased activity of the indirect pathway¹⁹. Together, these changes induce excessive, excitatory STN activity and inhibitory GPi activity that, as a net result, lead to increased thalamocortical inhibition¹⁷. From a clinical point of view, this inhibition results in bradykinesia (**Figure 3**). This model is likely oversimplified; however, it has contributed enormously to establishing functional neurosurgery

approaches in PD. In the 1950 and 1960s, ablative surgical procedures such as pallidotomy and thalamotomy were developed to improve motor signs and symptoms of PD²⁰. Later on, animal studies showed the strong antiparkinsonian effect of STN lesions. Subsequently, less invasive and reversible methods such as deep brain stimulation (DBS) were developed to target basal ganglia motor circuits²⁰. Nowadays, DBS of the STN or GPi is well established with the aim to decreasing pathological basal ganglia output to ameliorate motor symptoms in PD.

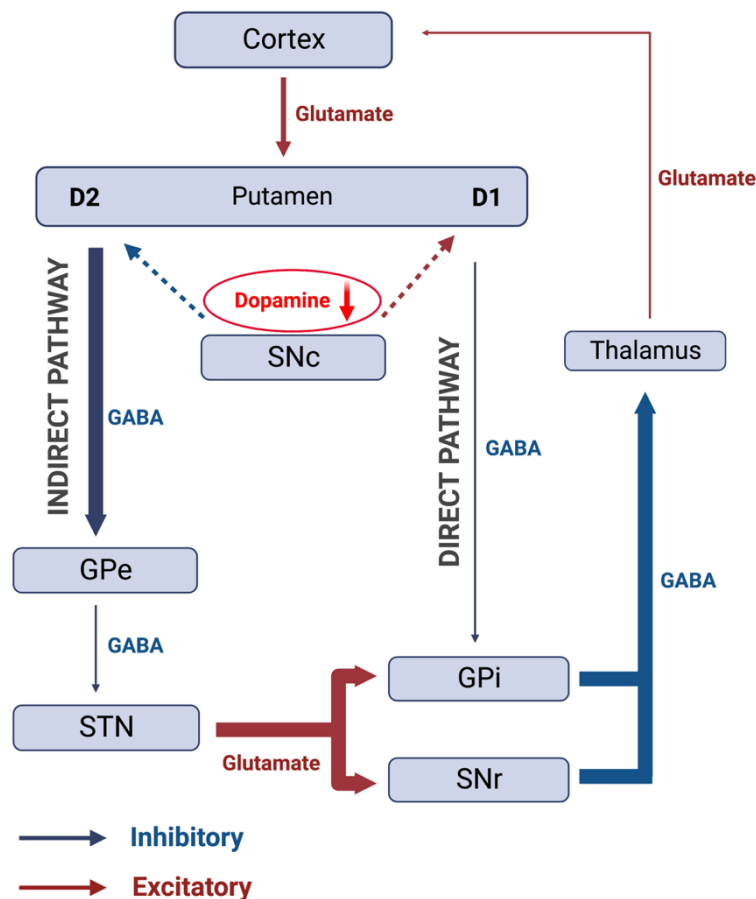


Figure 3. Schematic overview of basal ganglia circuit pathology in PD. Degeneration of SNc DA leads to dopamine deficiency that causes hyperactivation of the indirect pathway and hypoactivation of the direct pathway. As a result, increased GABAergic output from the GPi leads to increased inhibition of the thalamus and subsequent suppression of movements (Figure adapted from McGregor 2019¹⁷). Figure created with Biorender.

1. 1. 3. Aetiology

The aetiology of sporadic PD is complex and involves multiple contributors, including genetic, epigenetic and environmental risk factors^{9,21}. Advancing age is considered the main risk factor for idiopathic or sporadic PD, the most common form reported in adults. Environmental risk factors include solvents, heavy metal exposure and pesticides, which have been introduced and

heavily used after the second world war²¹. A retrospective study in former professional soccer players further identified traumatic head injury as a risk factor for PD²². Population-based studies have also revealed predictive factors that are associated with decreased risk of developing PD including caffeine consumption, cigarette smoking and anti-inflammatory drugs⁵. Genetic and epigenetic risk factors include polymorphic risk variants, pathogenic gene mutations, histone modification and methylation. Large-scale genome-wide association studies (GWAS) have provided insights into the genetic components of PD and identified around 90 independent genetic susceptibility loci associated with increased lifetime risk of PD^{23,24}. GWAS allows the calculation of so-called polygenic risk scores that are based on the weighted sum of multiple genetic risk variants of different effect sizes in order to estimate the individual's predisposition for PD²⁵. Interestingly, several GWAS PD genetic risk loci represent so-called pleomorphic risk loci, which are found near single genes causing Mendelian forms of PD, such as *SNCA*, *LRRK2* or *GBA*²³. Whilst rare, deleterious variants within these genes can lead to clinical manifestation of familial PD, it is postulated that more common variants may increase the risk for sporadic PD²³.

1. 1. 4. Monogenic forms of PD

Genetic linkage analysis in large kindreds has identified familial forms of PD that are inherited in both an autosomal recessive or dominant manner²⁶. Monogenic forms of PD only account for approximately 5-10% of familial PD^{27,28}. They usually manifest much earlier in life than sporadic PD, with either juvenile (onset < 21 years) or early-onset parkinsonism (onset between 21-50 years)²⁹. Monogenic forms of PD are clinically heterogeneous and may present with additional motor and non-motor phenotypic features including developmental delay, intellectual disability, seizures and other types of movement disorders, commonly referred to as Parkinson-plus-syndrome or atypical parkinsonism³⁰.

In 1997, *SNCA* (Synuclein Alpha), encoding the protein α -synuclein, was discovered as a causal gene for familial PD³¹. Since then, rapid advances in next generation sequencing technologies have accelerated the discovery of novel disease-causing genes (**Figure 4**). To date, mutations in over twenty genes have been associated with both monogenic PD and atypical parkinsonian syndromes^{30,32}. Some of the autosomal dominantly inherited forms of PD resemble idiopathic PD (*e.g.* *SNCA*, *LRRK2* (Leucine Rich Repeat Kinase 2), *GBA* (Glucosylceramidase Beta 1), *VPS35* (Vacuolar protein sorting ortholog 35), *DNAJC13* (DnaJ Heat Shock Protein Family (Hsp40) Member C13)), while autosomal-recessive inherited forms (*e.g.* *PRKN* (Parkin), *PINK1* (PTEN-induced kinase 1), *DJ-1*, *ATP13A2* (ATPase Cation Transporting 13A2),

FBXO7 (F-Box Protein 7), *PLA2G6* (Phospholipase A2 Group VI), *SYNJ1* (Synaptojanin 1), *DNAJC6* (DnaJ Heat Shock Protein Family (Hsp40) Member C6), *SPG11* (Spastic Paraplegia 11)) often present as complex, early-onset PD^{23,26,30}. Given that variants in many of these genes have also been identified as risk factors for sporadic PD in GWAS, it has become increasingly clear, that both monogenic and sporadic PD share common genetic determinants and that distinct molecular pathways may converge into common pathways that ultimately lead to degeneration of DA neurons²⁶.

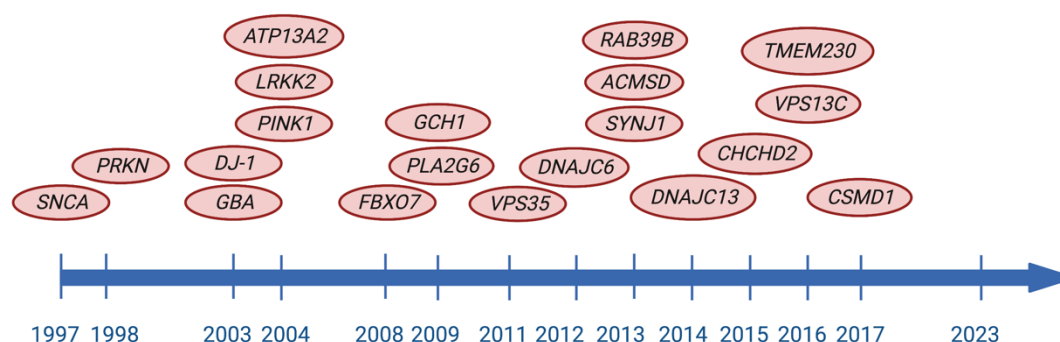


Figure 4. Timeline of gene discovery in monogenic PD. Since discovery of the PD-causing gene in 1997, the genetic landscape on monogenic PD has change considerably. Figure created with Biorender.

1. 1. 4. 1. Juvenile-onset forms of PD

Juvenile-onset forms of PD are mainly caused by genetic alterations and differ significantly from later-onset sporadic forms of PD, both in terms of molecular pathology and disease manifestation³³. In the majority of juvenile-onset cases, the clinical phenotype is complex or atypical and involves additional neurological, neurodevelopmental and neuropsychiatric features³⁴. Additional movement disorders such as dystonia or pyramidal signs and abnormal eye movements are common³⁴. Abnormal imaging features and extra-neurological manifestations may accompany specific forms of juvenile-onset PD and provide diagnostic clues³⁴. Depending on the underlying condition, neurodevelopmental abnormalities might precede the occurrence of parkinsonism and initially mask a non-progressive disease course. **Table 1** provides a summary on the main clinical, pathological and molecular features in juvenile-onset, early-onset and late-onset forms of PD^{33,35}. Clinical criteria of parkinsonism in the context of the immature and developing brain are not yet established, however, there are a number of disorders that manifest during infancy, childhood or adolescence with symptoms highly reminiscent of adult parkinsonism. A recent review proposed a classification for paediatric parkinsonism (onset 0–18 years) based on: (i) the age of onset, (ii) clinical symptoms,

(iii) outcome and (iv) aetiology³⁶. This clinical classification includes six subgroups including developmental parkinsonism, infantile and early childhood degenerative parkinsonism, parkinsonism in the setting of neurodevelopmental disorders, parkinsonism in the setting of multisystemic brain diseases, juvenile parkinsonism/dystonia-parkinsonism and acquired parkinsonism³⁶. Developmental parkinsonism encompasses diseases with a non-degenerative aetiology and normal development in early-treated patients. This group is particularly important to identify as diagnostic delay can often lead to neurological and neurodevelopmental sequelae. The other proposed forms of parkinsonism are associated with a more progressive disease course. To date, mutations in >70 genes have been linked to early-onset parkinsonism or syndromes presenting with parkinsonism as part of their clinical presentation³⁴. Most of the conditions have an autosomal-recessive inheritance, followed by dominant and X-linked mutations and in rare cases mitochondrial inheritance³⁴. From a molecular perspective, the underlying disease mechanisms are very heterogeneous and impact on the disease course, treatment response and outcome. In infancy, parkinsonism mainly presents as hypokinetic-rigid syndrome as described by García-Cazorla et al. and is usually caused by inborn errors of metabolism affecting monoamine synthesis³⁷. Primary or secondary neurotransmitter disorders may lead to dopamine deficiency, dopamine toxicity and/or nigrostriatal neurodegeneration – these include disorders of dopamine synthesis [aromatic L-amino acid decarboxylase (AADC) deficiency, tyrosine hydroxylase (TH) deficiency] and transport [Dopamine Transporter Deficiency (DTDS), Vesicular Monoamine Transporter 2 (VMAT2) deficiency]. In childhood- and juvenile-onset forms of PD, common genetic causes include mutations in *PRKN*, *PINK1*, *HTT*, *ATP13A2*, *ATP1A3*, *SYNJ1*, *DJI* and *FBX07*³⁴. There is also a variety of neurometabolic disorders that present with childhood- or juvenile parkinsonism, including diseases of Neurodegeneration with Brain Iron Accumulation, metal storage disorders, lysosomal and mitochondrial disorders and more recently cellular and synaptic trafficking disorders. While many of these monogenetic conditions are only amenable to symptomatic treatment, it is nevertheless important to exclude potentially treatable inborn errors of metabolism, which may respond dramatically to levodopa or other targeted treatments.

	Juvenile onset PD (onset <21 years)	Early-onset PD (EOPD) (onset 21-50 years)	Late-onset, sporadic PD (LOPD) (onset >50 years)
Clinical features			
Parkinsonian features	Bradykinesia/Hypokinesia, rigidity, tremor	Bradykinesia/Hypokinesia and rigidity > tremor	Tremor > bradykinesia/Hypokinesia, rigidity
Additional neurological features	Muscular hypotonia, dystonia, spasticity, ataxia	Dystonia (focal), spasticity	Dystonia, cognitive impairment
Additional neurodevelopmental features	Developmental delay, intellectual disability	-	-
Additional neuropsychiatric features	Sleep disturbances, behavioural problems, anxiety, psychosis	Anxiety, depression (>LOPD)	Sleep disorders, anxiety, depression, apathy, psychosis
Disease course	Rapidly progressive	Slower disease progression than LOPD	Variable (faster progression with higher age at onset)
Treatment response	Depending on the underlying condition, often poor response to common anti-parkinsonian drugs	Often responsive to levodopa, but early motor fluctuations (dyskinesias, end-of-dose wearing-off, on-off phenomenon)	Variable (tailored approach)
Pathological features	Substantia nigra neuronal loss (few studies available)	Lewy body inclusions, substantia nigra neuronal loss	Lewy body inclusions, substantia nigra neuronal loss
Disease aetiology and mechanisms	Genetic/Metabolic Primary and secondary neurotransmitter disorders, mitochondrial disorders, lysosomal disorders, NBIA, metal storage disorders, autophagy dysfunction, dysfunction of intracellular and synaptic trafficking	Genetic/Metabolic Mitochondrial and lysosomal dysfunction, NBIA, metal storage disorders, autophagy dysfunction	Multifactorial (genetic, environmental) α -synuclein misfolding and aggregation, mitochondrial dysfunction, autophagy dysfunction

Table 1. Overview on clinical, pathological and molecular disease features in juvenile-onset, early-onset and late-onset PD. Differences in clinical phenotypes, histopathological findings and disease mechanisms in juvenile-, early- and late-onset form of PD.

1. 1. 5. Molecular disease pathways in monogenic forms of PD

The discovery of novel disease-causing genes in families with PD has revealed novel molecular disease mechanisms and biological pathways involved in PD pathogenesis²⁵, such as protein misfolding and aggregation, vesicle-mediated transport and membrane trafficking, lipid metabolism, neuronal synaptic transmission, mitochondrial and endosomal-lysosomal dysfunction and programmed cell death²⁵. Subcellular localisation of proteins predicted to be involved in PD pathogenesis are found in the cytosol, mitochondria and in organelles associated with vesicular trafficking, the Golgi network and lysosomes-endosomes^{25,26}. Selective dopaminergic neurodegeneration likely results from the combined interaction of these distinct disease mechanisms³⁰. It is now increasingly acknowledged that mutations in genes involved in three major, interrelated molecular disease pathways contribute to neurodegeneration: (i) abnormal protein aggregation and lysosomal dysfunction, (ii) mitochondrial dysfunction and (iii) dysfunction of cellular and synaptic trafficking processes and endosomal dysfunction^{30,38} (**Figure 5**).

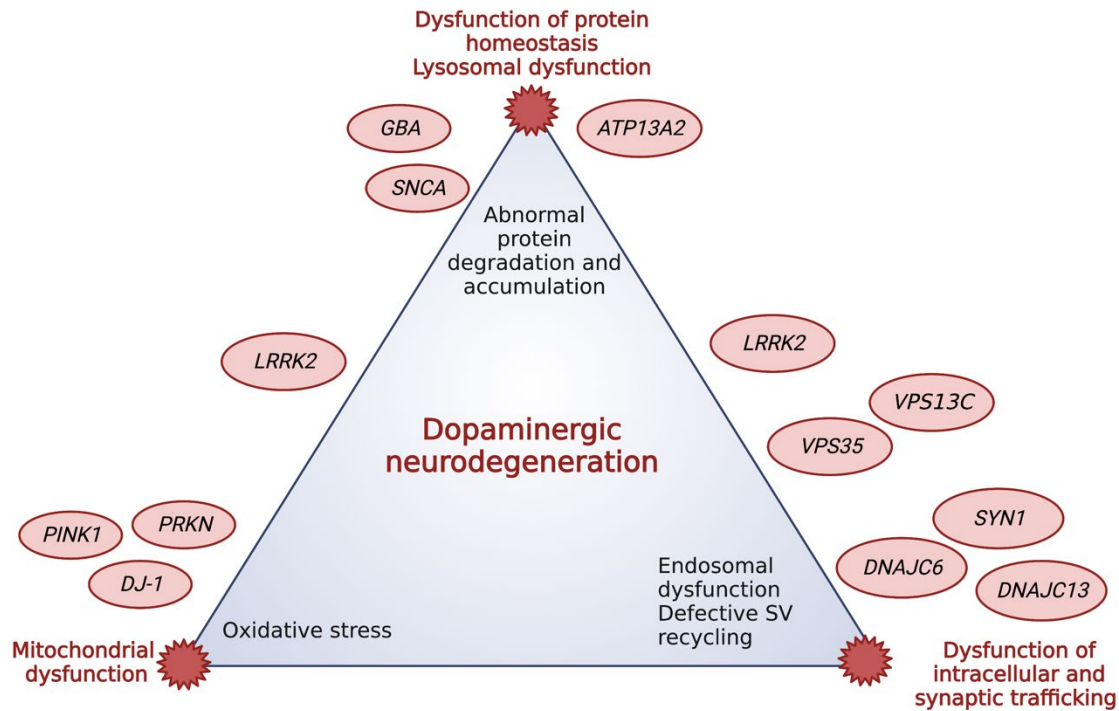


Figure 5. Disease mechanisms in PD. Corner points indicate important molecular disease mechanisms that, in a complex interplay, contribute to the dopaminergic neurodegeneration in PD. Red circles represent genes that have been associated with sporadic or monogenic PD (Figure adapted and modified from Domingo A, Klein C.³⁰). Figure created with Biorender.

1. 1. 5. 1. Protein aggregation and lysosomal dysfunction

Abnormal protein homeostasis and impaired lysosomal activity leading to abnormal protein degradation and accumulation, was one of the first pathophysiological mechanisms identified in PD. Postmortem brain studies revealed aggregated forms of α -synuclein in presynaptic terminals³⁹ and along the axons⁴⁰. Mutations in a number of genes associated with familial PD including *SNCA*, *LRRK2*, *VPS35* and *ATP13A2* support the hypothesis of altered proteostasis and an impaired lysosomal-autophagy system (LAS)⁵. *SNCA* mutations are associated with increased expression of α -synuclein but also increased risk for misfolding and oligomerisation of α -synuclein and formation of large insoluble fibrils that constitute Lewy bodies⁵. Overexpression of α -synuclein in transgenic mice has been associated with loss of dopaminergic terminals in the dorsal striatum⁴¹, deficits in dopamine release and alterations in synaptic vesicle (SV) localisation⁴². *LRRK2* is highly expressed in MSNs and encodes a large multi-domain protein kinase with multiple functions. Pathogenic mutations in *LRRK2* lead to increased GTPase or kinase activity that then results in impaired lysosomal and autophagy function⁴³. Discovery of *GBA1* as the most common genetic risk factor in PD has further highlighted the role of inefficient protein clearance and lysosomal dysfunction in PD. *GBA1*

encodes the lysosomal enzyme GCase, which localises to the endo-lysosomal lumen. GCase deficiency leads to increased intracellular α -synuclein levels⁴⁴ and the formation of pathological high-molecular α -synuclein species that are associated with increased neurotoxicity⁴⁵. The gene *VPS35* encodes the vacuolar protein sorting-associated protein 35, which is part of a retromer complex involved in sorting newly synthesised lipids and proteins, directing them to the endosomes, the cell surface and the Golgi apparatus⁴⁶. Vps35-deficient mice show increased α -synuclein levels in nigral DA neurons⁴⁷. *ATP13A2*, causing Kufor–Rakeb syndrome characterised by juvenile-onset parkinsonism, encodes a 5 P-type ATPase that is present in lysosomes and autophagosomes⁴⁸. Loss of *ATP13A2* results in decreased cellular secretion of α -synuclein⁴⁹. iPSC disease models of several monogenic forms of PD associated with mitochondrial dysfunction (*PRKN*, *PINK1*, *DJ-1*) dysfunction⁵⁰ showed accumulation of oxidised dopamine quinones that promoted the accumulation of pathological α -synuclein protofibril intermediates⁵¹.

1. 1. 5. 2. Mitochondrial dysfunction

First evidence for mitochondrial dysfunction in PD came from William Langston's observation that synthetic heroin contaminated with MPTP can cause parkinsonism in humans and animals⁵². MPP⁺, the active metabolite of MPTP, is a mitochondrial complex I inhibitor and causes a decrease in ATP production and an increase in levels of reactive oxygen species (ROS)⁵². ATP production through the respiratory chain is an essential energy supply for proper synaptic function, in particular SV recycling⁵³. Impairment of the respiratory chain capacity has further been reported in familial PD caused by mutations in the genes *PRKN*, *PINK1*, *DJ-1*, *VPS35* and *LRRK2*. Dysfunction of the respiratory chain subunits is associated with loss of mitochondrial membrane integrity and impaired mitochondrial oxidative phosphorylation that ultimately leads to increased oxidative stress and bioenergetic defects^{54–57}. Of note, early-onset mitochondrial cytopathies such as *POLG*-related disorders or mitochondrial respiratory chain defects (e.g. Complex I deficiency and Complex III deficiency) that manifest with juvenile parkinsonism further highlight the role of dysfunctional mitochondrial respiratory chain in PD^{36,58,59}. Other mechanisms of mitochondrial dysfunction in PD include defective mitophagy, the selective clearance of dysfunctional mitochondria by autophagy, to ensure mitochondrial homeostasis and quality control⁶⁰. PINK1-/Parkin-dependent mitophagy is a well-characterised quality control pathway. PINK1 phosphorylates parkin and ubiquitin and thereby promotes activation and mitochondrial stabilisation of parkin. Mutations in both *PINK1* and *PRKN* lead to decreased mitophagic flux in patient-derived neurons with decreased phosphorylation of ubiquitin and impaired recruitment of parkin to mitochondria upon mitochondrial

depolarisation⁵⁴. iPSC-derived models of genetic PD caused by *PINK1* and *PRKN* mutations also show enlarged and elongated mitochondria, while *VPS35* and *PRKN* mutant neurons showed excessive mitochondrial fragmentation due to defective fission and fusion⁵⁴. Further mechanisms of mitochondrial dyshomeostasis in PD include alterations in axonal transport of mitochondria in *SNCA* and *LRRK2* mutated neurons and dysregulation of mitochondrial Ca^{2+} handling in *GBA1*, *PRKN* and *SNCA* mutant neurons⁵⁴.

1. 1. 5. 3. Dysfunction of intracellular and synaptic trafficking pathways

Recently, identification of mutations in novel disease-causing genes such as *DNAJC6*, *DNAJC13* and *SYNJ1* has introduced the concept of impaired intracellular and synaptic trafficking processes in juvenile- and early-onset PD^{61–69}. Striatal DA neurons are characterised by a complex and extensive axonal arborisation that requires a highly effective cellular trafficking machinery⁷⁰. A high metabolic turnover and increased oxidative stress as well as a intrinsic pacemaker activity in DA neurons also requires rapid clearance of damaged organelles (e.g. mitochondria) and misfolded proteins.

Intracellular trafficking pathways include secretory and endocytic pathways, endocytosis and lysosomal pathways as well as distinct vesicle trafficking pathways in the soma and the synapse⁷¹. The endo-lysosomal system (E-L) plays a pivotal role in maintaining neuronal homeostasis. The E-L system is mainly located in the neuronal soma. However, SV recycling at the presynaptic terminal is an integral component of the E-L system⁷². Mutations in an increasing number of genes involved in distinct intracellular trafficking pathways have been associated with monogenic and sporadic PD (**Figure 6**).

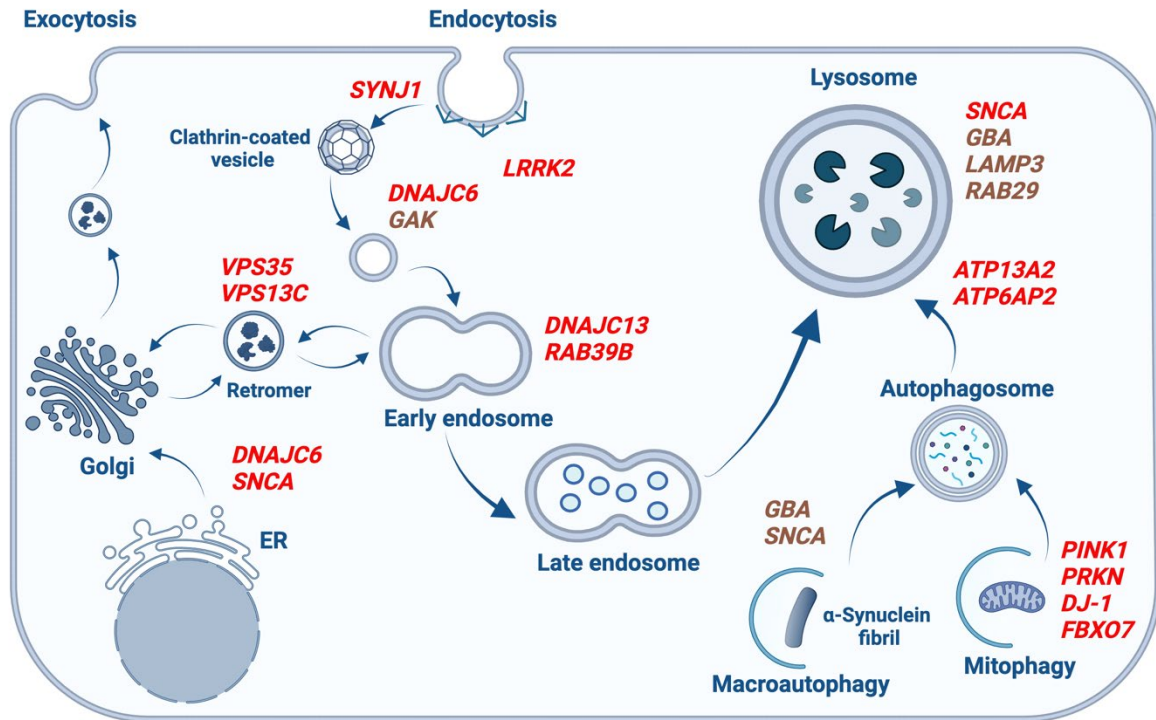


Figure 6. Intracellular trafficking pathways affected in monogenic and sporadic PD. Genes associated with monogenic and sporadic PD encode proteins that are involved in distinct intracellular trafficking pathways, in particular endocytic and endo-lysosomal pathways. Genes highlighted in red represent monogenic forms of PD, while genes highlighted in brown are associated with increased risk for PD (Figure adapted and modified from Abeliovich et al. 2016⁷¹ and Hasegawa et al. 2017⁷³). Figure created with Biorender.

Retromer complexes are responsible for the trafficking between early endosomes and trans-Golgi network (TGN) and from the endosome to the cell surface. Mutations in the genes *VPS35* and *VPS13C*, encoding components of the retromer complexes, are associated with autosomal-dominant, late-onset PD (*VPS35*) and autosomal-recessive, early-onset PD (*VPS13C*)^{74,75}. Genetic defects in both genes impair endosomal-TGN trafficking. Mutations in *VPS35* also functionally increase LRRK2 kinase activity and thus contribute to abnormal SV endocytosis (SVE)^{76,77}. Mutations in *ATP13A2* cause autosomal-recessive early-onset PD also referred to as Kufor-Rakeb syndrome. An *ATP13A2* knockout mouse model shows lysosomal dysfunction and autophagy defects⁷⁸, while patient fibroblasts harbouring *ATP13A2* mutations showed decreased mitochondrial ATP synthesis, increased oxygen consumption as well as decreased autophagic flux and impaired lysosomal degradation capacity^{79,80}. Mutations in *DNACJ13*, encoding the receptor mediated endocytosis 8 protein, have been identified in families with autosomal-dominant PD⁶⁶. *DNAJC13* gain-of-function variants lead to dysfunction of endosomal trafficking in the soma and postsynaptic compartment⁶⁶. Recently, knockdown and

overexpression experiments in *C. elegans* identified *DNAJC13* as a positive modulator of autophagy⁸¹.

Identification of mutations in PD-causing and PD-risk genes involved in SVE including *DNAJC6* (auxilin), *SYNJ1* (synaptojanin 1), *SH3GL2* (endophilin A1) and *LRRK2* (leucine-rich repeat kinase 2) has introduced the concept of **dysfunction of synaptic trafficking** (Figure 7).

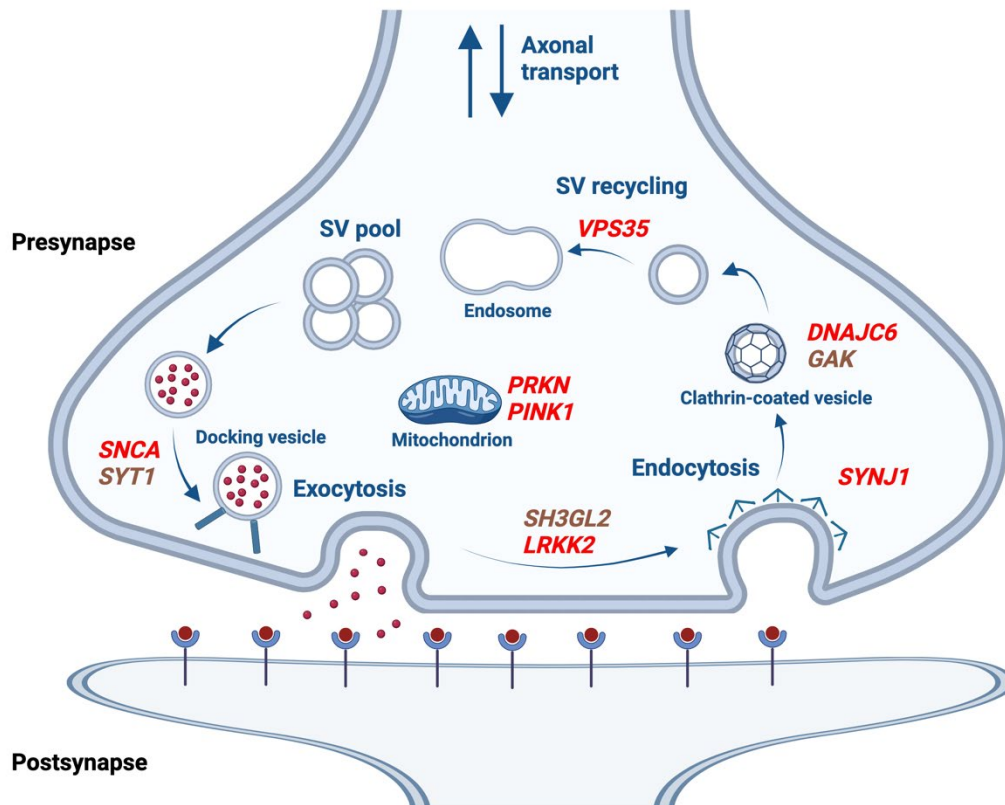


Figure 7. Synaptic trafficking pathways affected in monogenic and sporadic PD. The majority of “synaptic” genes associated with monogenic and sporadic PD affect components of the SV recycling process or SV exocytosis. Mutations in genes involved in mitochondrial function also highlight the importance of synaptic energy homeostasis. Genes highlighted in red represent monogenic forms of PD, while genes highlighted in brown are associated with increased risk for PD (Figure adapted and modified from Abeliovich et al. 2016⁷¹ and Zou et al. 2021⁸²). Figure created with Biorender.

Auxilin, synaptojanin and endophilin A1 are proteins that are involved at various stages of clathrin-mediated endocytosis (CME) at the presynaptic terminal^{83,84}. The co-chaperon protein Auxilin 1 and the phosphoinositol phosphatase synaptojanin 1, in conjunction with other accessory proteins, play important roles in the uncoating of clathrin-coated vesicles (CCVs). Mutations in *DNAJC6* and *SYNJ1* have been identified in families with autosomal-recessive, early-onset PD^{61–63,68,69}. *SH3GL2*, encoding the protein endophilin A1, is a known risk gene for sporadic PD^{24,85}. Endophilin A1 induces membrane bending in both SV curvature and autophagosome formation^{86,87}. Endophilin 1 knockout mice exhibit impaired synaptic

transmission and accumulation of CCVs⁸⁸. LRRK2 has serine/threonine kinase activity that mediates phosphorylation of endophilin A1, synaptojanin 1 and auxilin 1. Normal LRRK kinase activity is vital for proper SVE⁸⁹. Phosphorylation of auxilin 1 by mutated LRRK2 results in differential clathrin-auxilin binding with subsequent disruption of SVE and accumulation of CCVs in the dopaminergic synapse⁹⁰. LRRK2 kinase-deficient transgenic mice show decreased numbers of SV and accumulation of CCVs at presynaptic dopaminergic terminals⁹¹.

1. 1. 6. Dopaminergic dyshomeostasis

Disorders of dopamine synthesis and transport such as tyrosine hydroxylase (TH) deficiency, aromatic l-amino acid decarboxylase (AADC) deficiency or dopamine transporter deficiency syndrome (DTDS) manifest with complex childhood-onset parkinsonism⁹². GTP cyclohydrolase 1, encoded by the *GCHI* (GTP Cyclohydrolase 1), is involved in the biosynthesis of tetrahydrobiopterin (BH4), an essential co-factor for the synthesis of dopamine, serotonin, adrenaline and noradrenaline. Autosomal dominant mutations in *GCHI* typically lead to DOPA-responsive dystonia, while rare *GCHI* variants are associated with increased risk for PD⁹³. The pathogenic mechanisms underlying dopaminergic neurodegeneration in inherited forms of childhood-onset parkinsonism but also in early-onset and sporadic forms of PD have not yet been entirely elucidated. It has become increasingly clear that dopamine toxicity, in particular dopamine oxidation, plays an important role in dopaminergic neurodegeneration. In DTDS, for example, accumulation of extracellular dopamine leads to oxidative stress and proinflammatory cytokine-induced apoptosis⁹⁴. In another early-onset parkinsonism caused by mutations in the monoamine antiporter *VMAT2*, there is impaired release of dopamine and likely accumulation of cytosolic dopamine. Cytosolic dopamine can lead to auto-oxidation and the buildup of ROS and highly-reactive dopamine metabolites such as 3,4-dihydroxyphenylacetaldehyde (DOPAL)^{50,95}. Cytosolic dopamine is oxidised by iron, which generates DA quinones that can aggregate into dark pigmented neuromelanin polymers, a characteristic feature of catecholaminergic neurons of the SNc. Neuromelanin usually has a protective function, but in the case of cytosolic dopamine over-burden, it can induce a neuroinflammatory response when released from degenerating neurons⁹⁶. Oxidised dopamine metabolites can form protein adducts that lead to protein misfolding and aggregation as well as mitochondrial and lysosomal dysfunction^{95,97}. Accumulation of ROS and DA quinones is neurotoxic and ultimately constitutes a key process in dopaminergic neurodegeneration⁹⁶.

1. 1. 7. Preferential dopaminergic vulnerability

Selective degeneration of mDA neurons is responsible for the main motor symptoms in PD. Although investigation of disease-causing genes has clearly elucidated important molecular disease mechanisms in PD (**Figure 5**), it still remains unclear why mDA neurons are selectively more vulnerable than other neuronal populations, especially given that many of these genes (i) have a broad expression profile in the brain and (ii) are involved in generic cellular pathways.

To address this question, one has to consider the unique anatomical and electrophysiological characteristics of mDA neurons. It is estimated that each mDA neuron gives rise to approximately 1 to 2.5 million synapses in the striatum and forms a complex unmyelinated axonal arbor⁹⁸. This extensive axonal architecture imposes a major metabolic burden on mDA neurons. mDA neurons also exhibit autonomous pacemaker activity to support sustained neurotransmission⁹⁹. These unique axonal-architectural and electrophysiological features render mDA neurons more vulnerable to DA-related and other stressors⁹⁸. It is now well established that a combination of several factors negatively affect the mDA neuron energy homeostasis and thus lead to further detrimental sequelae including oxidative stress, mitochondrial dysfunction, impaired proteostasis and autophagy^{76,98}. Firstly, a higher mitochondrial turnover in mDA neurons results in increased levels of ROS and oxidation of accumulated cytosolic dopamine. Oxidation of free cytosolic dopamine generates reactive DA quinones that are neurotoxic and induce protein aggregation¹⁰⁰. DA quinones also impair lysosomal GC-activity and induce lysosomal dysfunction⁵⁰. Compared to DA neurons of the ventral tegmental area (VTA), mDA neurons of the SNc are more vulnerable due to their higher rate of mitochondrial oxidative phosphorylation and oxidative stress, smaller reserve capacity, higher density of axonal mitochondria and a more complex axonal arborisation¹⁰¹. Secondly, disturbance of SVE impairs reuptake of dopamine into recycled SV and thus results in accumulation of cytosolic dopamine and impaired neurotransmission⁹⁰. Thirdly, the pacemaker activity of mDA neurons leads to increased intracellular influx of Ca^{2+} via L-type (Cav1.3 subtype) calcium channels¹⁰². Intracellular calcium activates the Ca^{2+} -sensor protein phosphatase calcineurin that is involved in the initiation of SVE by dephosphorylation of endocytic proteins. Excess amount of Ca^{2+} can be removed by mitochondria in order to re-equilibrate intracellular Ca^{2+} homeostasis and ensure sequential cycles of SVE. It has been shown that L-type-channel mediated calcium influx is accompanied by mitochondrial calcium influx and increased mitochondrial oxidative stress¹⁰³. Increased levels of intracellular Ca^{2+} together with oxidative stress directly promote α -synuclein aggregation¹⁰⁴. Accumulation of

distinct isoforms of α -synuclein affect various stages of CME and thus impair SV regeneration⁷⁶. A vicious circle of increased mitochondrial oxidative stress, lysosomal dysfunction and α -synuclein pathology thus contribute to selective dopaminergic vulnerability¹⁰⁵.

1. 1. 8. Synaptic and axonal degeneration in PD

Evidence for synaptic and axonal alterations in PD come from both human studies and animal models^{106,107}. Reduced expression of the dopamine transporter (DAT) in selective imaging of presynaptic terminals in PD patients (DaTSCANTM) has fostered the hypothesis that progressive degeneration of dopaminergic axon terminals is an early event in PD disease pathology¹⁰⁶. Positron emission tomography imaging studies using a specific DAT radioligand, (¹²³I) β -CIT SPECT DAT, or a recently developed and more sensitive radioligand, [¹⁸F]-(E)-N-(3-iodoprop-2-enyl)-2 β -carbofluoroethoxy-3 β -(4-methyl-phenyl) nortropane (¹⁸F-FE-PE2I), shows significant reduction of dopamine terminals in early PD patients^{108,109}. Progressive loss of dopaminergic terminals in SNc has also been found in postmortem studies using quantitative immunohistochemistry for TH and DAT. In brain sections of PD patients, 35–75% loss of dopaminergic terminals occurs in the putamen 1-3 years after diagnosis, increasing to 70-90% 5 years after diagnosis¹⁰⁶. Kordower et al. showed that PD patients in early disease (Hoehn and Yahr Stage 1) have only minor differences in TH-immunostaining in the SNc compared to controls, while in the putamen, there is already a marked reduction of TH-labelled fine fibers indicating an early loss of axonal terminal structures¹¹⁰. Only in advanced stages of PD (Hoehn and Yahr Stage 3-5) is TH-staining reduced throughout the entire nigrostriatal system¹¹⁰. Immunofluorescence analysis in DA neurons of patients with sporadic PD showed a significant reduction of axonal transport proteins that might contribute to accumulation and aggregation of α -synuclein¹¹⁰. Studies with induced pluripotent stem cells provide further evidence for early axonal pathology in PD. mDA neurons generated from patients harbouring *SNCA* triplication and *LRRK2* (G2019S) mutations showed reduced neuronal connectivity and neurite length as well as axonal blebbing and fragmentation indicating axonal degeneration^{111,112}. Evidence for early synaptic alterations in PD have also come from several animal studies modelling familial monogenic PD¹⁰⁷. α -synuclein pathology plays a pivotal role. In a transgenic *SNCA* mouse model, accumulation and aggregation of α -synuclein led to a redistribution of important presynaptic proteins involved in SV exocytosis and consecutive reduction in dopamine release and synaptic failure¹¹³. More than half of the known PD-causing genes are involved in synaptic function and protein homeostasis including *LRRK2*, *VPS35*, *PRKN*, *PINK1*, *DJ-1*, *ATP13A2*,

FBX07, *DNAJC6*, *DNAJC13* and *SYNJI*¹¹⁴. It is thus likely that a variety of different disease mechanisms affecting synaptic and axonal homeostasis lead to early synaptic and axonal abnormalities and consecutive dying-back degeneration¹⁰⁶. Besides nigrostriatal synaptic pathology, postmortem studies also showed a significant reduction of spine density in MSNs in the striatum indicating loss of excitatory corticostriatal and thalamostriatal glutamatergic synapses¹¹⁵.

1. 1. 9. Therapeutic approaches in PD

The current symptomatic treatment of sporadic and familial PD consists of various dopamine replacement strategies and DBS to improve motor symptoms. However, these approaches do not delay or halt disease progression. The dopamine precursor L-Dopa or levodopa remains the first line treatment for PD, combined with inhibitors of AADC (e.g. carbidopa, benserazide) or catechol-O-methyltransferase (e.g. entacapone, tolcapone) to prevent peripheral breakdown of L-dopa and improve its bioavailability⁵. Monoamine oxidase type B inhibitors (e.g. selegiline, rasagiline, safinamide) as monotherapy or adjunct therapy, increase synaptic availability of dopamine by inhibiting breakdown of dopamine and may be useful for the treatment of “OFF” motor fluctuations seen in patients under long-term levodopa/carbidopa therapy. Dopamine agonists (e.g. pramipexole, ropinirole, apomorphine hydrochloride), targeting mainly D2-type dopamine receptors, are typically used in early stages of disease due to their lower risk for dyskinesias but can have substantial side effects including impulse control disorders⁵. Development of pump (DuopaTM Pump) and patch systems, which allow continuous delivery of levodopa/carbidopa or other agents can sometimes aid treatment of motor fluctuations in advanced PD¹¹⁶. Novel pharmacological approaches in the treatment of PD include disease-modifying drugs that target molecular abnormalities in distinct cellular pathways, in particular α -synuclein and LRRK2-associated disease pathology. Strategies include inhibition of α -synuclein synthesis, α -synuclein aggregation and α -synuclein uptake using small molecules, antisense oligonucleotides or short interfering RNAs¹¹⁷. Immunotherapies or autophagy-enhancing agents have also been developed to promote clearance of intra- and extracellular α -synuclein.

DBS is a non-lesional neurosurgical technique that places adjustable electrodes into specific brain targets involved in motor control. In patients with advanced PD, DBS of the subthalamic nucleus (STN-DBS) is a well-established palliative approach for the treatment of motor fluctuations and dyskinesia¹¹⁸.

Gene therapy is a rapidly evolving technology to replace, silence or modify mutated genes¹¹⁹. Gene delivery is based on non-replicating viral vectors such as adeno-associated virus (AAV) or lentivirus, which both demonstrate a good safety and efficacy profile in humans¹²⁰. The AAV virus does not integrate into the host genome in contrast to lentiviruses, but also promotes long-term transgene expression and has thus been favourably used in human trials so far. Stereotactic intraparenchymal injection allows targeted delivery specifically to the affected brain areas. In sporadic PD, gene therapy aims at increasing dopamine availability in the nigrostriatal pathway, for example by delivering neurotrophic factors to support the health and survival of DA neurons and modulating affected basal ganglia motor circuitries¹²¹. To enhance dopamine synthesis, viral vectors that deliver genes encoding dopamine synthesis enzymes including *AADC*, *TH* and GTP cyclohydroxylase have been used in the clinic. Stereotactic intraputamin injection of adeno-associated serotype 2 viral vector encoding human *AADC* (AAV-hAADC-2) improved motor function and reduced tremor, bradykinesia and rigidity with an overall increase of UPDRS total and UPDRS-III scores, though no control group was included in these studies so far^{122,123}. Two AAV-*AADC* phase 2 studies are ongoing¹²¹. Another approach uses a lentiviral vector encoding *GCH*, *TH* and *AADC* (LV-*GCHI-TH-AADC*) (ProSavin or OXB-102). Patients experienced a significant reduction of the UPDRS-III off-state score with only mild side effects^{124,125}. In addition to loss of DA neurons, PD patients also suffer loss of endogenous neuronal growth factors, in particular glial cell-line derived neurotrophic factor (GDNF) and neurturin (NRTN). GDNF and NRTN are involved in intracellular signalling that leads to activation of Nurr1, an important regulator of DA neuron development and *AADC*, *TH*, *DAT* and *VAMT2* gene expression¹²⁶. Direct protein infusion of GDNF has been investigated in several rodent and primate models of PD and showed excellent efficacy but failed in human phase 1 trials¹²¹. Viral delivery of the *NURT* gene, a GDNF homolog, also failed to demonstrate efficacy in phase 2 trials^{127,128}. A third gene therapy approach in sporadic PD aims at modulating basal ganglia circuitries, in particular the “direct” and “indirect” pathway. In PD, dopaminergic neurodegeneration leads to decreased activation of the “direct” pathway and decreased inhibition of the “indirect” pathway that ultimately result in STN hyperactivation and decreased thalamocortical excitation¹²¹. The STN contains mainly glutamatergic neurons. Glutamate decarboxylase (GAD) is the rate-limiting enzyme in the conversion of excitatory glutamate to inhibitory gamma-aminobutyric acid (GABA)¹²⁹. AAV-*GAD* delivery was thus proposed to restore the inhibitory GABAergic output in the STN and normalise excessive thalamocortical excitation. AAV-*GAD* phase 1 and 2 studies demonstrated good safety and efficacy with significant improvement of motor UPDRS scores^{130,131}.

For juvenile complex parkinsonism, gene therapy has already been applied in AADC deficiency with encouraging results. In children, stereotactic infusion of AAV2-hAADC to the midbrain (SN and ventral tegmental area) resulted in increased dopamine metabolism, almost complete resolution of (often painful) oculogyric crisis and improved motor function with gain of head control and independent sitting in a substantial number of patients¹³². In separate studies, bilateral intraputaminial delivery of AAV-hAADC-2 resulted in marked motor improvement, though the treatment was more effective in younger patients¹³³. In DTDS, an infantile form of complex parkinsonism, a study using an iPSC-derived mDA neuron model and knockout mouse model of DTDS showed reconstitution of dopamine transporter expression, rescue of neurodegeneration and an improved motor phenotype in mice⁹⁴. Gene therapy in monogenic parkinsonism, particularly when applied in the early disease stages, constitutes a promising therapy approach that has the potential to significantly alter or halt the progressive disease course.

1. 2. *DNAJC6*-related disease: key clinical and molecular features

1. 2. 1. Gene discovery and key clinical features

An association between the gene *DNAJC6* and juvenile parkinsonism was first reported in 2012⁶¹. Edvardson et al. described two brothers of Palestinian origin harbouring a homozygous loss-of-function mutation in *DNAJC6*. Both presented with normal psychomotor and cognitive development. At the age of 7 and 11 years, respectively, they developed motor symptoms reminiscent of PD including bradykinesia, rigidity, asymmetric rest tremor, postural instability, hypomimia and dysarthria. The disease course was rapidly progressive in the older brother leading to wheelchair dependence at age of 13 years, while the younger brother manifested a slightly slower disease course with loss of ambulation at the age of 18 years. In 2013, Koroğlu et al. described a more complex form of parkinsonism in 4 patients from a large consanguineous kindred of Turkish origin harbouring homozygous loss-of-function mutations in *DNAJC6*. They presented with a rapidly progressive parkinsonism manifesting between 10 and 11 years of age. In addition, they suffered from intellectual disability and seizures⁶². Elsayed et al. further reported on a girl from a consanguineous family of Yemeni origin with a homozygous nonsense mutation in *DNAJC6*. She presented with parkinsonian symptoms at the age of 10.5 years, and also suffered from hallucinations, psychosis and seizures⁶⁴. While in these patients, onset of parkinsonism was in childhood or adolescence, Olgiati et al. and Li et al. described 5 patients from 3 unrelated families of Caucasian origin presenting with parkinsonism between 21 and 44 years of age and a generally slower disease course^{63,134}. These patients harboured missense

varies considerably between individual donors (**Figure 9**). The gene expression pattern aligns with *DNAJC6* RNA expression in different human brain regions with high expression in the cerebellum, corpus callosum, frontal and occipital cortex, and moderate expression in the SNc, putamen and striatum⁶².

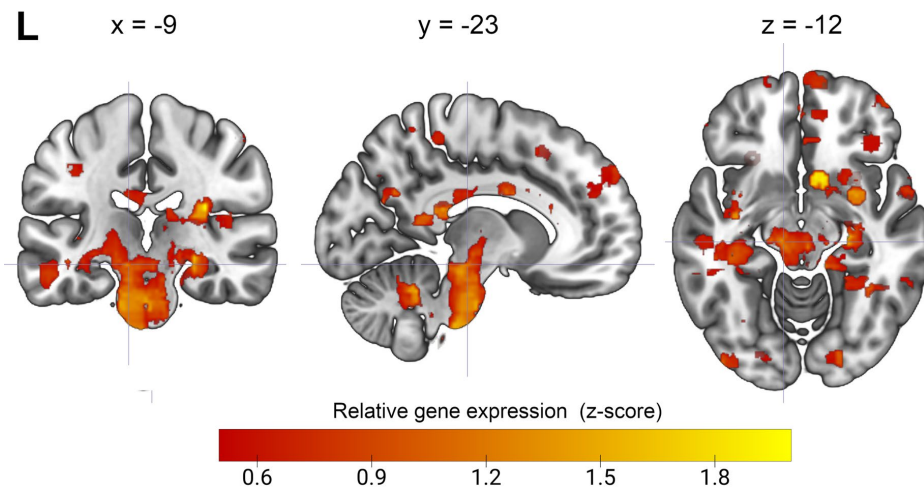


Figure 9. Mapping of human whole-brain *DNAJC6* expression. This image shows z-scores of increased *DNAJC6*-expression, averaged from 6 donors and overlaid onto a standard Montreal Neuroimaging Institute (MNI) brain template. Coordinates (in mm) indicate crosshair positions in axial (x), sagittal (y), and transversal (z) directions, centered on a region of maximal expression in close to the left SNc (z = 1.240). Data are from the Allen Human Brain Atlas, obtained via the Neurosynth database (<https://neurosynth.org/genes/DNAJC6/>).

1. 2. 3. Auxilin 1 – structure and function

DNAJC6 encodes auxilin 1, a brain-specific co-chaperone protein. Auxilin 1 belongs to the DNAJ homolog C protein/Hsp40 co-chaperone family, a subclass of the heat shock protein family. DNAJC proteins are characterised by a common and highly conserved histidine-proline-aspartic acid domain (J-domain) that binds to heat shock cognate protein 70 (Hsc70)¹³⁸. Auxilin 1 is a 100 kDa protein with three different domains: a J-domain located at its carboxy-terminus (C-terminus), a central domain that binds to clathrin and the endocytic proteins AP2 and dynamin, and a catalytically inactive phosphatase and tensin-like (PTEN) domain located at the amino-terminus (N-terminus) that binds to plasma membrane lipids phosphatidylinositol (4,5)-biphosphate (**Figure 10**)¹³⁸. *In vivo*, the J-domain and the clathrin-binding domain are both required for clathrin uncoating. The PTEN-like domain is required for recruitment of auxilin 1 to CCVs¹³⁹. In humans, auxilin 1 has a ubiquitously expressed homologue, called cyclin-G-associated-kinase (GAK or auxilin 2). In addition to the clathrin-binding and J-domain, GAK has a cyclin-G Ser/Thr-dependent kinase domain at the N-terminus and serves

as a co-chaperone for Hsc70 in non-neuronal cells¹⁴⁰. In the auxilin knockout mouse model, GAK can partially compensate for auxilin deficiency¹⁴¹.

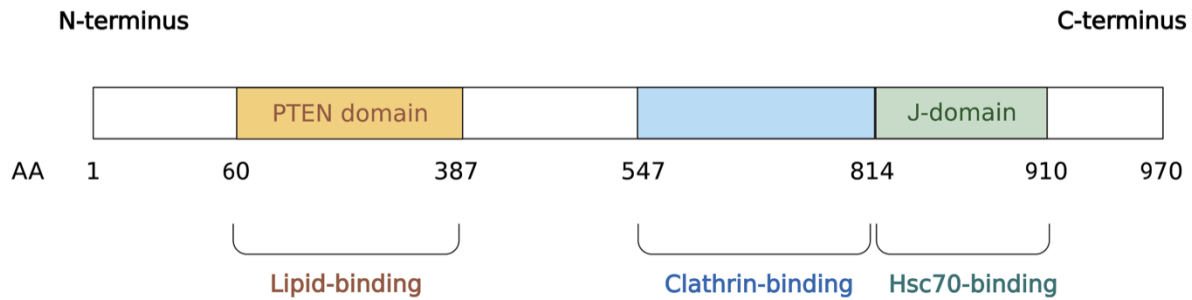


Figure 10. Schematic protein domain organisation of auxilin. Auxilin 1 has three major protein domains: a PTEN-like-domain, that binds to membrane lipids, a central clathrin-binding domain and a J-domain, that binds Hsc70 (Figure adapted from Ungewickell E. et al.¹⁴²). AA: amino acid. Figure created with Biorender.

1. 2. 4. Role of auxilin in clathrin-mediated endocytosis

CME is a complex and highly-coordinated vesicular transport mechanism involving over 50 specific presynaptic proteins with distinct functions^{83,143}. CME occurs via five steps: (i) initiation and nucleation, (ii) cargo selection, (iii) clathrin coat assembly, (iv) vesicle scission and (v) uncoating^{83,144,145}. CME initiates with the recruitment of adaptor proteins including AP-2, AP-180, epsins, and proteins of the clathrin assembly lymphoid myeloid leukaemia protein family (CALM, or PICALM family) by binding to plasma membrane lipids (phosphatidylinositol(4,5)- bisphosphate [PI(4,5)P₂])^{83,84}. The adaptor proteins, in particular FCHO1/2 and AP2, recruit further scaffold proteins to initiate membrane curvature and start the endocytic process⁸³. Subsequently, binding of clathrin and other coat-associated proteins leads to the assembly of the clathrin lattice⁸³. In addition to the clathrin coat, the actin cytoskeleton participates actively in membrane bending by filament polymerisation. After membrane insertion, dynamin and BAR proteins contribute to neck restriction and subsequent fission of the vesicle. Synaptojanin dephosphorylates PI(3,4)P₂ to prepare the binding of auxilin to phosphatidylinositol 3-phosphate (PI(3)P) and PI(3,4)P₂ lipids via its PTEN-domain¹⁴⁶. Through its clathrin-binding domain, auxilin strongly binds to the carboxy-terminal of a clathrin heavy chain in a ratio of 3:1¹³⁸. Via its J-domain, auxilin subsequently recruits the Hsc70 protein. Hsc70 is a member of the Hsp70 molecular chaperone protein family that is expressed ubiquitously¹⁴². The formation of the clathrin-auxilin-Hsc70 complex stimulates the Hsc70 ATPase activity and subsequently initiates dissociation of the clathrin-coat. Two models of how the auxilin-Hsc70 complex promotes clathrin coat disassembly, have been proposed. The first model, also referred to as the “steric wedge model”, proposed that binding of Hsc70 to the

clathrin C-terminal ends under each coat vertex works as a “wedge” and sterically hinders spontaneous, loosening fluctuations between clathrin triskelia and finally lead to coat disassembly^{83,147,148}. The other model, also called “wrecking ball”, is based on entropic forces generated by binding of Hsc70 to flexible polypeptides under each coat. Recruitment of APT to Hsc70 would enhance this entropic motion and lead to intermolecular collisions with the coat and distortion of the clathrin lattice, which finally triggers disruption of the clathrin coat^{83,148,149} (**Figure 11**). Uncoated vesicles are subsequently recycled via the endosomal pathway.

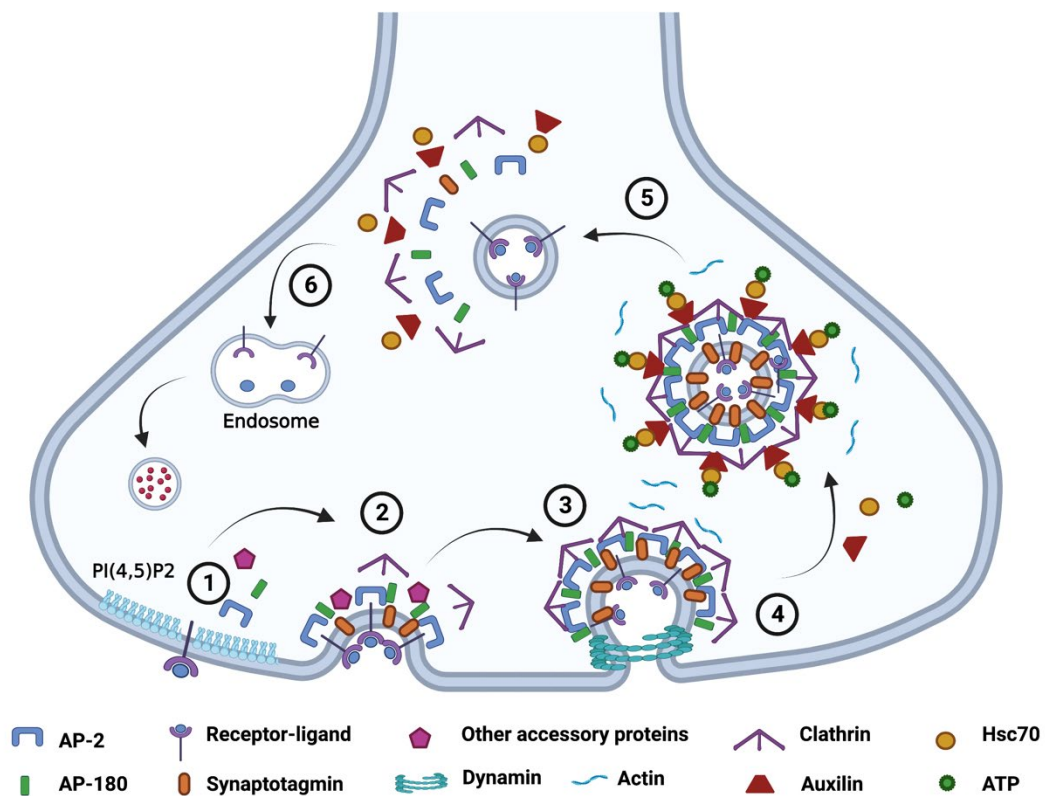


Figure 11. Schematic overview of clathrin-mediated endocytosis. 1) Initiation of CME with recruitment of key endocytic adaptor proteins to the plasma membrane lipids PI(4,5)P2 and nucleation. 2) Selection and enrichment of cargo at the site of the forming vesicle. 3) Formation of the clathrin coat and membrane bending. 4) Dynamin-mediated scission of the vesicle. 5) Recruitment of auxilin 1 and HSc70 to the clathrin-coated vesicle with subsequent ATP hydrolysis and uncoating. 6) Recycling of the naked vesicles via the endosomal pathway. Figure created with Biorender.

1. 2. 5. Role of Auxilin in other intracellular trafficking pathways and signalling

Auxilin is a co-chaperone that together with other Hsp40/DNAJ proteins such DNAJC5 (CSP α), cognate of Hsp40-3, DNAJA1 homologs, DNAJB1 and DNAJB2 belongs to the synaptic chaperone compartment, which has an integral role in synaptic protein homeostasis¹⁴⁸. Synaptic neurotransmission requires a large set of highly-specialised proteins including

neurotransmitter receptors, SV exo- and endocytosis proteins, and scaffolding proteins of the active zone and the post synaptic density¹⁵⁰. Many of these proteins undergo rapid conformational changes and interact in sequential protein-protein interactions that generate constant proteostatic stress¹⁵⁰. Co-chaperones assist chaperones in the folding of specific protein substrates, their assembly and stability and regulate their activity. The synaptic co-chaperones *DNAJC6* (auxilin 1), *DNAJC5* (CSP α) and *DNAJC13* (RME-8) are involved in distinct steps of SV recycling¹⁵¹. Interestingly, many DNAJ proteins have been linked to PD and parkinsonism highlighting the importance of synaptic protein homeostasis and trafficking in PD pathology (**Table 2**)^{61,62,156–158,63–66,152–155}.

Gene	Protein	Biological function	Mode of inheritance	Clinical phenotypes	Reference
<i>DNAJC5</i>	Cystein string protein α	Synaptic protein folding	Autosomal dominant	Adult cerebroid neuronal lipofuscinosis, with seizures, movement disorders, dementia, parkinsonism reported in some individuals	155-157
<i>DNAJC6</i>	Auxilin 1	Uncoating of clathrin-coated vesicles	Autosomal recessive	Juvenile and early-onset PD, with developmental delay intellectual disability, seizures, neuropsychiatric features	61-65
<i>DNAJC10</i>	Endoplasmic reticulum DNAJ domain-containing protein 5 (Erdj5)	ER-associated degradation of misfolded proteins	PD-risk gene	Sporadic PD	152
<i>DNAJC12</i>	DNAJC12	Protein interaction with aromatic amino acid hydrolases, folding of PAH	Autosomal recessive	HPA, dystonia, developmental delay, early-onset parkinsonism	153, 154
<i>DNAJC13</i>	Receptor-mediated endocytosis 8 (RME8)	Retromer-associated endosomal trafficking, regulation of endosomal clathrin dynamics	Autosomal dominant	Late onset PD with slow disease progression	66, 158
<i>DNAJC26</i>	Cyclin G-dependent kinase A (GAK), Auxilin 2	Uncoating of clathrin-coated vesicles	PD-risk gene	Sporadic PD	24

Table 2. Overview of DNAJ proteins associated with sporadic or monogenic PD and parkinsonism. Biological function of known DNAJ proteins and their associated clinical phenotypes. *DNAJC* = *DnaJ* Heat Shock Protein Family (*Hsp40*) Member, *PAH* = *Phenylalanine hydroxylase*, *HPA* = *hyperphenylalaninemia* (Table adapted from Roosen D. et al.¹⁵¹).

A recent study has shown that auxilin also takes part in the uncoating of other clathrin-coated vesicles in the cell¹⁵⁹. Together with clathrin, coat protein complex I and II (COPI and COPII) constitute the three major types of cellular coated vesicles. COPI and II coats share structural similarities with the clathrin coat and are involved in the early secretory pathway in the Endoplasmic reticulum (ER) and Golgi compartment. COPI mediates the sorting and trafficking of proteins and lipids between Golgi and the ER¹⁶⁰, while COPII assists in the formation of membrane transport vesicles that mediate protein transport from the ER¹⁶¹. Auxilin co-precipitates with a COPI subunit and loss of auxilin results in impaired trafficking between ER and Golgi and a delay in COPII vesicle fusion¹⁵⁹. Further evidence comes from the R857G

auxilin knock-in mouse model mimicking the human pathogenic R927G mutation in the J-domain of auxilin¹⁶². The knock-in mice show accumulation of coated structures around the Golgi apparatus indicating impaired uncoating as well as dystrophic alterations of the Golgi apparatus.

In *Drosophila*, auxilin is crucial for Notch signalling, a developmental pathway that regulates neural stem cell proliferation, survival, renewal and differentiation^{163,164}. Interestingly, Notch signalling is also an important regulator of DA neuron specification in *Drosophila*¹⁶⁵.

1. 2. 6. Clathrin-mediated endocytosis in physiological and pathological conditions

CME is a ubiquitous and specialised form of cellular membrane trafficking. In neuronal synapses, CME plays a fundamental role in efficient and fast SV recycling, which is vital for sustained neurotransmission. Physiologically, CME also regulates surface protein expression, plasma membrane homeostasis and remodeling upon environmental and nutritional changes, inter- and intracellular developmental signalling, and viral entry^{83,144}. By regulation of signal transduction CME influences important cellular functions such as cell growth and differentiation, patterning and development, chemotaxis and immune responses^{144,166}. CME terminates signal transduction by retrieving activated receptors from the plasma membrane surface and directing ligand-receptor complexes to the endosomal-lysosomal system for subsequent degradation¹⁴⁴. In contrast, CME activates or amplifies signalling cascades by directing internalised ligand-receptors to the endosomal system for recycling and retrograde trafficking to the cell surface¹⁴⁴. Clathrin itself is further involved in other intracellular trafficking pathways such as endosomal complex required for transport-dependent cargo sorting at endosomes as well as protein trafficking from the TGN network¹⁴⁴. In addition, clathrin is involved in neurotransmitter loading by timely acidification of SV. The clathrin coat inhibits vacuolar ATPases (vATPases) located on the SV membrane surface, which are necessary for neurotransmitter loading. Clathrin coat removal immediately restores vATPase function and allows neurotransmitter loading¹⁶⁷.

Given the importance of CME in many important cellular processes, it is not surprising that dysfunction of CME leads to disease. Loss of function of central CME components such as clathrin, dynamin, AP2 or epsin are not compatible with life and lead to early embryonic lethality^{144,168,169}. Mutations in other CME-associated proteins have been described in large

number of human disorders including cancer, myopathies, neuropathies, metabolic and genetic syndromes, as well as psychiatric and neurodegenerative diseases¹⁴⁴. The critical role of CME in SV recycling and neurotransmission implies that perturbation of this system leads to neurological dysfunction. During embryonic development, CME is involved in crucial neural developmental signalling pathways such as RTK, TGF- β /DPP, Hedgehog, Wnt and Notch¹⁷⁰. In neural progenitor cells located within the proliferative ventricular zone, also referred to as radial glial (RG) cells, CME regulates asymmetrical distribution of cell fate determinants to balance proliferation of NPCs and neurogenesis¹⁷¹. Upon asymmetrical division of RG cells, developing immature neurons migrate to the subventricular zone and differentiate into neurons. In the early stage of migration, CME regulates adhesion or de-adhesion, while later on, CME is involved in neural polarisation, which is important for axonal and neurite outgrowth at the axonal growth cones¹⁷¹. In mature neurons, CME ensures SV recycling and neurotransmission, but also regulates transmembrane receptor signalling, which is crucial for synaptogenesis, synaptic pruning and dendritic growth arborisation¹⁷¹. Given the importance of CME in diverse brain-specific functions, mutations in genes encoding CME-associated proteins have been associated with a variety of neurological disorders including movement disorders^{61–66,155}, neurodevelopmental disorders^{172–177}, neuromuscular disorders^{178,179} and epilepsy^{65,67,69,174–177,180–182} (**Table 3**). Many of these disorders present in infancy or childhood and show overlapping clinical phenotypes. Secondary dysfunction of CME has also been reported in Parkinson's disease, Alzheimer's disease⁸⁴, Huntington's disease¹⁸³ and Charcot-Marie Tooth disease¹⁷⁸.

Gene	Function in CME	Inheritance	Clinical phenotypes	Reference
SYT1	Calcium sensor (SV exocytosis), vesicle fission	De novo	Neurodevelopmental disorder, Early onset dyskinetic movement disorder with cognitive impairment	172, 173
SYT2	Calcium sensor (SV exocytosis), vesicle fission	Autosomal dominant	Lambert-Eaton myasthenic syndrome, Non-progressive motor neuropathy	179
DNM1	Scission of clathrin-coated vesicles, intracellular membrane trafficking (from endosomes and Golgi apparatus)	Autosomal recessive, de novo	Developmental and Epileptic encephalopathy, Status epilepticus with progressive bilateral mesial temporal sclerosis, Epileptic Encephalopathy with Hypo- and Dysmyelination, Mild Epilepsy and Autism	174-177, 180-182
DNM2	Scission of clathrin-coated vesicles, intracellular membrane trafficking (from endosomes and Golgi apparatus)	Autosomal dominant	Charcot-Marie-Tooth neuropathy, Centronuclear neuropathy	178
SYNJ1	Regulation of membrane resident phosphatidylinositol, membrane curvature formation	Autosomal recessive	Early-onset PD with generalized seizures, Intractable epilepsy and Tauopathy, Early-onset seizures with neurological decline,	67-69
DNAJC6	Uncoating of clathrin-coated vesicles	Autosomal recessive, de novo	Juvenile and early-onset PD, with developmental delay intellectual disability, seizures, neuropsychiatric features	61-65
DNAJC13	Regulation of endosomal clathrin dynamics	Autosomal dominant	Late onset PD with slow disease progression	66, 155, 156

Table 3. Overview on CME-associated genes associated with a wide spectrum of neurological disorders. Biological function of CME-associated genes and their associated clinical phenotypes. Gene abbreviations: SYT1/2 = Synaptotagmin 1/2, DNM1 = Dynamin 1/2, SYNJ1 = Synaptojanin 1; DNAJC6 = DnaJ Heat Shock Protein Family (Hsp40) Member C6, DNAJC1 = DnaJ Heat Shock Protein Family (Hsp40) Member C13.

1. 2. 7. Animal and cellular models of DNAJC6-related parkinsonism

To date, auxilin deficiency has been investigated in several animal models and in a human primary cell line. A conventional auxilin knockout mouse model ($^{-/-}$) using auxilin knockout embryonic stem cells showed increased early postnatal mortality at stage P21, while one-week old surviving pups had a 40% reduced body weight compared to their wild-type littermates but normal life-span¹⁴¹. Analysis of brain lysates revealed significantly increased GAK protein levels, the ubiquitously expressed auxilin homologue, which may indicate a compensatory mechanism for the loss of auxilin, though the uncoating efficiency of auxilin was clearly higher than GAK¹⁴¹. The protein expression levels of other endocytic synaptic proteins such as clathrin, AP-2, dynamin 1, synaptojanin 1, epsin1, amphiphysin 1 and Hsc70 were not altered in whole brain lysates. Immunofluorescence and electron microscopy studies in primary cortical neurons and brain slices of deep cerebellar nuclei revealed clustering of clathrin coat components and accumulation of CCVs and empty clathrin cages at auxilin knockout synapses, while the number of SV remained unchanged¹⁴¹. Analysis of SVE at hippocampal synapses

demonstrated a significantly reduced rate in auxilin knockout neurons, most likely due to sequestration of clathrin-coat components and subsequent impairment of CME.

The R857G auxilin mouse recapitulating the human pathogenic R927G *DNAJC6* mutation has features of parkinsonism including progressive bradykinesia and gait disturbances¹⁶². Electron microscopy analysis of striatal synaptic terminals revealed impaired SV recycling with reduced numbers of SV per synaptic area as well as accumulation of TGN-derived CCVs and dystrophic alterations of the Golgi apparatus. Immunoprecipitation analysis demonstrated an interaction of auxilin with a Golgi-resident clathrin adaptor protein. These findings highlight the role of auxilin in the regulation and trafficking of trans-Golgi-derived CCVs. Striatal brain sections further showed accumulation of lipofuscin and lipids in dopaminergic neurons. Accumulation of lipofuscin has been previously reported in patients with familial PD indicating lysosomal dysfunction¹⁸⁴.

Lipid defects have also been observed in a *Drosophila* auxilin knock-in model. *Drosophila* knock-in animals were created by introducing the R1119G, homologous to the human pathogenic R927G mutation, under an endogenous promoter control (*dAux*^{R1119G})¹⁸⁵. The *dAux*^{R1119G} mutants developed age-dependent progressive motor deficits, seizure-like behavior and neurodegeneration¹⁸⁵. Shotgun lipidomics of fly heads revealed alterations in lipid metabolism with reduced membrane lipids that contain long-chain polyunsaturated fatty acids, including phosphatidylinositol lipid. Both lipid species are important for SV recycling and organelle function. Synaptojanin-1 is an endocytic protein that binds to membrane lipids and is involved in CME, where it regulates the dissociation of endocytic clathrin adapters. Similar to *DNAJC6*-associated parkinsonism, loss-of-function mutations in *SYNJ1* are associated with juvenile- or early-onset parkinsonism, epilepsy, developmental delay and additional neurological features^{69,185}. Neuronal overexpression of Synaptojanin-1 rescued the functional deficits in the *dAux*^{R1119G} mutants and partially restored lipid deficits presumably because Synj1 may help to recruit auxilin to the Golgi apparatus where it is involved in trafficking of lipid transport vesicles¹⁸⁵.

The role of synaptojanin 1 and its interaction with auxilin has also been investigated in the auxilin knockout mouse model. Auxilin KO mice ($-/-$)¹⁴¹ demonstrate dystrophic dopaminergic axon terminals in the dorsal striatum¹⁸⁶ similar to those of the SJ1-KI^{RQ} mouse¹⁸⁷. An Aux-KO/SJ1-KI^{RQ} double mutant mouse model demonstrates shorter lifespan and more severe

synaptic abnormalities including increased dystrophic dopaminergic nerve terminals. The synergistic impact of *DNAJC6* and *SYNJ1* mutations demonstrate that DA neurons are highly vulnerable to defects in CME.

Recently, another study demonstrated progressive PD-like behavioural abnormalities accompanied by nigral DA neuronal loss in auxilin KO mice^{141,188}. In whole-brain homogenates, the authors found increased levels of clathrin, while other endocytic protein levels remained unchanged. Electron microscopy analysis and CCV proteomics revealed SV sorting deficits. In addition, there was evidence of striatal dopamine dyshomeostasis with significantly decreased levels of dopamine metabolites 3-Methoxytyramine (3-MT) and homovanillic acid (HVA), cytoplasmic accumulation of DOPAC and delayed reuptake of dopamine. Auxilin KO mice also showed mislocalisation of dopamine transporter (DAT) in membrane deformities and increased presynaptic autophagy.

A *Drosophila* auxilin knockdown model using RNAi (*auxRNAi*) showed reduced levels of auxilin in DA neurons¹⁸⁹. The *auxRNAi* flies demonstrated progressive locomotor function with reduced climbing abilities and lifespan compared to controls. Auxilin deficiency in combination with α -synuclein overexpression led to a significant loss of DA neurons in the corresponding cell clusters in *auxRNAi* flies (PPM1/2 clusters). Reduced auxilin expression also made *auxRNAi* flies more sensitive to paraquat, a toxin which is widely used to induce parkinsonism in animal and cell models. These findings suggest that DA neurons are more vulnerable in the state of auxilin deficiency.

Recently, Wulansari et al. developed a humanised *DNAJC6* model using human embryonic stem cells modified by clustered regularly interspaced short palindromic repeat associated system 9 (CRISPR-Cas9)-mediated gene editing to mimic the human *DNAJC6* gene mutation c.801-2 A>G¹⁹⁰. In human midbrain organoids (hMLOs) at *in vitro* differentiation stage DIV15 and DIV30, they found reduced expression of early (LMX1A and EN1) and late (NURR1) midbrain-specific markers indicating defects in ventral midbrain patterning¹⁹⁰. Global transcriptomics analysis of mutant and wild-type hMLOs at stage DIV15 revealed that down-regulated genes in mutant hMLOs are enriched in “midbrain development”, “DA neuron differentiation” and “Wnt signalling pathway”. Wnt is an important signalling pathway involved in early ventral midbrain patterning and its activation is dependent on CME. In mutant hMLOs, downregulation of Wnt-signalling was caused by disturbance of CME due to loss of

DNAJC6. Defective WNT-LMX1A autoregulation resulted in a decreased yield of TH+DA neurons and reduced expression of midbrain-specific markers in late hMLOs. In mutated, differentiated neural stem cell cultures, they further found an increase in mitochondrial ROS levels and a decrease in mitochondrial membrane potential indicating mitochondrial dysfunction. In addition, mutant neurons showed increased expression of the autophagosome components p62 and LC3II and decreased expression of the lysosomal markers LAMP1+/LC3+. LAMP1+/M6PR+-late endosomes, which are involved in Golgi-to-lysosome vesicular transport, were significantly decreased and enlarged, pointing towards a perturbation of lysosomal vesicular transport due to loss of *DNAJC6*¹⁹⁰.

Overall in auxilin deficiency, there appears to be a deleterious combination of several mechanisms that ultimately lead to dopaminergic neurodegeneration.

1. 3. Induced pluripotent stem cell technology

1. 3. 1. Introduction

In 1961, James A. Till and Ernest A. McCulloch discovered that stem cells derived from mouse bone marrow have the potential to differentiate into different somatic cell types and called them pluripotent stem cells¹⁹¹. Pluripotent stem cells have the ability to self-renew and differentiate into somatic cell types derived from one of the three primary germ layers: ectoderm, endoderm, or mesoderm. In 1981, Thomson et al. isolated the first human embryonic stem cells (hESC) from blastocysts¹⁹². However, the use of hESC in research has important ethical limitations and is regulated by law in many countries. In 2006, Shinya Yamanaka reported the ground-breaking reprogramming of mature adult somatic cells to so-called induced pluripotent stem cells (iPSC) with four basic transcription factors, encoded by the genes *OCT3/4*, *SOX2*, *KLF4* and *MYC*¹⁹³. For their discovery, Shinya Yamanaka and John B. Gordon were awarded the Nobel Prize in Medicine in 2012. iPSC disease models, or so-called “disease in a dish” models, can be derived from different, more easily accessible tissues or body fluids such as skin biopsies (fibroblasts), peripheral blood (peripheral blood mononuclear cells), hair follicles (keratinocytes) and urine (renal tubular cells)¹⁹⁴. iPSC can be expanded efficiently and differentiated to disease-specific cell types. Moreover, the preservation of the patient’s unique genetic background allows investigation of cellular and molecular phenotypes attributed to patient genotype. iPSC technology has revolutionised the field of disease modelling and boosted the development of cell-based regenerative medicine, high-throughput drug screening platforms and personalised medicine¹⁹³.

Rapid development of site-specific-nuclease-mediated gene-editing technologies such as zinc finger nucleases (ZAF) and Transcription activator-like effector-based nucleases (TALENs) or more recently, CRISPR-Cas9 has opened further promising research applications for iPSC-based disease modelling and clinical trials¹⁹⁵. CRISPR-Cas9 technology has an excellent targeting efficiency with low off-target effects. CRISPR-Cas9 allows generation of so-called isogenic controls, mutation-corrected lines generated from mutant lines, that maintain the specific genetic background and minimise the risk of random genetic mutations and epigenetic variations during iPSC-reprogramming. Isogenic controls are crucial in iPSC-disease-modelling to unravel true disease-associated phenotypes that can be attributed to the mutation being studied and thus strengthen the robustness of the model. CRISPR-Cas9 also enables generation of knock-in (KI) and knockout (KO) iPSC lines to study the corresponding gene function or confirm a disease phenotype related to a specific mutation. Development of novel CRISPR-Cas9 systems continuously improves the specificity and efficiency of editing, genome stability, and target accuracy¹⁹⁶.

1. 3. 2. Limitations and challenges of iPSC-based research

Genetic and epigenetic variations of iPSC can cause substantial variation in differentiation capacities and molecular phenotypes¹⁹⁷. Genetic alterations include aneuploidy, copy number variants (CNV), and single nucleotide variants (SNV) as well as karyotype abnormalities, which can be acquired during reprogramming or maintenance of iPSCs¹⁹⁷. Aberrant DNA methylation at specific loci or even incomplete reprogramming cause epigenetic variation. A study of undifferentiated hiPSCs by the Human Induced Pluripotent Stem Cells Initiative, however, has revealed that the variation in the genetic background of the donors is mostly responsible for the variability in hiPSC production¹⁹⁸. To minimise variability in iPSC generation, different strategies can be applied. Firstly, the use of non-integrated reprogramming technologies prevents transgene insertion while a thorough check of genomic integrity after reprogramming (SNP arrays, clearance of transgenes and methylation status) helps to exclude abnormal iPSC lines from further downstream studies¹⁹⁷. Secondly, the use of appropriate control lines such as age-matched healthy controls and, in addition, isogenic control lines are increasingly essential to confirm robust disease phenotypes¹⁹⁷. Thirdly, increasing the number of patient and control biological replicates is recommended to reduce variability.

1. 3. 3. iPSC reprogramming technologies

1. 3. 3. 1. Integrating reprogramming strategies

Initially, delivery of four transcription factors was based on viral vectors such as lentiviruses or retroviruses that integrate into the host genome. Integrating viral transfection carries the risk of aberrant genomic insertion with activation of oncogenes, inactivation of tumor suppressor genes or reactivation of the transgenes themselves¹⁹³. In particular MYC, one of the reprogramming factors, has oncogenic potential and has shown sporadic tumour formation in the offspring of iPSC-derived chimeric mice¹⁹⁹.

1. 3. 3. 2. Non-integrating reprogramming strategies

Development of novel, integration-free transfection systems significantly advanced reprogramming methodology and improved safety and efficacy for downstream clinical applications²⁰⁰. Non-integrating delivery is based on viral systems such as Sendai viruses, adenoviruses or episomal plasmids or other viral-free, transient transfection methods including piggyBack transposons, synthetic modified mRNA or miRNA²⁰⁰. Among them, Sendai Virus and episomal plasmid delivery are now well established reprogramming methods and most commonly used in the laboratory setting.

1. 3. 4. Embryonic development of the brain as the basis for iPSC-based neuronal differentiation strategies

During human embryogenesis, the one-dimensional blastula differentiates into three types of tissues in a process called gastrulation: the ectoderm from which skin and nervous system develop, the mesoderm from which result connective tissue, muscle, bone and vasculature and the endoderm which gives rise to the internal organs²⁰¹. *In vivo*, development of the central nervous system (brain and spinal cord) initiates with the formation of the neural tube, followed by regional neural patterning and neuro- and gliogenesis²⁰². Human pluripotent stem cells migrate underneath the ectoderm and transform to neuroepithelia or neural stem cells following inhibition of BMP (bone morphogenetic protein) signalling and activation of FGF (fibroblast growth factor) signalling. *In vivo*, neural patterning starts around week 3 and is governed by distinct temporal and spatial expression of morphogens along two axes: the anterior-posterior (A-P) and the dorsal-ventral (D-V) axis. A-P patterning defines regionalisation of the forebrain, mid-hindbrain, and anterior spinal cord and is governed by *FGF*, *WNT* (wingless/int1) and *RA* (retinoic acid) morphogens, while D-V patterning defines forebrain and spinal cord development and is regulated by *WNT*, *BMP*, and *SHH* (sonic hedgehog)²⁰². Neural patterning

allows formation of region-specific neural progenitor subtypes that, during neurogenesis, acquire defined neural or glial identities. *In vitro*, neural progenitor specification and differentiation follows the same principle and is controlled by supplementing media with distinct morphogens and signalling molecules that mimic A-P/D-V patterning.

1. 3. 4. 1. Midbrain dopaminergic neuron development

Dopaminergic neuron development requires the tightly coordinated interaction of complex gene networks that follow defined spatial and temporal expression patterns²⁰³. In the mature mouse analogous to the human brain, mDA neurons localise into three main nuclei: the retrorubral field (RrF) or A8 area, the substantia nigra pars compacta (SNc) also referred to as A9 area and the ventral tegmental area (VTA) called A10 area²⁰³. From a clinical point of view, SNc/A9 mDA neurons are the most disease-relevant mDA subpopulation, as they selectively degenerate in PD. SNc DA neurons give rise to the nigrostriatal pathway, while VTN DA neuron projections form the mesocortical pathway and RrF DA neuron projections the mesolimbic pathway (**Figure 12**). In the adult human ventral midbrain, the total number of DA neurons is about 400'000 – 600'000²⁰⁴. To date, various protocols have been developed to generate functional human SNc/A9 mDA neurons from pluripotent stem cells based on the principles of central nervous system embryology²⁰⁵.

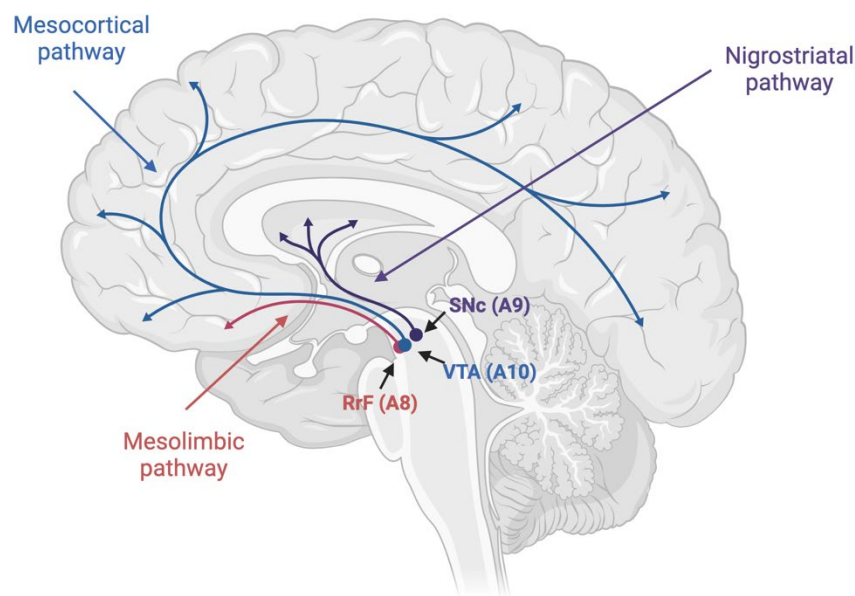


Figure 12. Localisation of dopaminergic cell clusters in the human ventral midbrain and their associated pathways. Midbrain dopaminergic cell populations in the substantia nigra pars compacta (SNc or A9 area) project to the dorsal striatum; DA neurons in the ventral tegmental area (VTA or A10 area) project to the prefrontal cortex, the limbic system and the nucleus accumbens while DA neurons in the retrorubral field (RrF or A8 area) project to the nucleus accumbens, the limbic system and the hippocampus. Figure created with Biorender.

1. 3. 4. 2. Ventral midbrain patterning

During formation of the neural tube (neurulation), two main gene expression signalling centers arise: the isthmus organizer (IsO) and the midbrain floor plate (mFP)²⁰³. The IsO develops at the midbrain-hindbrain boundary (MHB) at mouse embryonic stage E7.5 through mutual inhibition of the transcription factors *OTX2* (orthodenticle homolog 2) in the midbrain and *GBX2* (gastrulation brain homeobox 2) in the hindbrain^{206–208}. The coordinated expression of *OTX2* and *GBX2* is required for the activation of *WNT1* in the midbrain and *FGF8* (fibroblast growth factor 8) in the hindbrain. The mFP, which controls ventral patterning, develops at mouse embryonic stage E8 upon secretion of the morphogen *SHH* at the most ventral region of the neural tube and is characterized by expression of *FOXA2* (Forkhead box protein A2). *FOXA2*, together with *FOXA1*, is an essential coordinator in ventral patterning and upregulates *SHH*, *FERD31* (Fer3-like) and *LMX1A/B* (LIM homeobox transcription factor 1a/b)²⁰⁹. *FOXA2* also directly upregulates *SHH* and represses *GLI*. In the mFP, *SHH* builds a concentration gradient that regulates D-V patterning with lower concentration upregulating *NKX6-1* (NK6 Homeobox 1) and *OTX2* in the basal plate and higher concentration upregulating *FOXA2* (Shh-Foxa2 network) in the midbrain. Spatial and temporal expression of *SHH* thus plays an important role in ventral patterning (**Figure 13**).

1. 3. 4. 3. Specification of mDA progenitors

The specification of mDA progenitors in the mFP involves several transcription factors including *WNT1*, *LMX1A*, *LMX1B* and *MSX1*²¹⁰. *WNT1* integrates information from both signalling centers and is mainly expressed at the MHB. *WNT1* coordinates the development of both posterior midbrain and anterior hindbrain via regulation of *OTX2*^{211–213} but is also involved in the specification of mDA progenitors in the mFP through regulation of *LMX1A* via β -catenin²¹⁴. In the mFP, *LMX1A/B* upregulate each other and *MSX1*. While *WNT*/ β -catenin and *LMX1A/B* are roofplate genes, they form an important autoregulatory loop in the mFP that, together with the *SHH-FOXA2* network, is necessary for the specification of mDA neurons and suppression of lateral cell fates such as midbrain basal plate and hindbrain^{215,216}. *LMX1B* is also required for the differentiation of mDA progenitors²¹⁷ (**Figure 13**).

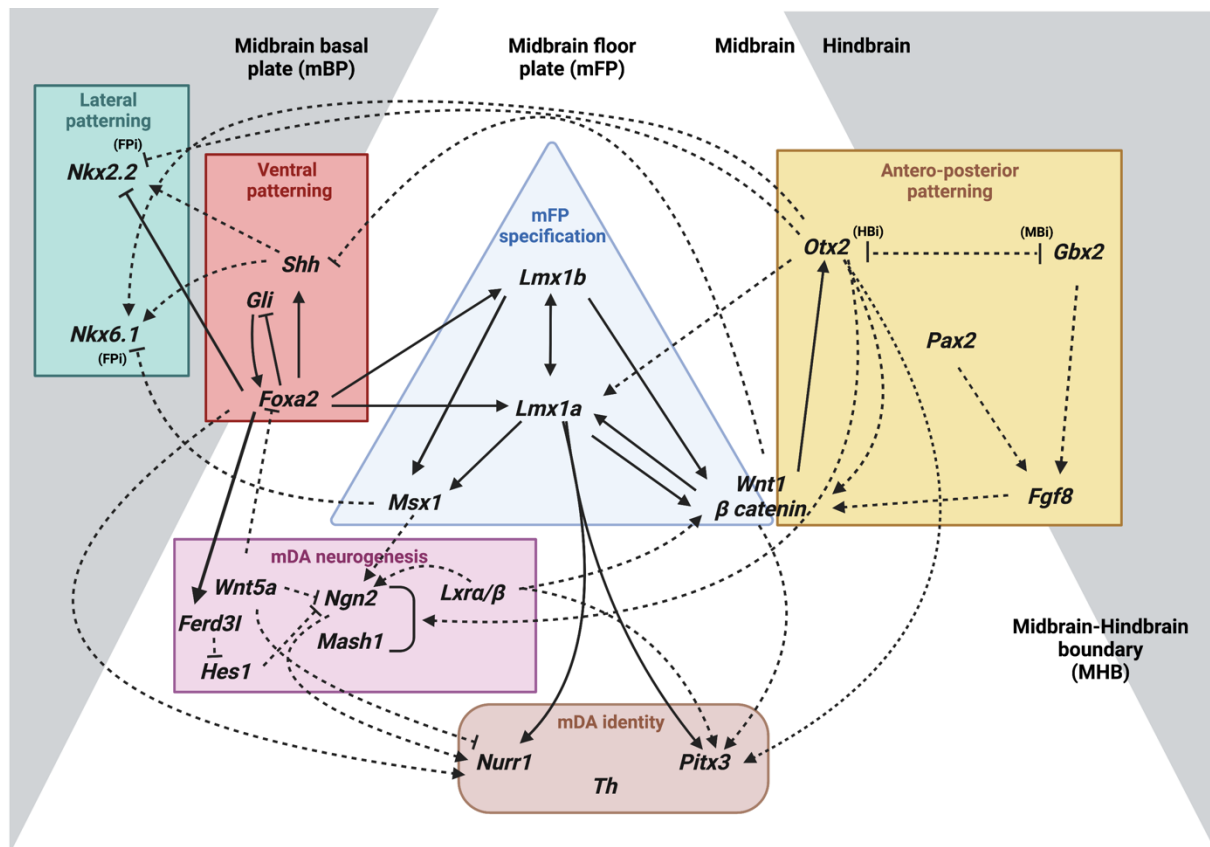


Figure 13. Overview of genetic networks involved in the development of midbrain DA neurons and formation of the midbrain-hindbrain. mDA neuron development includes 1) mFP specification (blue) that is controlled by spatial and temporal regulation of ventral (red) and antero-posterior patterning (yellow) followed by mDA neurogenesis (purple) and final acquisition of mDA identity (Figure adapted from Arenas et al. 2015²⁰³). Figure created with Biorender.

1. 3. 4. 4. mDA neurogenesis

In the inner ventricular zone (VZ) of the mFP, radial glial cells undergo neurogenesis and generate postmitotic neuroblasts that are characterised by *NURR1* (Nuclear receptor-related factor 1) expression²⁰³. mDA neurogenesis is mainly regulated by *MSH1* (mouse achaete-schute homolog 1) and *NGN2* (neurogenin 2). Both genes receive direct and indirect information from two important networks, the *SHH-FOXA2* and the *LMX1A/B-WNT1-OTX2* networks. *WNT5A* and *LXRα/β* constitute additional morphogens involved in mDA neurogenesis and are mainly expressed in mFP radial glia (*LXRα/β*) and postmitotic neuroblasts (*WNT5A*)^{203,218}. For mDA neurogenesis, *WNT1/β-catenin* suppresses *SHH* in the mFP, while *FOXA2* dose-dependently induces *FERD31* and *LMX1A*²⁰⁹. *LXRα* and *LXRβ* are both required to induce and maintain *LMX1B*, *WNT1* and *NGN2* during mDA neurogenesis.

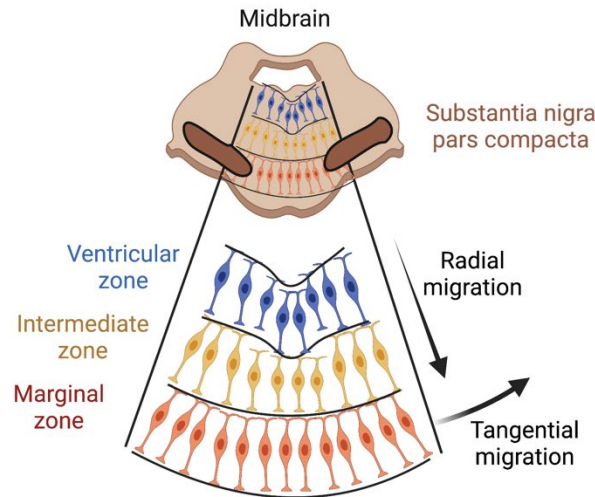


Figure 14. Overview of midbrain DA neuron migration. After neurogenesis, postmitotic neuroblasts migrate radially from the ventricular zone to the intermediate zone and differentiate into mDA neurons in the marginal zone, from where they migrate tangentially to the SNc (Figure adapted and modified from Arenas et al. 2015²⁰³). Figure created with Biorender.

1. 3. 4. 5. mDA migration, differentiation and survival

Postmitotic neuroblasts migrate radially through the intermediate zone (IZ) and differentiate into mDA neurons in the marginal zone (MZ) of the mFP (**Figure 14**). Differentiation of migratory postmitotic neuroblasts is under control of *OTX2*, *LMX1A/B*, *FOXA1/2* and the homeobox genes *EN1/2* (engrailed 1/2). Early transcription factor *LMX1A* directly regulates the expression of late transcription factors *NURR1* and *PITX33* (pituitary homeobox 3, or paired-like homeodomain transcription factor 3)^{219,220}. *NURR1* and *PITX3* are expressed in postmitotic mDA neurons from embryonic stage E10-10.5 on to adult stages and are important for the gradual acquisition of a mature dopaminergic phenotype. *NURR1* is crucial for the survival of mDA neuroblasts and controls a variety of genes that are expressed in mature mDA neurons such as *TH*, *SLC18A2/VMAT2* (solute carrier family-18 member-2/vesicular monoamine transporter-2), *SLC6A3/DAT* (solute carrier family-6 member-3/dopamine transporter) and *DDC/AADC*, *RET* (c-ret proto-oncogene), *BDNF* (brain-derived neurotrophic factor) and *CDKN1C* (cyclin-dependent kinase inhibitor 1C)^{126,221–224}. *NURR1* also controls *EN1*, which in turn regulates *PITX3* as well as *TH*, *SLC18A2/VMAT2* and *SLC6A3/DAT*. *PITX3* directly and indirectly (via retinoic acid) regulates *TH*, *VMAT2* and *DRD2* (dopamine receptor 2). Altogether, *NURR1*, *PITX3* and *EN1/2* are involved in terminal dopaminergic differentiation and support survival and maintenance of mature mDA. *FOXA2* is also crucial for the expression of *NURR1*, *EN1* and *DDC* in mDA neuroblasts and neurons and *TH* in mDA neurons²²⁵. From the MZ, mature mDA neurons migrate tangentially to reach their final destinations in the SNc (known as the A9 group).

1. 3. 5. Neuronal iPSC-based differentiation strategies

Before the era of iPSC technology, research into neurological disorders was mostly carried out with animal models, primary neuronal cells or immortalised cell lines¹⁹⁷. Animal models have contributed enormously to a better understanding of basic molecular disease mechanisms. However, species-specific differences in the genetic background and divergent neuronal network development often prevent the recapitulation of cardinal human disease phenotypes²²⁶. These differences have been a major hurdle in the development and translation of therapeutics and most of the successful drug studies in animal models have failed in human clinical trials, particularly in the field of neurodegenerative diseases²²⁶. The use of primary neuronal cells is limited due to the relative inaccessibility of fresh human brain tissue, while isolation of primary cells from postmortem tissue remains challenging due to their extreme sensitivity to alterations in oxygen levels and metabolite supply. Postmitotic primary neuronal cells are also difficult to expand and culture for extended periods²²⁷. Immortalised human cell lines offer several advantages including easy handling, unlimited expansion and low costs but carry the disadvantage of oncogenic or unique genetic characteristics that may interfere with the intended research studies²²⁷.

Neurological disorders often present with complex clinical phenotypes that are usually attributable to distinct neuronal or glial cell populations. Laboratory investigation of relatively pure human neuronal cell populations has been challenging. In this regard, iPSCs provide many advantages, in that they can be expanded efficiently and differentiated into virtually every somatic cell of the body using established protocols. To date, numerous neuronal iPSC differentiation protocols have been developed, which allow generation of distinct types of neurons (e.g. cortical neurons^{228,229}, GABAergic interneurons²³⁰, striatal neurons²³¹, dopaminergic neurons^{232–234}) and glial cells (e.g. astrocytes^{235–237}, oligodendrocytes^{238,239}, and microglia^{240,241}) (**Table 4**).

Cell type	Patterning factors	Neurotrophic factors	Reference
Cortical neurons	SMAD Inhibition (SB431542I, Noggin/dorsomorphin)	N2, B27, FGF2	228
	Dual SMAD Inhibition (with XAV939)	PD0325901, SU5402 and DAPT	229
GABAergic neurons	ROCK Inhibitor, SB431542I, BMPRIA, Dkk1, PM	N2, B27	230
Striatal neurons	SB431542, LDN193189, dorsomorphin, SHH, cyclopamin, activin A	BDNF, GDNF	231
Dopaminergic neurons	Dual SMAD Inhibition, SHH-C24II, CHIR99021	FGF8b, BDNF, AA, GDNF, DAPT, dbCAMP	232
	Dual SMAD Inhibition, FGF-8, SHH-C24II, LDN193189, SB431542, CHIR99021, purmorphamine	BDNF, GDNF, TGFb3, AA, dbCAMP, DAPT	233
	Dual SMAD Inhibition, SHH-C24II, Wnt, Dkk1 blocking antibody	FGF2, BDNF, GDNF, TGFb3, AA, FGF8, TGFb3, dbCAMP	234
Astrocytes	FGF2, CNTF, BMP2		235
	Dual SMAD inhibition, N-acetylcysteine, RA, purmorphamin, bFGF2, BDNF< GDNF, forskolin	EGF, LIF, FGF, CNTF (astrogligenic factors)	236
	Dual SMAD inhibition, CT1, JAG1	EGF, FGF2, CNTF	237
Oligodendrocytes	bFGF, FGF2, RA, purmorphamine	T3, NT3, IGF, PDGF-AA	238
	SB431542I, LDN, RA, PDGF, IGF-1, HGF, NT3	Insulin, T3, biotin, cAMP, AA	239
Microglia	FGF2, BMP4, activin A, LiCL, VEGF, TPO, IL-6, IL-3	M-CSF, IL-34, TGFb-2, CD200, CX3CI1	240
	BMP4, SCF, SCF, VEGFA, IL-3, TPO, M-CSF, FLT3, GM-CSF	IL-34, GM-CSF	241

Table 4. Selection of established iPSC neuronal differentiation protocols. Table adapted and modified from McComish et al.²⁴².

Many neuronal differentiation protocols are based on two-dimensional monolayer cultures, which are useful for imaging and morphological studies (e.g. dendrite complexity) as well as a variety of cell-based assays²⁴³. In 2013, Lancaster et al. developed self-organising cerebral organoids derived from floating cultures of embryoid body-like (EB) aggregates²⁴⁴. These organoids represent more physiological and complex three-dimensional structures containing a variety of neuronal cell types. 3D cultures can be used to study cell-cell interactions but also synaptogenesis or myelination in a context that is more reminiscent of an *in vivo* neuronal cytoarchitecture²⁴³. Generation of region-specific brain organoids (e.g. forebrain organoids²⁴⁵, midbrain-like organoids^{245,246}, cerebellar organoids²⁴⁷, hypothalamic organoids²⁴⁵) are useful to study areas or cell populations that are selectively affected in both acquired or inherited brain disorders (e.g. midbrain-organoids in PD, cortical organoids for a broad range of neurodevelopmental diseases). Recently, development of assembloids²⁴³, or fused organoids, allow the study of cell migration, inter-regional interaction and distinct brain circuits for

example in dorsal-ventral forebrain organoids²⁴⁸, cortico-thalamical assembloids or cortico-striatal assembloids²⁴⁹ (Table 5).

Organoid type	Patterning factors	Neurotrophic factors	Reference
Cortical organoid	Unguided, self-patterned differentiation		244
Region-specific organoids	Patterning factors	Neurotrophic factors	Reference
Forebrain organoid	Dorsomorphin, A83, CHIR99021, SB431542, Wnt3A	N2, B27, Neurobasal, BDNF, GDNF, Tgf-beta cAMP	245
Midbrain organoid	SB431542, CHIR99021, FGF8, purmorphamine	BDNF, GDNF, db-cAMP	245, 246
Cerebellar organoid	Wnti, SB431542l, Y-27632, gfCDM, FGF2	Neurobasal, N2,	247
Hippocampal organoid	SB431542, Y-27632, IWR1e,	N2, 40% oxygen	248
Hypothalamic organoid	SB431542, LDN193189, Wnt3A, SHH, purmorphamine	FGF2, CNTF	245
Fusion organoids	Patterning factors	Neurotrophic factors	Reference
Dorsal-ventral forebrain organoids	Human cortical spheroids: SMAD inhibition, FGF2, EGF Human subpallial spheroids: SMAD inhibition, IWP2, FGF2, IWP2, SAG	Human cortical spheroids: BDNF, N3, AA, cAMP, DHA Human subpallial spheroids: BDNF, N3	249
Cortico-striatal assembloids	Human cortical spheroids: SMAD inhibition, FGF2, EGF Human striatum spheroids: SMAD inhibition, activin A, IWP2, SR11237	Human cortical spheroids: BDNF, N3, AA, cAMP, DHA Human striatum spheroids: BDNF, N3, AA, cAMP, DHA, DAPT	250

Table 5. Selection of iPSC-based neuronal organoid differentiation protocols. Table adapted and modified from Koo et al.²⁵⁰.

1. 3. 5. 1. Established dopaminergic differentiation protocols

Differentiation of iPSC into mDA neurons is based on the temporal expression of different transcription factors *in vitro* to mimic embryonic development of mDA. In mouse models, Arenas and others have identified the basis of the complex spatial and temporal interplay of distinct genetic networks that contribute to the development of mDA neurons²⁰³. Early dopaminergic differentiation protocols were based on stromal-feeder-based neural induction, but the DA neurons generated by this protocol could not be transplanted *in vivo*²⁰⁵. In 2011, Kriks et al. from the Studer laboratory established an efficient floor-plate based protocol for the development of human DA neurons that efficiently engrafted *in vivo*²³³. The floor plate is a critical signalling center that is crucial for ventral midbrain development^{203,251}. In a first step, they used dual SMAD-inhibition (e. g. by adding SB431542 and LDN193189) to induce neural induction²⁵². The specificity of mDA is achieved by expression of characteristic markers.

Importantly, co-expression of *FOXA2* and *LMX1A* is a unique feature of DA precursors and differentiated DA neurons. CHIR99021 (CHIR), a potent GSK3b inhibitor, induces *LMX1A* expression in *FOXA2*⁺ floor plate precursors by strong activation of Wnt signalling²³³. To achieve floor plate induction and ventral patterning, additional morphogens are necessary. Purmorphamine, a small molecule agonist, activates SHH that is required for ventralisation and co-expression of *FOXA2/LMX1A*. Final midbrain DA neuron differentiation and maturation is achieved by exposure to BDNF and glial cell line-derived neurotrophic factor (GDNF) to induce DA neuron differentiation, to ascorbic acid (AA) and dibutyryl cyclic AMP (cAMP) to support survival and to transforming growth factor- β 3 (TGF β 3) and γ -secretase inhibitor (DAPT) to maintain midbrain DA neuron identity^{205,233}. The protocol by Kriks et al. was highly efficient with a yield of >70% *FOXA2/LMX1A*⁺ cells at day 11 and >70% *TH*⁺ cells at day 50 of differentiation. The floor plate strategy was subsequently used in many other protocols²³³. Kirkeby et al. established a similar approach by combining dual SMAD inhibition (SB and noggin) with EB formation for neural induction and dissociation to single cells at day 11 for terminal differentiation, and in contrast to the Kriks protocol, a dose-dependent activation of Wnt signalling by CT (inhibitor of glycogen synthase kinase 3 (GSK3))²³². The protocol yielded a relatively pure population of midbrain DA neurons expressing *LMX1A/FOXA2*, *EN1*, *NURR1* as well as *TH* and *AADC*. Based on embryological mDA neuron development, many other protocols have been developed since then, including 3D-approaches modeling the human midbrain region (midbrain-like organoids) reflecting the more complex *in vivo* cytoarchitecture²⁵³. The protocol established in our lab is based on the Kirkeby approach²³².

1. 3. 6. Modelling neurodevelopmental disorders with induced pluripotent stem cells

Neurodevelopmental disorders (NDD) include a spectrum of phenotypically and genetically heterogeneous diseases which are characterized by impaired language, cognitive, emotional and/or motor development resulting in significant dysfunction of communication, memory, learning, and motor abilities²⁵⁴. NDD include autism spectrum disorders and intellectual disability, which are frequently associated with complex paediatric neurological diseases. To date, more than 1500 genes have been linked to NDD (<https://sysnidd.dbmr.unibe.ch>). The study of human brain development in animal models remains somewhat limited since brain size, neuron density and connectivity and brain development differs considerably in rodents compared to humans²⁵⁴. Furthermore, postmortem human studies offer some possibilities to study early brain development though again has its limitations. In this regard, hiPSC model

systems provide a unique opportunity to study early developmental trajectories. hiPSC-derived neuronal cells can recapitulate brain development from embryogenesis to different stages of derived neuronal maturity²⁵⁴. It is well acknowledged that iPSC-derived neurons retain a fetal-like phenotype, though they are capable of forming functional synapses and neuronal circuitries²⁵⁵. 3D brain organoid cultures are thought to be similar to first trimester forebrain²⁴³. This limitation needs to be considered when studying later-onset neurological diseases²⁵⁶. However, for early-onset neurological diseases, the use of fetal-like neurons can potentially facilitate the study of perturbations in early developmental signalling pathways, neuronal patterning, synapse formation and network establishment. To date, numerous NDDs have been studied in iPSC disease models including classical Rett syndrome, Fragile X-syndrome and other distinct genetic syndromes such as Williams-Beuren syndrome, Timothy syndrome and many others^{254,257,258} (**Table 6**). Differentiation protocols for cortical neurons, neural progenitor cells and glutamatergic cells have been used to investigate underlying disease mechanisms. Interestingly, many of the identified molecular and cellular pathways have been linked to synaptic function²⁵⁷. Alterations in synaptic structure, function and connectivity, dendritic spine morphology and synaptic neurotransmission has led to the emerging concept of developmental “synaptopathies”^{255,257,259}. Mutations in genes encoding proteins that are involved in synapse development and function have been linked to both NDD and complex paediatric neurological disorders^{260–266}. These proteins localise to the presynaptic terminal, the synaptic cleft or the postsynaptic compartment. Depending on their localisation and function, alterations of synaptic proteins can potentially affect neurotransmitter synthesis, SV recycling, synaptic protein and mitochondrial homeostasis or postsynaptic receptor function and signalling that alter excitation and inhibition with subsequent perturbation of neuronal activity. Other emerging disease concepts in NDD include perturbation of key developmental signalling pathways (ASD) or transcription factors (Rett syndrome, FOXP1 syndrome) and chromatin remodeling.

Gene	Disorder Clinical phenotype	Inheritance	Molecular “synaptic” phenotype in iPSC-derived neuronal cell models	Reference
DDC	AADC deficiency	Autosomal recessive	Reduced neurite branching and synapse maturation defects	258
CACNA1A	Timothy syndrome	Autosomal dominant	Reduction in dendritic complexity and activity-dependent dendritic retraction	260
FMR1	Fragile X syndrome	X-linked	Impaired synaptic retinoic acid signalling, immature synaptic networks, delayed synaptic maturation, reduced synaptic activity	261, 262
MECP2	Rett syndrome	X-linked	Reduced dendritic spine density, altered electrophysiological properties, altered calcium signalling, fewer synapses	263
STXBP1	Developmental and epileptic encephalopathy	De novo, mosaicism	Impaired synaptic transmission and neurite outgrowth	264
SHANK3	Phelan McDermid syndrome	De novo	Defects in excitatory synaptic transmission	265
UBE3A	Angelman syndrome	Maternal imprinting	Decreased spontaneous excitatory synaptic activity and activity-dependent synaptic plasticity	266

Table 6. Selected iPSC-derived neuronal NDD models associated with synaptic dysfunction. Genes associated with a variety of NDD and their associated synaptic dysfunction. Gene abbreviations: DDC = Dopa Decarboxylase, CACNA1A = calcium voltage-gated channel subunit alpha1 A, FMR1 = fragile X messenger ribonucleoprotein 1, MECP2 = methyl-CpG binding protein 2, STXBP1 = syntaxin binding protein 1, SHANK3 = SH3 and multiple ankyrin repeat domains 3, UBE3A = ubiquitin protein ligase E3A.

1.3.7. Modelling neurodegenerative disorders with induced pluripotent stem cells

Neurodegenerative disorders are group of disorders that are characterized by progressive loss of neurons that lead to disruption of structure and function of the central (and peripheral) nervous system²⁶⁷. In terms of their aetiological origin, neurodegenerative disorders are highly heterogeneous and include both genetic and environmental factors as well as pathophysiological changes associated with ageing²⁶⁷. Infancy or childhood-onset neurodegenerative diseases are nearly always inherited and comprise a spectrum of neurometabolic disorders²⁶⁸. They often present as multi-organ systemic diseases and, in contrast to adult-onset neurodegenerative diseases, also typically have associated neurodevelopmental features.

The aetiological complexity and later disease-onset poses significant challenges when establishing *in vitro* models for adult-onset neurodegenerative disorders²⁶⁷. Nevertheless, iPSC-disease models have been increasingly used in the study of both adult- and childhood-onset neurodegenerative disorders with differentiations directed towards disease-relevant neuronal cell populations such as cortical neurons (e.g. Alzheimer disease, lysosomal storage disorders,

mitochondrial disorders), striatal GABAergic interneurons (e.g. PD), motor neurons (e.g. ALS), medium spiny neurons (e.g. Chorea-Acanthocytosis), dopaminergic neurons (e.g. PD), and astrocytes (e.g. Huntington disease, PD, ALS)^{94,269–277}. To overcome the issue of iPSC-related immaturity, different aging strategies have been developed including progerin-induced ageing²⁷⁸, stress loading²⁷⁹, telomerase manipulation²⁸⁰ or *ad hoc* aging promoters²⁸¹. Direct conversion of somatic adult cells to neurons using transcription factors²⁸² or miRNAs²⁸³ (iN technology) also confers several advantages for modeling late-onset neurodegenerative diseases. It has been demonstrated that directly induced neurons (iN) retain ageing signatures of donor fibroblasts and also preserve the epigenetic memory²⁸⁴. The lack of expandability however, is a clear limitation in iN. Finally, use of co-culture systems (e.g. neuron-glia, neuron-astrocytes), 3D organoids and prolonged culture time also contribute to improving the immature stage of iPSC-derived neurons. Indeed, a recent study showed that human cortical organoids reach postnatal stages between 250 and 300 days of culture²⁸⁵.

Neurodegenerative diseases such as Alzheimer's disease, PD, amyotrophic lateral sclerosis and Huntington's disease share some common pathogenic mechanisms including abnormal protein accumulation and distribution, reduced mitochondrial activity, accumulation of reactive oxygen species (ROS), enhanced inflammation by astrocytes/microglia, and impaired neuron-glia interactions²⁸⁶. The accumulation of protein deposits as intracellular inclusions and/or as extracellular aggregates in specific neuronal cell-types enriched in distinct regions of the brain is a major hallmark of neurodegenerative diseases, e.g. accumulation of neurofibrillary tangles (phosphorylated tau) and amyloid plaques (amyloid β peptide) in pyramidal neurons (Alzheimer's disease), accumulation of Lewy bodies (α -synuclein) in DA neurons (PD) or aggregated huntingtin in striatal neurons (Huntington's disease). hiPSCs-based disease models provide excellent opportunities to study disease-associated protein pathology in relevant human, otherwise non-accessible neuronal cell populations.

In PD, pharmacological- and especially genetic-based animal models have provided key insights into the molecular pathology underpinning disease. However, they also have substantial limitations, and above all limited translation of therapeutic approaches²²⁶. In recent years, many human iPSC-derived neuronal models have been established, in particular for monogenic PD^{44,90,292–299,94,190,234,287–291} (**Table 7**). These models have contributed enormously to unravelling the complex interplay of molecular disease mechanisms that drive dopaminergic

neurodegeneration and have also provided excellent platforms for drug screening and gene therapy approaches³⁰⁰.

Gene	Neuronal model	Cellular phenotype	Reference
SNCA	Dopaminergic cells	Increase in α synuclein protein levels Increase in oxidative stress Vulnerability to cell stressors	295-296
LRKK2	Dopaminergic cells	Increase in α -synuclein protein levels Increase in oxidative stress Vulnerability to cell stressors Mitochondrial dysfunction Defective autophagy Morphological abnormalities	90, 287-288, 297-299
GBA	Dopaminergic cells	Increase in α synuclein protein levels Mitochondrial dysfunction	44, 289
PINK1	Dopaminergic cells	Increase in oxidative stress Vulnerability to cell stressors Mitochondrial dysfunction	291-293
VPS35	Dopaminergic cells	Increase in GluR1 cluster intensity Decreased autophagic flux Increased accumulation of α -synuclein Mitochondrial dysfunction, increased membrane potential and impaired mitochondrial respiration	294
DNAJC6	Dopaminergic cells Midbrain-like organoids	Increase in α synuclein protein levels Mitochondrial and lysosomal dysfunction Neurodevelopmental defects	190
SLC6A3	Dopaminergic cells	Impairment of Dopamine transporter activity Apoptotic neurodegeneration associated with TNF α -mediation neuroinflammation Dopamine toxicity	94

Table 7. Selection of iPSC-derived neuronal disease models for monogenic PD. Genes associated with monogenetic forms of PD and their associated molecular dysfunction. Gene abbreviations: SNCA = synuclein Alpha, LRKK2 = leucine-rich repeat kinase 2, GBA = glucocerebrosidase, PINK1 = PTEN induced kinase 1, VPS35 = vacuolar protein sorting 35, DNAJC6 = DnaJ Heat Shock Protein Family (Hsp40) Member C6, SLC6A3 = Solute Carrier Family 6 Member 3 (Table adapted and modified from Bose et al. 2022³⁰⁰).

1. 4. Research Hypothesis and Aims

1. 4. 1. Background

Autosomal recessive *DNAJC6* mutations cause a progressive, early-onset movement disorder characterised by juvenile-onset parkinsonism-dystonia, while heterozygous *DNAJC6* mutations are associated with a later-manifesting early-onset PD^{61–64}. *DNAJC6*-related juvenile-parkinsonism is a complex movement disorder with additional neurological, neurodevelopmental and psychiatric features including neurodevelopmental delay, intellectual disability, seizures, behavioural abnormalities, anxiety and sleep disorders⁶⁵. Currently, there are no disease-modifying treatments available for *DNAJC6*-related parkinsonism-dystonia, and patients often respond poorly to common antiparkinsonian medications. DaTScan™ imaging in juvenile patients demonstrates degeneration of presynaptic dopaminergic terminals, while

cerebrospinal fluid (CSF) analysis can show low HVA and reduced levels of proteins associated with dopamine metabolism⁶⁵.

DNAJC6 encodes auxilin 1, a neural-specific protein that is involved in CME, an important cellular membrane trafficking process. Auxilin 1 drives the uncoating of CCVs in CME. In neurons, CME is vital for recycling of SV to sustain synaptic neurotransmission and has additional important roles in the regulation of developmental and synaptic signalling cascades. Auxilin KO mouse models and *Drosophila* knockdown models demonstrated impaired CME with abnormalities in SV recycling, dystrophic dopaminergic nerve terminals, dopamine dyshomeostasis and dopaminergic neurodegeneration. During the course of this PhD, a midbrain organoid *DNAJC6* model was published, providing important proof of concept for my proposed study. Human midbrain organoids showed mitochondrial and lysosomal defects as well as neurodevelopmental abnormalities. Patient-derived cell models are useful to study disease mechanisms in a humanised system with the patient's preserved genetic background and allows application of much-needed and clinically translatable therapeutic approaches.

1. 4. 2. Hypothesis

I hypothesise that mutations in *DNAJC6* lead to impaired function of auxilin and subsequent impairment of the uncoating process in CME. It is most likely that disturbance of CME affects a number of CME-associated processes including SV recycling at presynaptic terminals, but also developmental signalling cascades regulated by CME. DA neurons are highly sensitive to any form of cellular stress due to their high metabolic turnover and intrinsic pacemaker activity. Given the importance of CME for rapid SV recycling in pacemaker neurons, it is most likely that defects in CME will adversely affect DA neurons. Generation of patient-derived mDA neurons will allow me to study the underlying disease mechanisms in *DNAJC6*-parkinsonism. This dopaminergic neuronal cell model will also serve for a first proof-of-concept viral gene therapy approach and prepare the path for future clinical translation.

1. 4. 3. Research aims and methodology

The proposed workflow for this project is outlined in Figure 15. The aims of my PhD are as follows:

1. Comprehensive clinical characterisation of a *DNAJC6* patient cohort

- by participating in the endophenotyping of six patients diagnosed in our laboratory
- by undertaking a comprehensive review of all *DNAJC6* patients published to date

2. Cellular reprogramming of *DNAJC6* patient fibroblast lines and subsequent comprehensive characterisation

- by using Sendai-Virus-based reprogramming to generate induced pluripotent stem cells
- by using a range of different assays to confirm patient mutations, genomic integrity and pluripotent characteristics of generated iPSC lines

3. Development of an iPSC-derived 2D dopaminergic neuronal cell model and subsequent comprehensive characterisation

- by differentiating iPSC lines towards mDA neurons based on an established, modified protocol by Kirkeby et al.²³²
- by using qRT-PCR and immunocytochemistry methods to confirm early midbrain dopaminergic identity at day 11 of differentiation and mature midbrain dopaminergic identity at day 65 of differentiation.

4. Investigation of the effects of *DNAJC6* deficiency at a cellular and molecular level in the iPSC-derived dopaminergic neuronal cell model

- by using a range of different assays including:
 - Immunoblot analysis to assess auxilin protein levels
 - FM1-43 uptake assay and electron microscopy analysis to assess CME and synaptic vesicle homeostasis
 - Immunohistochemistry analysis to study neuronal maturity of generated mDA neurons
 - Bulk RNA seq analysis to investigate deregulated genes and associated pathways in mDA neurons

5. Development of a lentiviral gene therapy approach and analysis of its effects on specific cellular phenotypes

- by generating a *DNAJC6*-containing lentiviral vector and transfecting patient- and control-derived mDA neurons at day 24 of differentiation
- by evaluating correction of key cellular disease phenotypes in day 65 mDA using previously established assays

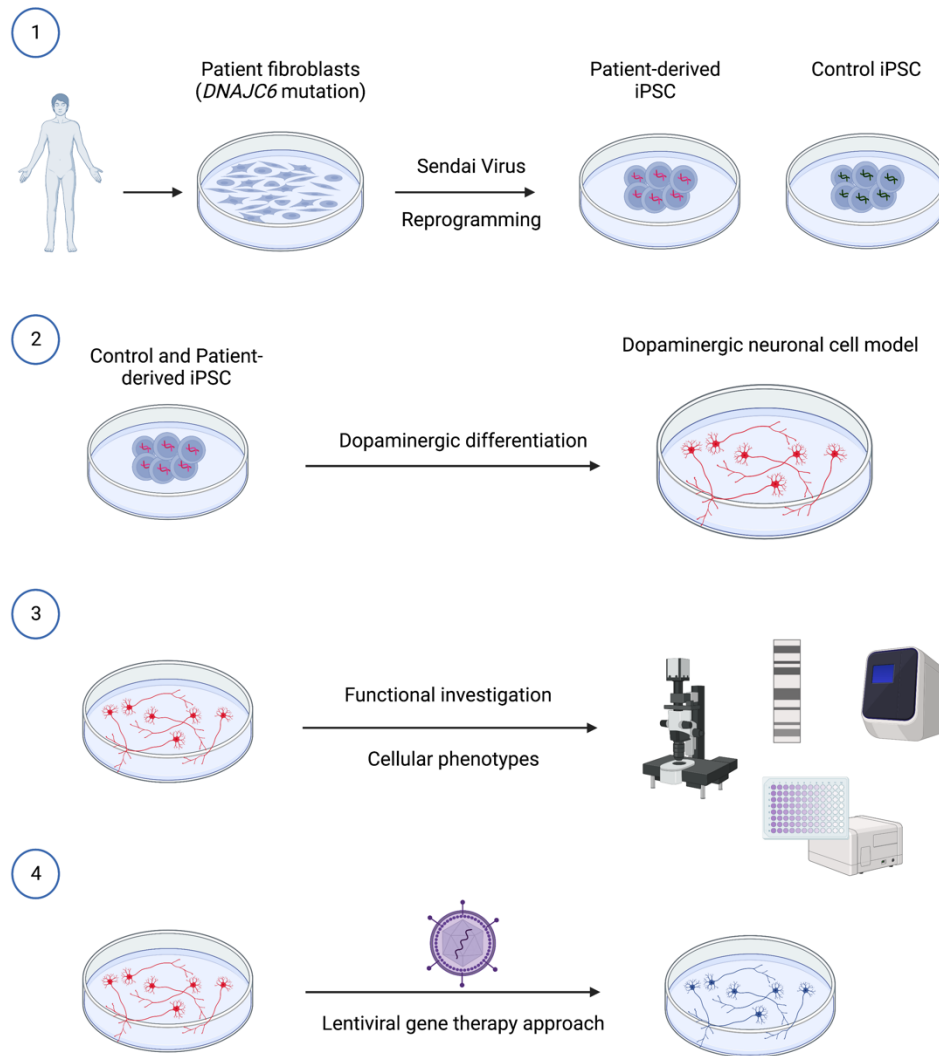


Figure 15. Schematic overview on the development of a patient-derived dopaminergic neuronal cell model to investigate disease mechanisms in DNAJC6-related parkinsonism-dystonia. 1) Patient fibroblasts will be reprogrammed to hiPSC. 2) Patient and age-matched healthy and isogenic control lines will be differentiated to midbrain dopaminergic neurons. 3) This dopaminergic neuronal cell model will be used for investigation of disease mechanisms. 4) A lentiviral gene-therapy approach will be applied to correct cellular disease phenotypes.

CHAPTER 2

Materials and methods

2. 1. Introduction

In the following chapter, I will describe the methods employed in this PhD. Some sections have been adapted from publications arising from this research, including Ng J*, Cortès-Saladelafont E*, Abela L* et al, 2020⁶⁵ and Abela L et al, 2024³⁰¹.

2. 2. *DNAJC6* patient cohort characterisation

2. 2. 1. Patient cohort recruitment for study

At the GOS-Institute of Child Health, Prof. Kurian established a research cohort of 232 children with undiagnosed movement disorders between 2012 and 2018. These patients were recruited for research from Prof Kurian's Movement Disorder Neurogenetic Clinic at Great Ormond Street Hospital and also through international referrals. From this cohort, we identified 25 children with juvenile parkinsonism based on the following study inclusion criteria: 1) onset of bradykinesia <21 years of age, 2) at least one of the following signs: resting tremor, rigidity, postural instability. All patients underwent detailed clinical examination by Prof. Kurian or, if based outside of the UK, another paediatric movement disorder specialist. A detailed study of patient clinical history, molecular genetic features and neuroimaging findings was carried out by me in collaboration with Dr. Joanne Ng and Dr. Elisenda Cortès-Saladelafont. Written informed consent was obtained from all participating families, and the study was approved by the local ethics committees (reference 13/LO/0168).

2. 2. 2. Molecular genetic investigations

2. 2. 2. 1. Autozygosity mapping and whole-exome sequencing

From the subgroup of children presenting with juvenile parkinsonism, we focused on two consanguineous families whose affected children presented with a strikingly similar phenotype. Both families originated from the same region in Pakistan: Family A had three affected children (A:III-1, A:III-4 and A:III-5) and Family B two affected children (B:IV-2, B:IV-4), respectively. In order to find recessively inherited disease genes, we first performed autozygosity mapping studies, followed by whole-exome sequencing (WES). SNP genotyping analysis was performed as described previously by Dr. Esther Meyer and Dr. Elisenda Cortès-Saladelafont³⁰². WES was undertaken for two children (A:III-1 and B:IV-2) by UCL Genomics with following parameters: average WES coverage as previously reported³⁰³; average *DNAJC6* coverage of 30X; and minimum coverage of 10X for 82% of the genes.

2. 2. 2. 2. Sanger sequencing

In order to verify variants identified on WES and confirm familial segregation, we performed Sanger sequencing (Dr. Esther Meyer and Dr. Elisenda Cortès- Saladelafont). Primers were designed based on the genomic *DNAJC6* sequence (Ensembl transcript ENST00000371069; NCBI reference sequence NM_001256864) using Primer3 software (<http://bioinfo.ut.ee/primer3/>). PCR conditions were as follows: initiation 95°C for 5min, 40 cycles (denaturation 95°C for 45 s, annealing 60°C for 1 min, elongation 72°C for 1min), 72°C for 5 min. PCR products were purified with MicroCLEAN (Web Scientific) and processed for sequencing using the Big Dye Terminator v1.1 Cycle Sequencing Kit (Thermo Fisher Scientific). Sequencing was carried out on an ABI PRISM 3730 DNA Analyzer (Applied Biosystems Inc.) and results were analysed with Chromas (<http://technelysium.com.au/wp/chromas/>).

2. 2. 3. Cerebrospinal fluid neurotransmitter analysis

In the context of routine diagnostic lumbar puncture (LP) for CSF neurotransmitter analysis within the clinical setting, CSF samples were collected, snap frozen in liquid nitrogen and stored at -80°C using standardised protocols³⁰⁴. Analysis of samples was performed at the National Neurometabolic Laboratory (Queen Square) using high pressure liquid chromatography with electrochemical detection (HPLC) and reversed phase column³⁰⁴. Seven anonymised control paediatric CSF samples with normal neurotransmitter profiles and no signs of movement disorders or intake of medications were provided by the Neurometabolic Laboratory (National Hospital for Neurology and Neurosurgery, Queen Square, London). Processing of samples and storage was performed in accordance with the UK Royal College of Pathologists guidelines.

2. 2. 4. Patient fibroblast immunoblotting

Fibroblast protein isolation and immunoblotting was performed by Dr. Joanne Ng as previously described³⁰³. The following primary antibodies were used: Auxilin and GAK (gift from Professor Green, National Institutes of Health, Washington, USA) and GAPDH horseradish peroxidase (HRP)-conjugate (Cell signalling).

2. 2. 5. Patient CSF immunoblotting

CSF samples were available from Patient A-III:1, A-III:4 and B-IV:4 as well as two age-matched controls. CSF protein isolation and immunoblotting was undertaken by Dr. Joanne Ng as previously reported³⁰⁵. The following antibodies were used: Auxilin (gift from Professor Green, National Institutes of Health, Washington, USA), GAK (gift from Professor Green,

National Institutes of Health, Washington, USA), tyrosine hydroxylase (Millipore, AB152), dopamine transporter (Millipore, AB1766), dopamine receptor 2 (Millipore, AB5084P), vesicular monoamine transporter 2 (Santa Cruz, sc- 7721) and transferrin (Santa Cruz, sc- 365871) as a loading control.

Image J software was used to assess relative protein quantification and protein levels were normalised to the loading control. For each protein, the mean % optical densitometry of three replicates was analysed with standard error mean (SEM). Prism 8 software was used for statistical analysis and data was tested for Gaussian distribution prior to analysis. Data were compared by student t-test.

2. 3. Fibroblast culture

Human dermal fibroblasts (HDF) of Patient A-III:1 and Patient B-IV:4 were collected for metabolic investigations prior to this study and stored at the Department of Biochemistry, University of Oxford (NHS service) (Patient A-III:1) and Willink Metabolic Unit, Manchester Centre for Genomics Medicine (NHS service) (Patient B-IV:4), respectively. After obtaining written consent (Reference 13/LO/0168 and Reference 13/LO/0171), a vial was transferred to the Enzyme Unit, Chemical Pathology, Camelia Botnar's laboratories, Great Ormond Street Hospital, London, for further expansion and stored at -80°C. HDF from Patient C and Patient II-4 were obtained in collaboration with Dr Toni Pearson (Washington University School of Medicine, St. Louis, USA) and Dr Simon Edvardson (Hadassah University Hospital, Jerusalem, Israel), respectively. Written informed consent was obtained from Patient A-III:1 and Patient B-IV:4 (Reference 13/LO/0168), consent for Patient C & Patient II-4 is covered by their local ethics committees. Fibroblasts were maintained in DMEM Medium [Gibco] supplemented with 10% FCS [Dunn School], 1% Penicillin/Streptomycin (P/S) [10'000 U/ml] in T25 cm² flasks.

2. 4. Generation and maintenance of hiPSC lines

2. 4. 1. Reprogramming human dermal fibroblasts using CytoTune Kit

hiPSCs were generated according to an adapted protocol from the CytoTune-iPS 2.0 Sendai Reprogramming Kit (Invitrogen). HDF were thawed and maintained in T25 cm² flasks for 5 days in the above-mentioned medium with media change every second day. Two days prior to infection, HDF were washed with PBS, collected with 0.05% Trypsin/EDTA 1x (Gibco), counted and plated in a 12-well plate with densities of 0.75x10⁵, 1x10⁵, 1.25x10⁵, 1.5x10⁵ and 2.0x10⁵ per well. On the day of infection (Day 0),

the wells reaching 90% confluency were selected and infected with the Sendai virus at a Multiplicity of Infection (MOI) of 3. Infected HDF were incubated with the virus supernatant overnight and medium was changed on day 1 (24 hours post-infection), day 3 and day 5. At day 5, 3 x 6-well plates were coated with gelatin (0.1%, Sigma) for 1h at 37°C and subsequently used for plating of irradiated mouse embryonic fibroblasts (MEF) at a density of 500,000 cells/well in MEF medium. For the preparation of conditioning medium, MEF cells were plated in 3 x T75 cm² flasks at a density of 4 million cells/flask and cultured for 7 days in KOSR medium (KnockOut DMEM [Gibco], 20% KnockOut Serum Replacement [Gibco], 1% L-Glutamine [Invitrogen, 200 mM], 1% P/S, 1% Non-essential Amino Acids [Sigma, 100x], 0.1% β -Mercaptoethanol [Invitrogen, 50mM], 10 ng/ μ l FGF2 [Miltenyi Biotech, 100 μ g/ μ l]). Conditioning medium (15ml per flask) was collected every day, sterile-filtered and stored at -80°C. At day 6, infected HDF were washed with PBS, collected with 0.05% Trypsin/EDTA 1x and counted. Subsequently, they were plated onto the MEF plates prepared at day 5 in a density of 8,000 cells/well for 2 plates and 16,000 cells/well for the third plate, respectively. A control plate without MEF coating was prepared with infected HDF as well. On day 7, MEF medium was replaced with KOSR conditioning medium. 1ml of KOSR medium was exchanged every other day, and, when iPSC colonies started to emerge around day 20, subsequently changed every day.

2. 4. 2. iPSC culture

Around 30-35 days post-infection, colonies were inspected for typical iPSC morphology and picked manually. Around 10-12 colonies were picked per patient and transferred to a well of a 6-well plate previously plated with MEF cells at a density of 500,000 cells/well. Individual clones were fed with KOSR medium on a daily basis and passaged with ReLeSR when reaching about 80% confluency. At passage 6, 3 clones from each patient were frozen, while another 3 clones were further expanded and transferred to Matrigel-coated plates once stable (around passage 10-11). iPSC lines were cultured in mTeSR complete medium (StemCell Technologies) supplemented with 1% P/S.

2. 4. 3. Generation of CRISPR-Cas9-corrected iPSC line

Generation of a CRISPR-Cas9-corrected iPSC line for Patient 2-1 was carried out by Applied StemCell Inc. In brief, two single guide RNAs (sgRNA) were designed to target the *DNAJC6* genomic locus and tested in HEK293 cells for Cas9-mediated cleavage efficiency. Cas9 endonuclease induces a double strand break. Patient 2-1 iPSCs were subsequently co-transfected (Neon transfection system, Invitrogen) with sgRNAs and a single-stranded oligo

donor for endogenous homology repair. Single cells were culture in 96-well plates for 14 days and subsequently transferred to 24-well plates for further expansion. Genomic DNA was extracted from each clone and the targeted sequence PCR-amplified. PCR products were sequenced to confirm bi-allelic correction of the homozygous *DNAJC6* mutation.

2. 5. Characterisation of patient-derived iPSC

2. 5. 1. Assessment of genomic integrity of iPSC lines

Genomic DNA was extracted from iPSC pellets following manufacturer's instructions from the DNeasy Blood & Tissue kit (QIAGEN). Genomic integrity was analysed with the Illumina Human CytoSNP-12v2.1 beadchip array. Raw data was analysed with BlueFuse multi software (Illumina) using the following algorithm settings: Minimum Del Size – backbone (Kb) = 5000, Minimum Dup Size – backbone (Kb) = 5000, Minimum LOH Region Size (Mb) = 3.0, Sex Mismatched Calling = no, CGH Region = 10, LOH Region = 200.

2. 5. 2. Confirmation of patient mutations in HDF and iPSC lines

Sanger sequencing was performed by Dr. Katy Barwick (Genetics Research Assistant in the Kurian lab) to confirm patient mutations in the corresponding iPSC lines. gDNA was extracted using the DNeasy Blood & Tissue kit (QIAGEN). PCR reaction was prepared with 2 µl of sample gDNA, 0.8 µl of specific primer mix (0.4 µl F + 0.4ul R), 10 µl Taq DNA polymerase BioMix Red (Bioline), and 7.2 µl of nuclease-free water in a total volume of 20 µl. PCR conditions were as following: initiation 95°C for 5min, 40 cycles (denaturation 95°C for 45 s, annealing 60°C for 1 min, elongation 72°C for 1min), 72°C for 5 min. Primer sequences are listed in **Table 2. 1**. PCR products were checked on a 1.5% agarose gel and subsequently purified with MicroCLEAN Kit (Clent Life Science) and processed for sequencing with the BigDye Terminator v1.1 Cycle Sequencing Kit (Thermo Fisher Scientific). Sequencing reactions were run on the ABI PRISM 3730 DNA Analyzer (Applied Biosystems) and results were analysed with Sequencher and Chromas software.

Patient line / Mutation	Primer Sequence (5'-3')	Melting Temperature
Patient 1 & 2 c.766C>T (DNAJC6 Exon 6)	F: CAATGGAGAATGGCTGATTTGAT R: TACATCTGTGCCTAGCCTGC	65.9 63
Patient 3 c.2416C>T (DNAJC6 Exon 16)	F: ACACAAGAGTTAGAGGCCACT R: TCAGAGAGACACATTTCAGGCA	59.5 63.7
Patient 4 c.801-2A>G (DNAJC6 Exon 7)	F: ATACTTATCACTGGTGATCCTCCT R: TCACCGTCTACCTAGTTGCTC	60.7 60.9

Table 2. 1. Forward (F) and Reverse (R) primers for confirmation of corresponding DNAJC6 mutations by Sanger Sequencing in Patient iPSC lines.

2. 5. 3. RNA purification and cDNA production

RNA was purified using the DNase Kit (Invitrogen) to eliminate double stranded DNA. The reaction volume contained 1 µg of RNA sample, 1 µl of DNase I Reaction Buffer, 1 µl of DNase I and nuclease-free water to a total of 10 µl. The reaction was carried out at RT for 15min. 1 µl of EDTA was added to inactivate DNase I and the mix incubated at 65°C for another 10 min. Purified RNA was then used for cDNA production using the SuperScript III Reverse Transcriptase (Invitrogen). 1 µl of RNA was mixed with 1 µl of oligo (dT) primers (Thermo Fisher Scientific), 1µl dNTP mix (Thermo Fisher Scientific), and 1 µl nuclease-free water in a total volume of 10ul. Reverse transcription was carried out on a PCR machine at 65°C for 5min. The PCR plate was then placed on ice for more than 1min. Subsequently, 4 µl 5x first strand buffer, 1 µl DTT (0.1 M), 1 µl SuperScript III RT, and 1 µl of nuclease-free water was added. The mixture was run on a PCR machine for 60min at 50°C, followed by 15min at 70°C. cDNA was finally diluted 1:25 with nuclease-free water.

2. 5. 4. Sendai Virus clearance

Sendai Virus clearance was performed to confirm elimination of the four Yamanaka factors (*OCT4*, *KLF4*, *C-MYC* and *SOX2*) in the corresponding iPSC lines (**Table 2. 2**). The PCR was carried out according to instructions from the CytoTune-iPS Sendai Reprogramming Kit. The PCR mixture was prepared with 10 µl cDNA and 10 µl AccuPrime SuperMix (Thermo Fisher Scientific) and the reaction was carried out on a PCR machine with the following conditions: initiation 95°C for 5min, 35 cycles (denaturation 95°C for 30 s, annealing 55°C for 30 s, elongation 72°C for 30 s), 72°C for 5 min. PCR products were loaded on 2% agarose gel using SeV genome as a positive control and an embryonic cell line (H9) as negative control.

Primer name	Primer Sequence (5'-3')	PCR Product size (bp)
Sev Genome F SeV Genome R	GGATCACTAGGTGATATCGAGC ACCAGACAAGAGTTTAAGAGATATGTA TC	181
Sev OCT4 F SeV OCT4 R	CCCGAAAGAGAAAGCGAACCAG AATGTATCGAAGGTGCTCAA	483
Sev SOX2 F SeV SOX2 R	ATGCACCGCTACGACGTGAGCGC AATGTATCGAAGGTGCTCAA	451
Sev c-MYC F SeV c-MYC R	TAACTGACTAGCAGGCTTGTCG TCCACATACAGTCCTGGATGATGATG	532
Sev KLF4 F SeV KLF4 R	TTCCTGCATGCCAGAGGAGCCC AATGTATCGAAGGTGCTCAA	410
Sev KOS2 F SeV KOS2 R	ATGCACCGCTACGACGTGAGCGC AATGTATCGAAGGTGCTCAA	451
GAPDH F GAPDH R	ATCCCATCACCATCTTCCAG CCATCACGCCACAGTTTCC	382

Table 2. 2. Forward (F) and Reverse (R) primers for Sendai Virus Clearance PCR.

2. 5. 5. PluriTest

Genomic DNA was extracted from iPSC pellets using the DNeasy Blood & Tissue kit (QIAGEN). The Epi-Pluri-Score analysis was performed by Cygenia, Epigenetic Diagnostics, Aachen, Germany. The epigenetic pluripotency marker is based on the combination of DNA methylation levels at three specific CpG sites located within two genes: *ANKRD46* (methylated in pluripotent cells) and *C14orf115* (non-methylated in pluripotent cells).

2. 5. 6. PCR analysis of pluripotency markers

A PCR analysis was performed to confirm upregulation of the following pluripotency marker genes: *REX1*, *ESG1*, *SOX2*, *NANOG*, *OCT4* and the house-keeping gene *GAPDH* (Table 2. 3). For the PCR reaction 2 µl of sample cDNA, 0.8 µl of primer mix (0.4 µl F + 0.4 µl R), 10 µl of Taq DNA polymerase BioMix Red (Bioline), and 7.2 µl of nuclease- free water was mixed in a total volume of 20 µl. PCR conditions were adjusted for the genes as follows: *REX1*, *ESG1*, *SOX2*, *NANOG* and *GAPDH* required initiation 95°C for 5min, 35 cycles (denaturation 95°C for 30 s, annealing 60°C for 45 s, elongation 72°C for 1 min), 72°C for 5 min. *OCT4* required initiation 95°C for 5min, 35 cycles (denaturation 95°C for 30 s, annealing 58°C for 45 s, elongation 72°C for 1 min), 72°C for 5 min. PCR products were separated on a 1.5% agarose gel (*REX1*, *ESG1*, *NANOG* and *GAPDH*) and 2% agarose gel (*SOX2*), respectively, with the

GeneRuler 100bp DNA Ladder (Thermo Scientific). PCR bands were visualised using the Bio-Rad Gel Doc Imager and analysed with Image Lab software (Bio-Rad).

Primer name	Primer Sequence (5'-3')	PCR Product size (bp)
REX1 F REX1 R	CAGATCCTAACAGCTCGCAGAAT GCGTACGCAAATTAAGTCCAGA	305
ESG1 F ESG1 R	ATATCCCGCCGTGGGTGAAAGTTC ACTCAGCCATGGACTGGAGCATCC	243
SOX2 F SOX2 R	GGGAAATGGGAGGGGTGCAAAAGAGG TTGCGTGAGTGTGGATGGGATTGGTG	151
NANOG F NANOG R	CAGCCCCGATTCTTCCAGTCCC CGGAAGATTCCCAGTCGGGTTCACC	343
OCT4 F OCT4 R	CGAAACCCACACTGCAGCAG CCTGGCACAACTCCAGGTTT	402
GAPDH F GAPDH R	ATCCCATCACCATCTTCCAG CCATCACGCCACAGTTTCC	382

Table 2. 3. Forward (F) and Reverse (R) primers for Pluripotency PCR.

2. 5. 7. Immunocytochemistry for pluripotency markers

Cells were washed 3x with PBS (Invitrogen), fixed with 4% paraformaldehyde (PFA) for 10 minutes at RT and blocked in blocking solution (PBS, 10% FBS, 0.1% Triton-X100 [Sigma]) for 30 min and subsequently incubated with primary antibodies overnight at 4°C. Blocking buffer for immunostaining contained Triton-X100 except for the cell surface markers TRA-1-60 and TRA-1-81. Primary antibodies for pluripotency markers were used in following dilutions: OCT4 (1:50, Santa Cruz), NANOG (1:500, Millipore), TRA-1-60 (1:200, Santa Cruz), TRA-1-81 (1:200, Millipore). The next day, cells were washed 3x with PBS and incubated with secondary antibodies in blocking solution in the dark at RT for 45min. Secondary antibodies were used in following dilutions: Alexa Fluor® 594 Goat Anti-mouse IgG (1:400; Alexa Fluor, Life Technologies), Alexa Fluor® 488 Goat Anti-mouse IgG (1:400, Alexa Fluor, Life Technologies). DAPI was used in a concentration of 1:1,000 for nuclear staining. Imaging was performed on the Olympus IX71 inverted TC scope for assessment of pluripotency

2. 5. 8. Spontaneous *in vitro* differentiation assay

For Patient 1 and 2 iPSCs lines, two 6-wells were harvested with TripleE and resuspended in KOSR medium with Thiazovivin (Cambridge Biosciences) in a nonadherent bacterial dish (6

cm²) to grow EBs. Media was changed on day 2. On day 4, EBs were transferred on plates previously coated with gelatin 0.1% (Sigma-Aldrich) for mesoderm differentiation or Matrigel for ectoderm and endoderm differentiation. Differentiations were cultured for 16 days with media change every other day. The gelatin-coated wells were fed with DMEM medium supplemented with 20% FCS, while the Matrigel-coated wells were fed with KOSR medium. For Patient 3 and 4 spontaneous *in vitro* differentiation was performed according to manufacturer instructions from the STEMdiff™ Trilineage Differentiation Kit (StemCell Technologies). Imaging was performed on the Olympus IX71 inverted TC scope

2. 6. Midbrain dopaminergic differentiation of control and *DNACJ6* patient lines

2. 6. 1. mDA neuron differentiation protocol

Patient and control iPSC lines were differentiated towards mDA neurons according to a published protocol²³² with minor modifications.

On day 0, iPSC cells were harvested from 4 confluent wells of a 6-well plate with TrypLE™ (Invitrogen) and plated on 10 cm non-adherent bacterial dishes in Embryonic Body medium (EB medium containing DMEM/F12:Neurobasal (1:1) [Thermo Fisher Scientific] enriched with N2 supplement 100x [1:100, Thermo Fisher Scientific], B27 minus vitamin A supplement 50X [1:50, Thermo Fisher Scientific], 1 % L-Glutamine [200 mM, Invitrogen], 1 % P/S, Rock inhibitor Y27632 from day 0 to day 2 [0.5 µM, Cambridge Bioscience], SB431542 [10 µM, Cambridge Bioscience], LDN193187 [100 nM, Sigma], CHIR99021 [0.9 µM, Tocris Bioscience], Recombinant modified human Sonic Hedgehog C24II (SHH) [200 ng/ml, R&D Systems], Purmorphamine (from day 2) [0.5 µM, Cambridge Bioscience]). Cells were cultured over 4 days to allow EB formation with a medium change at day 2. Concomitantly, 6 wells of a 12-well plate were coated with Poly-L-ornithine (PO) (15 µg/ml, Sigma) for 2 days, washed with PBS, then coated for another 2 days with Fibronectin (FN) (5 µg/ml, Invitrogen) and Laminin (LN) (5 µg/ml, Sigma).

On day 4 of differentiation, EBs were collected and plated on previously coated 12 well plates in Neural Differentiation Medium (ND medium containing DMEM/F12:Neurobasal (1:1) [Thermo Fisher Scientific] enriched with N2 supplement 100 X [1:200, Thermo Fisher Scientific], B27 minus vitamin A supplement 50X [1:100, Thermo Fisher Scientific], 1 % L-Glutamine [200 mM, Invitrogen], 1 % P/S, SB431542 (day 0 to day 6) [10 µM, Cambridge

Bioscience] and LDN193187 (day 0 to day 9) [100 nM, Sigma], CHIR99021 (day 0 to day 9) [0.9 μ M, Tocris Bioscience], recombinant modified human Sonic Hedgehog C24II (SHH) (day 0 to day 9), [200 ng/ml, R&D Systems] and Purmorphamine (day 0 to day 9) [0.5 μ M, Cambridge Bioscience]). Medium was changed every other day until day 11. Concomitantly, 6 wells of a 12-well plated were again coated with PO, FN and LN.

On day 11, cells were harvested with AccumaxTM (Sigma) and plated in droplets ($1-1.5 \times 10^4$ cells) onto pre-coated 12-well plates in Final Differentiation medium (FD medium containing Neurobasal [Thermo Fisher Scientific] enriched with N2 supplement 100 X [1:200, Thermo Fisher Scientific], B27 minus Vitamin A supplement 50X [1:100, Thermo Fisher Scientific], 1 % L- Glutamine [200 mM, Invitrogen], 1 % P/S, Ascorbic Acid (0.2 mM, Sigma), BDNF (20 ng/ml, Miltenyi Biotech). Drop plating was carried out as following: cells were incubated with AccumaxTM at 37°C for 5 min, harvested and centrifuged at 300g for 5min. The pellet was re-suspended in some FD medium and 100 μ l of the cell solution was plated in a single droplet in the middle of a well. Droplets were incubated for 1h and medium was added thereafter. Cells were fed every other day. On day 14, the FD medium was supplemented (FDf medium) with GDNF (20 ng/ml, Miltenyi Biotec) and N6,2'-O-Dibutyryl adenosine 3',5'-cycle monophosphate sodium salt [db-cAMP (0.5 mM, Sigma)].

On day 30, cells were incubated with AccumaxTM at 37°C for 30min, collected and drop-plated on PO/FN/LN coated plates and/or Lab-TekTM II chamber slides. FDf medium was supplemented (FDf+D medium) with γ -secretase inhibitor DAPT (2.5 μ M, Tocris Bioscience) until collection at day 65.

2. 6. 2. Day 11 immunocytochemistry for midbrain progenitor markers

At day 11 of differentiation, cells were washed 3x with PBS and fixed in 4 % PFA at RT for 10 min. Subsequently, cells were blocked in blocking solution (PBS, 10 % FBS, 0.1 % Triton X-100 [Sigma]) at RT for 1 h and incubated with primary antibodies overnight at 4°C. Primary antibodies were used as following: FOXA2 (1:500; BD PharmingenTM), LMX1A (1:2000; Millipore) (**Table 2. 5**). The next day, cells were washed 3x with PBS and incubated with secondary antibodies in blocking solution in the dark at RT for 45min. Secondary antibodies were used in following dilutions: Alexa Fluor® 594 Goat Anti-mouse IgG (1:400; Alexa Fluor, Life Technologies), Alexa Fluor® 488 Goat Anti-mouse IgG (1:400, Alexa Fluor, Life Technologies). DAPI was used in a concentration of 1:1,000 for nuclear staining. Images were

acquired on the Olympus IX71 inverted TC scope. Images were processed using ImageJ software (National Institutes of Health).

2. 6. 3. Real-Time Quantitative Reverse Transcription Polymerase Chain Reaction (qRT-PCR) at day 11 and day 65 of differentiation

RNA was extracted and cDNA produced as previously described. cDNA samples were then diluted 1:1 with nuclease-free water. A master mix was prepared with 10 µl of MESA BLUE qPCR 2X MasterMix Plus for SYBR® Assay (Eurogentec) and 1 µl of the respective primer mix (forward and reverse) (**Table 2. 4**). 9 µl of diluted cDNA was mixed with 11 µl of MESA BLUE qPCR 2X MasterMix Plus in a PCR plate and centrifuged at 2000 rpm for 2min. Each target gene was plotted in triplicates for each sample. GAPDH was used as housekeeping gene for normalisation. qRT-PCR was carried out on the StepOnePlus™ Real-Time PCR System (Applied Biosystems) with the following protocol: initiation at 95°C for 5 min, 40 cycles (denaturation 95°C for 15 s, annealing/elongation at 60°C for 1 min, elongation 72°C). Gene expression was analysed using the $\Delta\Delta C_T$ method. As a control for normalisation an iPSC line was used.

$$\Delta C_T = M_T \text{ target} - M_T \text{ GAPDH}$$

$$\Delta\Delta C_T = \Delta C_T \text{ sample} - \Delta C_T \text{ control}$$

$$\text{Fold change (FC)} = 2^{-(\Delta\Delta C_T)}$$

Primer Name	Forward sequence	Reverse sequence
AADC	TGCGAGCAGAGAGGGAGTAG	TGAGTTCCATGAAGGCAGGATC
EN1	CGTGGCTTACTCCCCATTTA	TCTCGCTGTCTCTCCCTCTC
EN2	CCTCCTGCTCCTCCTTTCTT	GACGCAGACGATGTATGCAC
DAT	TCACCAACGGTGGCATCTAC	CACTCCGATGGCTTCGATGA
FOXA2	CCGTTCTCCATCAACAACCT	GGGGTAGTGCATCACCTGTT
GAPDH	TTGAGGTCAATGAAGGGGTC	GAAGGTGAAGGTCGGAGTCA
LMX1A	CGCATCGTTTCTTCTCCTCT	CAGACAGACTTGGGGCTCAC
LMX1B	CTTAACCAGCCTCAGCGACT	TCAGGAGGCGAAGTAGGAAC
NANOG	TTGGGACTGGTGGAAGAATC	GATTTGTGGGCCTGAAGAAA
NURR1	TCGACATTTCTGCCTTCTCCTG	GGTTCCTTGAGCCCGTGTCT
OCT4	TCTCCAGGTTGCCTCTCACT	GTGGAGGAAGCTGACAACAA
PITX3	GAGCTAGAGGCGACCTTCC	CCGGTTCCTGAACCACACCC
SNCA	GGAGTGGCCATTCGACGAC	CCTGCTGCTTCTGCCACAC
TH	CGGGCTTCTCGGACCAGGTGTA	CTCCTCGGCGGTGTACTCCACA

Table 2. 4. Forward and Reverse (R) primers for qRT-PCR at day 11 and day 65.

2. 6. 4. Day 65 immunocytochemistry for mature midbrain markers

Day 65 mDA neurons were fixed in 4 % paraformaldehyde for 10 min at RT, blocked in blocking solution (PBS, 10 % FBS, 0.3 % Triton X-100 [Sigma]) at RT for 1 h and subsequently incubated with primary antibodies overnight at 4°C (**Table 2. 5**). The next day, cells were washed 3x in PBS and incubated with secondary antibodies at RT for 45 min. Secondary antibodies were used in following dilutions: Alexa Fluor® 594 Goat Anti-chicken IgG (1:400; Alexa Fluor, Life Technologies), Alexa Fluor® 488 Goat Anti-mouse IgG (1:400; Alexa Fluor, Life Technologies), Alexa Fluor® 488 Goat Anti-rabbit IgG (1:400; Alexa Fluor, Life Technologies), Alexa Fluor® 594 Goat Anti- rabbit IgG (1:400; Alexa Fluor, Life Technologies), Alexa Fluor® 594 Goat Anti-mouse IgG (1:400; Alexa Fluor, Life Technologies), Alexa Fluor® 633 Goat Anti-mouse IgG (1:400; Alexa Fluor, Life Technologies). DAPI was used in a concentration of 1:1000 for nuclear staining. Slides were mounted with ProLong Gold Antifade Mountant (Invitrogen). Images were acquired on the LSM710 Zeiss confocal microscope.

Name	Use, concentration	Source, catalogue number
beta-actin	IB 1:5000	Sigma-Aldrich, A1978
Auxilin	IB 1:3000	Gift Prof. Lois E. Greene
AP-2	IB 1:2000	BD Transduction, 610501
Clathrin HC	IB 1:200	Santa Cruz Biotechnology, sc-12734
CCASP3	ICC 1:400	Cell Signaling, 9661S
FOXA2	ICC 1:500	BD Pharmingen, 561580
LMX1A	ICC 1:500	Millipore, AB10533
MAP2	ICC 1:400	Sigma-Aldrich, M9942
NeuN	ICC 1:100	Millipore, MAB377
TH	ICC 1:400	Aves Labs, TYH

Table 2. 5. List of antibodies used for immunocytochemistry (ICC) and immunoblotting (IB).

2. 7. Immunoblotting

2. 7. 1. Protein extraction and determination of concentration

Cells were lysed and the pellets resuspended in 200 µl RIPA lysis and extraction buffer (Thermo Fisher Scientific) containing 1x Protease and Phosphatase Inhibitor cocktail (Thermo Fisher Scientific) for 30 min at 4°C, vortexed for 1min and incubated on ice for 30min. Following centrifugation at 13.000 rpm for 15min, the supernatant was collected and protein concentration

determined using the PierceTM BCA Protein Assay Kit (Thermo Fisher Scientific) according to the manufacturer's recommendations. Protein absorbance was measured at 562nm on a Spectramax i3x Microplate reader (VWR).

2. 7. 2. Immunoblotting

10 µg (auxilin, AP-2), respectively 20 µg (clathrin) of protein lysates were vortexed, spun down and denatured at 95°C for 5 min in 100 mM dithiothreitol (DTT) and 1x Laemmli buffer (Bio-Rad). Protein samples mixtures were loaded on a 4-20% Mini-PROTEAN® TGXTM Stain free Protein Gel (Bio-Rad) and separated at 300 V and 400 mA for 15 min in 1x Tris/Glycine/SDS buffer (Bio-Rad) Running buffer on a Mini-PROTEAN Tetra Vertical Electrophoresis Cell for Mini Precast Gels apparatus (Bio-Rad). Proteins were then transferred onto a Trans-Blot TurboTM Mini PVDF Transfer membrane (Bio-Rad) using a Trans-Blot TurboTM Transfer System (Bio-Rad). Membranes were blocked in 5 % milk in Tris Buffered Saline (TBS, Sigma) with 0.1 % Tween 20 (Sigma) for 1 h at RT and subsequently incubated with primary antibodies (**Table 2. 5**) in 1 % milk in TBS – 0.1 % Tween 20 overnight at 4°C with constant gentle shaking. The following day, membranes were washed and incubated with appropriate horseradish peroxidase-conjugated antibody secondary antibody (HRP-conjugated Anti-Rabbit IgG and Anti-Mouse IgG, Cell Signaling) in 1 % milk in TBS – 0.1 % Tween 20 for 1 h at RT. Membranes were visualised with ChemiDocTM MP (Bio-Rad), using Clarity Western ECL Substrate (Bio-Rad). ImageJ software (National Institutes of Health [NIH]) was used for protein quantification, and normalisation performed against a housekeeping gene, typically β-actin.

2. 8. FMTM1-43 dye uptake assay

At day 30 of differentiation, mDA neurons were plated on Labteck slides (NuncTM). At day 70 of differentiation mDA neurons were incubated with HBSS medium (Thermo Fisher Scientific) supplemented with 2 mM Ca²⁺ and 2 mM Mg²⁺ for 10 minutes at 37°C. Subsequently, mDA neurons were stimulated with HBSS medium (Thermo Fisher Scientific) supplemented with 2 mM Ca²⁺, 2 mM Mg²⁺, 5 µg/ml FMTM1-43x (Thermo Fisher Scientific), 10 µM NBQX (Tocris Biosciences) and 60 mM KCL for 2 min at 37°C. NBQX, a specific inhibitor of AMPA and KA ionotropic glutamate receptors, was used to block recurrent activity. The cells were then incubated with HBSS medium (Thermo Fisher Scientific) supplemented with 2 mM Ca²⁺, 2 mM Mg²⁺ and FMTM1-43x 5 µg/ml for 15 min at 37°C to allow complete endocytosis. Afterwards, mDA neurons were carefully washed with HBSS without Ca²⁺ and Mg²⁺ (Thermo Fisher Scientific) and fixed at RT for 10 min with 4% PFA diluted in HBSS medium without

Ca²⁺ and Mg²⁺. Fixed neuronal cultures were imaged using the confocal microscope Zeiss LSM710 and processed using ImageJ software (NIH). Mean fluorescence intensity of synaptic boutons was quantified as an average from 15 randomly selected regions of interest (ROI) in four images from three independent biological experiments.

2. 9. Electron microscopy analysis

At day 30 of differentiation, mDA neurons were plated on glass cover slips. At day 65-70 of differentiation, mDA neurons were prefixed with 2% PFA and 1.5% glutaraldehyde in 0.1 M phosphate buffer pH 7.3. Subsequently, samples were postfixated in 1% OsO₄, 1.5% K₄Fe(CN)₆, and 0.1M sodium cacodylate, dehydrated, and flat embedded in Araldite resin (Araldite CY212, Agar Scientific) at the UCL Biosciences Electron microscopy core facility. Ultrathin sections (70 nm) were collected on copper mesh grids (EMS). Images were acquired on a Jeol 1400 Flash transmission electron microscope at 100 kV equipped with a Gatan RIO camera (Gatan, Pleasanton, CA). Image morphometric analysis was performed using ImageJ software (NIH). Structures with sagittal diameter comprised between 20 and 60 nm were classified as SVs, while those with a sagittal diameter bigger than 60 nm were classified as intra-terminal cisternae. SVs touching AZ were classified as docked SVs.

2. 10. Bulk RNA seq analysis

Total RNA was isolated using the RNeasy® mini kit (Qiagen) following manufacturer's instructions. RNA libraries were prepared from 100 ng of total RNA using KAPA mRNA HyperPrep kit (Roche) according to the manufacturer's protocol. Sequencing was performed on an Illumina NextSeq 500/550 High Output single-end (~30 M reads/sample) at the UCL Genomics, GOS ICH. The obtained FASTQ files were uploaded onto the Galaxy web platform (www.usegalaxy.org) and subsequently analysed using the quality control features FastQC and MultiQC in Galaxy³⁰⁶. Fastp (v.0.20.1) was used to filter the FASTQ files³⁰⁷, trimming per quality (mean quality > Q20) and discarding low quality (phread quality > 15) reads. Reads were mapped to the human reference genome (GRCh38) using HISAT2 (v.2.1.0)³⁰⁸. Counts for genes were extracted with featureCounts (v.1.6.4) excluding duplicates, multimapping reads and chimeric fragments³⁰⁹. EdgeR (v.3.24.1)³¹⁰ was used to analyse differential gene expression, filtering low counts at 1 minimum counts per million, in at least three samples³¹¹. Comparisons were performed for disease status (all patients versus control) and disease-corrected genotype (Patient 2-1 versus CRISPR-corrected Patient 2-1). Differentially expressed genes (DEGs) with

a false discovery rate correction (FDR) < 0.05 and absolute fold change >2 were considered as statistically significant and only protein-coding DEGs were used for further analyses. Heat maps were generated from the row-scaled z-score of normalised counts obtained by EdgeR with complete-linkage Euclidean hierarchical clustering. Gene ontology (GO) enrichment was performed using PANTHER v14³¹² for biological processes, and SynGO (v.1.1)³¹³ for synaptic localisation and function, with Fisher's Exact test correction of FDR < 0.05.

2. 10. Generation and transfection of a *DNAJC6* lentiviral vector

2. 10. 1. Generation of a lentiviral *DNAJC6* expression plasmid

A lentiviral *DNAJC6* plasmid was generated by replacing the human *DAT* coding sequence in a previously developed plasmid (pCCL-hSYN-DAT-IRES-EGFP) by the human *DNAJC6* gene coding sequence. The lentiviral backbone containing the human *DAT* gene (pCCL-hSYN-DAT-IRES-EGFP) and a mock plasmid expressing only *GFP* (pCCL-hSyn-EGFPv2) was kindly provided by Dr Joanne Ng (UCL, Institute of Women's Health, UCL).

2. 10. 1. 1. DAT plasmid verification

50 ng of DAT plasmid DNA was added to one vial of One Shot™ TOP10 Chemically Competent *E. coli* bacteria (Thermo Fisher Scientific) and incubated for 30 min on ice. To promote uptake of plasmid DNA, bacteria cells were heat shocked at 42°C for 30 s and incubated on ice for a further 5 min. Then, 500 µl of SOC Medium (Takara) was added to the cells and the mixture was agitated at 37°C for 1 h (200-225 rpm). 500 µl of the culture mixture was seeded on a dry agar plates containing 50 µg/ml Kanamycin and incubated at 37°C for 20 hours. Single bacterial colonies were picked and grown in 3 ml mini cultures of LB medium at 37°C and agitated at 200-225 rpm over-night. The next day, plasmid DNA was extracted using a plasmid purification kit (Miniprep Kit (QIAGEN) according to manufacturer's recommendations. In brief, 1ml of the culture mix was collected in a 1.5ml Eppendorf tube and centrifuged at 6000g for 5 min. The supernatant was removed and 250 µl of the P1 resuspension buffer was added to the pellet and lysed with 250 µl of P2 lysis buffer for 5 min at room RT. Subsequently, the mixture was neutralised with 350 µl of N3 for a further 5 min at RT and centrifuged at 14000 rpm for 10min. Resulting supernatant was then transferred into a supplied spin column and centrifuged at 14000 rpm for 1 min and the flow-through was discarded. Columns were then washed with 750 µl of PE buffer containing ethanol to remove salts, centrifuged at 14000 rpm for 1 min, and the flow-through discarded. Residual ethanol was removed with a second step of at 14000 rpm for 1 min and DNA eluted with 50 µl of EB elution

buffer, after centrifugation for 1 min at 14000 rpm. DNA concentration was measured using a UV-Vis spectrophotometer NanoDropTM 1000 in ng/μl. Bacterial amplification of the DAT plasmid was analysed using restriction enzyme digestion of 1 μg of DNA. The restriction enzyme 5 BamHI (Thermo Fisher Scientific) was used to generate a 600 bp fragment of the DAT plasmid. A master mix was prepared with 5 μl Buffer (Anza red 10x) use 1:10, 2 μl Enzyme 5 BamHI and 33 μl H₂O per sample. 40 μl of master mix was added to 10 μl of DNA and the mix was digested at 37°C for 45 min. Subsequently, 30 μl of sample mixture and 10 μl of Quick-Load® 1 kb DNA Ladder were loaded on a gel and run for 45 min at 110 V in 1xTBE buffer.

2. 10. 1. 2. Removal of the *DAT* gene from the DAT plasmid

In order to remove the *DAT* gene from the DAT plasmid, two restriction enzymes were used: SgrDI (Thermo Fisher Scientific) and 6 NheI (Thermo Fisher Scientific). A first master mix was prepared with 5 μl Buffer (Tango 10x) use 1:5 to get Tango 2x, 2 μl Restriction enzyme SgrDI and 3 μl H₂O. Each sample was prepared with 20 μl of master mix and 10 μl of DNA (2 μg) and digested at 37°C for 45 min. A second master was prepared with 5 μl Buffer (Anza red 10x) use 1:10, 2 μl restriction enzyme 6 NheI and 13 μl H₂O. 20 μl of master mix was added to each sample from the first digest (total volume 50 μl) and the digest was carried out at 37°C for 45 min.

A 0.7% agarose gel was prepared with 50 ml 1xTBE and SYBRTM Safe. The digested samples together with the Quick-Load® 1 kb DNA Ladder was run at 110 V for 45 min. The digested backbone plasmid was cut out from the gel at 8.5 kb and purified using the QIAquick Gel Extraction Kit (Qiagen). Plasmid DNA was solubilized in a ratio of 1:3 with QG buffer and the gel incubated for 10 min at 50°C, vortexed and incubated for another 10min. DNA was precipitated with 110 μl of isopropanol and transferred to a spin column for centrifugation at 13.000 rpm for 1min. The flow through was discarded. 500 μl of QG buffer was added and the mixture centrifuged at 13.000 rpm to remove agarose traces. Subsequently, the sample was washed with 750 μl of PE buffer, centrifuged at 13.000 rpm for 1 min and the flow through discarded. The column was then transferred to a new 1.5ml tube. DNA was eluted with 30 μl of pre-warmed EB Buffer, incubated at 50°C for 4 min and centrifuged at 13.000 rpm for 1 min. DNA concentration was measured using the UV-Vis spectrophotometer NanoDropTM 1000.

2. 10. 1. 3. Cloning of the *DNAJC6* gene into the DAT plasmid

The *DNAJC6* gene sequence was designed with the assistance of Dr. John Counsell (UCL GOS-ICH). The synthesised DNA was resuspended in 20 µl H₂O to get a concentration of 50 µg/µl and incubated for 5 min at RT. In a PCR tube, a PCR mixture was prepared with 2 µl of the 5x In-Fusion® HD Enzyme (Takara), 4 µl of *DNAJC6* DNA and 4 µl of the empty plasmid. PCR was carried out at 50°C for 15min and the mix incubated on ice for 2min afterwards. The *DNAJC6* plasmid was purified and analysed as described above. The plasmid construct was diluted in LB medium with Kanamycin (50 µg/ml) in a ratio 1:10 and a stock of the plasmid bacterial culture was frozen down in 20% glycerol and stored at -80°C.

Isolation of plasmid DNA was performed using the PureLink™ HiPure Plasmid Filter Maxiprep Kit and the PureLink™ HiPure Precipitator Module (Thermo Fisher Scientific) according to the manufacturer's instructions. The Filtration Cartridge was inserted into the PureLink® HiPure Maxi Column. The column was then equilibrated with 30 ml of Equilibration Buffer EQ1. The LB culture was centrifuged at 4000 g for 10min and the medium removed. The cell pellet was resuspended in 10 ml Resuspension Buffer R3. Cell lysis was performed with 10 ml of Lysis Buffer L7 and incubated at RT for 5min. The lysate was then precipitated with 10 ml of Precipitation Buffer N3 and the DNA washed with 50 ml of Wash Buffer W8. A sterile 50 ml centrifuge tube was placed under the HiPure Filter Column and the DNA eluted with 15 ml of Elution Buffer E4. Subsequently, DNA was precipitated using the PureLink™ HiPure Precipitator Module according to the manufacturer's instructions. 10.5 ml of isopropanol was added to the elution column and incubate at RT for 2min. The precipitated DNA mixture was then loaded into a syringe, passed through the precipitator and the flow-through discarded. The DNA was washed with 5 ml of 70% ethanol, eluted with 750 µl of TE buffer, and stored at -20°C.

2. 10. 1. 4. Sequencing of the *DNAJC6* plasmid

Sequencing of the plasmid was performed by Dr Katy Barwick using dideoxy sequencing (Table 2.6).

Primer name	Primer Sequence (5'-3')
DNAJC6_plas_1F DNAJC6_plas_1R	AGTCGTGTCGTGCCTGAGAG ATCGCCCTTGGTGTATGATG
DNAJC6_plas_2F DNAJC6_plas_2bF DNAJC6_plas_2R	GGGCGGCTCTTCTCAAATCT CCAAATTCCATAGTCGGGTA ATCCGTTGCGTTGCTTGTTA
DNAJC6_plas_3F DNAJC6_plas_3R	TGTGTGACTTGTGGCTGAC TCTTGATGCTCTTGGTGAGA
DNAJC6_plas_4F DNAJC6_plas_4R	CGGTTTCATTCCGTTGGATA CTGGCTCTTGCTGCTTCTTA
DNAJC6_plas_5F DNAJC6_plas_5R DNAJC6_plas_5bR	GAGCAGAGCGATGACGAACT GTCCAGAGGGATGAAAGACG TGAACAGTGGGACTCGGTGA
DNAJC6_plas_6F DNAJC6_plas_6R	TCATCTGACCCGTTTCTCCA TTGAGGTTGCTGCCAGTTGT
DNAJC6_plas_7F DNAJC6_plas_7R	TTGGGTCTAGTAGTTTCGCTTC TCGTGGACCTTCTTGTCCT
DNAJC6_plas_8F DNAJC6_plas_8R	ACAACTGGCAGCAACCTCAA AGACGGCAATATGGTGGA

Table 2. 6. Primer sequences for plasmid confirmation.

Presence of the *DNAJC6* gene in the DNAJC6 plasmid (pCCL-hSYN-DNAJC6-IRES-EGFP) (**Figure 2. 1**), and its absence in the mock plasmid (pCCL-hSYN-EGFPv2JN) (**Figure 2. 2**) as well as presence of the human synapsin (*hSYN*) gene promoter and the *EGFP* reporter gene in both plasmids was confirmed.



Figure 2. 1. Schematic representation of the pCCL-hSYN-EGFPv2JN lentivirus mock plasmid sequence. CMV= human cytomegalovirus immediate early promoter, 5'LTR= truncated 5' long terminal repeat, ψ = packaging signal, RRE= Rev response element, cPPT= central polypurine tract, hSYN= human synapsin promoter, EGFP= enhanced green fluorescent protein, WPRE= woodchuck hepatitis virus posttranscriptional regulatory element, 3'LTR Δ U3= self-inactivating 3' long terminal repeat, SV40pA= simian virus 40 polyadenylation signal, NeoR/KanR= neomycin and kanamycin antibiotic resistance. The construct is not drawn on scale.



Figure 2. 2. Schematic representation of the pCCL-hSYN-DNAJC6-IRES-EGFP lentivirus plasmid sequence. The plasmid sequence is the same as the mock plasmid with an additional Internal Ribosome Entry Site sequence (IRES) between the *DNAJC6* gene and the *EGFP* gene.

2. 10. 2. Lentivirus Production

Previously, a T175 flask with 1.8×10^7 HEK 293T cells was prepared in DMEM high glucose pyruvate (Gibco®), 10% FBS, and 1:100 P/S. A DNA master mix was prepared with 40 µg transgene plasmid, 30 µg of the lentiviral packaging plasmid pCMVR8.74 (1 µg/µl; Addgene) and 10 µg of envelope expressing plasmid pMD2.G (1 µg/µl; Addgene). 5ml Opti-MEM I medium (Gibco®) was added and the mixture filtered through a 0.22 µm pore size membrane filter (Millipore) with hydrophilic polyethersulfone (PES) (Millipore), mixed with a filtered solution 1:20 of Opti-MEM I medium and 10 mM polyethylenimine (PEI) (Sigma-Aldrich). The mix was incubated for 30min at RT. 10 ml of the DNA-PEI mixture was added to a T175 flask with HEK 293T cells and culture at 37°C for 4 hours. Afterwards, the DNA-PEI was removed and 20ml of DMEM medium without P/S was added. The medium was collected after 3 days and centrifuged at 500 rpm for 5 min to remove cell debris. The viral supernatant was filtered through a 0.22 µm filter and centrifuged at 4600 rpm and 4°C for 24 hours. The supernatant was disposed and the 50ml tubes were placed upside-down on a dry paper towel for 1min. Afterwards, 30 µl of Opti-MEM I medium was added to the tube and incubated on ice for 60 min. The pellet was gently resuspended in the medium, aliquoted into cryovials and stored at -80°C.

2. 10. 2. 1. Lentiviral Vector Titration by qRT-PCR

HEK 293T cells were plated at a density of 10^5 cells per well in a 6-well plate and subsequently transduced with 10, 2, 0.4, 0.08 and 0 µl of virus in 1 ml of medium in order to quantify the total number of integrated genomes per cell. A previously validated qPCR assay was then used to determine the integrated vector copy number (VCN)³¹⁴. After 3 days of culture, gDNA was extracted from the cells using the commercial kit DNeasy Blood & Tissue Kit according to the manufacturer's recommendations and samples diluted to 20 ng/µl. Standard curves were calculated using a plasmid DNA template (pCCL-GFP) and a genomic DNA template (albumin gene).

Standard curve for plasmid DNA template

The mass of the standard plasmid DNA was calculated as following:

$$m = n [\text{bp}] * 1.096(10^{-21}) [\text{g/pb}]$$

where n = plasmid total bp (i.e. plasmid+insert)

pCCL-GFP n = 8025 bp

$$m = 8025 \text{ bp} * 1.096(10^{-21}) \text{ g/bp} = 8.7954(10^{-18}) \text{ g}$$

The plasmid mass was used for the calculation of plasmid gene copy numbers (Table 2.6).

Gene of interest copies * mass of single plasmid = mass of plasmid DNA needed

Gene copies		Mass of plasmid DNA (g)
300,000	$\times 8.7954(10^{-18})$	$2.64(10^{-12})$
30,000		$2.64(10^{-13})$
3,000		$2.64(10^{-14})$
300		$2.64(10^{-15})$
30		$2.64(10^{-16})$

Table 2. 6. Calculation of gene copy numbers using plasmid DNA mass.

The plasmid mass was used to calculate the concentration of the plasmid DNA (Table 2.7).

Gene copies	Mass of plasmid DNA (g)		Concentration of plasmid DNA (g/ μ L)
300,000	$2.64(10^{-12})$	/9 μ l	$2.93(10^{-13})$
30,000	$2.64(10^{-13})$		$2.93(10^{-14})$
3,000	$2.64(10^{-14})$		$2.93(10^{-15})$
300	$2.64(10^{-15})$		$2.93(10^{-16})$
30	$2.64(10^{-16})$		$2.93(10^{-17})$

Table 2. 7. Calculation of plasmid DNA concentration using plasmid DNA mass.

Finally, serial solutions (Table 2. 8) were prepared as following:

Stock solution: 350.6 ng/ μ L = 350,600 pg/ μ L

Predilution:

A) 5000 pg/ μ L from Stock Solution

B) 100 pg/ μ L from A)

	Initial conc. (g/μL) C_1	Volume of plasmid DNA (μL) V_1	Volume of diluent (μL)	Final Volume (μL) V_2	Resulting copies of WPRE sequence
1	$2.93(10^{-12})$	2.93 μl	97.07 μl	100 μl	300,000
2	$2.93(10^{-13})$	10 μl	90 μl	100 μl	30,000
5	$2.93(10^{-14})$	10 μl	90 μl	100 μl	3,000
4	$2.93(10^{-15})$	10 μl	90 μl	100 μl	300
5	$2.93(10^{-16})$	10 μl	90 μl	100 μl	30

Table 2. 8. Overview on serial dilutions for generation of the standard curve.

Standard curve for genomic DNA template

The mass of the standard gDNA was calculated as following:

$$m = n \text{ [bp]} * 1.096(10^{-21}) \text{ [g/pb]}$$

where n = haploid genome bp

Homo sapiens (haploid) = 3,000,000,000 bp = 3(10⁹) bp

$$m = 3(10^9) \text{ bp} * 1.096(10^{-21}) \text{ g/bp} = 3.288(10^{-12}) \text{ g} = 3.3 \text{ pg}$$

3.3 pg of genomic DNA contains 1 copy of albumin gene

The gDNA mass was used for the calculation of gDNA copy numbers (**Table 2. 9**).

Gene of interest copies * mass haploid = mass of gDNA needed

Gene copies		Mass of gDNA (pg)
300,000	× 3.3	990000
30,000		99000
3,000		9900
300		990
30		99

Table 2. 9. Calculation of gene copy numbers using genomic DNA mass.

The gDNA mass was used to calculate the concentration of the genomic DNA (**Table 2. 10**).

Gene copies	Mass of gDNA (pg)	/9µl	Concentration of gDNA (pg/µL)
300,000	990000		110000
30,000	99000		11000
3,000	9900		1100
300	990		110
30	99		11

Table 2. 10. Calculation of plasmid DNA concentration using genomic DNA mass.

Finally, serial solutions (**Table 2. 11**) were prepared as following:

Stock solution: 160.67 ng/µL = 160,670 pg/µL

	Initial conc. (g/µL) C ₁	Volume of gDNA (µL) V ₁	Volume of diluent (µL)	Final Volume (µL) V ₂	Resulting copies of albumin sequence
1	Stock				43,830
2	11000	6.85 µl	93.15 µl	100 µl	3,000
5	1100	10 µl	90 µl	100 µl	300
4	110	10 µl	90 µl	100 µl	30
5	11	10 µl	90 µl	100 µl	3

Table 2. 11. Overview on serial dilutions for generation of the standard curve.

qRT-PCR was carried out using the TaqMan® Universal PCR Master Mix (Applied Biosystems). A reaction master mix was prepared with 6.99 µl H₂O, 12.5 µl TaqMan® Universal PCR Master Mix, 0.23 µl Forward oligo and 0.23 µl Reverse oligo and 0.06 µl Probe per sample. 20 µl of the mix was added to 5 µl of samples/standards and mixed.

Standard curves were calculated using the following equation:

$$y=m*x+t$$

where y = C_T value and x =gene copy number

Lentivirus copy number per cell was calculated as following:

$$\text{Virus copy number per cell (VCN)} = (\text{copy number WPRE}/\text{copy number ALB}) \times 2$$

Lentivirus titer was calculated as following:

$$\text{Virus titer (iu/ml)} = \text{number of transduced cells at day 1} \times \text{VCN} / \text{volume of lentivirus used in titration (ml)}$$

From previously established lentivirus transfection experiments in mDA neurons in the Kurian laboratory, a MOI of 1.5 was used for neuronal infection. The amount of virus for infection was calculated as following:

$$\text{Amount of virus for infection (}\mu\text{l)} = (\text{Amount of cells}/\text{virus titer (iu/ml)}) \times 1000 \times \text{MOI}$$

where the amount of cells was assumed from drop plating 100 μl and a concentration of 15.000/ μl

2. 10. 3. Lentivirus transfection of mDA neurons

At day 28 of differentiation, mDA neurons seeded in a 12-well plate were transfected with a MOI of 1.5 with the pCCL-hSYN-DNAJC6-IRES-EGFP, and the pCCL-hSYN-EGFPv2 virus. For a MOI of 1.5, 72.5 μl of virus was added to 500 μl of FDF medium and incubated for 24 hours at 37°C. Afterwards, medium was replaced by fresh FDF medium and mDA neurons differentiated to day 65.

2. 10. 4. Immunoblotting of lentivirus-transfected mDA neurons

At day 65 of differentiation, protein was extracted and immunoblotting performed as described in Section 2.5.2.

2. 10. 5. FMTM1-43 dye uptake assay analysis in lentivirus-transfected mDA neurons

Lentivirus-transfected mDA neurons were plated on Labteck slides (NuncTM) at day 30 of differentiation. FMTM1-43 dye uptake assay was carried out as described in Section 2.6.

CHAPTER 3

Clinical and molecular genetic features of patients with *DNAJC6*-related parkinsonism

3. 1. Introduction

The advent of next generation sequencing has substantially changed the genetic landscape of movement and neurodegenerative disorders. Depending on the stratification of any given patient cohort, the diagnostic yield of WES may be anywhere between 32% and 56% for patients with paediatric movement disorders^{315–317}. While the number of novel genes is steadily increasing, detailed clinical characterisation of patients is essential to better define the phenotypic spectrum and disease course. At the time of analysis, the Neurogenetic Movement Disorders Clinics at Great Ormond Street Hospital harboured a large research cohort of 232 children with undiagnosed movement disorders. A subgroup of 25 children (16 singletons and 9 familial cases) with unresolved juvenile parkinsonism was further investigated. In this part of my PhD project, I was involved in the phenotypic characterisation of six patients from this cohort. Molecular genetic analysis using SNP array (UCL Genomics) and WES (BGI) was carried out by Dr Elisenda Cortès-Saladelafont, while molecular analysis of patient fibroblasts and CSF was performed by Dr. Joanne Ng. Some sections and figures have been adapted from publications arising from this research, including Ng J*, Cortès-Saladelafont E* and Abela L* et al., 2020⁶⁵.

3. 2. Results

3. 2. 1. Molecular genetic analysis

Clinical examination of 25 children with juvenile parkinsonism revealed five individuals from two consanguineous families originating from Pakistan with a remarkably similar clinical phenotype. The affected children underwent autozygosity mapping studies, which identified a 4.33Mb region of common homozygosity on chromosome 1, between rs640407 (64,267,606bp) and rs2566784 (68,602,735bp) (**Figure 3. 1A**). SNP genotyping was followed by WES in Patient A-III:1 and Patient B-IV:2, which identified 23,365 and 23,549 variants, respectively. Given familial consanguinity and a common haplotype in the affected children, WES data was filtered for recessively inherited pathogenic variants within the common region of homozygosity (**Figure 3. 1B**). WES revealed a single homozygous nonsense variant **c.766C>T (p.R256*)** in the gene *DNAJC6* (Chr1:65,248,219-65,415,869) both in A-III:1 and B-IV:2. In addition, WES data was interrogated for pathogenic variants in other genes causing juvenile parkinsonism, but no other variant was identified. Subsequent Sanger sequencing confirmed the homozygous mutation **c.766C>T (p.R256*)** in all five affected children (**Figure 3. 1C**). Family segregation analysis confirmed parents as obligate carriers and unaffected siblings as

either wild-type or heterozygous for this variant. WES/whole genome sequencing (WGS) from the remaining 20 children of the juvenile-parkinsonism subgroup was then interrogated for *DNAJC6* mutations and revealed a novel homozygous nonsense variant c.2416C>T (p.R806*) in a sixth unrelated patient (Patient C). The variant was confirmed by Sanger sequencing (**Table 3. 1**).

3. 3. Detailed endophenotyping of the *DNAJC6* study cohort

3. 3. 1. Family history

The parents of Family A and B are first-cousins originating from the same region in Pakistan. The parents of Patient C originate from Puerto Rico and are second-cousins with the maternal grandmother and the paternal grandmother being first cousins. The paternal grandfather of Family A was diagnosed with PD in his 50s. Two brothers (A- III:2 and A-III:3) of the affected siblings A exhibited mild learning difficulties but had no evidence of a movement disorder at the age of 17 and 15 years, respectively (**Table 3. 1**).

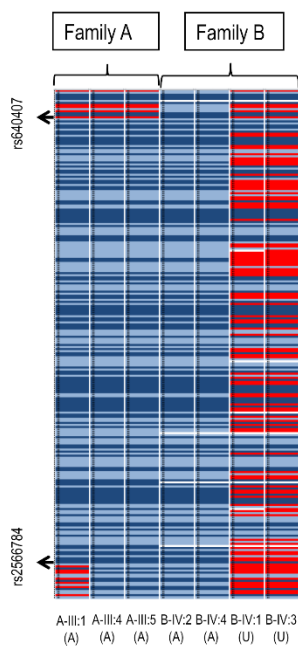
3. 3. 2. Early development and cognition

All six patients were born at term after an uneventful pregnancy. Affected siblings of Family A (A-III:1, A-III:4 and A-III:5) presented with primary microcephaly at birth (head circumference <0.4th centile) that was non-progressive over time. All siblings of Family A showed early developmental delay with slow progress over time and later manifested moderate learning difficulties. Patient B-IV:2 and B-IV:4 also presented with developmental delay by 6 months of age, and progressed slowly during infancy and childhood. They both achieved independent walking and spoken language by three years of age. Patient C showed a mild delay in attaining developmental milestones, she was able to walk and talk by two years of age.

A

	Family A				Family B			
	Start of Homozygous Region		End of homozygous region		Start of Homozygous Region		End of Homozygous Region	
	Reference SNP Cluster ID (rs number)	Physical Position (bp)	rs number	Physical Position (bp)	rs number	Physical Position (bp)	rs number	Physical Position (bp)
Chromosome 1	rs2819130	64 231 541	rs2772304	68 636 580	rs41285364	63 786 518	rs6687262	79 509 109
Chromosome 2					rs300758	72 184	rs809672	12 688 452
Chromosome 5					rs1859295	135 327 491	rs13153997	151 080 003
Chromosome 5					rs13358102	171 650 965	rs6887234	173 616 645
Chromosome 7					rs12669653	128 746 301	rs3800707	134 472 116
Chromosome 11	rs10836509	36 177 369	rs3133269	67 804 156				
Chromosome 12					rs4469939	77 288 346	rs2114926	101 093 560
Chromosome 17					rs9911464	32 468 227	rs7216307	42 413 481
Chromosome 18					rs292324	5 167 441	rs4800629	22 901 551

B



C

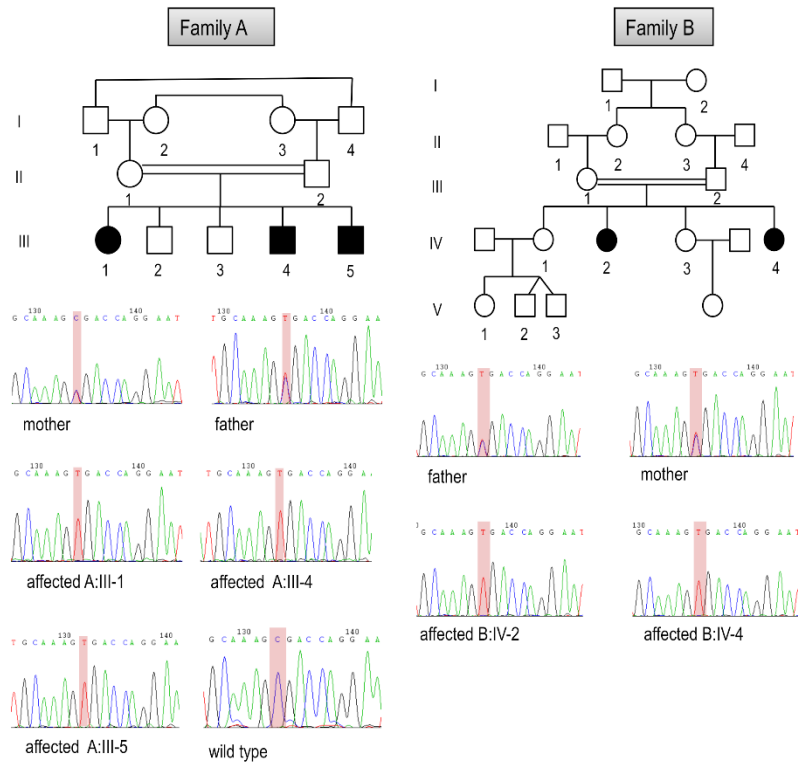


Figure 3. 1. Molecular genetic analysis. **A)** SNP array analysis showing homozygous regions present in Family A and B. The start and end point of each chromosome is indicated by the Reference SNP Cluster ID (rs number) and physical position. **B)** Heatmap graph demonstrating homozygous SNPs in light blue (AA) and dark blue (BB), heterozygous SNPs in red (AB) and “no calls” in white. **C)** Sanger Sequencing chromatograms show a homozygous DNAJC6 mutation c.766C>T (p.R256*) in all affected children of Family A (A-III:1, A-III:4 and A-III:5) and Family B (B-IV:2, B-IV:4). Parents have been identified as heterozygous carriers. Autozygosity mapping and WES have been performed by Dr. Elisenda Cortès-Saladelafont (Figure and legend from Ng J*, Cortès-Saladelafont E* and Abela L* et al., 2020)⁶⁵.

3.3.3. Movement disorder and treatment

All six patients developed motor symptoms either at the end of the first decade or beginning of the second decade, respectively (**Table 3. 2**). The movement disorder is characterised by progressive bradykinesia, tremor, rigidity and postural instability. Patient A-III:1 developed bradykinesia, tremor and rigidity at 10 years following a phase of acute encephalitis of uncertain aetiology. At 13 years, she lost ambulation, became wheelchair-bound with generalised cogwheel-rigidity and severe bradykinesia. She acquired multiple limb contractions over time. Treatment with levodopa resulted in improved motor function and speech 30 minutes post-dose, but marked drug sensitivity was evident and dosages above 150mg/day led to drug-related dyskinesias. Treatment with other substances such as trihexyphenidyl, benzhexol, procyclidine, clobazam, rotigotine and apomorphine did not show any clinical benefit. Patient A-III:4 and A-III:5 both presented with fine motor difficulties at the age of 8 years and subsequently manifested positional tremor, hypophonia, hypomimia, bradykinesia, cogwheel rigidity and postural instability over a period of 12 months. Both brothers improved under treatment with transdermal rotigotine and oral trihexyphenidyl, however, dosages had to be adjusted due to drug-induced dyskinesias. Patient B-IV:2 developed motor symptoms at the age 13 years with bradykinesia, hypomimia, tremor, generalised cogwheel rigidity and subsequent loss of ambulation and speech. Treatment was difficult and she did not response to medication with levodopa (maximum 10mg/kg/day), selegiline, rotigotine and trihexyphenidyl. Patient B-IV:4 presented at 7 years with bradykinesia, cogwheel rigidity and gait deterioration and lost her ambulation and speech at the age of 10 years. Treatment with levodopa initially evoked a good clinical response, but had to be ceased at a dosage of 5.5mg/kg/day due to emotional lability. Medication with trihexyphenidyl or chloral hydrate had no benefit, but she showed a modest response to pramipexole, which improved hypomimia and bradykinesia and reduced tremor. Patient C suffered deterioration of gait with frequent falls and postural instability at the age of 10 years. She lost her ability to run and over the next four years further deteriorated rapidly with progressive bradykinesia. Medication with levodopa improved tremor, gait and sialorrhea, but dosages above 200mg/day resulted in drug-related dyskinesias. At the age of 16 years, she developed increased drug-sensitivity to levodopa with clear on-off phenomena. In the on-state, she experienced peak-dose agitation, restlessness and dyskinesia, while 2-3 hours post-administration, she became akinetic and rigid in the off-state. Trihexyphenidyl improved rigidity but not bradykinesia.

Additional movement abnormalities were also frequently observed. Patient A-III:4 and A-III:5 developed upper limb dystonic posturing together with the onset of typical parkinsonian symptoms. As another sign of dystonia, Patient A-III:4 showed a striatal toe sign when walking. With further progression of the disease, Patient B-IV:2 and Patient C also suffered from dystonia with worsening anterocollis. Patient B-IV:2 manifested upper limb myoclonus. There was no evidence of spasticity in our patient cohort.

3. 3. 4. Additional neurological, neuropsychiatric and systemic features

In most patients, the movement disorder was accompanied by a variety of neurological, neuropsychiatric, and systemic features (**Table 3. 3**).

Neurological features

Patient B-IV:2 and Patient C both presented with seizures. At the age of 9 years, Patient B-IV:2 developed generalised tonic-clonic seizures responsive to lamotrigine therapy. Patient C manifested first seizures at the age of 2 years, characterised by staring episodes and loss of tone. At the age of 12 years she developed generalised tonic-clonic seizures and atypical absences that were controlled by lamotrigine and zonisamide.

Neuropsychiatric features

Behavioural and anxiety disorders, either isolated or attributed to drug side effects, were commonly reported. Patient A-III:1 suffered from emotional lability with onset of the movement disorder. Her brother, Patient A-III:4, also experienced anxiety, perseveration behaviour and sleep disorder. With the onset of parkinsonism at the age of 13 years, Patient B-IV:2 manifested anxiety and disrupted sleep pattern. Her sister, Patient B-IV:4, suffered from sleep disorder and emotional lability when she was under medication with levodopa at a dosage of 5.5mg/kg/day. Anxiety and emotional tension provoked episodes of generalised body shaking. Levodopa treatment had to be withdrawn subsequently. Patient C experienced severe psychiatric side effects four months after starting treatment with levodopa at a dosage of 200mg/day. She developed aggressive behaviour and needed treatment with quetiapine.

Systemic features

Gastrointestinal dysfunction was observed in the majority of our patients. Affected siblings of Family B (Patient B-IV:2 and B-IV:4) and Patient C manifested neonatal and infantile feeding difficulties. All affected siblings of Family A exhibited feeding difficulties, recurrent vomiting and sialorrhea requiring gastrostomy insertion. Further in the disease course, Patient B-IV:4

developed bulbar dysfunction and underwent gastrostomy. Patient C suffered remarkable weight loss due to severe bulbar dysfunction with sialorrhea, dysarthria and dysphagia.

3. 3. 5. Disease course over time

With the onset of the movement disorder, four patients (Patient A-III:1, Patient B-IV:2, Patient B-IV:4, Patient C) experienced a rapid decline in motor function and lost independent ambulation within 2 to 5 years. Two patients are still ambulant (Patient A- III:4, A-III:5), but also suffered gait deterioration. Along with the progression of the movement disorder, Patient A-III:1, B-IV:2 and B-IV:4 suffered cognitive deterioration and also lost their speech by the age of 13 years (Patient A-III:1, Patient B-IV:2) and 10 years (Patient B-IV:4), respectively.

3. 3. 6. Features on Neuroimaging

¹²³I-FP-CIT SPECT (DaTScan™) imaging was performed in three patients from our study cohort (Patient A-III:1, A-III:4, B-IV:4) and compared to a scan undertaken in one control subject. In patients, ¹²³I-FP-CIT SPECT imaging showed reduced tracer uptake or absent tracer uptake in the basal ganglia indicating impaired presynaptic dopamine uptake and striatonigral neurodegeneration (**Figure 3. 2, upper panel**). Brain magnetic resonance imaging (MRI) demonstrated mild to moderate generalised cerebral atrophy in four patients from our study cohort (Patient A-III:1, B-IV:2, B-IV:4, C), with additional cerebellar atrophy in two patients (Patient A-III:1, B-IV:4) (**Figure 3. 2, lower panel**).

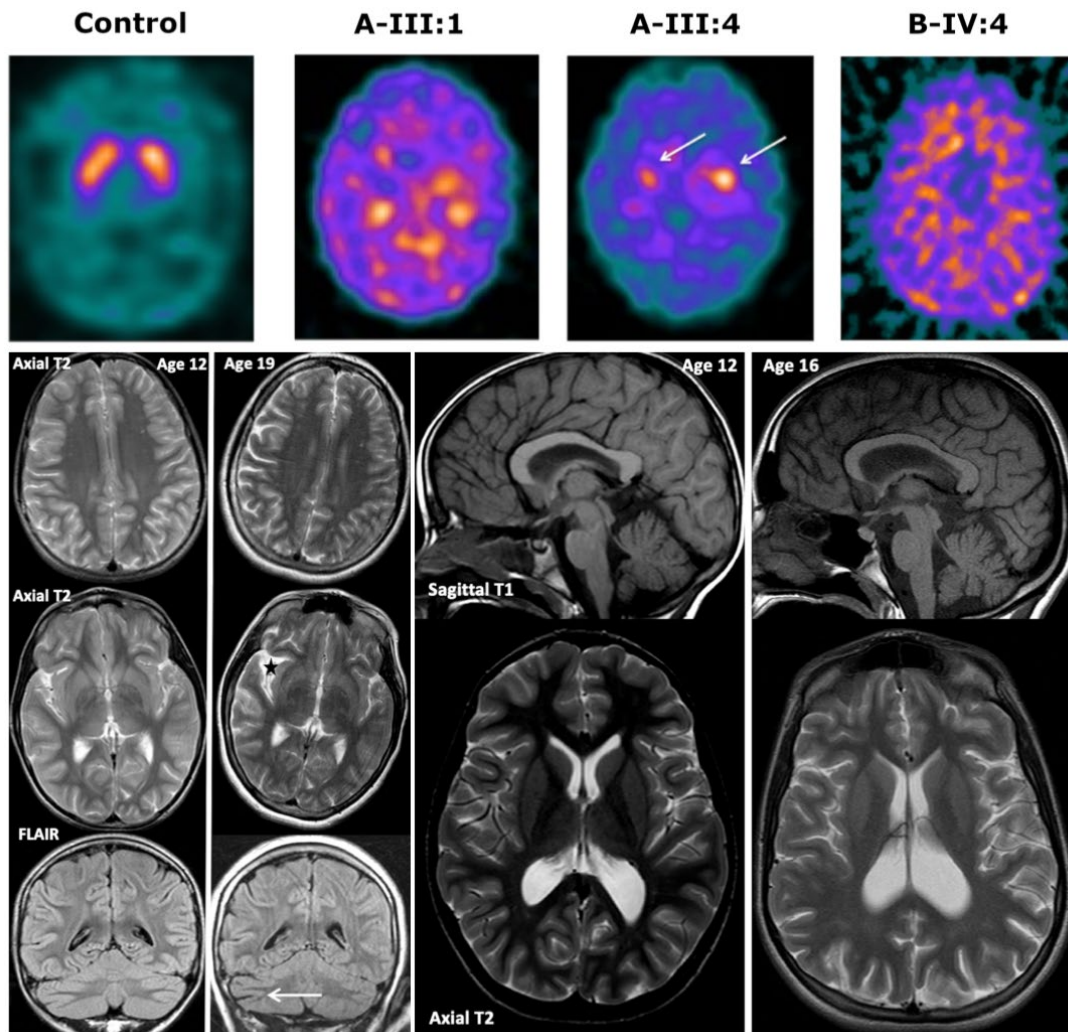


Figure 3. 2. Neuroimaging features in DNAJC6-patients. *Upper panel:* ^{123}I -FP-CIT SPECT (DaTScanTM) in Patients A-III:1, A-III:4 and B-IV:4 showing reduced (white arrows, A-III:4) or absent (A-III:1, B-IV:4) tracer uptake in basal ganglia and unspecific high background compared to the control. **Lower panel left:** Axial T2 and coronal FLAIR images at age 12 & 19 years (Patient A-III:1) demonstrating progressive right fronto-parietal and perisylvian (black star) and cerebellar (white arrow) atrophy over time. **Lower panel right:** Sagittal T1 and axial T2 MR images at age 12 and 16 years (Patient B-IV:4) showing mild cerebral and cerebellar atrophy (Figure Upper panel and legend adapted from Ng J*, Cortès-Saladelafont E* and Abela L* et al., 2020)⁶⁵.

3. 3. 7. Molecular studies

CSF neurotransmitter analysis demonstrated significantly reduced HVA levels in four patients, and borderline lower limit level in one patient. (**Figure 3. 3A**). HVA represents a dopamine degradation metabolite. 5-hydroxyindolacetic acid (5-HIAA), a serotonin degradation product, was not significantly reduced compared to controls (**Figure 3. 3A**). The HVA:5-HIAA ratio was reduced in four patients. These findings indicate impaired turnover and are reminiscent of TH deficiency, another inherited movement disorder with central dopamine deficiency. CSF

Auxilin protein levels were significantly reduced, while GAK protein levels were significantly increased indicating a potential compensatory mechanism (**Figure 3. 3B/C**). A range of presynaptic proteins involved in dopamine synthesis and metabolism showed reduced levels in CSF as well (**Figure 3. 3D**).

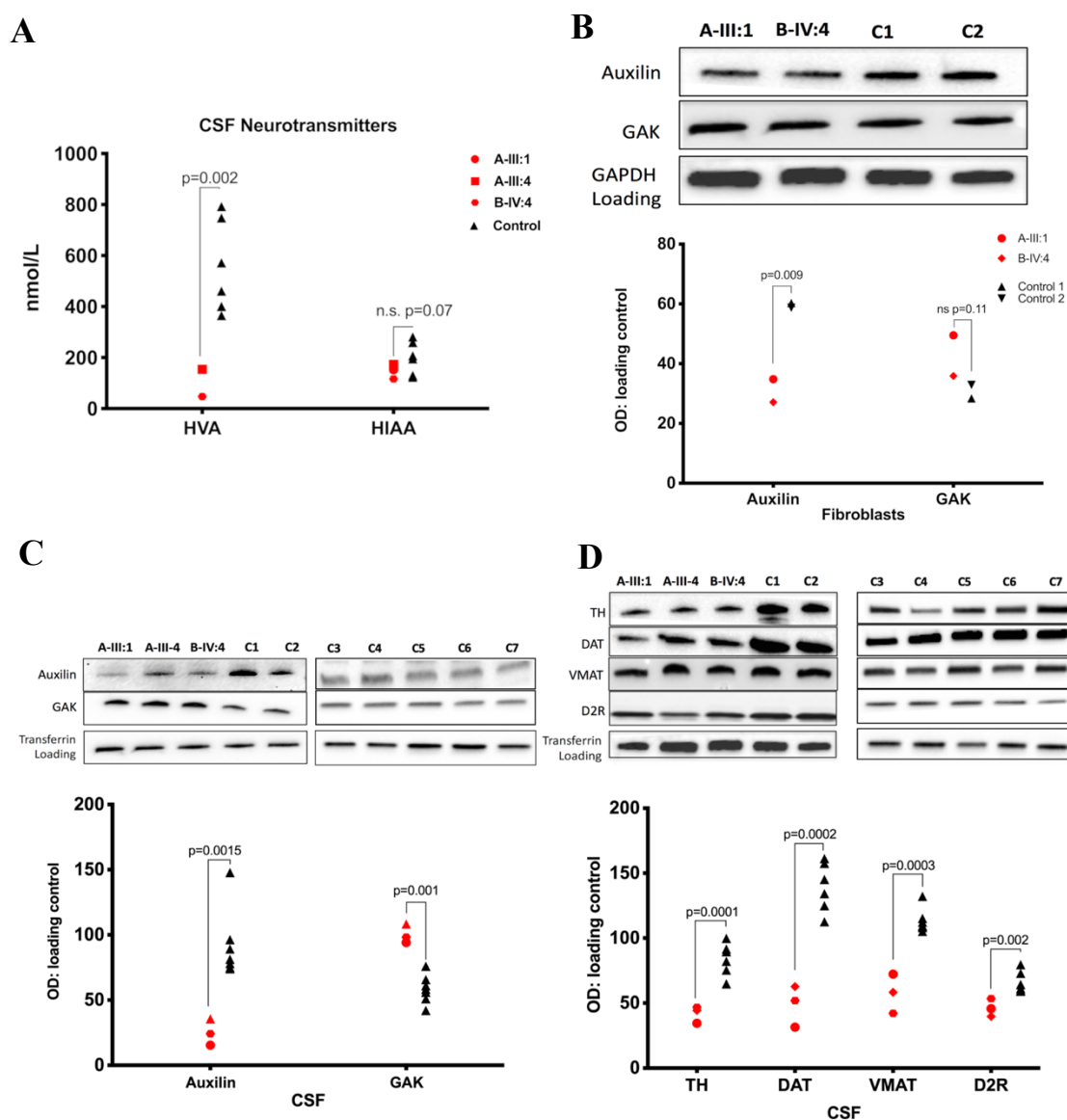


Figure 3. 3. CSF Neurotransmitter analysis and immunoblot analysis in patient fibroblasts and CSF. *A)* High performance liquid chromatography analysis indicating significantly reduced HVA (nmol/L) and normal HIAA levels (nmol/L) in patients (red shapes) compared to controls (black triangles). *B&C)* Immunoblot analysis of patient fibroblasts (*B*) and native CSF (*C*) demonstrating significantly decreased auxilin protein expression levels and increased GAK protein expression levels compared to controls. *D)* Immunoblot of patient CSF showing decreased protein expression levels for TH, DAT, VMAT and D2R compared to controls. Graphs show mean protein % optical density (OD) normalised to loading control in patients (red) and controls (black). Neurotransmitter analysis and immunoblotting has been performed by Dr. Jo Ng (Figure and legend adapted from Ng J*, Cortès-Saladelafont E* and Abela L* et al., 2020)⁶⁵.

3. 4. Literature review on *DNAJC6*-related disease

In order to provide an overview on all published *DNAJC6* cases to date and compare their phenotypic aspects with this cohort (**Table 3. 1. – 3. 3**), I performed a detailed literature review using Pubmed Database with following combined search terms: *DNAJC6*, auxilin and juvenile/early-onset parkinsonism.

3. 4. 1. Reported patients with biallelic *DNAJC6* mutations

In 2012, Edvardson et al reported autosomal recessive mutations in *DNAJC6* in two brothers of Palestinian origin with juvenile-onset parkinsonism⁶¹. Pregnancy, delivery and early psychomotor development was normal. Patient II-2 presented with bradykinesia, rigidity, postural instability, hypomimia and asymmetric tremor at the age of 11 years, while his brother, Patient II-4, developed bradykinesia at the age of seven years, and later suffered from rigidity, tremor and postural instability. Treatment with levodopa, amantadine and pramipexole did not improve motor symptoms, and both patients lost their ambulation at the age of 13 years (Patient II-2) and 18 years (Patient II-4), respectively. Brain MRI was normal in both patients. Homozygosity mapping followed by WES led to the identification of a homozygous splice site mutation in *DNAJC6*, predicted to cause protein truncation (**c.801-2 A->G**).

In 2013, the phenotypic spectrum further expanded with the identification of four individuals of a consanguineous Turkish family with progressive juvenile-onset parkinsonism and additional neurological features including intellectual disability, epilepsy and movement abnormalities⁶². Between the age of 10-11 years, they manifested with bradykinesia, resting and postural tremor, rigidity and postural instability, and in the further disease course, developed intermittent dystonic posturing, dysarthria and pyramidal signs. Treatment with levodopa (62.5mg) was effective, but accompanied by severe psychiatric and motor side effects. The disease course was progressive and all patients were wheel-chair bound or bed-ridden 10-15 years after the onset of symptoms. All individuals suffered from mild to moderate intellectual disability (IQ 40-63). Three patients (Patient 502, 502, 505) developed absence and generalised seizures between the age of 1- 5 years with good response to sodium valproate. The electroencephalogram (EEG) showed generalised epileptiform discharges in Patient 502, while it was normal in Patient 504 and 505. Brain MRI was normal except for Patient 402, where there was evidence of diffuse cerebral atrophy. Linkage analysis and homozygosity mapping followed by WES revealed a homozygous nonsense mutation **c.2200C>T (p.Q734X)** in *DNAJC6*.

In 2016, Olgiati et al. reported two novel homozygous *DNAJC6* variants in two third-cousin consanguineous families originating from small villages in the Netherlands and Southern Brazil as well as one sporadic Brazilian patient⁶³. These patients presented with a later-onset phenotype in the third to fifth decade of life, with slower disease progression and good response to dopaminergic treatments. The variant **c.2779A>G (p.Arg927Gly)** was detected in two probands of the Dutch family. First motor symptoms (bradykinesia, tremor) developed in the third decade and the disease progressed slowly. Brain MRI of both patients were normal, while 18F-DOPA-PET showed nigrostriatal abnormalities. The variant **c.2223A>T (p.Thr741=)**, predicted to affect splicing, was found in two individuals of a Brazilian family who developed Parkinson's symptoms at the age of 31 and 42 years, respectively. These patients showed a good response to levodopa and suffered typical motor complications (wearing off, dyskinesia). One of the patients (PAL 54) underwent bilateral STN-DBS, which markedly reduced parkinsonian symptoms. The third sporadic Brazilian patient had compound heterozygous *DNAJC6* variants **c.2038+3A>G** and **c.1468+83del**. He showed a mildly progressive disease course and was responsive to levodopa. He underwent bilateral pallidotomy.

Elsayed et al. identified a homozygous novel nonsense *DNAJC6* mutation **c.2365C>T (p.Gln789*)** in a patient from first-degree cousins of a Sudanese family originating from Yemen, who initially presented with vivid visual hallucinations at the age of 10 years⁶⁴. She subsequently developed marked bradykinesia, rigidity and postural instability accompanied by progressive cognitive decline. She also manifested spasticity, and over time suffered from seizures (no semiology available) and severe psychotic features including auditory hallucinations. The EEG demonstrated diffuse encephalopathy with focal epilepsy, while brain MRI was normal. The patient showed a mild improvement under medication with levodopa, but treatment was limited by drug-induced dyskinesia.

A homozygous **80kb-deletion** that includes exon 5-19 of the *DNAJC6* gene and the proximal promotor, as well as exon 1 and 2 of the *LEPR1* gene was reported in a 7-year old boy (Patient III-1) presenting with obesity, epilepsy and mental retardation, but without parkinsonian symptoms³¹⁸. The predicted loss of auxilin function would suggest that he would be at high risk of developing the motor features of *DNAJC6*-related disease, later in life.

In 2020, a systematic analysis of *DNAJC* genes in a large Chinese cohort with early-onset PD (EOPD) revealed novel compound heterozygous mutations in *DNAJC6*¹³⁴. The patient

presented with early-onset parkinsonism at the age of 44.3 years. He initially showed a good response to dopaminergic medication but then developed severe motor fluctuations with wearing off and dyskinesia. Treatment with STN-DBS resulted in a markedly improved motor symptoms. WES revealed two heterozygous missense variants **c.2687C>T (p.Thr896Met)** and **c.1577A>G (p.Asn526Ser)** in *DNAJC6*.

In 2020 and 2021, three interesting case reports with predominant dystonia further expanded the *DNAJC6*-associated phenotypic spectrum. Om Mittal et al. described a 16-year old boy born to consanguineous parents from Yemen who suffered from gait difficulties, generalised body stiffness and crying episodes since the age of 14 years¹³⁵. He additionally presented with facial dysmorphism, short stature, thin habitus and intellectual disability. Clinical examination revealed severe dysarthria, generalised dystonia affecting the upper and lower limbs, trunk and face with crying/moaning episodes and bradykinesia, rigidity, mild rest tremor of the upper limbs and postural instability. He also had pyramidal signs with spasticity in both legs. Treatment with levodopa elicited a good response, but he developed severe motor fluctuations with OFF-state dystonia and parkinsonism and ON-state dyskinesias. Brain MRI and EEG were both normal. WES identified a **homozygous single base pair deletion in exon 5, c.580del (p.Ser194ValfsTer138)** in *DNAJC6* resulting in a frameshift and premature truncation.

Ray et al. reported on an adolescent girl with normal psychomotor and cognitive development, who developed dystonic symptoms at the age of 16 years¹³⁶. She suffered from blepharospasm followed by limb, head, jaw and tongue tremor. One year later, she presented with bradykinesia, cogwheel rigidity as well as jaw opening, lingual and cervical dystonia. Treatment with trihexyphenidyl and clonazepam relieved blepharospasm. Botulinum toxin infiltration improved jaw opening and lingual dystonia. However, parkinsonian symptoms (bradykinesia, tremor) did not respond to levodopa treatment (maximum dose 450mg). Brain MRI was uneventful. Clinical WES identified a novel homozygous mutation **c.941T>G (p.Val314Gly)** in *DNAJC6*.

Garza-Brambila et al. published a case of an 11-year old girl suffering from gait and balance problems¹³⁷. She presented with a toe gait since the age of 16 months, and later developed a “cock-walk” gait with flexed elbows, reduced arm swing and an erect posture. A “cock-walk” gait is typically observed in acquired and hereditary manganism, spinocerebellar ataxia type 3 and with psychostimulant use^{319–322}. At the age of 8 years, she presented with parkinsonian

symptoms including progressive rest tremor in the upper limbs, bradykinesia and postural instability. Clinical examination further showed left torticollis and retrocollis, hypokinetic dysarthria and a “sardonic smile” alternating with hypomimia. Treatment with levodopa/benserazide at the age of 10 years markedly improved motor symptoms, though she did not continue on the medication. Brain MRI was unremarkable. A targeted gene panel for hereditary recessive causes of juvenile parkinsonism revealed a homozygous *DNAJC6* variant **c.2589delG (p.Met863Ilefs*15)**, previously reported as a probably pathogenic. After diagnosis she was treated with pramipexole 0.25 mg 3 times daily with marked improvement in the MDS-UPDRS scale.

	DNAJC6 Study Cohort						Previously published cases – juvenile onset parkinsonism											Previously published cases – early onset parkinsonism						Prev Pub
	A-III:1 ⁶⁵	A-III:4 ⁶⁵	A-III:5 ⁶⁴⁶⁵	B-IV:2 ⁶⁵	B-IV:4 ⁶⁵	C ⁶⁵	II-2 ⁶¹	II-4 ⁶¹	402 ⁶²	502 ⁶²	504 ⁶²	505 ⁶²	4202 ⁹⁶⁴	CR 1 ¹³⁵	CR 2 ¹³⁶	CR 3 ¹³⁷	GPS 313 ⁶³	GPS 314 ⁶³	PAL 50 ⁶³	PAL 54 ⁶³	BR-2652 ⁶³	CR 4 ¹³⁴	III-1 ³¹⁸	
Patient characteristics																								
Presenting age (y)/Gender	20/F	12/M	10/M	28/F	19/F	18/F	18/M	13/M	44/F	24/F	31/F	17/M	10/F	16/M	16/F	11/F	48/M	44/F	62/M	46/F	57/M	44/M	3/M	
Consanguinity	Y	Y	Y	Y	Y	Y	Y	Y	Y	Y	Y	Y	Y	Y	N	NR	N	N	N	N	N	NR	N	
Country of Origin	PK	PK	PK	PK	PK	PR	PL	PL	TR	TR	TR	TR	YM	YM	NR	NR	NL	NL	BR	BR	BR	NR	FR	
Genotype																								
DNAJC6 mutation	c.766 C>T	c.766 C>T	c.766 C>T	c.766 C>T	c.766 C>T	c.2416 C>T	c.801-2A>G	c.801-2A>G	c.2200 C>T	c.2200 C>T	c.2200 C>T	c.2200 C>T	c.2365 C>T	single base pair deletion Exon 5	c.941 T>G	c.2589 delG	c.2779 A>G	c.2779 A>G	c.2223 A>T	c.2223 A>T	c.2038+3 A>G and c.1468 +83del/-	c.2687 C>T and c.1577 A>G	80 KB Micro-del 1p31.3 Exon 5-19	
Recessive/ dominant	R	R	R	R	R	R	R	R	R	R	R	R	R	R	R	R	R	R	R	R	R	R	R	
Protein change	R256*	R256*	R256*	R256*	R256*	R806*			Q734 X	Q734 X	Q734 X	Q734 X	G789 *	Ser194ValfsTer138	V314 G	Met863Ilefs*15	R927G	R927G	Thr74 I=	Thr74 I=		T896M /N526S	-	
Predicted effect	PTV	PTV	PTV	PTV	PTV	PTV	Splice site	Splice site	PTV	PTV	PTV	PTV	PTV	PTV	Mis-sense	PTV	Mis-sense	Mis-sense	Splice site	Splice site	Splice site/-	Mis-sense	-	
CADD score	36	36	36	36	36	40	33	33	38	38	38	38	44	28.8	27.9	34	24,4	24,4	1,78	1,78	11,64/-	25.6 / 8.14	-	

Table 3. 1. Patient characteristics and Genotype in the Patient study cohort and previously published cases. Abbreviations: Pre Pub: Previously published; Y: Years of age; N: No; Y: Yes; PK: Pakistan; PL: Palestine; TR: Turkey; YM: Yemen; NL: Netherlands; BR: Brazil; FR: France; R: Recessive; D: Dominant; PTV: Protein truncating variant. **Blue represents juvenile-onset cases, red represents early-onset cases, orange represents a case without movement disorder but neurological and systemic features.**

	Study Cohort						Previously published cases – juvenile onset parkinsonism										Previously published cases – early onset parkinsonism						Pre Pub
	A-III:1 ₆₅	A-III:4 ₆₅	A-III:5 ₆₅	B-IV:2 ₆₅	B-IV:4 ₆₅	C ⁶⁵	II-2 ⁶⁰	II-4 ⁶⁰	402 ⁶²	502 ⁶²	504 ⁶²	505 ⁶²	4202 ⁹⁶⁴	CR ₁ ¹³⁵	CR ₂ ¹³⁶	CR ₃ ¹³⁷	GPS ₃₁₃ ⁶³	GPS ₃₁₄ ⁶³	PAL ₅₀ ⁶³	PAL ₅₄ ⁶³	BR-2652 ₆₃	CR ₄ ¹³³	III-1 ³¹⁸
Movement Disorder Phenotype																							
Onset of parkinsonism (y)	11	10	9	13	7	10	7	11	10	11	10	10	10	14	17	8	21	29	42	31	33	44.3	-
Initial symptoms	Brad, Tre, Rig	Fine motor difficulties	Fine motor difficulties	Brad, Tre, Rig, HyMi	Brad, Tre, gait deter	Gait deter, post Ins	Brad, Tre, Rig, post Ins, HyMi	Brad	Shuffling gait, Tre	Tre	Brad	Tre, Brad	Brad, Hall	Gait deter, Rig,	Blepharospasm Tre	Gait deter, Tre	Brad, Hand Tre	Brad, Hand Tre	Brad	Hand Tre	Hand Tre	NR	-
Bradykinesia	+	+	+	+	+	+	+	+	+	+	+	+	+	+	+	+	+	+	+	+	+	+	-
Tremor	+	+	-	+	-	+	+	+	+	+	+	+	-	+	+	+	-	+	+	+	+	+	-
Rigidity	+	+	+	+	+	+	+	+	+	+	+	+	+	+	+	+	+	+	+	+	+	+	-
Hypomimia	+	+	+	+	-	+	+	+	+	+	+	+	+	+	+	+	+	+	+	+	+	+	-
Postural instability	+	+	+/-	+	+	+	+	+	+	+	+	+	+	+	+	+	+	+	+	+	+	+	-
Dysarthria	Anarthric	+	+/-	Anarthric	NR	+	+	+	Anarthric	+	Anarthric	+	-	+	+	+	-	-	-	-	-	NR	-
Loss of ambulation (y)	13	Unsteady gait	-	13	10	15	18	13	39	21-26	26	20-25	12	NR	-	NR	NR	NR	NR	NR	NR	NR	-
Motor fluctuations	+	-	-	-	-	+	NR	NR	NR	NR	NR	NR	NR	+	-	+	-	-	+	+	+	+	-
Treatment																							
Response to levodopa/carbidopa (maximum dose)	Unsustained (150mg/day)	Not tried	Not tried	Unsustained (5.5mg/KG/day)	No resp (10mg/KG/day)	Some resp (200mg/day)	NR	No resp	Good	Good	The- rapy refu- sed	Good		Good	No resp	Good	Good, limited by psychiatric side effects	Good, limited by psychiatric side effects	Good, limited by psychiatric side effects	Good	Good	Good	-
Other effective treatments	-	RGT, TRH	RGT, TRH	-	PPX	TRH	-	-	-	-	-	-		-	TRH, BT (Dys-tonia)	PPX	-	-	-	STN-DBS	Palli-doto-my	STN-DBS	-

Table 3. 2. Movement Disorder Phenotype in the Patient study cohort and previously published cases. Abbreviations: Pre Pub: Previously published; NR: not reported; Brad: Bradykinesia; Tre: Tremor; Rig: Rigidity; Gait deter: Gait deterioration; post Ins: Postural instability; HyMi: Hypomimia; resp: Response. BT: Botulinum Toxin; PPX: Pramipexole; RGT: Rotigotin; TRH: Trihexyphenidyl. Blue represents juvenile-onset cases, red represents early-onset cases, orange represents a case without movement disorder but neurological and systemic features.

	Study Cohort						Previously published cases – juvenile onset parkinsonism										Previously published cases – early onset parkinsonism						Pre Pub
	A-III:1 ₆₅	A-III:4 ₆₅	A-III:5 ₆₅	B-IV:2 ₆₅	B-IV:4 ₆₅	C ⁶⁵	II-2 ⁶⁰	II-4 ⁶⁰	402 ⁶²	502 ⁶²	504 ⁶²	505 ⁶²	42029 ⁶⁴	CR ₁ ¹³⁵	CR ₂ ¹³⁶	CR ₃ ¹³⁷	GPS ₃₁₃ ⁶³	GPS ₃₁₄ ⁶³	PAL ₅₀ ⁶³	PAL ₅₄ ⁶³	BR-2652 ₆₃	CR ₄ ¹³⁴	III-1 ³¹⁸
Early development and cognition																							
Early development	D	D	D	D	D	D	NO	NO	NO	D	D	D	NO	NO	NO	D	NO	NO	NO	NO	D	NR	D
Cognition	CI	CI	CI	CI	CI	CI	NO	NO	CI	CI	CI	CI	CI	CI	NO	CI	NO	NO	CI	NO	NO	NR	NR
Additional neurological features																							
Microcephaly	+	+	+	-	-	-	-	-	-	-	-	-	-	NR	NR	NR	-	-	-	-	-	NR	-
Seizures	-	-	-	Gen	-	Gen (staring, atonic)	-	-	-	Gen, Abs	Gen, Abs	Gen, Abs	+	-	-	-	-	-	-	-	+	NR	+
Dystonia	+	+	-	+	-	+	-	-	+	+	+	+	-	+	+	+	-	-	-	-	-	NR	-
Spasticity	-	-	-	-	-	-	-	-	+	+	+	+	+	+	-	-	-	-	-	-	-	NR	-
Eye movements abnormal	+	-	-	-	-	-	Hypome-tric Sacc	-	-	-	-	-	-	NR	-	-	-	-	-	-	-	-	-
Myoclonus	-	-	-	Upper limb	-	-	-	-	-	+	Neg Mcl	-	-	-	-	-	-	-	-	-	-	-	-
Additional neuropsychiatric features																							
Psychiatric features	Anxiety	Anxiety, PsB, SD	-	Anxiety SD	SD	AD, AgB, mild BP	NR	NR	-	Psychosis after levodopa, AgB, Hall	-	-	Psychosis visual & auditory Hall	-	-	-	-	Psychosis	-	-	-	NR	-
Additional systemic features																							
Gastrointestinal dysfunction	+	+	+	-	+	+	-	-	-	-	-	-	-	-	-	-	-	-	-	-	-	NR	-
Other systemic features	Hypothyroid	-	-	-	-	-	-	-	Scoliosis, Pes cavus	-	Scoliosis, Pes cavus	-	-	Short stature, facial dysmorphism	-	-	-	-	-	-	-	NR	Obesity

Table 3.3. Additional clinical features in the Patient study cohort and previously published cases. Abbreviations: Pre Pub: Previously published; D: Delayed; NO: Normal; NR: Not reported; CI: Cognitive impairment; Gen: Generalised seizures; Abs: Absence seizures; AD: Attention deficit; AgB: Aggressive behaviour; PsB: Perseveration behaviour; Hall: Hallucinations; SD: Sleep disturbance; BP: Behavioural problems; Mcl: Myoclonus; Sacc: Saccades. **Blue represents juvenile-onset cases, red represents early-onset cases, orange represents a case without movement disorder but neurological and systemic features.**

3. 5. Synopsis of clinical findings in recessive *DNAJC6* disease

In total, including our study cohort of 6 patients, 23 patients harbouring **biallelic *DNAJC6* mutations** have been described^{61–64,134–137,318}.

Juvenile-onset parkinsonism

The majority of patients (16/23) presented with juvenile-onset parkinsonism at the end of the first or beginning of the second decade (mean age of onset 10.5 years). One patient with an 80 kb deletion encompassing exon 5-19 of the *DNAJC6* gene is asymptomatic from a motor perspective at 7 years of age but is potentially at high risk of developing a movement disorder over time. The movement disorder is characterised by typical parkinsonian symptoms, but shows a rapidly progressive disease course leading to loss of independent ambulation within 10-15 years after onset (**Box 3.1**). Patients with a juvenile-onset often suffer from additional movement abnormalities. Dystonia was the most common movement abnormality observed in 11 patients, followed by spasticity in 6 patients and myoclonus in 3 patients. In addition, the movement disorder was preceded by early developmental delay in 10 out of 16 patients and patients seem to suffer from additional neurological symptoms (epilepsy n=6; cognitive impairment n=13), neuropsychiatric issues (behavioural n=2, psychotic n=3 and anxiety n=3 disorders) as well as systemic features (gastrointestinal dysfunction n=5 and orthopaedic features n=2) (**Box 3.2**). Treatment of juvenile-onset *DNAJC6*-related parkinsonism can be difficult. Levodopa has been administered as a first-line treatment in the majority of patients. Only 6 juvenile-onset cases showed a moderate to good response to levodopa. In 2 cases, levodopa had to be withdrawn due to intolerable side effects. A few other agents including trihexyphenidyl (n=4), pramipexole (n=2) and rotigotine (n=2) have anecdotally shown clinical benefit in single case reports (**Box 3. 3**).

Predominant dystonia with juvenile-onset parkinsonism

Three patients presented with a predominant dystonic phenotype in the beginning: focal cranial dystonia (blepharospasm, jaw opening dystonia, lingual dystonia)¹³⁶, a dystonic gait (“cock walk” gait)¹³⁷ and generalised dystonia¹³⁵. All three patients developed parkinsonism shortly thereafter at the end of the first or in the second decade.

Early-onset parkinsonism

Six patients manifested with a **milder form of early-onset parkinsonism** with onset in their third or fourth decade (mean age of onset 33,3 years) with slower disease progression and preservation of ambulation in 4 of 6 patients (**Box 3.1**). In these patients, no additional movement abnormalities or neurological features including seizures or developmental delay were observed. One patient suffered from cognitive decline and another one from neuropsychiatric symptoms. Overall, patients with early-onset *DNAJC6*-related parkinsonism showed a good response to levodopa with improved motor function, though the dosage had to be adjusted in 3 cases due to marked drug-sensitivity. STN-DBS and bilateral pallidotomy have been undertaken in 3 patients (Patient PAL54, Patient BR2652 and CR4) with clinical benefit (**Box 3.3**).

Disease spectrum of <i>DNAJC6</i> parkinsonism-dystonia
Juvenile-onset parkinsonism with biallelic <i>DNAJC6</i> mutations <ul style="list-style-type: none">• Onset of parkinsonian symptoms (bradykinesia, resting tremor, rigidity, postural instability) at the end of the 1st decade or beginning of the 2nd decade• Neurological regression after onset of movement disorder• Loss of ambulation in mid-adolescence
Dystonia and juvenile-onset parkinsonism with biallelic <i>DNAJC6</i> mutations <ul style="list-style-type: none">• Predominant dystonia (focal cranial, dystonic gait ("cock walk"), generalized) followed by onset of parkinsonism at the end of the 1st decade or in the 2nd decade
Early-onset parkinsonism with biallelic <i>DNAJC6</i> mutations <ul style="list-style-type: none">• Onset of parkinsonian symptoms (bradykinesia, resting tremor, rigidity, postural instability) in the 3^d or 4th decade• Slow progression and better response to treatment
Early-onset parkinsonism with monoallelic <i>DNAJC6</i> mutations <ul style="list-style-type: none">• Onset of parkinsonian symptoms (bradykinesia, resting tremor, rigidity, postural instability) in the 3^d or 4th decade

Box 3.1. Overview of the disease spectrum of *DNAJC6*-related disorders.

Additional neurological, neuropsychiatric and systemic features in *DNAJC6* parkinsonism-dystonia.

- **Development/cognition:** Early developmental delay, intellectual disability
- **Neurological features:** Epilepsy, dystonia, spasticity, eye movement abnormalities, myoclonus
- **Neuropsychiatric features:** Behavioural disturbances, anxiety disorder, sleep disorders, psychosis
- **Systemic features:** Gastrointestinal complications, orthopaedic problems (scoliosis, pes cavus), hypothyroidism, short stature, facial dysmorphism

*Box 3.2. Overview of additional neurological, neuropsychiatric and systemic features in *DNAJC6*-parkinsonism-dystonia.*

Summary of effective treatments in *DNAJC6* parkinsonism-dystonia.

- **Dopaminergic agents:** levodopa (often accompanied by severe psychiatric side-effects and typical motor complications (drug-related dyskinesia, wearing-off effects)) (n=12)
- **Dopamine receptor agonists:** rotigotine (transdermal), pramipexole (selective D2-receptor agonist)
- **Anticholinergic agents:** trihexyphenidyl
- **Surgical treatments:** STN-DBS, bilateral pallidotomy

*Box 3.3. Overview of effective treatments in *DNAJC6*-parkinsonism-dystonia.*

3. 5. 1. Patients with heterozygous *DNAJC6* mutations

In addition to these 23 patients harbouring biallelic *DNAJC6* variants, 4 patients were reported with a monoallelic pathogenic *DNAJC6* variant (c.397A>T, c.626T>C, c.1855C>T, c.2517del), classified as novel or extremely rare in databases and predicted to be deleterious⁶³. Three of these patients presented with sporadic PD and one with familial parkinsonism with an onset between the third to fifth decade (mean age of onset 40.2 years). There was no further information available on the clinical presentation or the disease course of these patients.

3. 5. 2. Overview of molecular genetic features in recessive *DNAJC6*-related disease

The *DNAJC6* gene encodes 970 amino acids and harbours 19 exons (**Figure 3. 4**). Overall, in recessive disease, 15 different mutations have been identified including 4 nonsense, 6 missense, 3 splice site mutations, a homozygous single base pair deletion in Exon 5 and a homozygous 80 kb deletion in the chromosomal 1p31.3 region encompassing exon 5-19 from the *DNAJC6* gene^{61–64,318}. For patients with heterozygous variants, 3 missense variants and 1 nonsense variant have been reported⁶³. Mutations are located throughout the protein but clustering in key protein regions such as the PTEN, Clathrin-binding and J-domain is observed (**Figure 3. 4**). Missense variants or late splicing variants that may result in a partially functional protein seem to be associated with a milder and later-onset phenotype, whereas nonsense mutations or early splice site mutations predicted to cause complete protein deficiency or a non-functional protein are associated with a more severe, juvenile-onset phenotype.

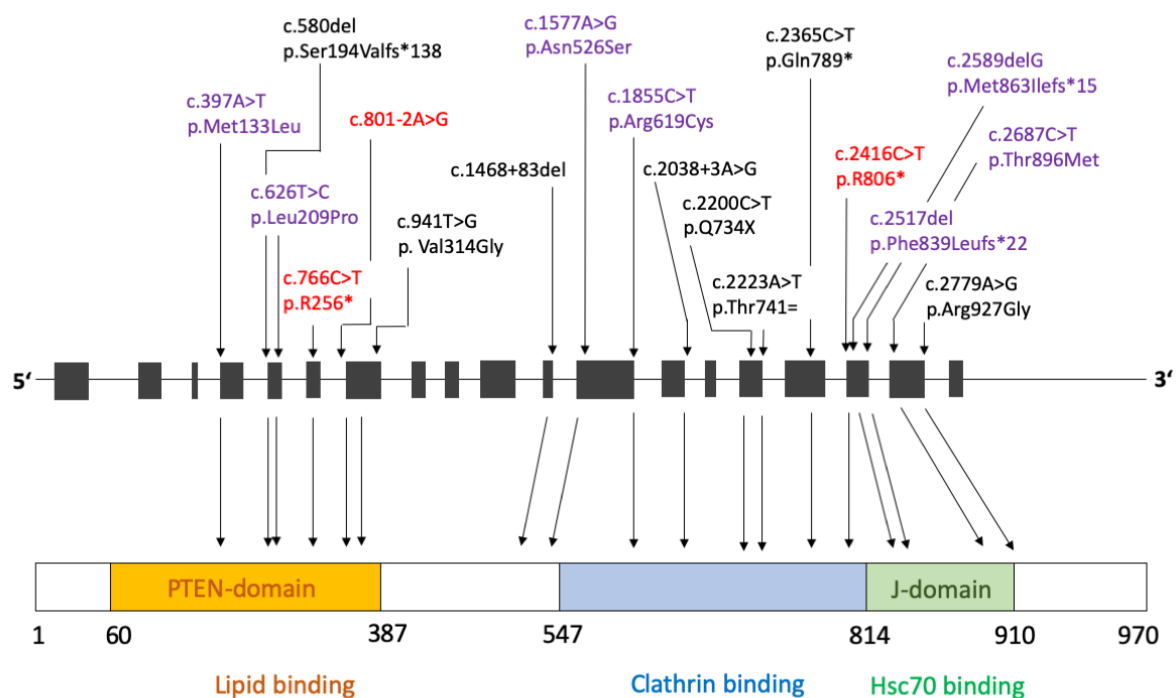


Figure 3. 4. Schematic representation of the *DNAJC6* transcript (upper part) and corresponding domains of auxilin 1 (lower part). All *DNAJC6* variants published to date in biallelic disease are coloured in black, mutations coloured in red are recessive variants identified in our study cohort, mutations coloured in purple are heterozygous variants (Figure modified from Olgiati et al. and Ungewickell et al.^{63,142}).

3. 5. 3. Diagnostic investigation in *DNAJC6* patients

DaTScanTM and brain MRI

DaTScanTM imaging showed abnormal tracer uptake in the basal ganglia in three patients of our study cohort. ¹⁸F-DOPA-PET was performed in two further published cases with a later-onset disease (Patient GPS 313 and GPS314) and similarly demonstrating striatonigral abnormalities⁶³.

Brain MRI was abnormal in four patients from our study cohort showing mild to moderate generalised cerebral atrophy and additional cerebellar atrophy in two patients. Another case (Patient 402) published by Köroglu et al. showed generalised atrophy⁶². MRI was not performed in the Patient III-1 with the 80kb microdeletion and no information on brain imaging was available in the Patient with the compound heterozygous missense variants c.2687C>T and c.1577A>G. The remaining other patients published to date (n=14) demonstrated normal brain MRIs.

EEG findings

Two patients from our study cohort (Patient B-IV:2 and Patient C) manifested generalised seizures. There were no EEG reports available from these patients. Another three published cases (Patient 502, 504, 505) were reported to have generalized and absence seizures⁶², and in a fourth case (Patient 420), seizure semiology was not specified⁶⁴. EEG data was available in four patients: For Patient 420, EEG demonstrated diffuse encephalopathy with focal epilepsy⁶⁴. For Patient 502 there were generalized epileptiform discharges⁶². EEG was normal in another two patients suffering from generalized and absence seizures (Patient 504 and 505)⁶².

Laboratory studies

Complete blood count and routine biochemistry analysis were normal where available⁶². CSF neurotransmitter analysis was performed in three patients of our study cohort only and demonstrated isolated reduced HVA, but to my knowledge has not yet been reported elsewhere in the literature for this disorder.

3. 6. Discussion

I took part in a comprehensive clinical and molecular characterisation of a cohort of six patients with bi-allelic *DNAJC6* mutations. Five patients from two consanguineous families originating from Pakistan and one unrelated patient presented with early neurodevelopmental delay,

juvenile parkinsonism and neurological regression thereafter and all were diagnosed with novel *DNAJC6* mutations. Overall, *DNAJC6* mutations are rare in juvenile-onset parkinsonism, but the phenotypic spectrum is further expanding and now includes cases with predominant dystonia at the beginning of the disease and later onset parkinsonism. In line with their clinical parkinsonism, DaTScanTM imaging in patients shows evidence of nigrostriatal neurodegeneration. Neurotransmitter findings in our cohort revealed isolated decreased HVA, which, together with early clinical findings, may mimic some primary neurotransmitter disorders. Molecular studies in CSF demonstrated reduced auxilin protein and increased GAK protein levels as well as reduced synaptic protein levels indicating disturbance of dopamine homeostasis.

In summary, clinical, imaging and molecular findings of this cohort provide additional insights into the disease spectrum and pathology underpinning *DNAJC6* parkinsonism-dystonia. In order to further elucidate the molecular disease mechanisms, three patients from our cohort donated fibroblasts, which were used for reprogramming to establish a dopaminergic neuronal cell model in this PhD project (Chapter 4-6).

CHAPTER 4

Human induced pluripotent stem cell reprogramming and characterisation

4. 1. Introduction

iPSC technology has substantially changed the way we can model human neurological diseases. iPSCs can be differentiated towards disease-relevant neuronal cell types that are otherwise difficult to access in order to study the underlying disease mechanisms. A further advantage of iPSC-derived *in vitro* models is the retention of the patient-specific genetic background, which allows studies in a truly humanised system, as well as generation of isogenic controls to confirm robust disease phenotypes. As a starting material for generation of desired cell types, iPSCs should always undergo stringent quality control assessments. A number of benchmarks have been established to evaluate molecular and cellular identity of iPSCs based on the initial characterisation of hESCs¹⁹². Genomic integrity, pluripotency and cellular morphology are key criteria in iPSC quality control. Different methods have been established over time including karyotyping, analysis of pluripotent cell surface markers by FACS or immunohistochemistry and analysis of pluripotent gene expression profiles as well as the ability to differentiate into all three germ layers using teratoma formation assay or *in vitro* spontaneous differentiation assay.

The following chapter describes the generation of iPSCs derived from patient dermal fibroblasts and subsequent assessment of Sendai virus clearance, genomic integrity and pluripotent identity.

4. 2. Reprogramming of patient's dermal fibroblasts into iPSC

4. 2. 1. Patient lines

HDF from four patients with bi-allelic *DNAJC6* mutations were taken with written informed consent and reprogrammed to hiPSCs. HDF from Patient 1 (A-III:1) and Patient 2 (B-IV:4) were taken by Dr. Joanne Ng in Prof Kurian's Neurogenetic Movement Disorders Clinic at Great Ormond Street Hospital. HDF from Patient 3 have been kindly provided by Dr. Toni Pearson at Columbia University Irving Medical Center, New York, and HDF from Patient 4 (II-4) have been kindly provided by Dr. Simon Edvardson and Prof. Orly Elpeleg at Hadassah, Hebrew University Medical Center, Jerusalem, Israel. Reprogramming of Patient 3 and 4 until Passage 6 was performed by Dr. Serena Barral. Detailed clinical characterisation of these patients is provided in Chapter 3. **Table 4. 1** provides a summary on the patient's genotype and phenotype.

Patient	iPSC lines	Sex	Age of onset	Clinical phenotype	Genotype
Patient A-III:1	<i>DNAJC6</i> Patient 1	F	11	Early onset parkinsonism-dystonia, developmental delay, neuropsychiatric features	c.766C>T, p.R256* Homozygous
Patient B-IV:4	<i>DNAJC6</i> Patient 2	F	7	Early onset parkinsonism-dystonia, developmental delay, neuropsychiatric features	c.766C>T, p.R256* Homozygous
Patient C	<i>DNAJC6</i> Patient 3	F	10	Early onset parkinsonism-dystonia, developmental delay, seizures	c.2416C>T, p.R806* Homozygous
Patient II-4	<i>DNAJC6</i> Patient 4	M	11	Early onset parkinsonism-dystonia	c.801-2 A>G Homozygous

Table 4. 1. Overview on clinical and genetic features of *DNAJC6* patients. iPSC lines were generated from four patients. Clinical phenotype is summarised in Chapter 3 of this thesis and in Ng J*, Cortès-Saladelafont E*, Abela L* et al. 2020⁶⁵ for Patient A-III:1, Patient B-IV:4 and Patient C, and in Edvardson et al. 2012⁶¹ for Patient II-4.

4. 2. 2. Control lines

Reprogramming of two healthy control iPSC lines (HDF 7301-05, Ctrl 582-06) and subsequent iPSC characterisation including karyotype analysis, Sendai Virus clearance and analysis of pluripotency markers by PCR and immunofluorescence analysis was previously performed by Dr. Serena Barral (HDF 7301-05 or Control 03) in Prof Kurian's laboratory at UCL Institute of Child Health and in Professor Ludovic Vallier's laboratory (Ctrl 582-06 or Control 05), Wellcome Trust-Medical research Council Cambridge Stem Cell Institute (Anne McLaren Laboratory for Regenerative Medicine, Cambridge, UK). These lines are regularly used by the Kurian group for disease-modelling projects.

4. 2. 3. Generation of a CRISPR-Cas9 corrected line for Patient 2-1

A CRISPR/Cas9 corrected line for Patient 2 was outsourced to Applied StemCell Inc. (Milpitas, CA). Initially, two sgRNAs were designed targeting the *DNAJC6* genomic locus and subsequently validated in HEK293 cells for CRISPR-Cas9 cutting efficiency. Patient 2 recipient iPSCs were then co-transfected with sgRNAs and a ssODN using the Neon transfection system (Invitrogen) to induce endogenous homology repair. Single cells were isolated in 96-well plates for 14 days and subsequently transferred to 24-well plates for further expansion. Correction of the homozygous *DNAJC6* mutation was confirmed by PCR analysis and both clones subsequently underwent karyotype analysis to confirm genomic integrity.

4. 2. 4. Sendai-Virus reprogramming

I reprogrammed HDF using the CytoTune™-iPS 2.0 Sendai Reprogramming Kit based on a modified Sendai Virus vector that carries four key transcription factors: OCT4, SOX2, KLF4 and C-MYC (**Figure 4. 1**). Sendai Virus is an RNA virus that does not integrate into the host genome and viral particles and reprogramming factor genes are gradually cleared from the host cell. Transfected HDF are then transferred to MEF on day 6 and closely monitored. Morphological changes usually become evident around day 11-12 after transduction and first colonies start to appear around day 20 post-transduction. For each patient line, 10-15 individual colonies are manually picked between day 30-35 post-transduction. Single clones are expanded individually and stabilised on MEF feeder cells. Around passage 10-11, the clones are transferred to feeder-free conditions on Matrigel/mTeSR1 (**Figure 4. 1**).

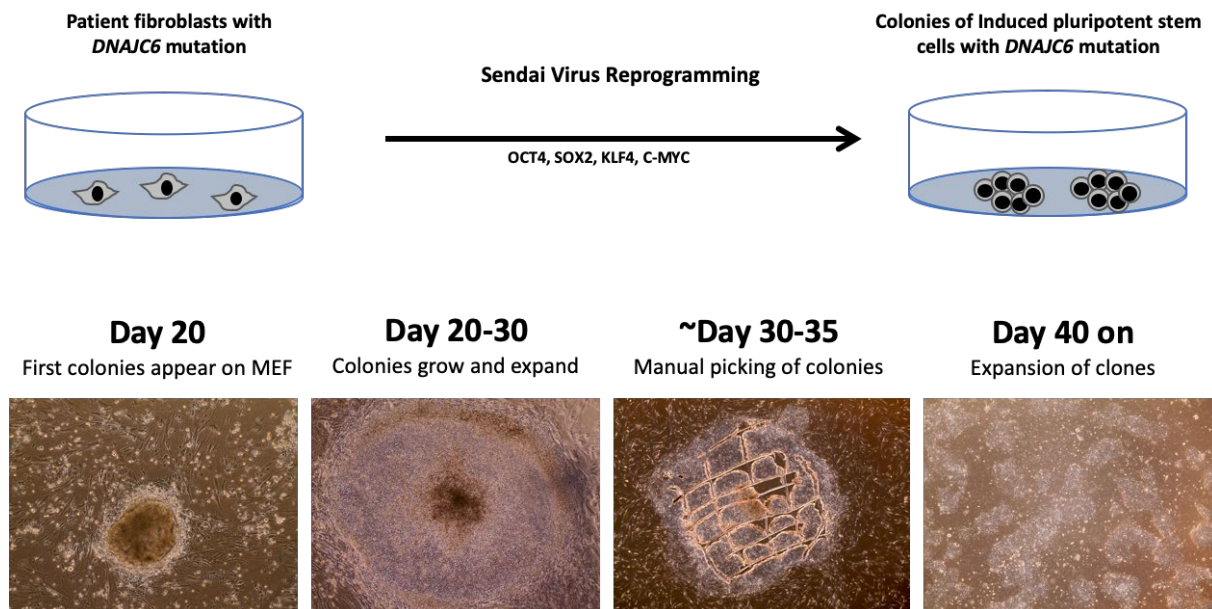


Figure 4. 1. Overview on Sendai Virus reprogramming. *Upper panel:* Schematic representation of the reprogramming process using the CytoTune™-iPS 2.0 Sendai Reprogramming Kit. **Lower panel:** Patient HDF are transfected at day 0 and transferred to MEF feeder cells at day 6. First iPSC colonies emerge around day 20 and are manually picked between day 30-35. iPSC manifested typical morphological features with sharp edges and high nuclear-to-cytoplasm ratio. The clones are individually expanded, stabilised and transferred to Matrigel and mTeSR1 medium.

4. 3. Characterisation of genomic integrity

4. 3. 1. Confirmation of a normal karyotype following reprogramming

During the process of reprogramming, genomic changes such as aneuploidy and chromosomal aberrations such as CNV and SNV can be acquired. These may alter the differentiation potential of iPSCs or induce tumorigenicity and thus severely impact further downstream applications and identification of true disease phenotypes^{323,324}. Of note, genetic variation can also be transferred from individual donor cells or be acquired during prolonged culture times³²³.

Confirmation of chromosomal integrity is thus of utmost importance before proceeding towards differentiation. Different techniques can be used to detect chromosomal aberrations. G-banding is a conventional karyotyping method that stains condensed chromosomes and is able to detect chromosomal imbalances greater than 5-10 megabases (Mb). With newer methods including array-based techniques, resolution has markedly improved. We used the Illumina CytoSNP-12-v2.1 BeadChip array, a high-throughput whole-genome scanning platform that incorporates around 300,000 SNPs targeting regions and can be carried out within a couple of days (3 days).

All newly reprogrammed iPSC lines were analysed using the Illumina CytoSNP-12-v2.1 array (**Table 4.2**). Patient 1 and 2 both had two clones (1-2, 2-2) that acquired significant chromosomal gains (>5 Mb). Clone 1-2 acquired a 34.6 MB gain and clone 2-2 a 113.6 Mb gain (represented in green, red circles) (**Figure 4. 2**). Both were excluded from downstream applications. The remaining iPSC lines (Patient 1-1, 2-1, 3-1, 3-2, 4-1, 4-2, CRISPR 2-1_A and CRISPR 2-1B) showed a normal karyotype.

Genotype	iPSC line	iPSC clone	Patient nomenclature in Abela et al. 2024 ³⁰¹
c.766C>T, p.R256* Homozygous	Patient 1	Patient 1-1 Patient 1-2	
c.766C>T, p.R256* Homozygous	Patient 2	Patient 2-1 Patient 2-2	Patient 1
c.2416C>T, p.R806* Homozygous	Patient 3	Patient 3-1 Patient 3-2	Patient 2
c.801-2 A>G Homozygous	Patient 4	Patient 4-1 Patient 4-2	Patient 3
c.766T>C	CRISPR 2-1	CRISPR 2-1_A CRISPR 2-1_B	CRISPR 2-1

Table 4. 2. Overview on generated iPSC lines and corresponding clones. The clones highlighted in red are used for final experiments.

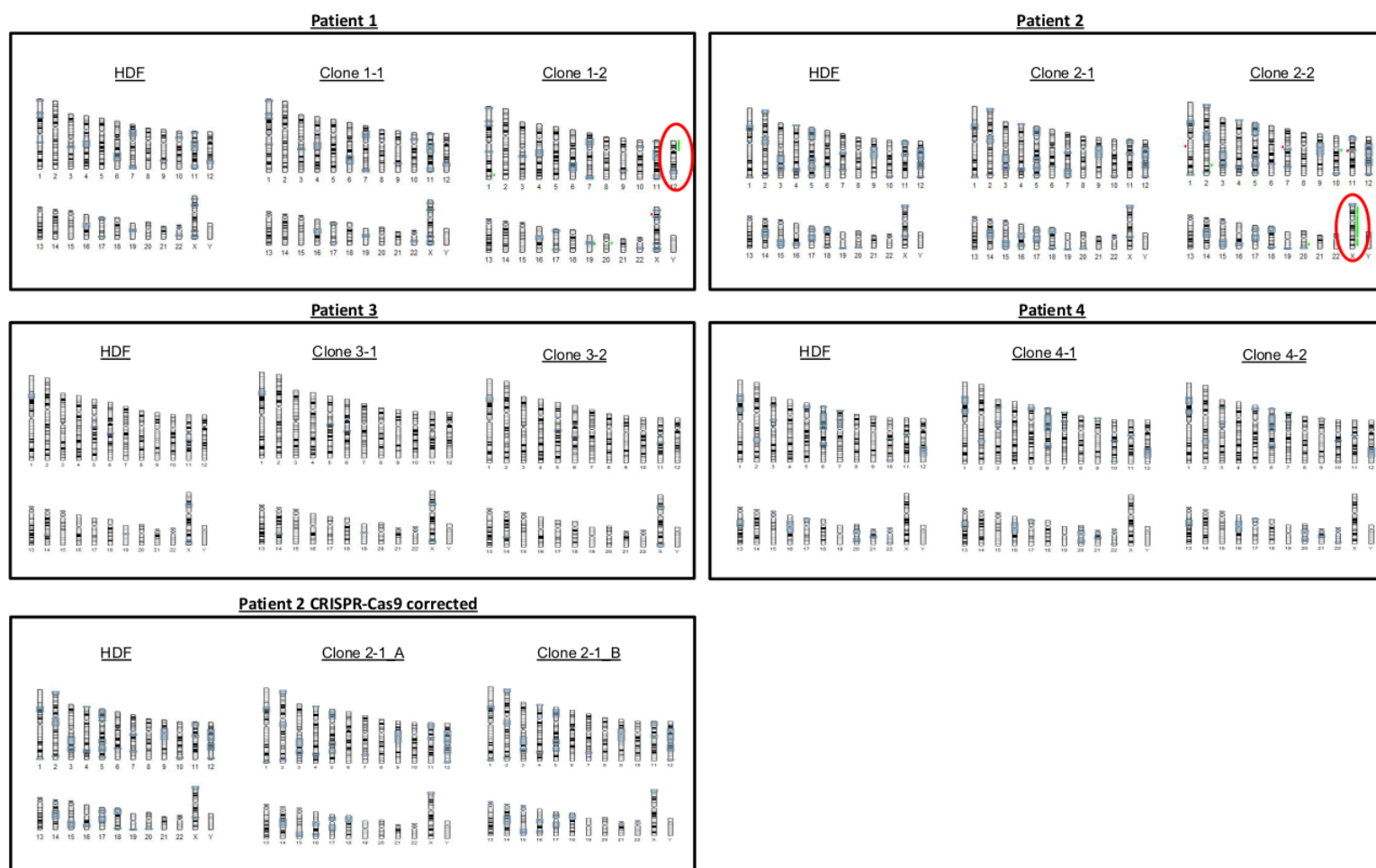


Figure 4. 2. Illumina CytoSNP-12-v2.1 BeadChip array analysis for newly generated DNAJC6 iPSC lines. Two clones were analysed for each patient line and compared to their corresponding fibroblast line. Clone 1-2 and clone 2-2 acquired a 34.6 Mb gain and a 113.6 Mb gain (green), respectively. The remaining iPSC lines retained chromosomal integrity pre- and post-reprogramming. Green lines indicate chromosomal gain (indicated in green). Blue regions represent loss of heterozygosity.

4. 3. 2. Retention of patient-specific mutations following reprogramming

In addition to the assessment of karyotypic abnormalities, it is crucial to confirm that patient-specific mutations have been retained during reprogramming. Genomic DNA was extracted from all newly generated iPSC lines. Dr. Katy Barwick subsequently performed Sanger sequencing for the patient-specific *DNAJC6* mutation. All iPSC lines retained their patient-specific mutation when compared to a healthy control line (**Figure 4. 3**).

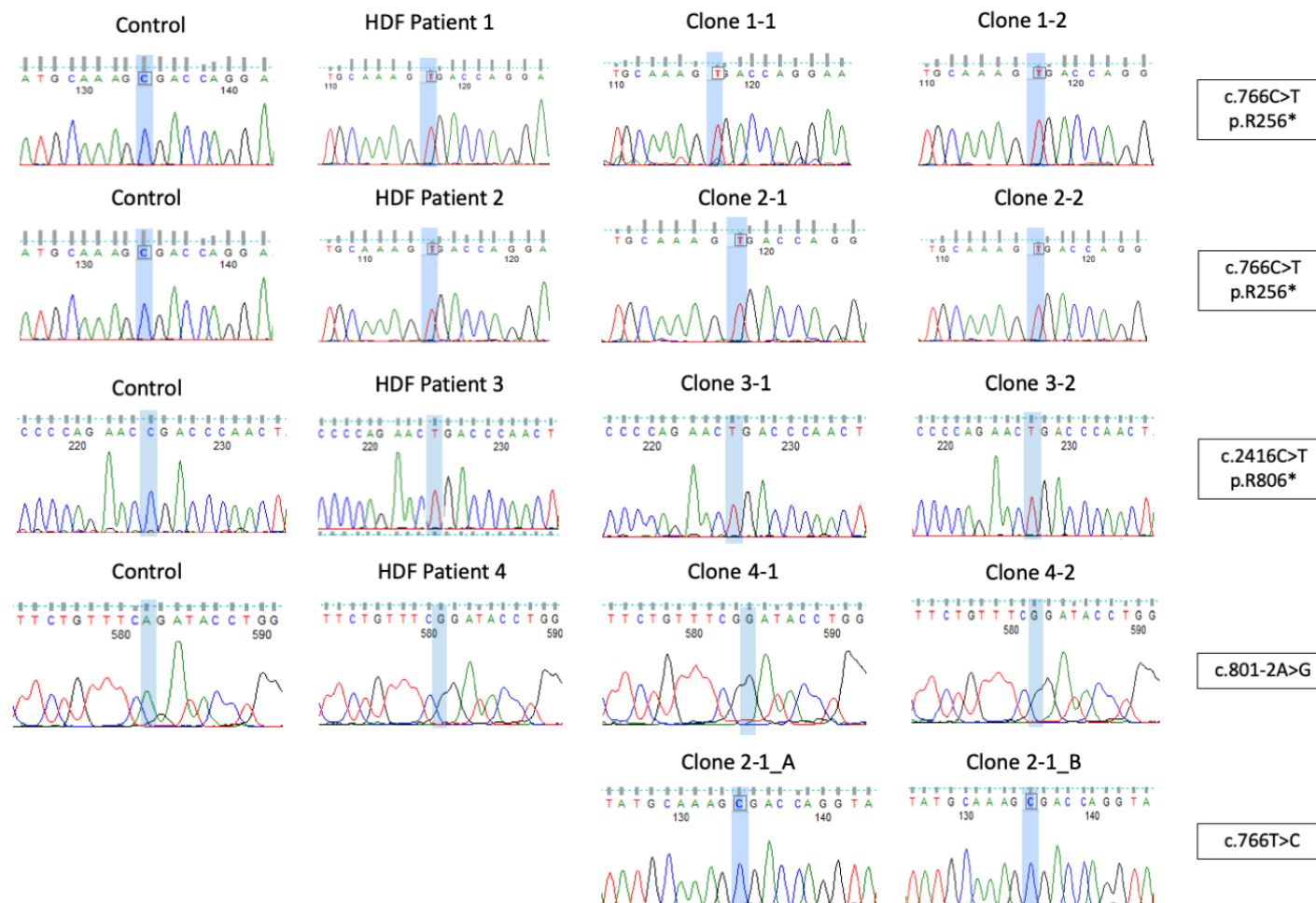


Figure 4. 3. Direct Sanger sequencing for specific DNJC6 mutations for all newly generated iPSC lines. Direct Sanger sequencing confirmed retention of the corresponding patient-specific mutation in all iPSC lines when compared to their corresponding fibroblast line (HDF). A control reference sequence showing the wild- type sequence is also included.

4. 4. Characterisation of pluripotent identity

4. 4. 1. Sendai Virus clearance of patient and control iPSC lines

Sendai Virus is a non-integrating RNA virus that is expelled from the cell with sequential passages. To confirm complete clearance of all viral particles and transgenes, I performed PCR using virus-specific markers. All iPSC lines proved negative for the respective reprogramming transgenes and the Sendai Virus backbone (**Figure 4. 4**).

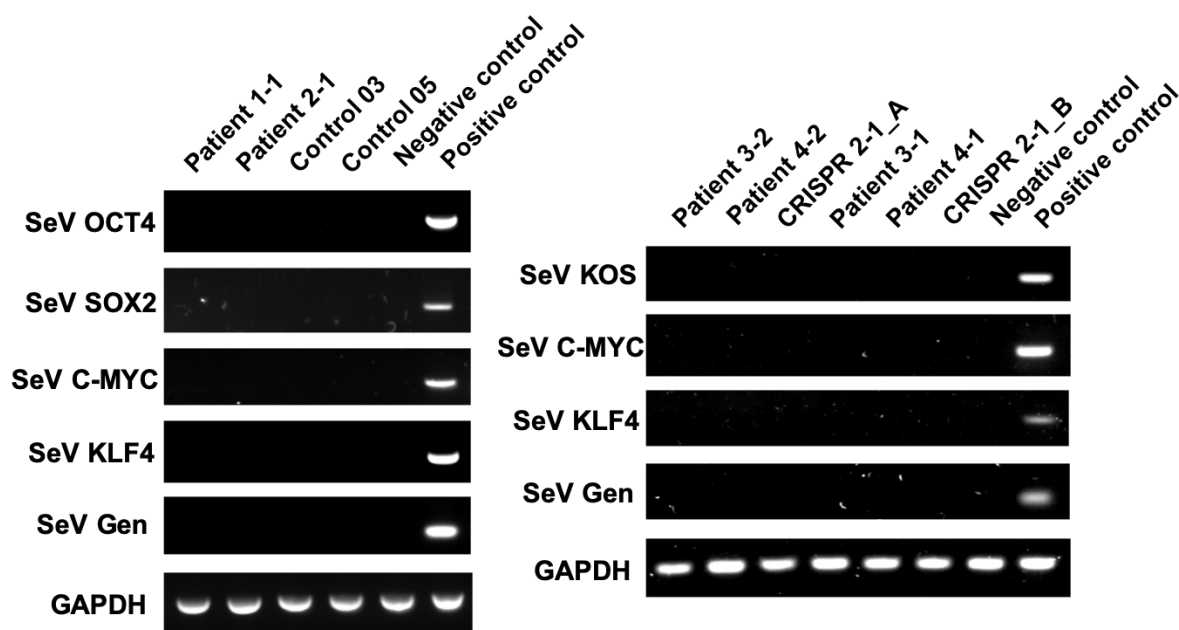


Figure 4. 4. Sendai Virus clearance in patient- and control iPSC lines. RT-PCR analysis confirms absence of the four virally delivered markers OCT4, SOX2, C-MYC, KLF4 and SeV genome in all indicated patient and control iPSC lines as well as in a human embryonic stem cell line as a negative control, while all the markers are present in the positive control line. A newer kit was used for the second reprogramming (Patient 3 and 4 and CRISPR-Cas9 corrected Patient 2 with SeV KOS replacing OCT4 and SOX2). GAPDH was used as a loading control.

4. 4. 2. Typical cellular morphology of patient and control iPSC lines

Undifferentiated cultured iPSCs exhibit typical morphological characteristics reminiscent of embryonic stem cells. They grow in compact colonies with well-defined borders and tightly packed cells in single layers. The cells have a high nuclear-to-cytoplasm ratio. Regular manual inspection of iPSC colonies is important to ascertain that all lines develop typical morphological features and to monitor the quality of the culture. All newly generated iPSC lines demonstrated typical iPSC morphology (**Figure 4. 5**).

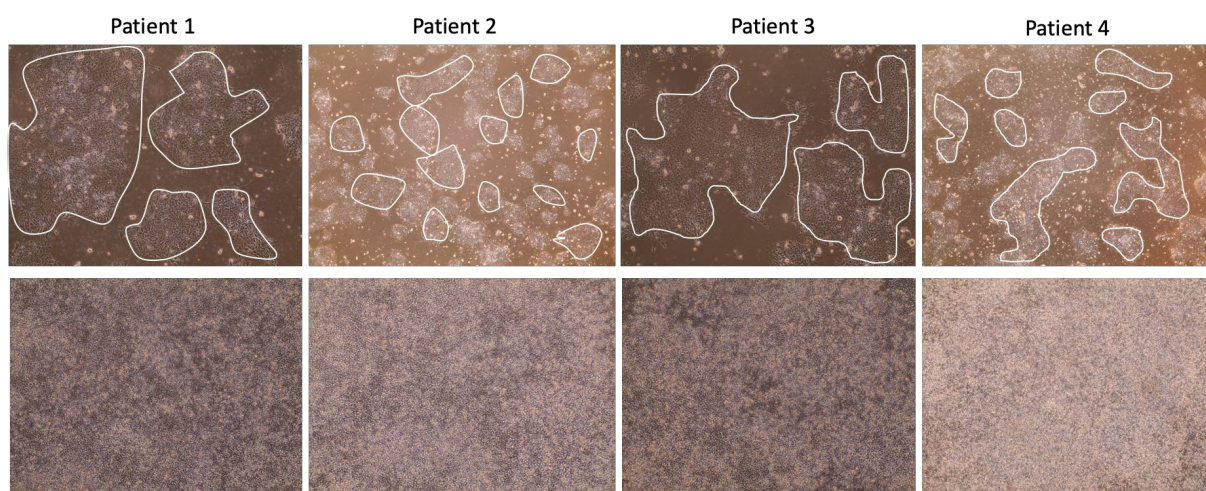


Figure 4. 5. Typical morphological aspects of iPSCs grown on Matrigel. Representative images of all newly generated patient iPSC lines. iPSC colonies demonstrate typical sharp edges (upper panel, demarcated with white lines). iPSC shown in a confluent state (lower panel) with cells demonstrating high nuclear-to-cytoplasm ratio. Images were acquired on an EVOS XL Core Tissue Culture Microscope at 10x magnification.

4. 4. 3. Expression of pluripotency markers in patient and control iPSC lines

During reprogramming, iPSCs acquire a distinct gene expression profile that is characteristic of non-differentiated cells. To confirm expression of several well-established pluripotency genes³²⁵, I selected a panel of pluripotency markers including *REX1*, *ESG1*, *SOX2*, *NANOG* and *OCT4* for RT-PCR. A human embryonic stem cell line was used as a positive control, and a fibroblast line (HDF) served as negative control. All patient and control lines expressed pluripotency markers (**Figure 4. 6**).

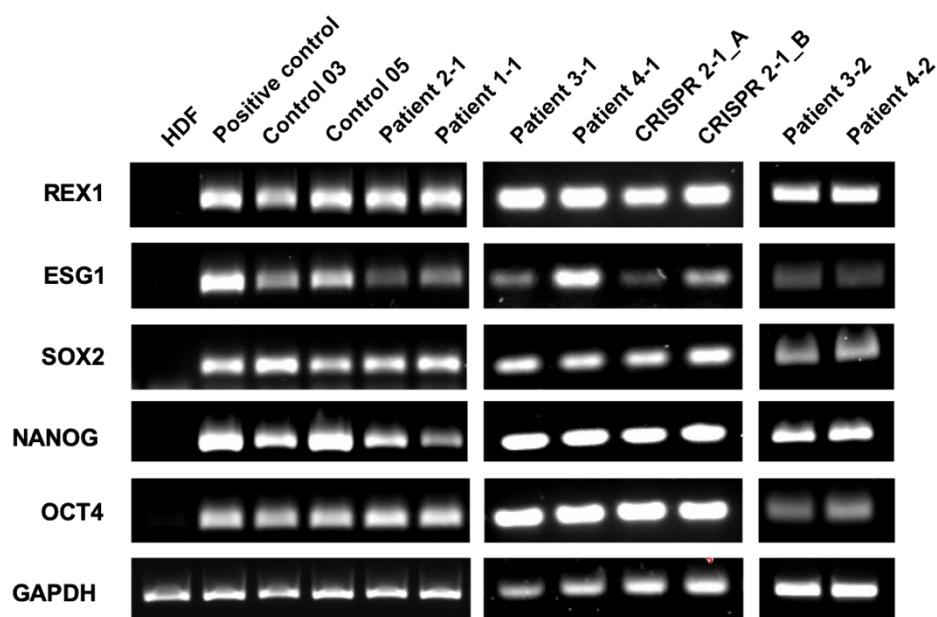


Figure 4. 6. PCR analysis for expression of pluripotency markers in patient and control iPSC lines. RT-PCR analysis demonstrated presence of common pluripotency markers including REX1, ESG1, SOX2, NANOG and OCT4 in all indicated patient and control iPSC lines as well as in a human embryonic stem cell line as a positive control. HDF represents a negative control sample. GAPDH is used a loading control.

Pluripotent identity of the generated iPSC lines was further investigated by immunocytochemistry using the cell surface markers TRA-1-60 and TRA-1-81 and the nuclear markers OCT4 and NANOG. Immunocytochemistry analysis demonstrated staining for these pluripotent markers in all patient and control lines (**Figure 4. 7**).

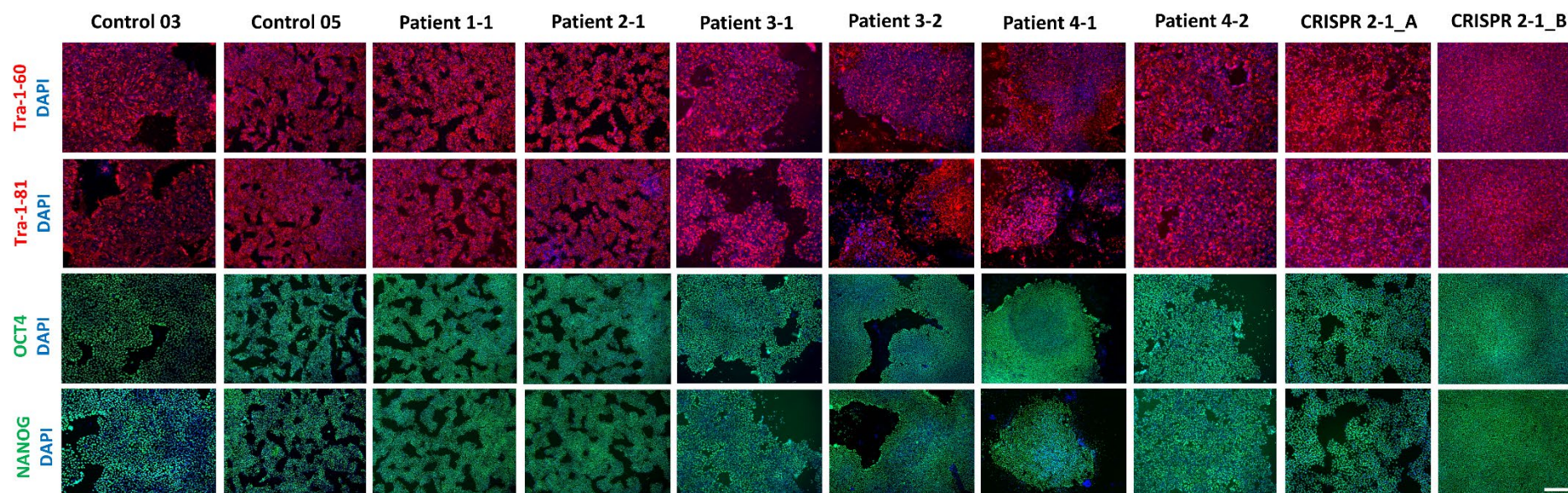


Figure 4. 7. Immunofluorescence analysis for pluripotency markers in patient and control iPSC lines. Immunofluorescence analysis showed expression of the pluripotency markers TRA-1-60, TRA-1-81 (red), OCT4, and NANOG (green) in all indicated patient and control iPSC lines. Nuclei were stained for DAPI (blue). Images of Control 05 have been kindly provided by Dr. Dimitri Budinger. Scale bar represents 100 μ m.

4. 4. 4. Pluripotent gene expression profiling in patient and control iPSC lines

PluriTest is a quantitative biomarker assay that provides a numeric value, the so-called Epi-Pluri-Score, that can differentiate between pluripotent and somatic cells based on differential gene expression profiles³²⁶. The score summarises the DNA methylation levels of two CpG sites in the genes *ANKRD46* and *C14orf115* as well as one CpG site within the pluripotency-associated gene *POU5F1* (also known as *OCT4*). *ANKRD46* is usually methylated in pluripotent cells, while *C14orf115* is unmethylated in pluripotent cells. The methylation values or β -values of the respective genes are then plotted against each other. The blue cloud refers to the DNA methylation profiles of 1,951 non-pluripotent cells, while the red cloud summarises DNA methylation profiles of 264 pluripotent cells. The Epi-Pluri-Score classified all patient and control iPSC lines as pluripotent clustering in the red cloud (**Figure 4. 8**).

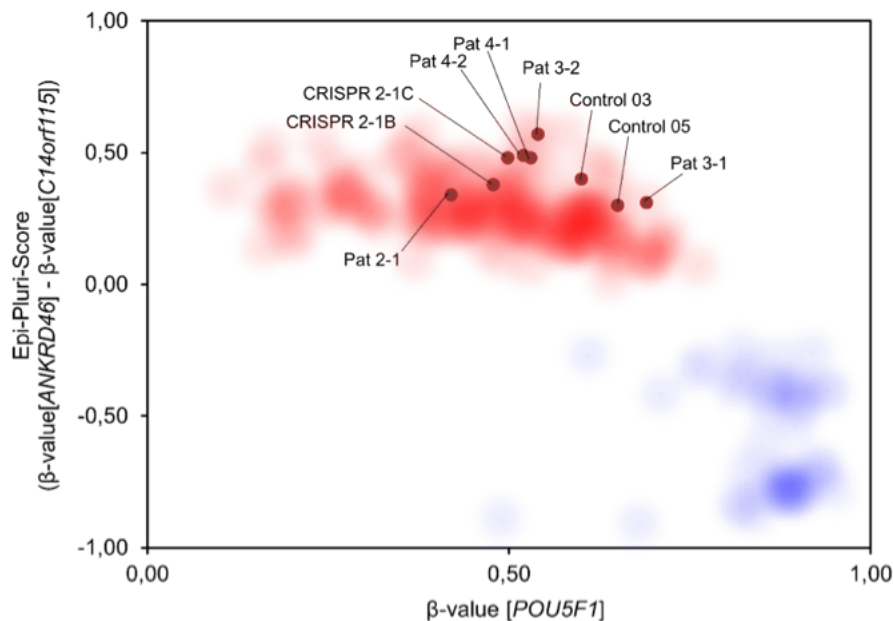


Figure 4. 8. Epi-Pluri-Score analysis in patient and control iPSC lines. The PluriTest Assay confirms that all indicated patient and control iPSC-lines are represented in the red, pluripotent cloud. The blue cloud represents somatic gene expression profile. (Figures provided by Cygenia). CRISPR 2-1B corresponds to CRISPR 2-1_A and CRISPR 2-1C corresponds to CRISPR 2-1_B.

4. 4. 5. *In vitro* spontaneous differentiation assay in patient and control iPSC lines

One of the cellular hallmarks of stem cells is the potential to differentiate into all three germ layers: the ectoderm, endoderm and mesoderm. Initially, an *in-vivo* teratoma assay was the most

widely used technique to assess trilineage differentiation potential. When implanted into immune-compromised mice, hESCs form heterogeneous tumours that contain tissue and cells from all three germ layers³²⁷. Formation of these tumours usually takes 6-12 weeks, followed by histopathological analysis. Due to the laborious, time-consuming and cost-prohibitive assay and in accordance with the 3R principles³²⁸, alternative *in vitro* assays have now been developed. For this project, I performed an EB-based spontaneous *in vitro* differentiation assay to induce mesoderm, endoderm and ectoderm formation. EBs are early embryonic structures that have the capacity to develop into all three embryonic germ layers³²⁹. EBs form spontaneously when cultured in suspension. I observed that all iPSC lines express markers indicative of mesoderm (smooth muscle actin [SMA] or Brachyury), neuroectoderm (neurons-specific class III beta-tubulin [TUBJ1]) and endoderm (SOX17) (**Figure 4. 9**). For Control 05, the STEMDiff Trilineage Differentiation Kit (StemCell Technologies) was used.

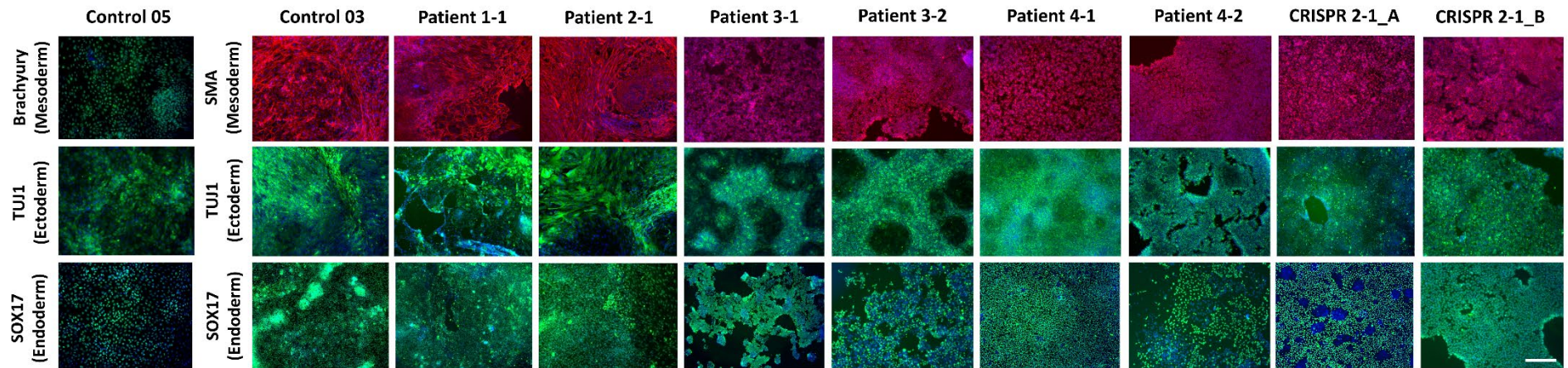


Figure 4. 9. Spontaneous in vitro differentiation in DNAJC6 and control iPSC lines. Cells were differentiated for 16 days and subsequently fixed and stained. Immunofluorescence analysis in all indicated patient and control iPSC lines showed positive staining for all three germ layers, indicated by smooth muscle actin (SMA) or Brachyury (mesoderm), neurons-specific class III beta-tubulin (TUJ1) (neuroectoderm) and SOX17 (endoderm). Nuclei were stained for DAPI (blue). Images of Control 05 have been kindly provided by Dr. Dimitri Budinger. Images were acquired using the inverted Fluorescence microscope Olympus IX71 at 20x magnification. Scale bar represents 100 μ m.

4. 5. Discussion

In this chapter, I have demonstrated successful reprogramming of patient-derived dermal fibroblasts from four patients harbouring pathogenic bi-allelic *DNAJC6* mutations. Subsequent comprehensive characterisation was performed for two clones of each patient line.

Generation and maintenance of human iPSCs for a variety of applications including disease modelling or therapeutic approaches requires stringent quality control assessments. High-quality iPSC cultures will minimise line variability, increase reproducibility and reliability of identified disease phenotypes. For the reprogramming of patient HDF, I have selected the CytoTune™-iPS 2.0 Sendai Reprogramming protocol, a non-integrating reprogramming strategy. Reprogramming was successful for all four HDF lines and provided iPSC colonies with typical morphological characteristics. Two clones per patient line were selected and further expanded. Once stabilised, each clone underwent comprehensive quality control assessments. Using the Illumina CytoSNP-12-v2.1 BeadChip array, genomic integrity was assured for all clones except two clones (1-2 and 2-2), which acquired significant chromosomal gains. These clones were excluded from further downstream experiments. Retention of patient-specific mutations post-reprogramming was demonstrated by Sanger sequencing for all iPSC lines. Pluripotent identity of the generated iPSC lines was assessed using several assays. PCR analysis confirmed expression of pluripotency markers *REX1*, *ESG1*, *SOX2*, *NANOG* and *OCT4*, while immunohistochemistry showed positive staining for the cell surface markers TRA-1-60 and TRA-1-81 and the nuclear markers OCT4, and NANOG. Gene expression analysis finally demonstrated a pluripotent gene expression profile for all patient and control iPSC lines. Trilineage differentiation potential, a typical characteristic of pluripotent cells, was demonstrated for all iPSC lines using an *in vitro* spontaneous differentiation assay based on EB formation.

Overall, reprogramming, clonal expansion and characterisation is a laborious and time-consuming process that takes about 6 months' time. For this PhD, I performed Sendai Virus reprogramming, a reliable method that has been established in my host laboratory and has been previously used for the generation of two control iPSC lines. Other reprogramming methods including integrating viral (lentivirus, retrovirus) and non-viral strategies (mRNA, miRNA) have similar timescales. The overall rather low reprogramming efficiency of these methods has been optimised with newer protocols such as a synergistic combination of modified mRNAs

encoding reprogramming factors and miRNA-367/302s³³⁰ or microfluidic technology³³¹. The number of cell lines being reprogrammed per person in one experimental round is limited (usually 2-4)³³². In order to reduce costs and time, attempts have been made to set up reprogramming platforms for large-scale iPSC production³³². Increasing efficiency and consistency of reprogramming protocols will ease the associated workload and allow generation of multiple patient and control lines, which will definitely contribute to the robustness of iPSC-derived disease models.

In June 2023, the ISSCR has released updated comprehensive Guidelines for Human Stem Cell Use in Research (<https://www.isscr.org/standards-document>). Basic characterisation includes acquisition of material, initial biobanking, establishing identity and authentication, transgene clearance and basic cell hygiene. Recommendations for assessing pluripotency include expression of undifferentiated stem cell markers and quantitative assay of differentiation into progenitors of three germ layers, and, for newly generated lines differentiation into one or more tissue cell types. For the generated iPSC lines in this PhD project, all the requirements have been fulfilled. Guidelines for genomic characterisation include different types of karyotype analysis such as SNP/CGH arrays, qPCR/ddPCR and FISH as well as next generation sequencing methods. Importantly, monitoring for genetic aberrations should be performed before and during the time of experiments. For this PhD project, assessment of pluripotency and genomic integrity of newly generated iPSC lines has been accomplished according to the proposed guidelines. In order to fully characterise the generated iPSC lines, whole genome sequencing of reprogrammed lines will become increasingly necessary in the future. According to the standards in my host laboratory, iPSCs were not kept in culture for longer than 3 months to minimise the risk of genetic aberrations.

In summary, I provide proof that all iPSC lines generated, except two clones, retain genetic integrity post reprogramming and show truly pluripotent characteristics. The generated iPSC lines are thus a reliable source for further downstream differentiation.

CHAPTER 5

Generation and characterisation of a midbrain dopaminergic neuronal cell model for *DNAJC6* parkinsonism-dystonia

5. 1. Introduction

Neurodegenerative disorders can often affect distinct neuronal cell populations as seen in PD, amyotrophic lateral sclerosis or distinct forms of dementia. Bi-allelic mutations in *DNAJC6* are associated with juvenile-onset parkinsonism and additional neurodevelopmental, neurological and neuropsychiatric features. In patients with homozygous *DNAJC6* mutations, DaTScanTM imaging demonstrates reduced tracer uptake in the basal ganglia indicating impaired presynaptic dopamine uptake and ultimately nigrostriatal neurodegeneration. Both clinical and imaging features clearly demonstrate involvement of the dopaminergic system. Dopaminergic neurons are thus specifically vulnerable to *DNAJC6* deficiency, though it is likely that other neuronal cell populations are affected as well given the complex neurodevelopmental phenotype. To generate a robust disease model for this PhD and investigate the underlying pathomechanisms in disease-relevant neurons, I opted to differentiate the generated iPSC lines into mDA neurons.

The following chapter describes the differentiation and basic characterisation of patient-derived mDA neurons. Some sections and figures have been adapted from publications arising from this research, including Ng J^{*}, Cortès-Saladelafont E^{*}, Abela L^{*} et al., 2020⁶⁵ and Abela et al., 2024³⁰¹.

5. 2. Results

5. 2. 1. Midbrain dopaminergic neuron differentiation

To differentiate iPSC into mDA neurons, I used a modified protocol based on Kirkeby et al. which combines dual SMAD-inhibition together with EB formation for efficient neural induction (**Figure 5. 1**)²³². Upon single cell dissociation at day 11 and day 30, mDA neurons reach terminal differentiation at day 60-65. Mature mDA neurons are characterised by expression of mature ventral midbrain markers, typical cell morphology and electrophysiological properties. Kirkeby et al. showed that hESC-derived VM grafts in a rat PD model showed GIRK2-expression, which is a typical marker of nigral A9 mDA neurons²³². The A9 mDA neuron population projects to the striatum *in vivo*, through the nigrostriatal pathway. Two clones each (except for Patient 1 and Patient 2), from four patient lines and a CRISPR-corrected line as well as two age-matched control lines were differentiated.

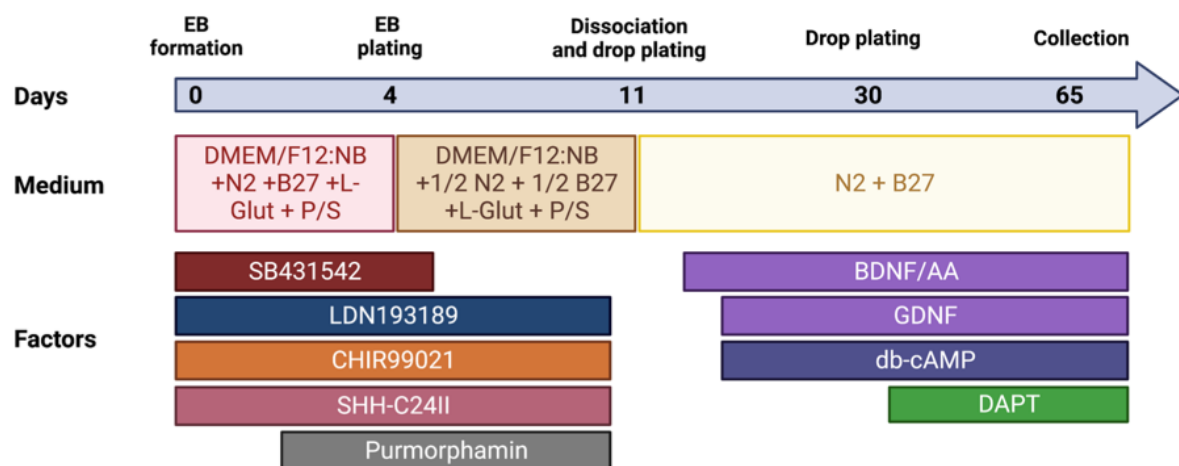


Figure 5. 1. Schematic overview of midbrain dopaminergic neuron differentiation. The protocol is adapted from Kirkeby et al. using dual SMAD inhibition (SB431542, LDN 193189) together with EB formation to induce neural induction. Ventral (SHH-C24II) and caudal (CHIR99021) patterning in neural progenitor cells induces midbrain precursor identity. Terminal differentiation and survival of mature mDA neurons is supported by a number of additional molecules (BDNF, AA, GDNF, db-cAMP and DAPT). Figure adapted from Kirkeby et al.²³²

5. 2. 2. Characterisation of midbrain dopaminergic progenitors

To ensure that neural progenitor cells gradually acquire midbrain identity driven by transient exposure to distinct morphogens, I examined gene expression profiles of neural progenitors at day 11 of differentiation. I used qRT-PCR to assess the expression of established pluripotency markers *OCT4* and *NANOG* as well as mDA precursor markers *FOXA2*, *LMX1A*, *LMX1B*, *EN1* and *EN2*. Normalized to iPSC, all patient and control mDA show downregulation of pluripotency-associated genes and upregulation of mDA progenitor genes (**Figure 5. 2**), indicating that the cells have lost their pluripotent identity and acquired neuronal lineage specific gene expression.

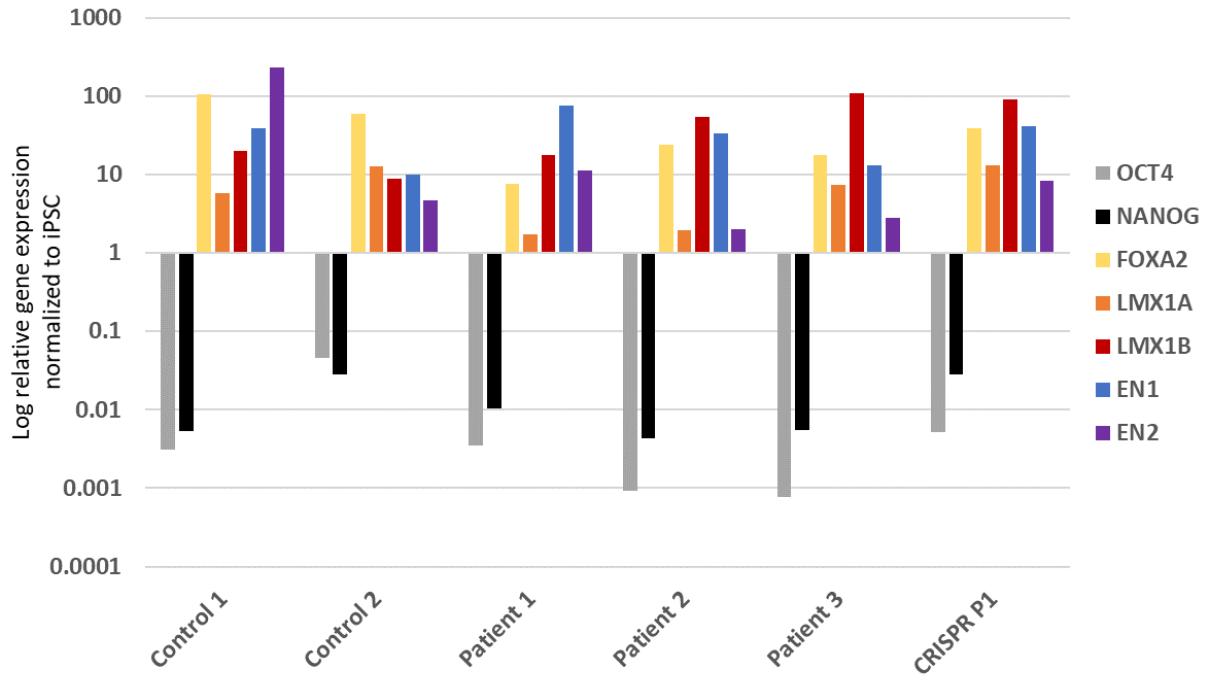


Figure 5. 2. qRT-PCR analysis at day 11 of differentiation. Expression of the indicated genes in patient- and control-derived mDA neurons is normalised to GAPDH and the corresponding iPSC-line of each patient and control (n=1).

5. 2. 2. 1. Patient lines show alterations in early ventral midbrain patterning

LMX1A and *FOXA2* are both expressed in early mDA progenitor cells. *LMX1A* is crucial for mDA specification and directly regulated by the morphogen *WNT1*. Together, they form the *LMX1A-WNT* autoregulatory loop, which is important for mDA differentiation of human ES but also for the suppression of alternative neural fates²¹⁰. *FOXA2* is an established floor plate marker and directly regulated by *SHH* in the ventral mesencephalon^{203,333}. Co-expression of both factors indicates midbrain floor plate identity^{203,215}. To specifically assess and quantify co-localisation of *LMX1A* and *FOXA2*, I performed immunocytochemistry analysis with subsequent manual counting. At day 11 of differentiation, all patient lines show significantly decreased numbers of *LMX1A/FOXA2*-double-positive cells with an average of 39.6% in patient lines compared to an average of 65.8% in control cells (**Figure 5. 3/5. 4**). Numbers of *FOXA2*-single-positive cells were comparable in both control and patient lines with an average expression of 74.6% in patient lines and 77.1% in control lines with no significant statistical difference (**Figure 5. 3/5. 4**). These findings indicate reduced *LMX1A* expression across all patient lines.

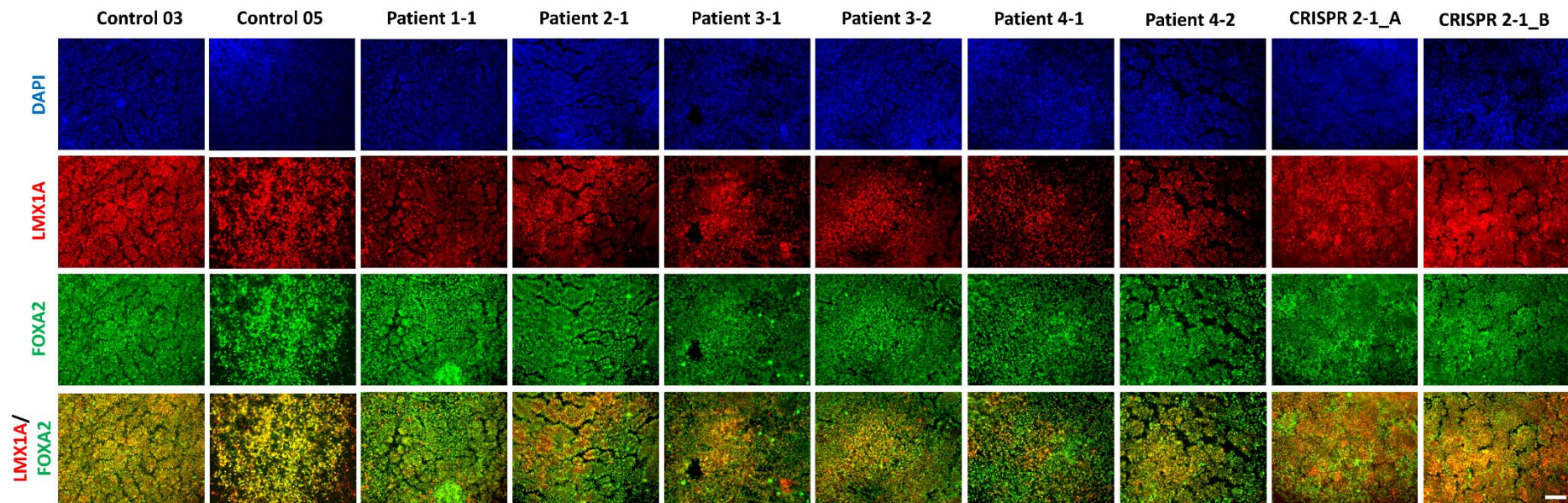


Figure 5. 3. Immunofluorescence analysis for LMX1A and FOXA2 in patient- and control-derived midbrain progenitor cells at day 11 of differentiation. Cells were fixed at day 11 of differentiation and stained with LMX1A (red), FOXA2 (green) and DAPI (blue). Representative immunofluorescence images in patient- and control-derived mDA neurons. Images were acquired using the Olympus IX71 inverted TC scope at 20x magnification. Scale bar = 100 μ m.

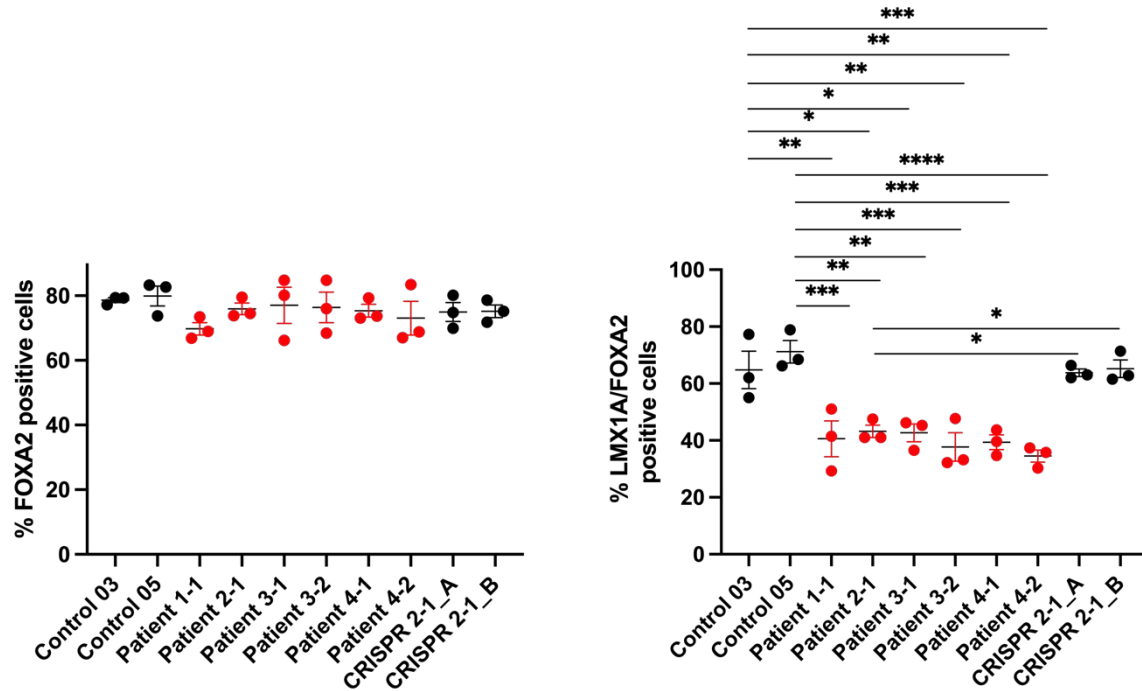


Figure 5. 4. Immunofluorescence quantification for LMX1A and FOXA2 at day 11 of differentiation. Quantification of total numbers of FOXA2-single-positive cells and LMX1A/FOXA2-double-positive cells in patient-and control-derived mDA neurons. Three images were analysed per differentiation with 600 nuclei counted per image. The software ImageJ was used for image processing and counting. No statistical significance was detected for FOXA2-single positive cells. Statistical significance was determined using one-way ANOVA followed by post-hoc Tukey's multiple comparison test. Error bars indicate \pm SEM ($n=3$ independent differentiations). *indicates statistically significant differences: * $p<0.05$; ** $p<0.01$, *** $p<0.001$, **** $p<0.0001$.

5. 2. 3. Characterisation of mature midbrain dopaminergic neurons

5. 2. 3. 1. Patient and control lines differentiate into midbrain dopaminergic neurons

Next, I assessed whether patient and control lines can effectively differentiate into mDA neurons until day 65 of differentiation. Manual inspection of day 65 cultures shows densely packed neuronal cell aggregations with formation of long neurites (**Figure 5. 5**).

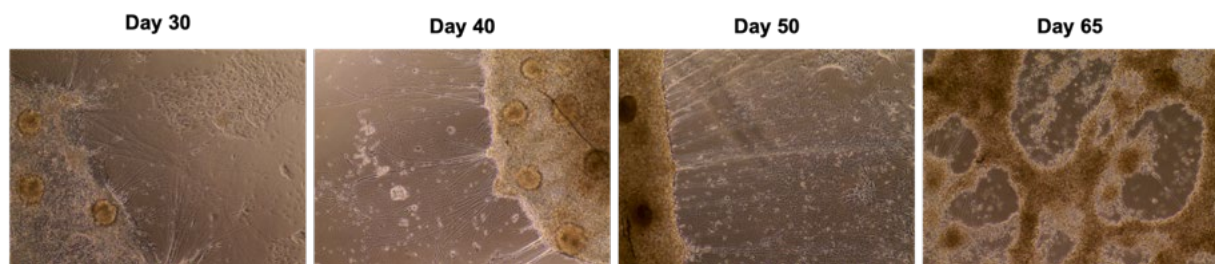


Figure 5. 5. Brightfield images of mDA neuronal cultures. Representative immunofluorescence images of differentiated mDA neuronal cultures. Day 65 mDA neurons are densely packed with evidence of long neurites. Images were acquired using the EVOSTM XL microscope at 10x magnification.

For day 65 neuronal cultures, I performed immunofluorescence analysis for the markers microtubule associated protein 2 (MAP2) and the enzyme TH. MAP2 belongs to the MAP2/Tau protein family which regulate and stabilise microtubule networks in axons and dendrites of post-mitotic neurons³³⁴. TH constitutes the rate-limiting enzyme in dopamine metabolism and is a characteristic marker of more mature dopaminergic neurons²⁰³. Co-staining of MAP2/TH therefore identifies differentiated dopaminergic neurons. Manual quantification of 1) single MAP2-single-positive cells showed an average of 49% and 47,2%, respectively, 2) MAP2/TH-double positive cells an average of 30,6% and 29,3%, respectively, and 3) TH-single-positive cells an average of 32,7% and 31.1%, respectively, in patient- and control-derived mDA neurons with no significant statistical difference between different lines (**Figure 5. 6/5. 7**).

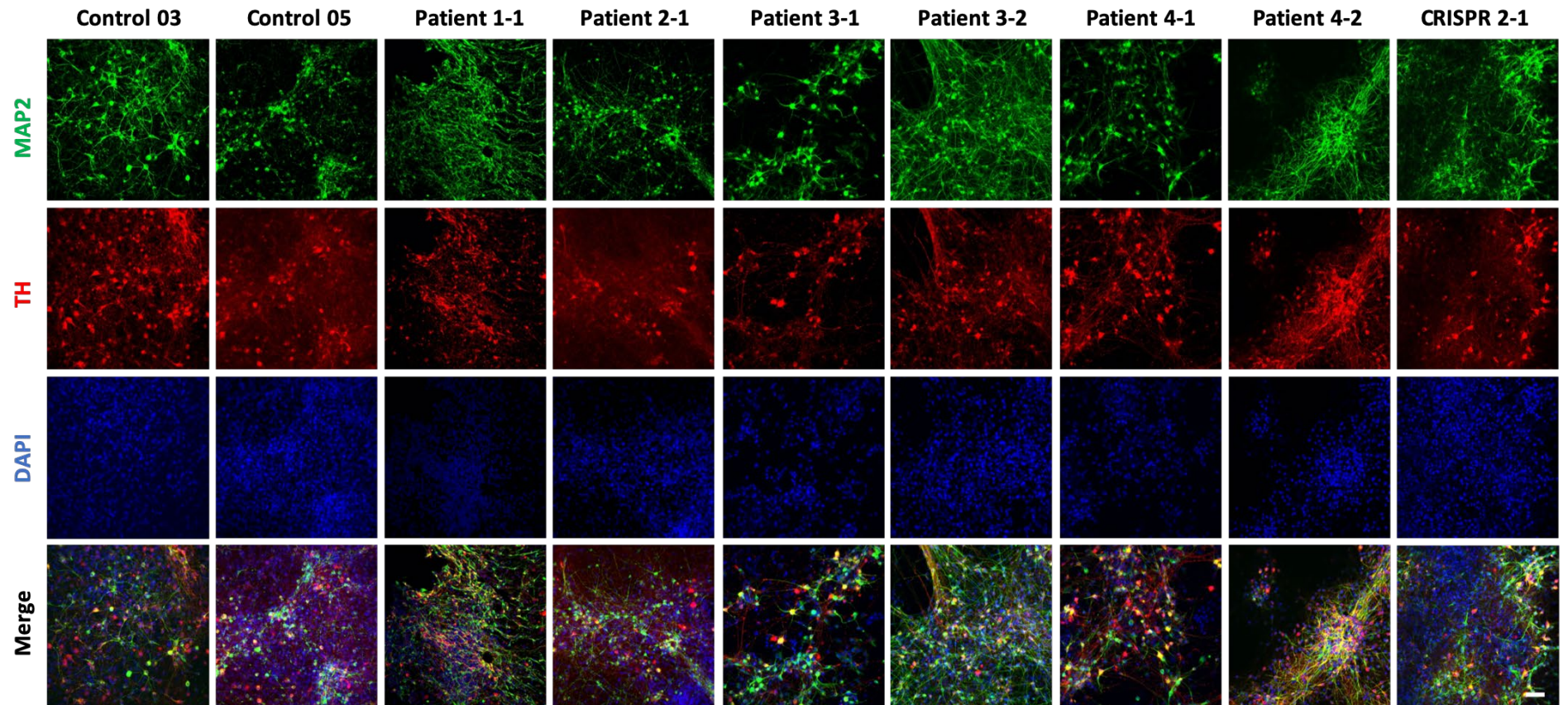


Figure 5. 6 Immunofluorescence analysis for TH and MAP2 in patient- and control-derived mDA at day 65 of differentiation. Cells were fixed at day 65 of differentiation and stained with TH (red), MAP2 (green) and DAPI (blue). Representative immunofluorescence images in patient- and control-derived mDA neurons. Images were acquired using the LSM710 Zeiss confocal microscope. Scale bar = 150 μ m.

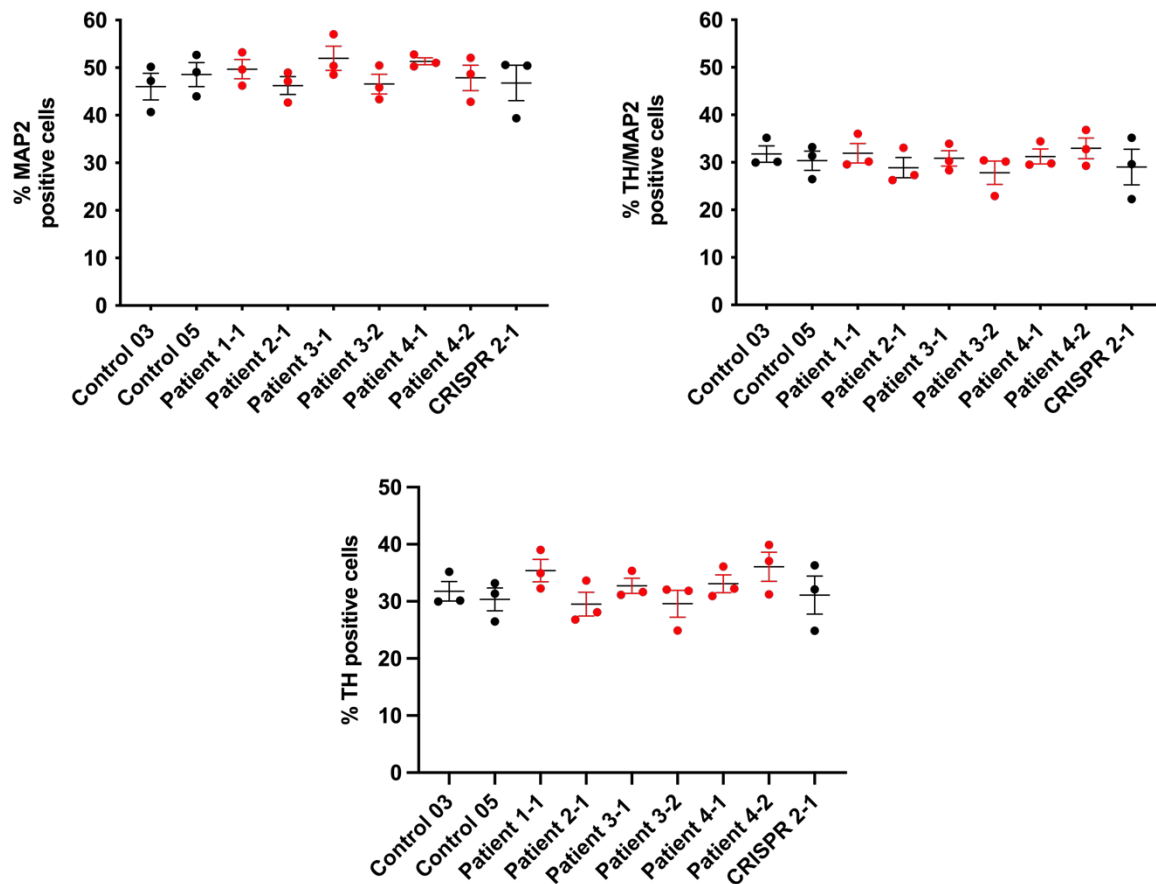


Figure 5. 7. Immunofluorescence quantification for TH and MAP2 at day 65 of differentiation. Quantification of total numbers of MAP2- and TH-single-positive cells and TH/MAP2-double-positive cells. Three images were analysed per differentiation and 600 nuclei counted per image. The software ImageJ was used for image processing and counting. No statistical significance was observed for MAP2- and TH-single positive cells and MAP2/TH-double-positive cells. Statistical analysis was performed using one-way Anova followed by post-hoc Tukey's multiple comparison test. Error bars indicate \pm SEM ($n=3$ independent differentiations).

As quality control did not reveal significant differences between the respective clones of each patient and the CRISPR line, I chose one patient clone for further downstream experiments: clone 2-1, 3-1 and 4-1. Of note, Patient 1-1 showed problems with differentiation including failure to differentiate, excessive overgrowth or early detachment of neuronal cultures. Due to these aberrant differentiation characteristics and the fact that the same *DNAJC6* mutation is present in Patient 2-1, Patient 1-1 was not used for further downstream experiments.

5. 2. 3. 2. Patient and control lines show upregulation of mature midbrain markers

For day 65 neuronal cultures I performed qRT-PCR analysis to evaluate expression of mature neuronal and dopaminergic markers including *AADC*, *TH*, *DAT*, *NURR1*, *PITX3* and *SNCA*. Compared to their respective iPSC lines, all patient and control lines showed upregulation the respective markers. Gene expression is normalised to *GAPDH* (Figure 5. 8).

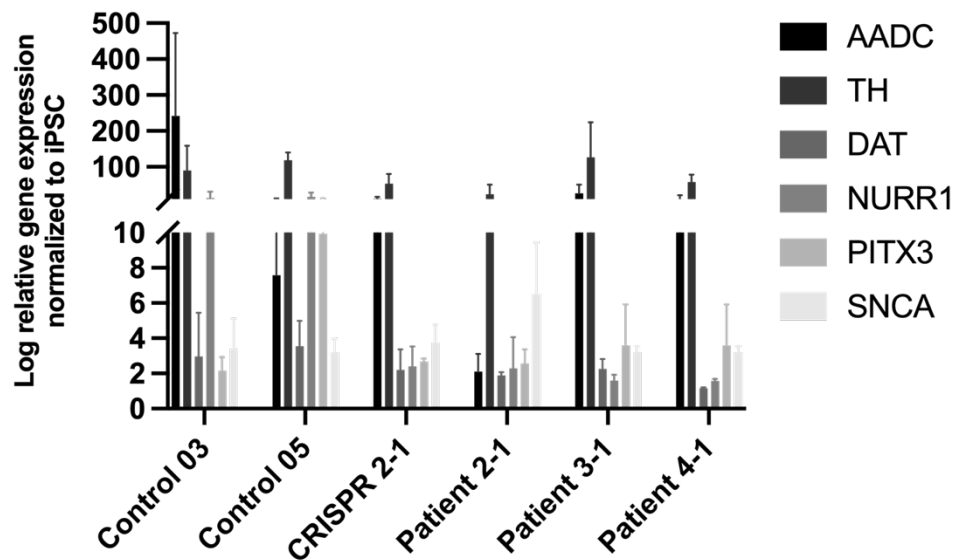


Figure 5. 8. qRT-PCR analysis for mature neuronal and dopaminergic markers at day 65 of differentiation. Expression of the indicated genes in patient- and control-derived mDA neurons is normalized to GAPDH and the corresponding iPSC-line of each patient and control (n=1) (Figure and legend adapted from Abela et al., 2024)³⁰¹.

5. 2. 3. 3. Patient lines show absence of neurodegeneration at day 65 of differentiation

TH/MAP2 staining did not reveal significant differences between patient- and control-derived neuronal cultures. I then performed cleaved caspase 3 (cCASP3) immunofluorescence staining. cCASP3 is a well-established marker for apoptosis and indicates DNA fragmentation. Manual counting of cCASP3-single-positive and cCASP3/TH-double-positive cells did not reveal significant differences between patient- and control-derived mDA neurons (**Figure 5. 9/5. 10**).

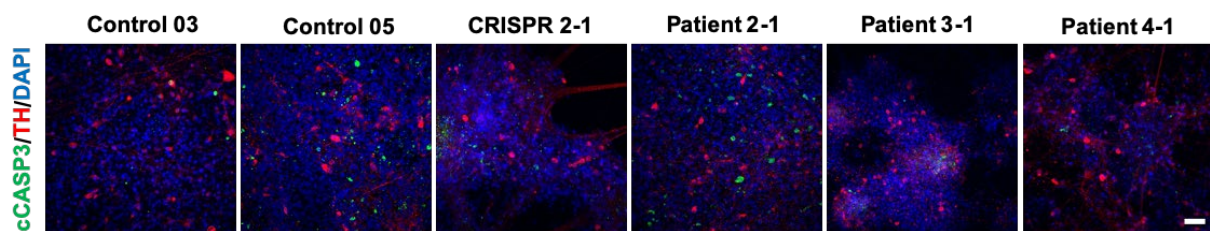


Figure 5. 9. Immunofluorescence analysis for cCASP3 in patient- and control-derived mDA at day 65 of differentiation. Cells were fixed at day 65 of differentiation and stained with TH (red), cCASP3 (green) and DAPI (blue). Representative immunofluorescence images in patient- and control-derived mDA neurons. Images were acquired using the LSM710 Zeiss confocal microscope. Scale bar = 150µm (Figure and legend adapted from Abela et al., 2024)³⁰¹.

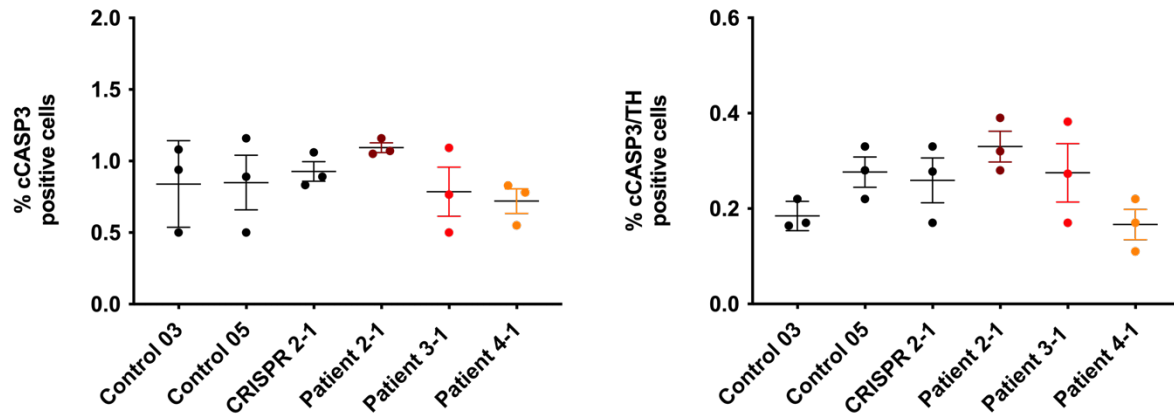


Figure 5. 10. Immunofluorescence quantification for cCASP3 at day 65 of differentiation. Quantification of total numbers of cCASP3-single-positive cells and cCASP3/TH-double-positive cells. Three images were analysed per differentiation and around 600 nuclei counted per image. The software ImageJ was used for image processing and counting. No statistical significance was detected for cCASP3-single positive cells and cCASP3/TH-double-positive cells. Statistical analysis was performed using one-way Anova followed by post-hoc Tukey's multiple comparison test. Error bars indicate \pm SEM ($n=3$ independent differentiations) (Figure and legend adapted from Abela et al., 2024)³⁰¹.

5. 2. 3. 4. Patient lines show neuronal maturation defects at day 65 of differentiation

Given that the majority of patients with homozygous *DNAJC6* mutations manifest neurodevelopmental delay, I examined another marker of neuronal maturity at day 65 of differentiation. Neuronal nuclear protein (NeuN) is a marker of mature, postmitotic neurons and localises primarily to the nucleus³³⁵. NeuN immunofluorescence staining of day 65 old mDA cultures shows significantly decreased numbers of NeuN-single-positive and TH/NeuN-double-positive cells in patient lines compared to control lines (**Figure 5. 11/5. 12**).

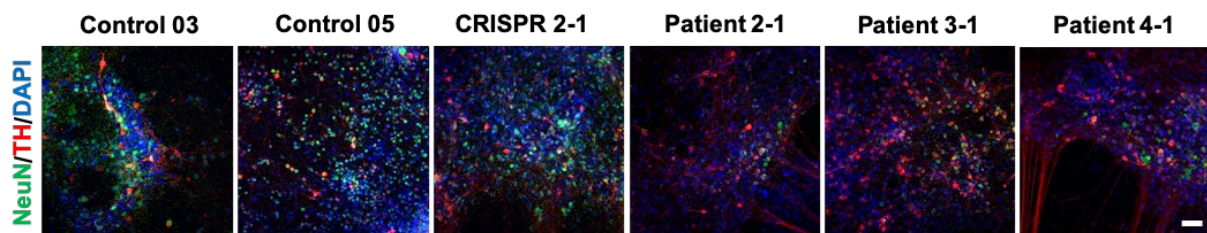


Figure 5. 11. Immunofluorescence analysis for NeuN in patient- and control-derived mDA at day 65 of differentiation. Cells were fixed at day 65 of differentiation and stained with TH (red), NeuN (green) and DAPI (blue). Representative immunofluorescence images in patient- and control-derived mDA neurons. Images were acquired using the LSM710 Zeiss confocal microscope. Scale bar = 150 μ m (Figure and legend adapted from Abela et al., 2024)³⁰¹.

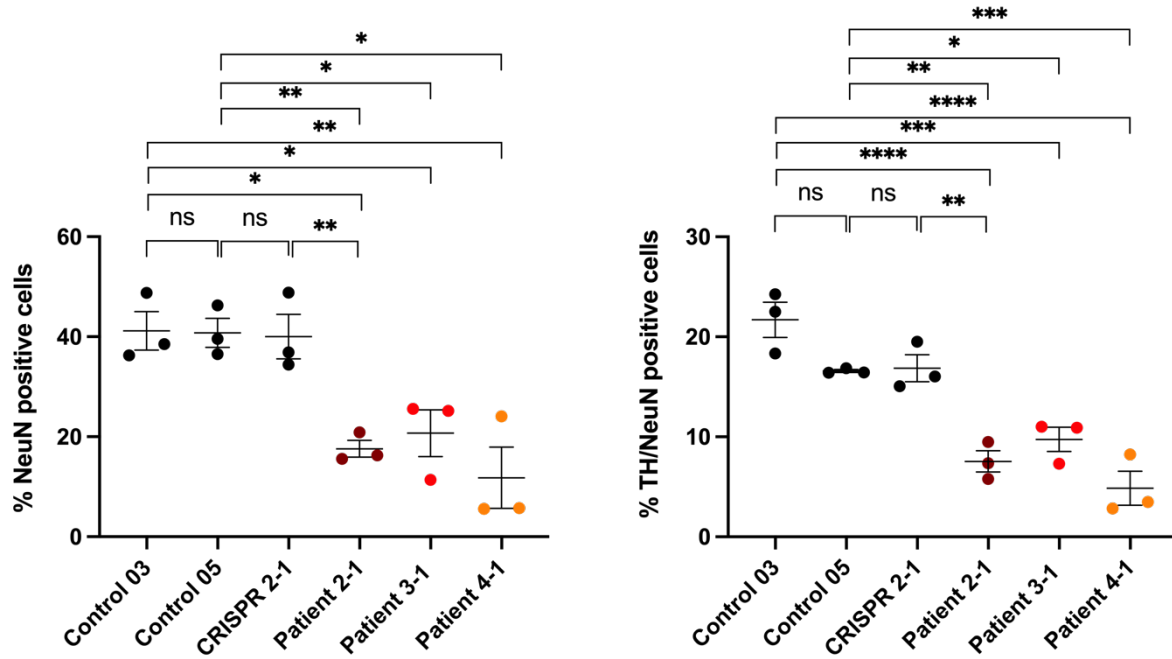


Figure 5. 12. Immunofluorescence quantification for NeuN at day 65 of differentiation. Quantification of total numbers of NeuN-single-positive cells and TH/NeuN-double-positive cells. Three images were analysed per differentiation and around 400 nuclei counted per image. The software ImageJ was used for image processing and counting. Statistical analysis was performed using one-way Anova followed by post-hoc Tukey's multiple comparison test. Error bars indicate \pm SEM ($n=3$ independent differentiations). *indicates statistically significant differences: * $p<0.05$; ** $p<0.01$, *** $p<0.001$. (Figure and legend adapted from Abela et al., 2024)³⁰¹.

5. 2. 3. 5. Patient lines show impaired primary neurite outgrowth

Neurite outgrowth is a complex developmental process in which differentiating neurons generate multiple cellular protrusions that later become axons and dendrites. Through their neurites, neurons connect to each other via synapses and build functional networks. CME is directly involved in the regulation of neurite outgrowth. Several CME-associated proteins regulate the endocytosis of adhesion molecules such as L1-CAM and N-cadherin¹⁷¹. I assessed neurite outgrowth by quantifying primary neurite protrusions from TH-positive mDA neurons. The number of primary neurites was significantly reduced in all patient lines compared to control lines (Figure 5. 13/5. 14).

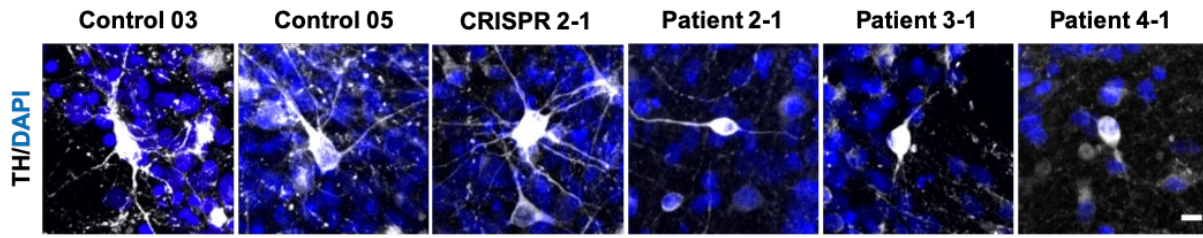


Figure 5. 13. Primary neurite outgrowth assessment in patient- and control-derived mDA at day 65 of differentiation. Cells were fixed at day 65 of differentiation and stained with TH (red) and DAPI (blue). Representative immunofluorescence images in patient- and control-derived mDA neurons. Images were acquired using the LSM710 Zeiss confocal microscope. Scale bar = 10 μ m (Figure and legend adapted from Abela et al., 2024)³⁰¹.

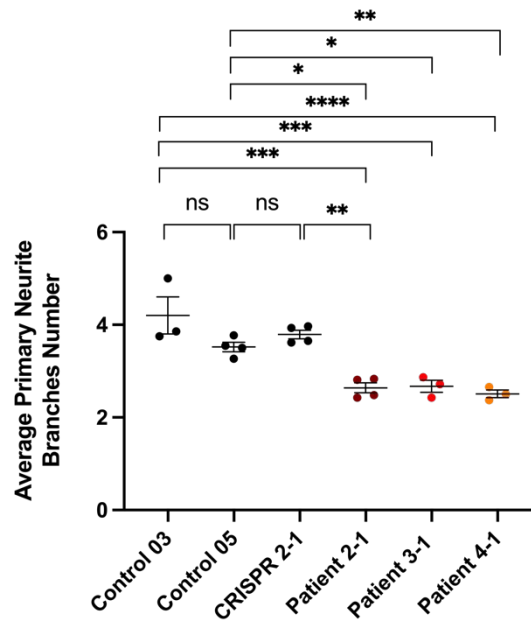


Figure 5. 14. Primary neurite quantification at day 65 of differentiation. Quantification of total numbers of neurites per neuron for patient- and control-derived mDA neurons. Four images were used per differentiation and neurites were counted from 5-8 TH-positive neurons per image. Statistical significance was calculated using the one-way ANOVA followed by post-hoc Tukey's multiple comparison test. Error bars indicate \pm SEM (n=3 independent differentiations, N=20-25 neurons per differentiation). *indicates statistically significant differences: * p <0.05; ** p <0.01, *** p <0.001, **** p <0.0001. (Figure and legend adapted from Abela et al., 2024)³⁰¹.

5. 3. Discussion

In this chapter, I have generated a 2D midbrain dopaminergic neuronal cell model for *DNAJC6* parkinsonism-dystonia. Patient and control iPSC lines were efficiently differentiated towards midbrain dopaminergic progenitors with successful downregulation of pluripotent markers and upregulation of midbrain precursor markers at day 11 compared to their respective iPSC lines. At this time point, immunohistochemistry analysis at day 11 showed reduced *LMX1A* expression across all patient lines compared to control and the CRISPR-corrected line (39,6%

vs 65,8), while *FOXA2* expression levels were similar in both patient and control lines (74.6% vs 77.1%). It is possible that reduced levels of *LMX1A* in patient lines are due to defective upstream regulation. *LMX1A* is expressed in the midbrain floorplate and a direct downstream target of *WNT1/β-catenin*. The Wnt signalling pathway is crucial during embryonic development and regulates patterning, organogenesis and angiogenesis as well as stem cell proliferation along with axis specification³³⁶. In the central nervous system, Wnt signalling is involved in the regulation of neuronal differentiation, axon outgrowth and guidance, dendrite formation as well as synaptic development and function³³⁷. Endocytosis, in particular CME, plays a key role in the activation and attenuation of the Wnt/β-catenin signalling pathway³³⁸. In murine cells, clathrin inhibitors as well as siRNA-mediated depletion of clathrin inhibited Wnt signalling³³⁶. Downregulation of *LMX1A* in patient lines is likely to reflect dysfunction of Wnt signalling due to *DNAJC6* deficiency and subsequently impaired CME. Chapter 6 will discuss disease-specific findings of impaired CME in this neuronal cell model. Indeed, a recent paper published during the course of this PhD demonstrated reduced *LMX1A* expression and impaired Wnt-Lmx1a signalling in human *DNAJC6* hMLOs at day 15 and 30 of differentiation¹⁹⁰.

I then differentiated patient and control lines towards mDA neurons until day 65 of differentiation. Both patient and control lines showed equal numbers of TH/MAP2-double-positive cells and a dopaminergic yield that is comparable to the original protocol²³². Quantification of the late apoptotic marker cCASP3 at day 65 confirmed absence of neurodegeneration in all patient lines. This finding differs somewhat from recently published work showing increased cCASP3 staining in human *DNAJC6* hMLOs and reduced numbers of mDA neurons at day 80 of differentiation¹⁹⁰. Differences in the protocol, use of a more complex 3D model and a later stage of differentiation at the time point of analysis may account for the divergent results and the lack of frank neurodegeneration observed in this 2D dopaminergic neuronal cell model.

As there were no obvious differences in TH/MAP2 expression between the clones from each patient, I continued with one clone per patient for further experimental analysis. qRT-PCR confirmed midbrain identity of day 65 neuronal cultures. All patient and control lines manifested upregulation of mature midbrain markers compared to their corresponding iPSC lines. The majority of patients with juvenile-onset *DNAJC6* parkinsonism-dystonia present with neurodevelopmental delay. To investigate, whether our model also exhibits neurodevelopmental features, I examined another marker of late neuronal differentiation at day

65 of differentiation, the neuronal nuclear protein (NeuN). All patient lines manifested decreased NeuN expression compared to controls. MAP2 is expressed shortly after the transformation of neuronal precursor cells to neurons³³⁹, while NeuN expression manifests when neurons exit the cell cycle and enter terminal differentiation³⁴⁰. Decreased NeuN expression in the light of normal MAP2 expression thus might highlight a delay in neuronal maturation. Immunohistochemistry analysis of late-expressed mDA markers such as *NURR1*, *DAT* or *PITX3* and comparison of gene expression to control lines instead of iPSC lines would constitute a necessary logical step to further investigate these findings.

Neurite outgrowth assays are commonly used as a marker of neuronal development and regeneration^{341,342}. Several components of the CME machinery are involved in the regulation of neurite outgrowth and growth cone motility¹⁷¹. Clathrin assembly protein AP-2 guides endocytosis of cell adhesion molecules L1-CAM and N-cadherin^{343,344}, AP-180 and CALM may have similar functions^{345,346}. In order to evaluate the impact of *DNAJC6* deficiency on neurite outgrowth, I assessed the sprouting of primary neurites in dopaminergic neurons at day 65 of differentiation, the very first step of neurite outgrowth. All patient lines exhibited significantly reduced numbers of primary neurites. Due to the very densely packed nature of 2D neuronal cultures, I was not able to track neurite length of single neurons. Notably, in TH-positive neurons, Wulansari et al. found significantly reduced fibre length in *DNAJC6* hMLOs¹⁹⁰.

In summary, I have successfully generated and characterised mDA neurons from patients with biallelic *DNAJC6* mutations. This dopaminergic neuronal cell model shows aberrant early ventral midbrain patterning and defects in neuronal maturation.

CHAPTER 6

Investigation of disease-specific phenotypes in the *DNAJC6* dopaminergic neuronal cell model

6. 1. Introduction

In the previous chapter, I have described the generation of patient-derived mDA neurons. Characterisation of day 11 and day 65 patient-derived mDA confirmed neural progenitor and derived-mature identity, respectively. I also identified potential aberration of early ventral midbrain patterning and defects in neuronal maturation. The following chapter focuses on exploring the effects of *DNAJC6* mutations on presynaptic SV recycling, given the essential role of auxilin in clathrin uncoating. I used a number of different assays including immunoblotting studies, the FM1-43 dye uptake assay and electron microscopy analysis to investigate disease-specific phenotypes in day 65 old mDA neurons. Some sections and figures have been adapted from a publication arising from this research, Abela L^{*} et al., 2024³⁰¹.

6. 2. Results

6. 2. 1. Patient lines show absent auxilin protein expression

In order to determine the effect of *DNAJC6* mutations on auxilin protein expression, immunoblotting studies were undertaken. Total cell lysates were extracted on day 65 of differentiation from Control 03, Control 05, Patient 2-1, Patient 3-1, Patient 4-1 and CRISPR 2-1. Western blot analysis shows absence of auxilin protein in all patient lines when compared to the control line and isogenic CRISPR line for Patient 2-1 (**Figure 6. 1**). The auxilin antibody is a polyclonal antibody targeting the C-terminal³⁴⁷. Truncated forms of the protein may therefore be missed by this antibody. However, the J-domain located at the C-terminal is essential for Hsc70 binding. Lack of this domain hinders formation of the Hsc70-auxilin complex and thus interferes with the uncoating process.

The absence of auxilin protein expression in mDA neurons is in contrast to the findings in patient CSF (**Figure 3.3**). However, protein levels in native CSF represent extracellular protein that may originate from other cellular sources (lymphocytes, monocytes) and do not necessarily represent intracellular neuronal levels. In addition, the ubiquitously expressed auxilin isoform GAK has a C-terminal domain with high sequence homology to auxilin. It is conceivable that the polyclonal auxilin antibody targeting the C-terminus may also capture the isoform GAK in the absence of auxilin in non-neuronal cells.

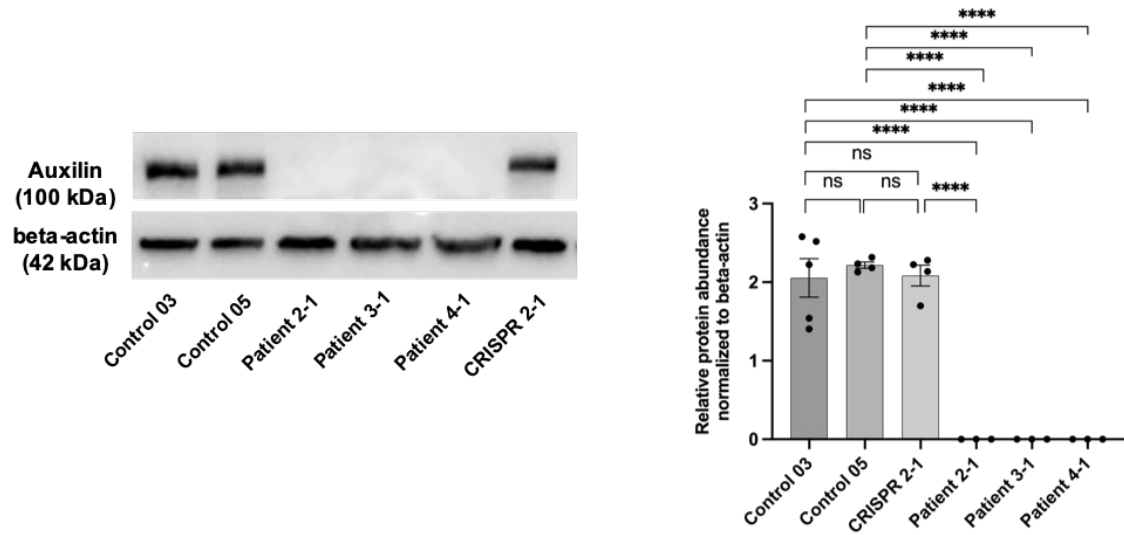


Figure 6. 1. Immunoblot analysis for auxilin protein in patient- and control-derived mDA at day 65 of differentiation. **A)** Representative immunoblot image for auxilin protein (100 kDa) and loading control, beta-actin (42 kDa) in Control 03, Control 05, Patient 2-1, Patient 3-1 and Patient 4-1 and CRISPR 2-1. **B)** Quantification of relative auxilin protein abundance, normalised to the loading control beta-actin ($n = 5, 4, 4, 3, 3$ independent differentiations, respectively). Statistical significance was evaluated using the Student's unpaired, two tailed t-test. Error bars indicate \pm SEM. *indicates statistically significant differences: * $p < 0.05$; ** $p < 0.01$, *** $p < 0.001$, **** $p < 0.0001$. (Figure and legend adapted from Abela et al., 2024)³⁰¹.

To evaluate the effect of auxilin deficiency on direct binding partners of auxilin, I further analysed protein expression of clathrin and AP-2³⁴⁸. Clathrin is a major coat protein and composed of three clathrin heavy and three clathrin light chains, the so called triskelia. Auxilin interacts with clathrin via its C-terminal domain. AP-2 is involved early in the formation and stabilisation of clathrin-coated pits and triggers clathrin polymerisation. Auxilin associates with the alpha-appendage domain of AP-2³⁴⁸. Protein levels varied significantly between the differentiations. However, repeated measurements showed no statistical difference between the control and patient lines (**Figure 6. 2**), indicating that auxilin deficiency does not affect protein expression levels of these key CME-associated proteins.

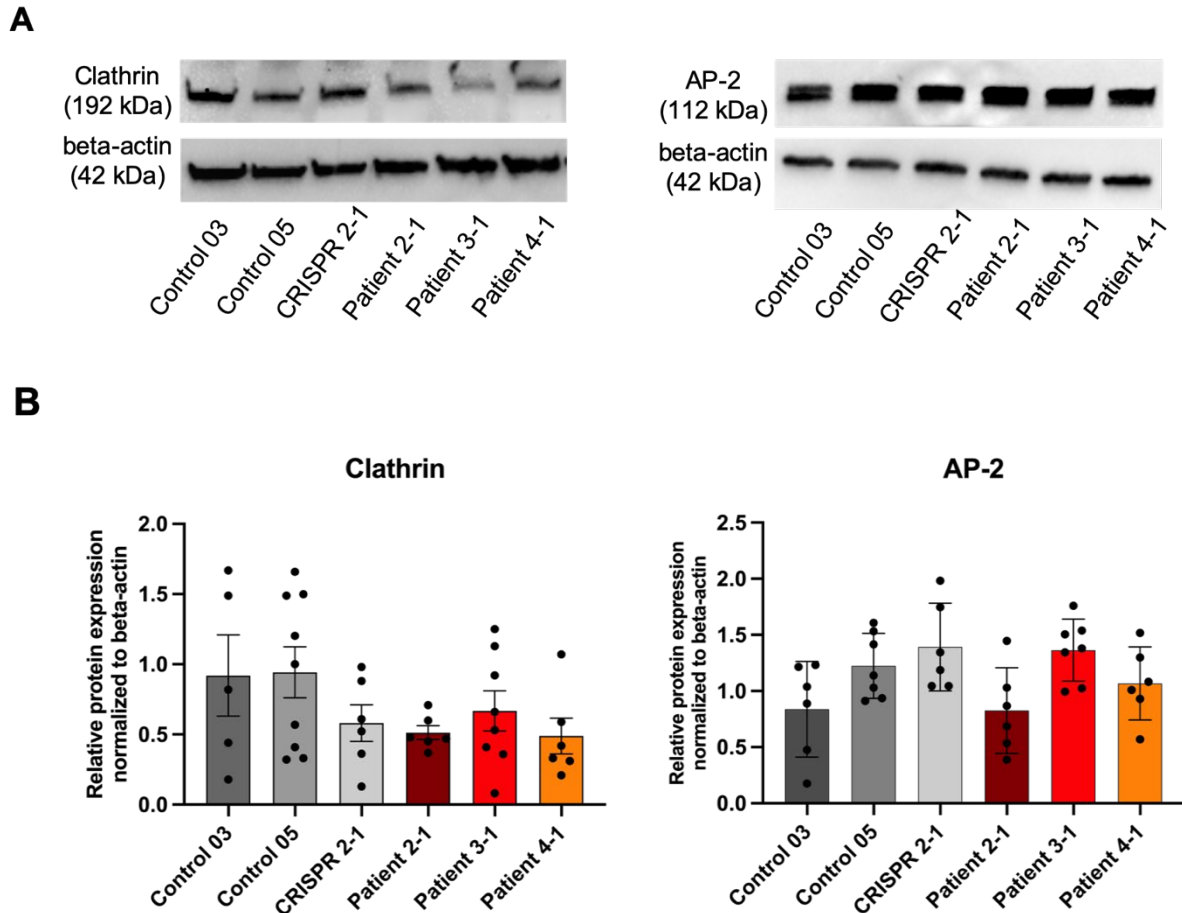


Figure 6. 2. Immunoblot analysis for CME-associated proteins in patient- and control-derived mDA at day 65 of differentiation. *A)* Representative immunoblot images for clathrin protein (192 kDa) and AP-2 protein (112 kDa) in Control 03, Control 05, Patient 2-1, Patient 3-1 and Patient 4-1 and CRISPR 2-1. *B)* Quantification of relative clathrin and AP-2 protein abundance, normalised to the loading control beta-actin ($n =$ samples from 5-9 independent differentiations). Statistical significance was determined using the one-way ANOVA followed by post-hoc Tukey's multiple comparison test. No difference was detected.

6. 2. 2. Patient lines show impaired clathrin-mediated endocytosis

Next, I sought to determine the effect of auxilin deficiency on CME using FM1-43 [N-(3-triethylammoniumpropyl)-4-(4-(dibutylamino)styryl) pyridinium dibromide] fluorescence imaging. FM1-43 is a styryl dye with a water-soluble polar head and a lipid-soluble hydrophobic tail separated by a central region that defines its spectral properties³⁴⁹. In aqueous solutions, FM1-43 dye is non-fluorescent, but when bound to membranes by its lipid-soluble hydrophobic tail, it becomes brightly fluorescent. In actively firing neurons, the dye binds to membrane lipids and is internalised within recycled SV (the outer membrane leaflet becomes the inner membrane in SV) and thus allows visualisation of SV endocytosis^{350,351}. Day 65 mDA neurons were incubated with FM1-43 dye and subsequently fixed and analysed. A 488nm laser

was used to excite the FM1-43 dye and at least 4 random images from three independent differentiations per line were acquired. Image analysis was carried out with Image J (NIH). Every image was corrected for its background fluorescence by measuring mean fluorescence intensity in a cell- and neurite-free area, which was subsequently subtracted from the whole image (“Subtract background” function in Image J). Mean fluorescence intensity was analysed in at least 15 defined regions of interest (ROI) per image each covering a presynaptic bouton. Patient images were compared to either their isogenic control or age-matched control. All patient lines show a reduction in mean fluorescence intensity compared to the control and CRISPR lines, respectively (**Figure 6. 3/6. 4**), indicating reduced uptake of FM1-43 dye and thus impaired CME.

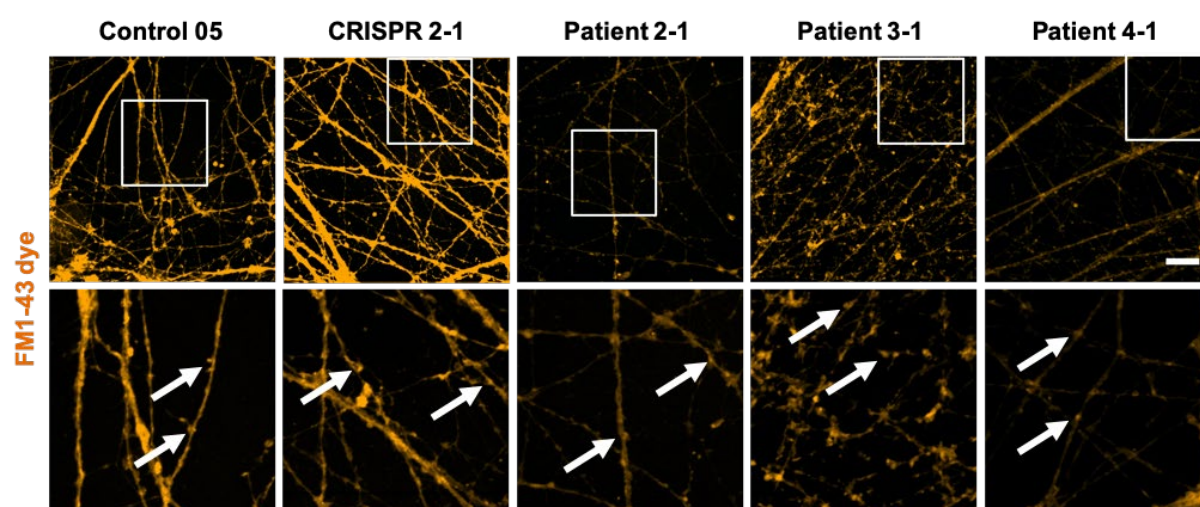


Figure 6. 3. FM1-43 uptake assay in patient- and control-derived mDA at day 65 of differentiation. Cells were incubated with FM1-43 dye, stimulated with potassium and subsequently fixed and analysed. Representative immunofluorescence images of FM1-43 uptake assay for Control-05, Patient 2-1, Patient 3-1 and Patient 4-1 and CRISPR 2-1-derived mDA neurons at day 65 of differentiation (upper panel). Lower panel: Arrows in the high-magnification images (lower panel) show representative synaptic boutons. Images were acquired using the LSM710 Zeiss confocal microscope. Scale bar = 20 μ m. (Figure and legend adapted from Abela et al., 2024)³⁰¹.

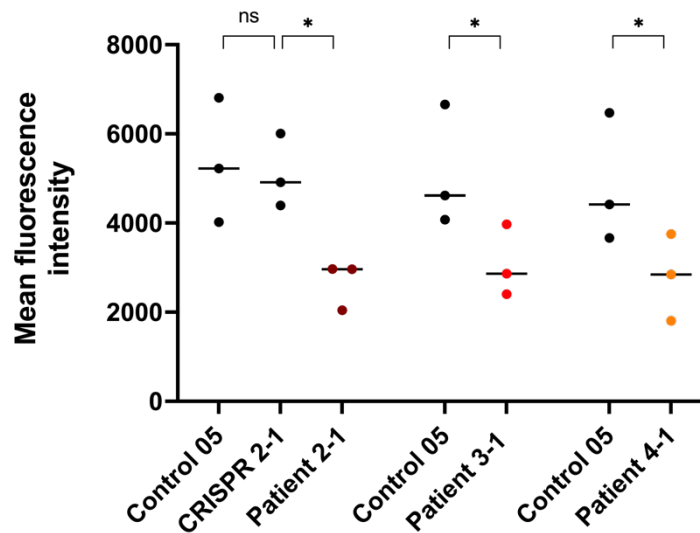


Figure 6. 4. Quantification of FM1-43 uptake assay at day 65 of differentiation. Quantification of FM1-43 mean fluorescence intensity in Patient 2-1, Patient 3-1 and Patient 4-1-derived mDA neurons relative to Control 05 and CRISPR 2-1, respectively. Statistical significance was determined using the Student's paired, two tailed t-test. Error bars indicate \pm SEM ($n=3$ independent differentiations, $N=60$ presynaptic boutons per differentiation). *indicates statistically significant differences: * $p<0.05$ (Figure and legend adapted from Abela et al., 2024)³⁰¹.

6. 2. 3. Patient lines show synaptic vesicle dyshomeostasis

To investigate the downstream effects of impaired CME on presynaptic SV homeostasis, electron microscopy analysis was performed. Electron microscopy represents the gold-standard for synapse imaging due to its superior spatial resolution. We analysed synapses from neuronal cultures without prior labeling of dopaminergic neurons. Neuronal processes were traced and synapses identified in the presence of vesicles and other organelles including mitochondria, endosomes, endoplasmic reticulum and a terminal dense zone. All patient lines show a significantly reduced number of SV at the presynaptic terminal compared to the controls and the corresponding CRISPR line (**Figure 6. 4/ 6. 5**). Analysis of other morphometric parameters shows variable results in patient lines. Synaptic area is significantly increased in Patient 3-1 versus both controls. Active zone (AZ) length is significantly increased in both Patient 2-1 and 3-1 versus Control 05, but not versus Control 03, and it remains unchanged in Patient 4-1 versus both controls. The number of docked SVs/AZ length is reduced in Patient 2-1 versus both Control 03 and the isogenic control, but remains unchanged in Patient 3-1 and 4-1.

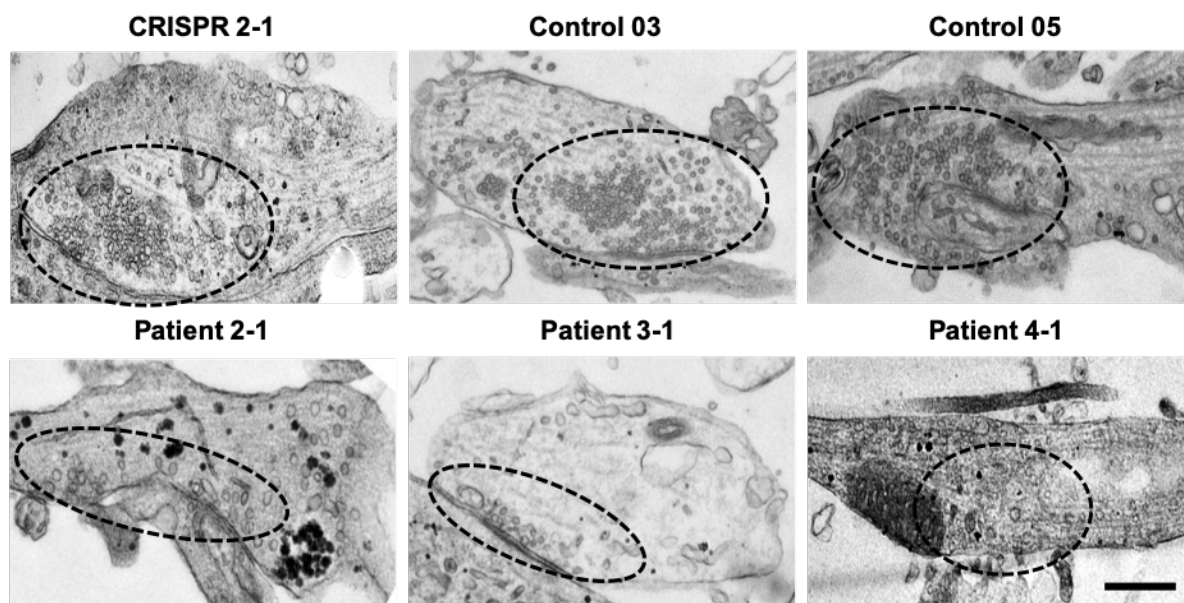


Figure 6. 4. Electron microscopy analysis in DNAJC6- and control-derived mDA neurons at day 65 of differentiation. Cells were fixed, flat embedded in Araldite resin and subsequently imaged on a Jeol 1400 Flash transmission electron microscope. Representative images of presynaptic terminals in in Control 03, Control 05, Patient 2-1, Patient 3-1 and Patient 4-1 and CRISPR 2-1-derived mDA neurons at day 65 of differentiation. Scale bar = 500nm. Electron microscopy analysis has been performed by Dr. Erica Tagliatti (Figure and legend adapted from Abela et al., 2024)³⁰¹.

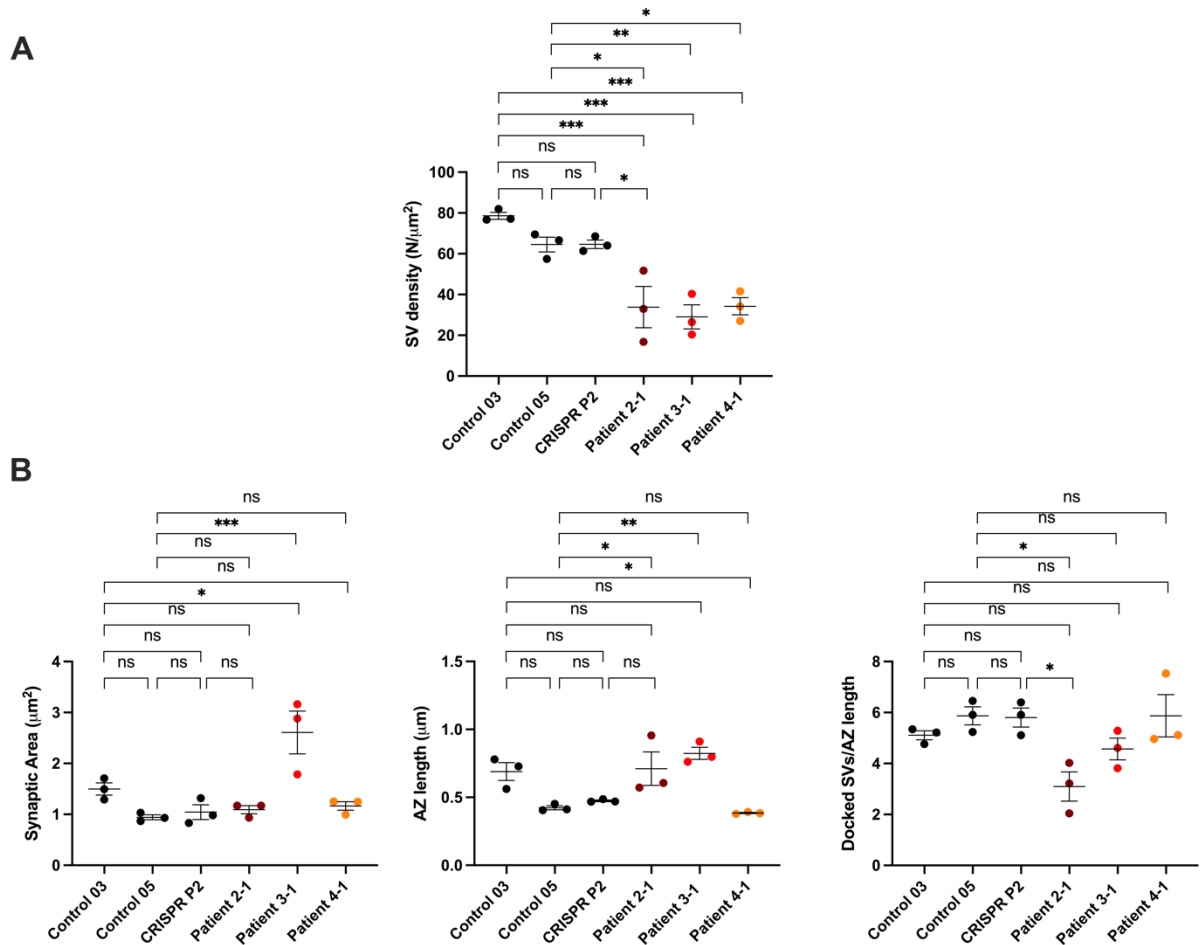


Figure 6. 5. Quantification of EM morphometric analysis. A) Quantification of SV density. B) Quantification of synaptic area, AZ length and docked SV. Statistical significance was determined using the ordinary one-way ANOVA followed by post-hoc Tukey's multiple comparison test. Error bars indicate \pm SEM ($n=3$ independent differentiations, $N=20$ synapses per differentiation). *indicates statistically significant differences: * $p<0.05$; ** $p<0.01$, * $p<0.001$, **** $p<0.0001$. Electron microscopy analysis has been performed by Dr. Erica Tagliatti (Figure and legend adapted from Abela et al., 2024)³⁰¹.**

6. 2. 4. Patch clamp analysis in Patient 2-1 shows decreased amplitude of events

To investigate the effect of diminished SV numbers of synaptic neurotransmission, patch clamp analysis was performed in Patient 2-1 and the corresponding isogenic control CRISPR 2-1. Spontaneous excitatory post-synaptic currents (sEPSCs) were recorded in Patient 2-1 and its isogenic control (**Figure 6. 6**). sEPSCs most probably represent glutamatergic activity since samples were not labelled for dopaminergic neurons prior to the analysis. Patient 2-1 shows similar a resting membrane potential and frequency of events compared to CRISPR 2-1, but has a significantly reduced amplitude of events (**Figure 6. 6**). An isolated decrease in the amplitude of events could result from a reduced number of SVs and a subsequent decrease in

neurotransmitter release, or, could be associated with impaired synaptic maturation. Further electrophysiological studies on other patient and control lines was unfortunately not possible within the time constraints of my PhD.

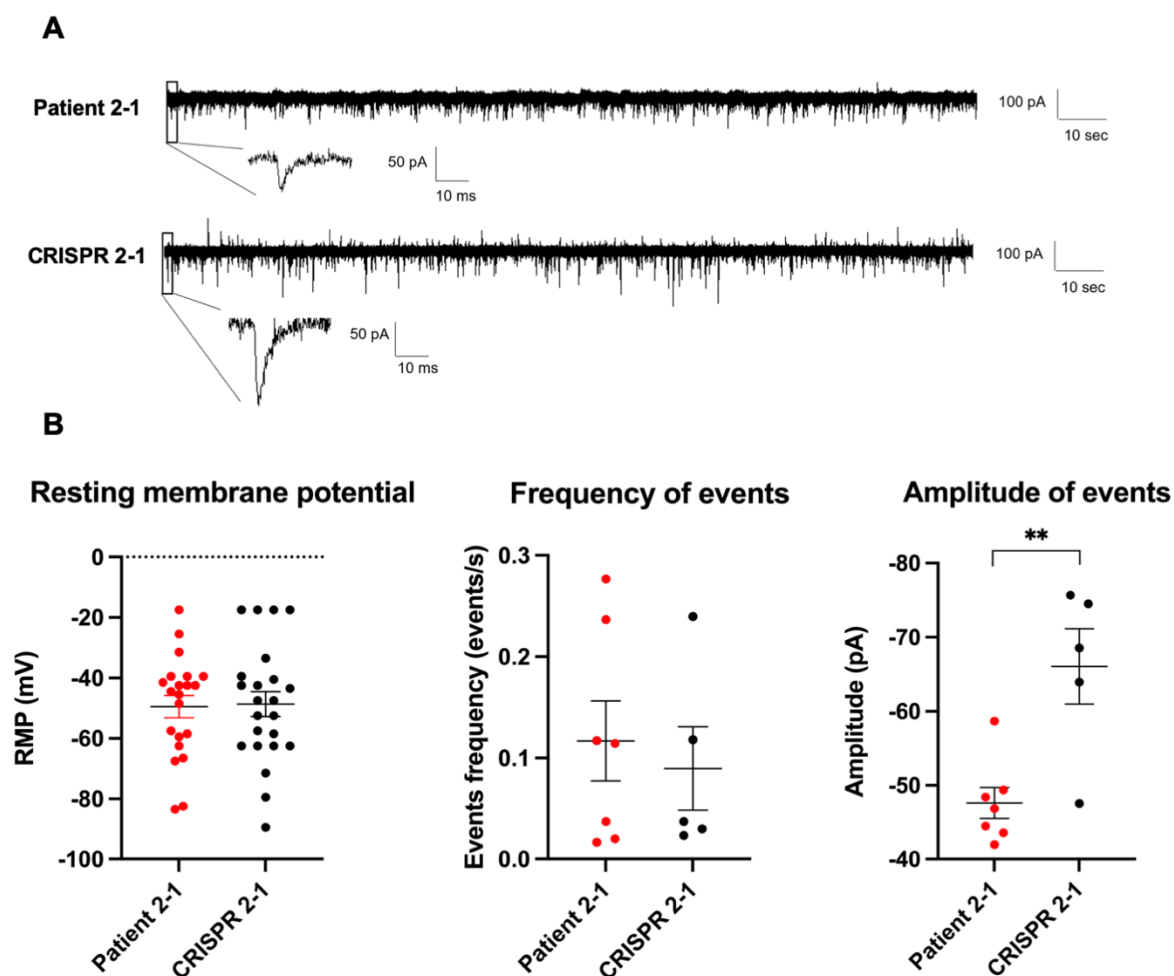


Figure 6. 6. Electrophysiological analysis in day 65 mDA neurons of Patient 2-1 and the isogenic control CRISPR 2-1. *A)* Recordings of spontaneous excitatory post-synaptic currents (sEPSCs) in Patient 2-1 and the isogenic control CRISPR 2-1. *B)* Analysis of resting membrane potential, frequency of events and amplitude of events in Patient 2-1 and the isogenic control CRISPR 2-1. *indicates statistically significant differences: * $p < 0.05$; ** $p < 0.01$. Electrophysiological analysis has been performed by Clara Zourray (Figure and legend adapted from Abela et al., 2024)³⁰¹.

6. 3. Discussion

Auxilin is an essential co-chaperone protein involved in the clathrin uncoating step in CME. In this chapter, I have shown that auxilin protein levels are severely reduced in all three patient-derived lines thereby confirming the deleterious effects of the respective *DNAJC6* mutation (c.766C>T (Patient 2-1), c.2416C>T (Patient 3-1), c.801-2A>G (Patient 4-1). Notably, levels of key CME-associated proteins such as clathrin and AP-2 were not affected, though of course, protein levels are not necessarily reflective of protein function. Uncoating of clathrin-coated

vesicles is essential to sustain rapid recycling of SV for neurotransmitter loading. In patient-derived mDA neurons, I have also shown that auxilin deficiency results in reduced uptake of FM1-43 dye at the presynaptic terminal in all patient lines indicating impaired SV endocytosis. Disturbance of SV endocytosis is likely to affect the process of SV cycling. We used electron microscopy analysis to investigate the effects of impaired CME on presynaptic SV homeostasis and found reduced numbers of SV in all patient-derived lines. Notably, we observed other more variable changes in synaptic morphology, where findings were not consistent across all patient lines. An increase in synaptic area as observed in Patient 3-1 versus both controls could indicate changes in homeostatic plasticity of the neuronal network. Reduced numbers of docked SVs/AZ length in Patient 2-1 versus all controls indicates possible impairment of SV cycling with fewer SV available for exocytosis. Preliminary electrophysiological findings in Patient 2-1 with reduced amplitude of events of sEPSCs could possibly support the EM findings and indicate disruption of SV cycling. These alterations in synaptic morphology may be caused by 1) developmental defects in maturation and refining/pruning of synapses or 2) impairments of homeostatic plasticity that alter the properties of synapses.

In summary, this *DNAJC6* neuronal cell model shows key disease features of auxilin deficiency and impairment of CME. The model further reveals defects in synaptic homeostasis and possibly also synaptic development although further experimental studies are needed to confirm this observation. Nevertheless, given the crucial role of CME in regulating developmental and synaptic signalling pathways, defects in synaptic development would not be surprising in *DNAJC6*-related disease.

CHAPTER 7

Transcriptome profiling of patient-derived midbrain dopaminergic neurons

7. 1. Introduction

With the advent of next-generation sequencing technologies, there are now novel unbiased bioinformatic approaches to analyse big datasets. These technologies can be used to study the transcriptome, which comprises the entire collection of RNA molecules in a biological sample³⁵². It is highly dynamic and reflects global gene expression in biological samples or cells. RNA sequencing analysis (RNA-seq) explores the major type of RNAs, so called messenger RNAs (mRNA) that are derived from protein-coding genes. RNA-seq has been developed almost 15 years ago and provides a high-throughput sequencing method to map and quantify the transcriptome³⁵². RNA-seq is most commonly used to assess differential gene expression in biological samples to better understand the regulation or dysregulation of gene networks in health and disease. Other applications comprise the analysis of translational dynamics (the translome), RNA structure (the structurome) and RNA-RNA or RNA-protein interactions³⁵³. RNA-seq can be applied to a large number of cells or tissue (bulk RNA seq analysis) to assess changes in gene expression. Usually, bulk RNA-seq measures the average expression levels of individual genes across millions of cells. More advanced methods such as single-cell RNA-seq and spatially resolved RNA-seq allow the study of specific cell types and cell-to-cell interactions³⁵³. In the field of iPSC disease modelling, RNA-seq analysis provides an unbiased approach to study changes in gene expression patterns and associated pathways, to gain insight into key molecular disease mechanisms. For this PhD project, I decided to perform bulk RNA-seq analysis in order to get a first impression of disease-specific changes in gene expression. I used the Illumina Next Seq 500/550 sequencing workflow (Methods Chapter 2, 2.8).

Some figures have been adapted from a publication arising from this research, Abela L^{*} et al., 2024³⁰¹.

7. 2. Results

Patient and control mDA neurons were cultured until day 65 of differentiation. Total RNA was extracted from three independent differentiations per line and a total of 12 samples was sent for RNA sequencing: 9 patient lines and 3 isogenic controls. Three non-isogenic age-matched controls (Control 03) were already available from previous bulk RNA-seq analysis in our laboratory²⁵⁸. Bulk RNA sequencing was undertaken at UCL Genomics, UCL GOS ICH. With guidance from Dr. Giada Rossignoli, I performed analysis of the raw data including quality

control of the reads and subsequent trimming, reads mapping to a reference genome, counting the reads mapped to genes, creation of a count matrix and extraction and annotation of differentially expressed genes (DEGs) using the Galaxy platform (<https://usegalaxy.org>). DEGs are represented with a threshold P-value <0.05 and an absolute Fold Change (FC) >2 .

In order to get a comprehensive impression of disease- and non-disease associated gene expression patterns, I conducted several comparisons. First, I compared Patient 2-1 to both the isogenic and non-isogenic control. Next, I compared the isogenic to the non-isogenic control to identify non-disease-associated gene expression patterns, which are shared between Patient 2-1 and the isogenic control due to the same genetic background. In a second step, I compared all three patients together to the non-isogenic control due to the lack of isogenic controls for Patient 3-1 and Patient 4-1. I used heat map analysis to demonstrate differential gene expression patterns between control and patient groups. Principal component analysis constitutes another useful and frequently used technique to reduce dimensionality and demonstrate transcriptome differences between patient and control groups.

7. 2. 1. Patient lines show differential gene expression profiles compared to control lines

7. 2. 1. 1. Patient 2-1 compared to its corresponding isogenic CRISPR 2-1 line

Analysis of Patient 2-1 compared to the isogenic control CRISPR 2-1 revealed a total of 1096 protein-coding DEGs, of which 593 DEGs were underexpressed and 503 DEGs were overexpressed (**Fig. 7. 1A**). Gene ontology (GO) analysis of underexpressed DEGs for biological processes using the PANTHER platform (<https://geneontology.org>) showed underexpression of developmental processes including *Multicellular Organism Development*, *System Development*, *Nervous System Development*, *Multicellular Organismal Process* and *Anatomical Structure Development* (**Fig. 7. 1B**). GO analysis of overexpressed DEGs for biological processes included *Cilium and Organelle Assembly*, as well as *Microtubule Organization and Processes* (**Fig. 7. 1C**).

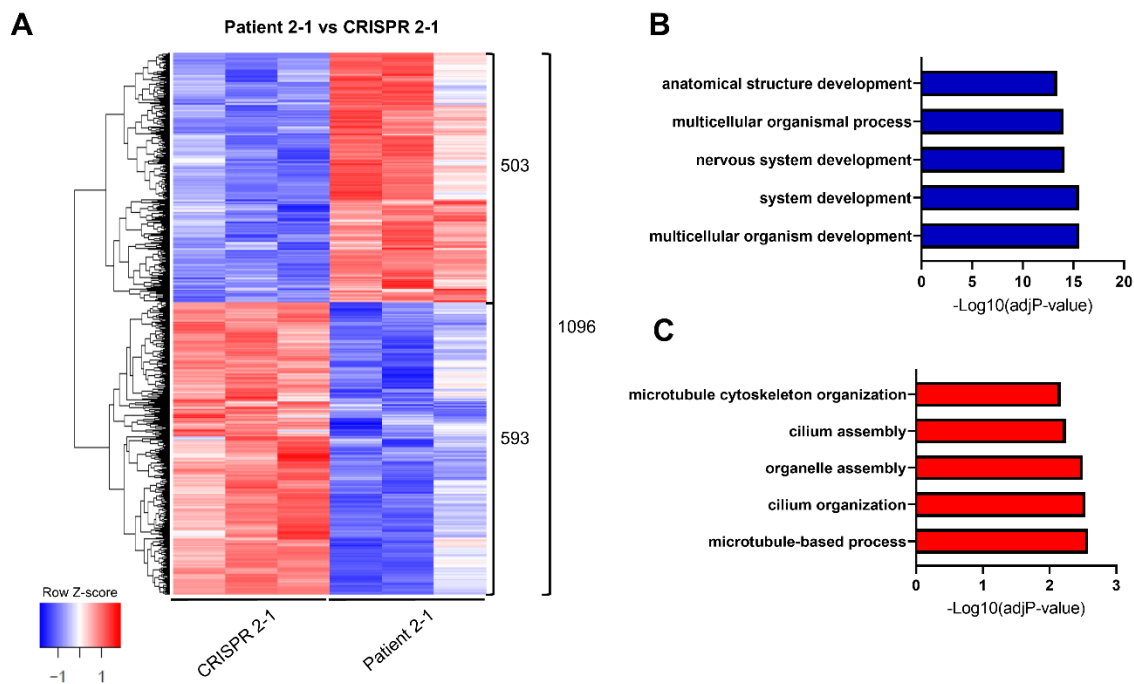


Figure 7. 1. Heat map and GO term enrichment analysis for biological processes in Patient 2-1 versus CRISPR 2-1. *A)* Heat map with hierarchical clustering of protein-coding DEGs in Patient 2-1 compared to CRISPR 2-1 ($n = 3$). *B)* Top five GO terms of underexpressed DEGs (blue) for biological processes. *C)* Top five GO terms of overexpressed DEGs (red) for biological processes.

GO analysis of underexpressed DEGs for cellular compartments using the Enrichr platform (<https://maayanlab.cloud/Enrichr/>) revealed *Collagen-Containing Extracellular Matrix*, *Neuron Projection*, *Synaptic and Exocytic Vesicle membrane* and *Potassium Channel Complex* (**Fig. 7. 2**). Overexpressed DEGs for cellular compartments include *Motile Cilium*, *Clathrin-Sculpted Gamma-Aminobutyric Acid Transport Vesicle*, *Clathrin-Sculpted Gamma-Aminobutyric Acid Transport Vesicle Membrane*, *Cilium* and *Lytic Vacuole Membrane* (**Fig. 7. 2**).

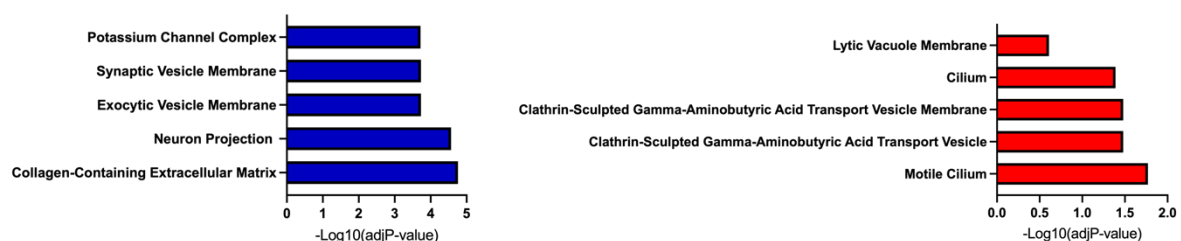


Figure 7. 2. GO term enrichment analysis for cellular compartments in Patient 2-1 versus CRISPR 2-1. *Left side:* top five GO terms of underexpressed DEGs (blue) for cellular compartments. *Right side:* top five GO terms of overexpressed DEGs (red) for cellular compartments.

7. 2. 1. 2. Patient 2-1 compared to Control 03

Analysis of Patient 2-1 compared to the non-isogenic Control 03 showed a total of 2769 protein-coding DEGs, of which 1745 DEGs were underexpressed and 1024 DEGs were overexpressed (**Fig. 7. 3A**). GO analysis of underexpressed DEGs for biological processes included a range of developmental processes including *Developmental Process*, *Multicellular Organism Development*, *System Development*, *Anatomical Structure Development* and *Morphogenesis* (**Fig. 7. 3B**). GO analysis of overexpressed DEGs for biological processes revealed *Organonitrogen Compound Biosynthetic Process*, *Amine Biosynthetic Process*, *Cellular Process*, *Cellular Nitrogen Compound Biosynthetic Process* and *Translation* (**Fig. 7. 3C**).

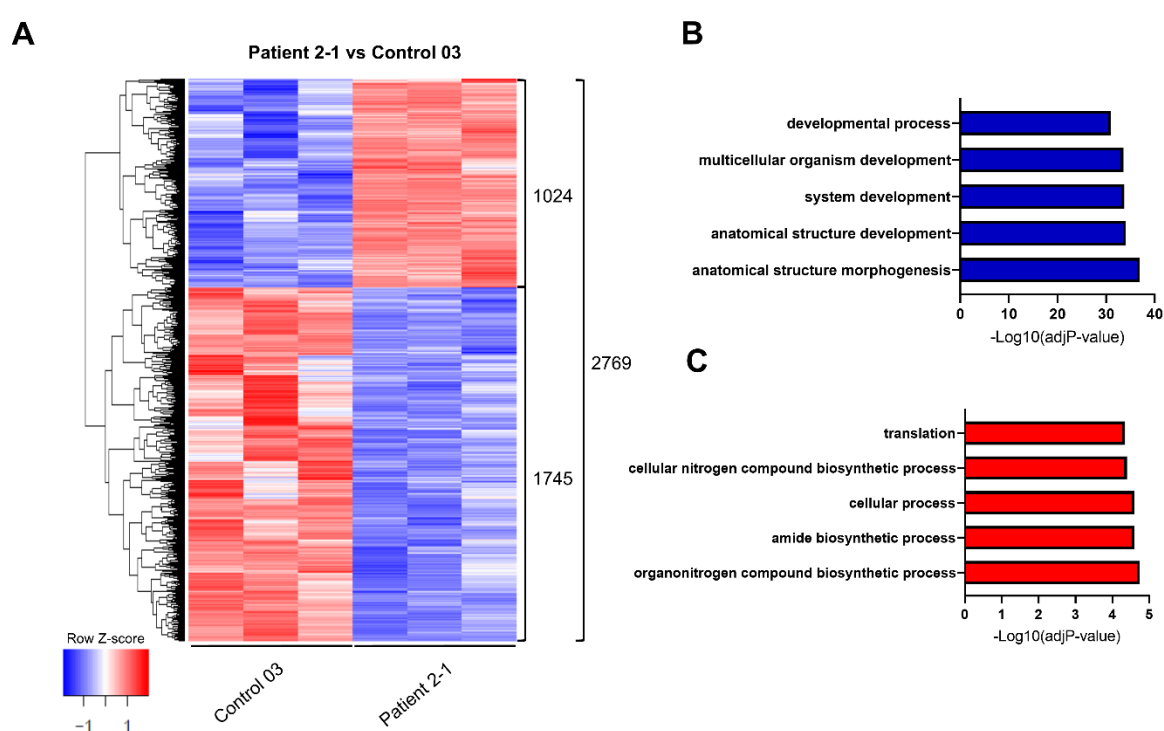


Figure 7. 3. Heat map and GO term enrichment analysis for biological processes in Patient 2-1 versus Control 1. **A)** Heat map with hierarchical clustering of protein-coding DEGs in Patient 2-1 compared to Control 03 ($n = 3$). **B)** Top five GO terms of underexpressed DEGs (blue) for biological processes. **C)** Top five GO terms of overexpressed DEGs (red) for biological processes.

GO analysis of underexpressed DEGs for cellular compartments revealed *Collagen-Containing Extracellular Matrix*, *Endoplasmic Reticulum Lumen*, *Basement Membrane*, *Focal Adhesion* and *Cell-Substrate Junction* (**Fig. 7. 4**). Overexpressed DEGs for cellular compartments include *Ribosome*, *Clathrin-Sculpted Gamma-Aminobutyric Acid Transport Vesicle*, *Clathrin-Sculpted Gamma-Aminobutyric Acid Transport Vesicle Membrane*, *Polysomal Ribosome* and *Small Ribosomal Subunit*.



Figure 7. 4. GO term enrichment analysis for cellular compartments in Patient 2-1 versus Control 03. Left side: top five GO terms of underexpressed DEGs (blue) for cellular compartments. Right side: top five GO terms of overexpressed DEGs (red) for cellular compartments.

7. 2. 1. 3. All Patients compared to Control 03

Analysis of all Patients compared to Control 03 revealed a total of 2939 protein-coding DEGs, of which 1722 DEGs were underexpressed and 1217 DEGs were overexpressed (**Fig. 7. 5A**). GO analysis of underexpressed DEGs for biological processes showed *Anatomical Structure Morphogenesis and Development*, *System Development*, *Multicellular Organism Development* and *Developmental Process* (**Fig. 7. 5B**). GO analysis of overexpressed DEGs for biological processes revealed *Cytoplasmic Translation*, *Translational Initiation*, *Protein targeting to ER*, *Establishment of Protein Localisation to ER* and *Organic Substance Biosynthetic Process* (**Fig. 7. 5C**).

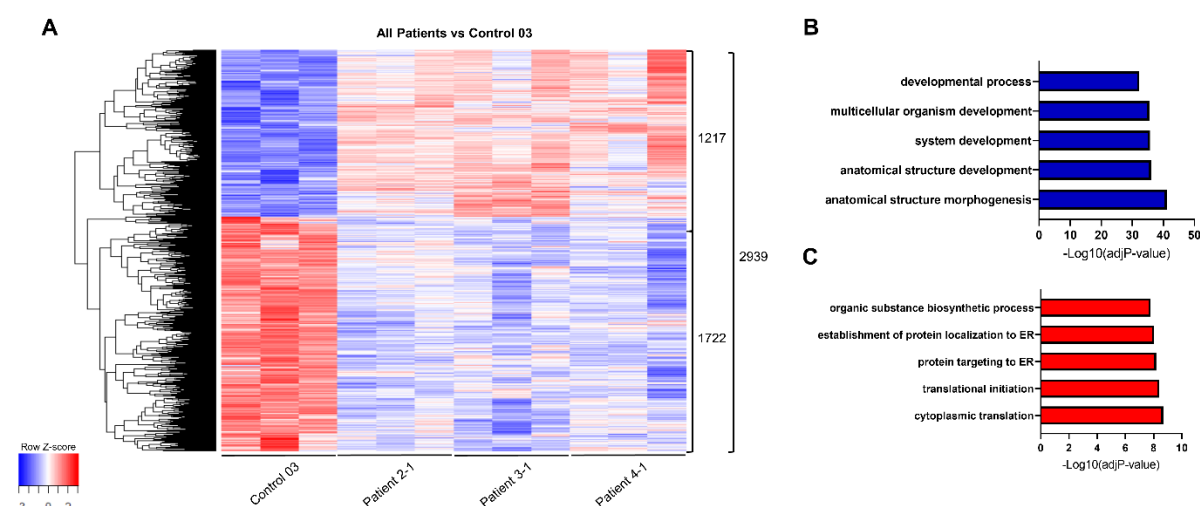


Figure 7. 5. Heat map and GO term enrichment analysis for biological processes in all Patients versus Control 1. A) Heat map with hierarchical clustering of protein-coding DEGs in all Patients compared to Control 03 ($n = 3$). B) Top five GO terms of underexpressed DEGs (blue) for biological processes. C) Top five GO terms of overexpressed DEGs (red) for biological processes.

GO analysis of underexpressed DEGs for cellular processes identified *Collagen-Containing Extracellular Matrix*, *Basement Membrane*, *Endoplasmic Reticulum Lumen*, *Intracellular Organelle Lumen*, *Cell-Substrate Junction* and *Focal Adhesion* (**Fig. 7. 6**). GO analysis of

overexpressed DEGs include *Polysomal Ribosome*, *Chitosome*, *Ribosome*, *Cytosolic Large Ribosomal Subunit* and *Large Ribosomal Subunit*.

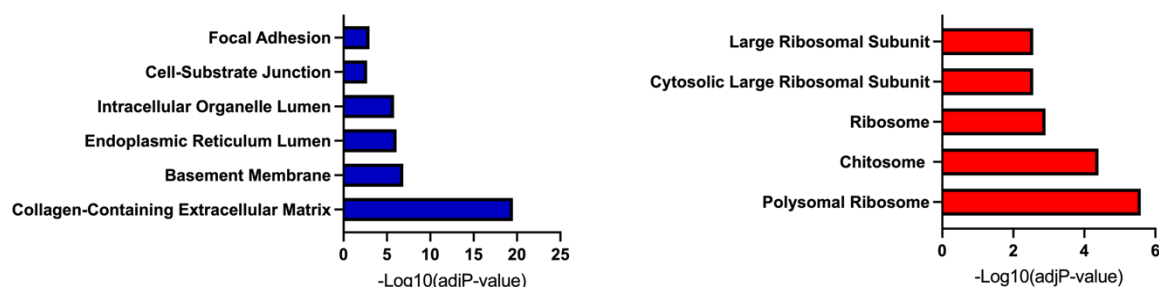


Figure 7. 6. GO term enrichment analysis for cellular compartments in all Patients versus Control 03. Left side: top five GO terms of underexpressed DEGs (blue) for cellular compartments. Right side: top five GO terms of overexpressed DEGs (red) for cellular compartments.

7. 2. 1. 4. CRISPR 2-1 compared to Control 03

To further clarify disease-associated gene expression patterns, I also compared CRISPR 2-1 to Control 03. Heat map analysis revealed a differential pattern of gene expression, which is not surprising given the different genetic backgrounds. I found a total of 2701 protein-coding DEGs, of which 1626 DEGs were underexpressed and 1075 DEGs were overexpressed (**Fig. 7. 7A**). GO analysis of underexpressed DEGs for biological processes revealed *External Encapsulating Structure Organization*, *Extracellular Structure Organization*, *Extracellular Matrix Organization*, *Anatomical Structure Morphogenesis* and *Circulatory System Development*. GO analysis of overexpressed DEGs for biological processes identified *Cell-Cell Adhesion Via Plasma-Membrane Adhesion Molecules*, *Nervous System Development*, *Homophilic Cell Adhesion Via Plasma Membrane Adhesion Molecules*, *Cellular Process* and *Cholesterol Biosynthetic Process*.

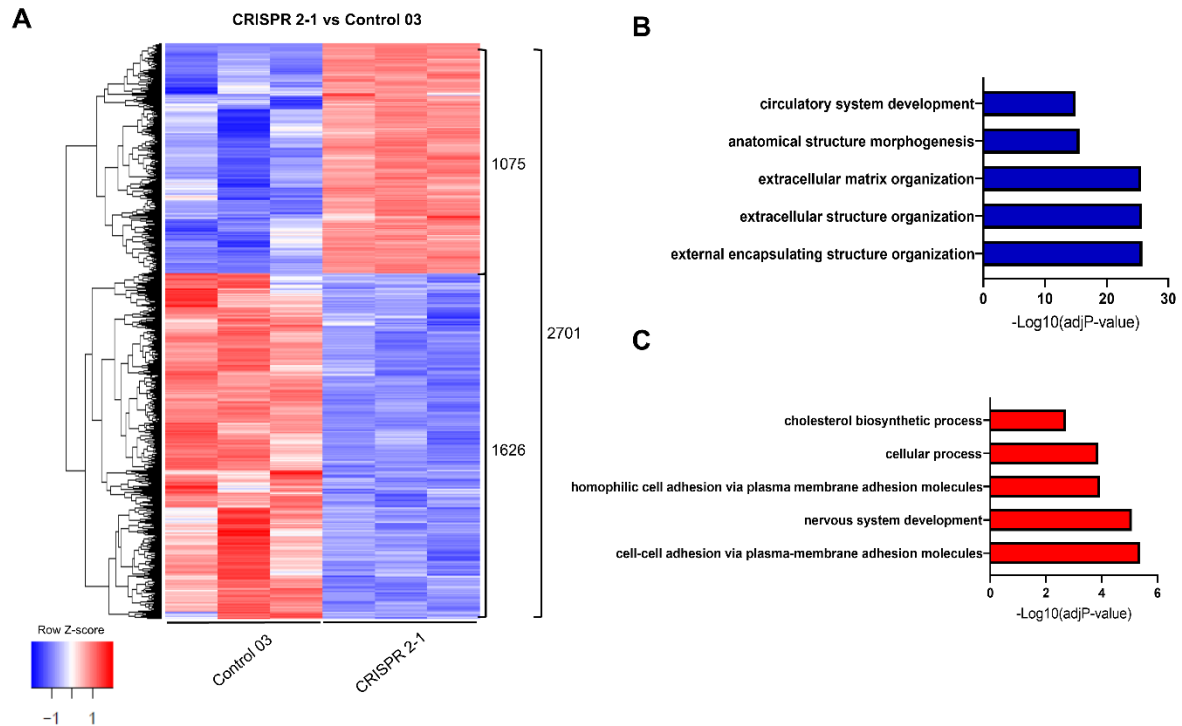


Figure 7. 7. Heat map and GO term enrichment analysis for biological processes in CRISPR 2-1 versus Control 03. *A)* Heat map with hierarchical clustering of protein-coding DEGs in CRISPR 2-1 compared to Control 03 ($n = 3$). *B)* Top five GO terms of underexpressed DEGs (blue) for biological processes. *C)* Top five GO terms of overexpressed DEGs (red) for biological processes.

GO analysis of underexpressed DEGs for cellular processes showed *Collagen-Containing Extracellular Matrix*, *Endoplasmic Reticulum Lumen*, *Cell-Substrate Junction*, *Basement Membrane* and *Intracellular Organelle Lumen* (**Fig. 7. 8**). GO analysis of overexpressed DEGs include *Cytosolic Large Ribosomal Subunit*, *Large Ribosomal Subunit*, *Ribosome*, *Neuron Projection* and *Rough Endoplasmic Reticulum Membrane*.

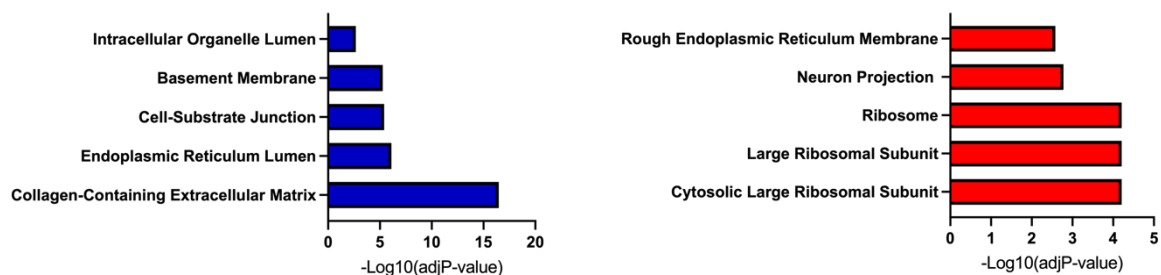


Figure 7. 8. GO term enrichment analysis for cellular compartments in CRISPR 2-1 versus Control 03. *Left side:* top five GO terms of overexpressed DEGs (red) for cellular compartments. *Right side:* top five GO terms of underexpressed DEGs (blue) for cellular compartments.

7. 2. 3. GO term enrichment analysis for biological processes in patient lines compared to control lines reveals dysregulation of developmental processes

In general, GO term enrichment analysis showed lower $\log_{10}(\text{adjP-values})$ for GO terms of overexpressed DEGs than $\log_{10}(\text{adjP-values})$ for GO terms of underexpressed DEGs indicating a stronger biological influence of underexpressed DEGs. In the following analysis, I therefore focused on underexpressed DEGs.

GO term analysis of underexpressed DEGs for biological processes in Patient 2-1 versus both controls and in all Patients versus Control 03, respectively, revealed dysregulation of a number of common developmental processes including *Anatomical Structure Development*, *Multicellular Organism Development* and *System Development* (**Fig. 7. 1, Fig. 7. 3, Fig. 7. 5**). Nervous System Development appeared among the top five GO terms of underexpressed DEGs in Patient 2-1 versus CRISPR 2-1, while in Patient 2-1 versus Control 03, Nervous System Development only appeared among the top 75 GO terms with a $\log_{10}(\text{adjP-value})$ of 3.98, and among the top 50 GO terms in all Patients versus Control 03 with a $\log_{10}(\text{adjP-value})$ of 4.27.

7. 2. 4. GO term enrichment analysis for cellular compartments in patient lines compared to control lines highlights vesicle membrane compartments

Analysis of underexpressed GO terms for cellular compartments in Patient 2-1 versus CRISPR 2-1 highlights dysregulation of genes involved in vesicle membrane pathways (**Fig 7. 2**). Genes associated with the cellular compartment *Synaptic Vesicle Membrane* include several membrane transporters including the vesicular glutamate transporters *SLC17A6* (Solute Carrier Family 17 Member 6), *SLC17A7* (Solute Carrier Family 17 Member 7) and *SLC17A8* (Solute Carrier Family 17 Member 7), as well as two vesicular monoamine transporters *SLC18A1* (Solute Carrier Family 18 Member A1) and *SLC18A2* (Solute Carrier Family 18 Member A2). *SLC18A2* or *VMAT2* is involved in the loading of dopamine and serotonin into SVs. Underexpression of this gene may result in impaired neurotransmitter loading with subsequently impaired neurotransmission. Indeed, mutations in *SLC18A2* cause "Infantile-Onset and Brain Dopamine-Serotonin Vesicular Transport Disease", a rare, infantile-onset movement disorder characterised by parkinsonism and dystonia, developmental delay, mood disturbances and autonomic dysfunction³⁵⁴. Functional studies revealed severely impaired vesicular transport function³⁵⁴. Further genes associated with the cellular compartment *Synaptic Vesicle Membrane* include *RPH3A* (Rabphilin-3A), which is part of the SV membrane and involved in SV trafficking and calcium-triggered exocytosis; *SYNPR* (Synaptoporin) and *SV2B*

(Synaptic Vesicle Glycoprotein 2B), which are intrinsic SV membrane proteins. In Patient 2-1 and in all Patients versus Control 03 the cellular compartment *Synaptic Vesicle Membrane* and *Exocytic Vesicle Membrane* only appeared among the top 75 underexpressed GO terms with a $\log_{10}(\text{adjP-value})$ of 0.39 and 0.43 (*Synaptic Vesicle Membrane*), respectively, and a $\log_{10}(\text{adjP-value})$ of 0.4 and 0.43 (*Exocytic Vesicle Membrane*), respectively.

The top five overexpressed GO terms for cellular processes in Patient 2-1 versus both CRISPR 2-1 and Control 03 include *Clathrin-Sculpted Gamma-Aminobutyric Acid Transport Vesicle* and *Clathrin-Sculpted Gamma-Aminobutyric Acid Transport Vesicle Membrane*, while in all Patients versus Control 03, these GO terms only appear among the top 10 and top 15 overexpressed GO terms, respectively. Eight genes localize to these cellular compartments including *DNAJC5* (DnaJ (Hsp40) homolog, subfamily C, member 5), *GAD1/2* (glutamate decarboxylase 1 and 2), *HSPA8* (heat shock 70kDa protein 8), *RAB3A* (member RAS oncogene family), *SLC32A1* (solute carrier family 32 (GABA vesicular transporter), member 1), *SYT1* (synaptotagmin 1) and *VAMP2* (vesicle-associated membrane protein 2 (synaptobrevin 2)). *DNAJC5* is a co-chaperone protein for the SNARE protein SNAP-25 and involved calcium-dependent exocytosis. *GAD1* and *GAD2* are involved in the synthesis of glutamate, while *SLC32A1* transports GABA to SV. *RAB3A* is a small GTP-binding protein involved in the membrane transport between different intracellular compartments, in particular in calcium-dependent exocytosis and associates with SV. *VAMP2* is a SNARE protein of SV and involved in exocytosis. It is therefore possible that overexpression of these genes might be to compensate for disruption of GABA- and glutamate-associated SV cycling.

7. 2. 5. GO term enrichment analysis in CRISPR 2-1 compared to Control 03 allows differentiation of disease-associated and non-disease-associated gene expression patterns

Analysis of common underexpressed GO terms for biological processes in Patient 2-1 versus Control 03 and in CRISPR 2-1 versus Control 03 revealed *Anatomical Structure Morphogenesis*, while analysis of common overexpressed GO terms for biological processes include *Cellular Processes*.

Analysis of common underexpressed GO term for cellular compartments in Patient 2-1 versus Control 03 and in CRISPR 2-1 versus Control 03 showed *Collagen-Containing Extracellular Matrix*, while analysis of common overexpressed DEGs for cellular processes included

translation-associated processes such as *Ribosome*, *Polysomal Ribosome* and *Ribosomal subunits*. These finding suggests that the aforementioned common GO terms for biological processes and cellular compartments are likely to not be disease-associated features and rather a component of genetic background in Patient 2-1 and CRISPR 2-1.

To investigate whether the process of CRISPR-Cas9 generation might be responsible for differences in gene expression patterns, I further compared underexpressed GO terms for biological processes in Patient 2-1 versus CRISPR 2-1 (**Fig. 7. 1**) with overexpressed GO terms in CRISPR 2-1 versus Control 03 (**Fig. 7. 7**). The analysis revealed one common GO term, namely *Nervous System Development*. Two possible explanations may account for this finding: 1) the technical process of CRISPR-Cas9 generation (and potential off-target effects) may have affected gene expression patterns associated with *Nervous System Development*, 2) correction of the respective *DNAJC6* mutation may have resulted in overexpression of genes associated with *Nervous System Development*. To further investigate this finding, I compared gene expression patterns associated with *Nervous System Development* across all patients and control lines (Section 7. 3).

7. 2. 6. Analysis of genes associated with Nervous System Development, Dopaminergic Neurogenesis and Clathrin-mediated Endocytosis

GO term enrichment analysis revealed several important biological processes and cellular compartments that might contribute to the observed cellular phenotypes. *Nervous System Development* was among the top five underexpressed GO terms for biological processes in Patient 2-1 versus CRISPR 2-1, but also emerged (with a lower ranking) in the comparison of Patient 2-1/all Patients versus Control 03. *Synaptic Vesicle Membrane* emerged among the top five underexpressed GO terms for cellular compartments in Patient 2-1 versus CRISPR 2-1. As reconstitution of the SV membrane is an essential function of CME, I analysed genes associated with the GO term *Clathrin-Mediated Endocytosis*. Finally, I wanted to explore whether there were defects in dopaminergic neurogenesis given the experimental findings of aberrant ventral midbrain patterning. *Dopaminergic Neurogenesis* emerged as number 1 in the GO term enrichment analysis of Patient 2-1 versus CRISPR 2-1 using the WikiPathway 2023 Human analysis with a log10(adjP-value) of 2.0 (**Fig. 7. 9**).

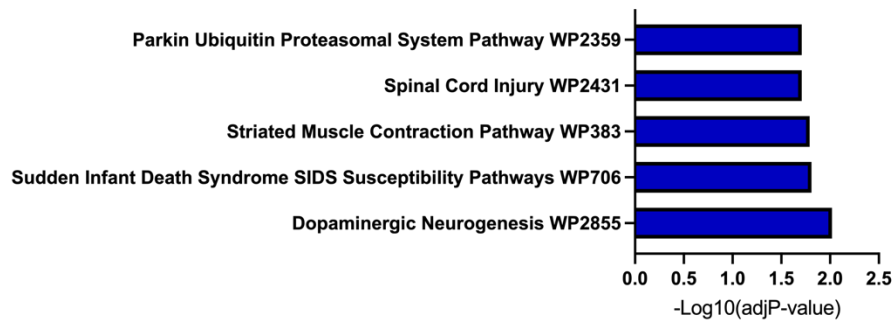


Figure 7. 9. GO term enrichment analysis for pathways in Patient 2-1 versus CRISPR 2-1. Top five underexpressed GO terms using WikiPathway 2023 Human (<https://maayanlab.cloud/Enrichr/>).

To unravel DEGs associated with the GO terms *Nervous System Development*, *Clathrin-Mediated Endocytosis* and *Dopaminergic Neurogenesis*, I extracted the corresponding genes from the Pathcards platform (<https://pathcards.genecards.org/>): *Nervous System Development* with a total of 1169 genes; *Clathrin-Mediated Endocytosis* with a total of 146 genes; and *Dopaminergic Neurogenesis* with a total of 30 genes.

	CLATHRIN-MEDIATED ENDOCYTOSIS	DOPAMINERGIC NEUROGENESIS	NERVOUS SYSTEM DEVELOPMENT
PATIENT 2-1 versus CRISPR 2-1			
Underexpressed genes (total 593 DEGs)	<i>AMPH, DNAJC6, TACR1, TF</i>	<i>DDC, FOXA2, LMX1A, LMX1B, NEUROD1, NR4A2, SLC18A2</i>	<i>ACVR1C, ADGRG6, PAX6, CACNA1G, CFC1, CNTN2, COL2A1, COL4A2, DPYSL5, DPYSL3, DSCAML1, EBF1, EFNA1, EFNA3, EOMES, EPHA5, EPHA6, FOXA2, FOXP1, GFRA2, GFRA3, H2AC6, H2AC8, H2AJ, H2BC4, H2BC5, H2BC6, H2BC7, H2BC8, H2BC11, H2BC12, H2BC15, H2BC21, H3-3B, H4C5, HIF3A, HEY2, MAPK13, MYOG, NEUROD1, NOG, NRP2, LHX9, PKP1, POU3F2, PSMB8, MEIS1, RND1, SALL4, SCD5, SCN7A, SEMA3E, SLIT1, SRGAP2, TRPC5, TUBA1A, TUBB2B, TUBB4A, RGMA, VAV3, ZIC3</i>
Overexpressed genes (total 503 DEGs)	<i>REPS1, SLC18A3, STAM2</i>	-	<i>COL9A2, CNTN6, CHL1, CXCL12, EFNA5, FGF10, ISL1, LHX2, MYH14, PTPRC</i>
PATIENT 2-1 versus CONTROL 03			
Underexpressed genes (total 1745 DEGs)	<i>BTC, DAB2, DNAJC6, FZD4, ITSNI, LRP2, NECAP2, STON1, STON2, TACR1, WNT5A</i>	<i>ALDH1A1, EN1, FOXA2, GLI2, LMX1A, LMX1B, MSX1, NEUROD1, NKX6-1, NR4A2, SLC18A2, SHH</i>	<i>ADGRG6, ADGRV1, AGRN, AJUBA, AKT2, ALCAM, ARHGEF28, BOC, CACNA1C, CACNA1H, CACNG4, CDK2, CD36, CNTN6, COL2A1, COL3A1, COL4A1, COL4A2, COL4A4, COL4A5, COL5A1, COL5A2, COL5A3, COL6A2, COL6A3, COL9A1, COL9A3, CXCL12, DSCAML1, DOCK1, DSP, EFNA4, EFNB2, EFNB3, EPHA4, EPHA5, EPHA6, EPHB4, ERBB2, FOXA1, FOXA2, FOXC1, FOXH1, FOXP1, FURIN, HES1, HEY2, H2AX, H3C6, H4C8, HNF4G, ITGA5, ITGA2, ITGB3, ITGAV, ITSNI, KLF5, LAMA1, LAMA2, LAMB1, LAMC1, LEF1, LFNG, LGI3, LYN, MAFB, MAML2, MAMLD1, MBP, MEIS1, MMP2, MAPK13, MSII, MYO10, NCAM1, NEUROD1, NKX6-1, NOG, NOTCH1, NTN1, NTN3, PAX6, PCK1, PLXNB1, PMP22, POU3F2, PRX, PSMB8, PTGDS, PTPRC, EBF1, RARG, RGMA, ROBO1, RUNX1, SALL1, SALL4, SEMA5A, SHH, SLIT1, SLIT2, SLIT3, SLC2A4, SMAD3, SNC7A, SOX9, SPTB, TEAD2, TCF3, TCF4, TCF7, TCF7L2, TFDP2, TLN1, TRPC4, TRPC6, TUBB6, YAP, VAV3, WWTR1</i>
Overexpressed genes (total 1016 DEGs)	<i>ARPC3, COPS3, DNM3, NECAP1, SH3GL3, SLC18A3, TGFA, VAMP2</i>	<i>CDKN1C</i>	<i>ARPC3, CACNG2, CACNG3, CDKN1A, CEBPA, CNOT9, DHH, DNM3, EFNA5, EPHA2, IAPP, ISL1, KRT10, LHX2, LIN28A, MAPK8, MED8, MED10, MED27, MET, NGEF, NRTN, NR5A1, PLXNC1, POLR2K, POU3F1, PSMB1, PSMC4, PSMD8, PSMD10, PRSS8, RARB, RPLP2, RPL18, RPL21, RPL24, RPL27, RPL31, RPL39, RPL39L, RPS13, RPS16, RPS18, RPS21, RPS26, RPS27, RPS29, RPS4X, TBX6, UPF3B, GCK, SCN4A, SEMA7A, TCHH, TUBA4A</i>

ALL PATIENTS versus CONTROL 03

Underexpressed genes (total 1722 DEGs)	<i>BTC, DAB2, DNAJC6, FZD4, ITSNI, LDLR1P1, LRP2, NECAP2, TACR1, STON1, STON2, WNT5A</i>	<i>EN1, FOXA2, GLI2, LMX1A, LMX1B, MSX1, NEUROD1, NKX6-1, NR4A2, SHH, SLC18A2</i>	<i>ADGRG6, ADGRV1, AGRN, AJUBA, AKT2, ALCAM, ANK1, ARHGEF28, BOC, EBF1, CACNA1C, CACNA1H, CACNG4, CD36, CDK2, CFC1, COL2A1, COL3A1, COL4A1, COL4A2, COL4A5, COL5A1, COL4A4, COL5A2, COL5A3, COL6A2, COL6A3, COL9A1, COL9A3, CNTN6, CXCL12, DOCK1, DSP, EFNA4, EFNB2, EFNB3, EPHA4, EPHA5, EPHA6, EPHA7, EPHB4, ERBB2, FOXA1, FOXA2, FOXC1, FOXH1, FOXPI, FURIN, H2AX, HES1, HEY2, HNF4G, H4C8, ITGA2, ITGA5, ITSNI, KLF4, KLF5, KMTD2, LAMA2, LAMB1, LAMC1, LEF1, LFNG, MAML2, NCAM1, NEUROD1, NTN1, NTN3, MAMLI, MAMLD1, MMP2, MYO10, PBX1, PAX6, PCK1, PLXNB1, PMP22, POU3F2, PSMB8, PTGDS, NKX6-1, MEIS1, MSII, RGMA, RUNX1, H3C6, RARG, SCN7A, SALL1, SALL4, SEMA5A, SHH, SOX9, SLIT1, SLIT2, SLIT3, SMAD3, SRF, TEAD2, TCF3, TCF4, TCF7, TLN1, SPTB, TRPC4, TRPC5, TRPC6, TUBB6, VAV3, WWTR1, YAPI, ZIC3, ZFPM2</i>
Overexpressed genes (total 1217 DEGs)	<i>ARPC3, CD3G, COPS3, NECAP1, SH3GL3, SLC18A3, TGFA, UBA52, VAMP2,</i>	<i>CDKN1C, FGF8, TH</i>	<i>ARPC3, CACNG2, CACNG3, CCND3, CDKN1A, CEBPA, CHL1, CNOT9, DHH, DLL3, DSC1, EFNA5, EPHA2, GCK, GRB10, HMGCR, IAPP, ISL1, KRT10, KRT18, LHX2, LIN28A, LPL, MAPK8, MED8, MED10, MET, NGEF, NRTN, NR5A1, PLXNC1, POLR2K, POU3F1, PRSS8, PSMB1, PSMC4, PSMD8, PSMD10, RARB, RPLP2, RPL5, RPL8, RPL9, RPL18, RPL18A, RPL21, RPL22L1, RPL27, RPL31, RPL32, RPL34, RPL35, RPL38, RPL39, RPL39L, RPL41, RPS8, RPS13, RPS16, RPS18, RPS21, RPS29, RBPJ, RPL24, RPS11, RPS27, RPS55, RPS4X, SEMA7A, TCHH, TUBA4A, UBA52, UPF3B</i>
CRISPR 2-1 versus CONTROL 03			
Underexpressed genes (total 1626 DEGs)	<i>BTC, DAB2, EGFR, FZD4, IGF2R, ITSNI, LDLR1P1, LRP2, NECAP2, STON2, WNT5A</i>	<i>EN1, NKX6-1, SHH, GLI2, ALDH1A1, MSX1</i>	<i>ADGRG6, AGRN, AJUBA, AMH, ARHGEF28, BOC, CACNA1C, COL3A1, COL4A1, COL4A3, COL4A5, COL5A1, COL5A2, COL5A3, COL6A3, CNTN6, CXCL12, DAG1, DOCK1, DSC2, DSP, EFNB2, EFNB3, EGFR, EPHA4, EPHB4, ERBB2, FGF10, FGFR1, FOXA1, FOXH1, FURIN, HES1, H3C6, H4C8, HNF4G, ITGA2, ITGAV, ITSNI, KIF4A, KMT2D, KLF5, LAMA2, LAMB1, LYN, MAML2, MMP2, MSII, MYH14, MYO10, NFKB1, NKX6-1, NTN1, NTN3, PCK1, PLXNB1, PMP22, PPARA, POU3F2, PTGDS, PTPRC, RARG, RUNX1, SALL1, SCN7A, SHH, SLIT3, SOX9, TCF4, TCF7, TEAD2, TLN1, TRPC4, TRPC6, YAPI</i>
Overexpressed genes (total 1075 DEGs)	<i>AMPH, DN3M3, OCRL, SH3GL3, SH3KBP1, SLC18A3, TGFA, TF, UBC, VAMP2</i>	<i>OTX2</i>	<i>AGAP2, AKT3, CACNA1I, CACNG2, CACNG3, CDKN1A, CEBPA, DCX, DLL3, DN3M3, DOK4, EFNA1, EFNA3, EPHA2, EPHA8, EPHB3, GCK, GFRA2, H2AJ, H2AC8, H2BC5, H2BC6, H2BC7, H2BC8, H2BC11, H2BC15, H2BC21, H3-3A, H3-3B, H4C5, HMGCR, IAPP, LIN28A, LGI1, KDM6A, KRT10, MED10, NELL2, NGEF, NR6A1, NR5A1, NRTN, NTN4, PKP1, POU3F1, PRSS8, PSMB1, PSMD10, RARB, RBBP5, RBBP7, RL5, RPL9, RPL12, RPL17, RPL21, RPL24, RPL27, RPL32, RPL34, RPL38,</i>

RPL39, RPL39L, RPL41, RPS18, RPS21, RPS26, **RPS27**, RPS29, RPS4X, SEMA4A, SEMA7A, SH3KBP1, TBX6, TCHH, TUBA1A, TUBB2B, TUBA4A, **UBC**, UNC5A, ZNF467

Table 7. 2. Overview on significantly under- and overexpressed genes associated with Clathrin-Mediated Endocytosis, Dopaminergic Neurogenesis and Nervous System Development. Genes involved in Clathrin-Mediated Endocytosis (146 genes), Dopaminergic Neurogenesis (30 genes) and Nervous System Development (1169 genes) in Patient 2-1 versus CRISPR 2-1, Patient 2-1 versus Control 03, all Patients versus Control 03 and in CRISPR 2-1 versus Control 03, respectively. Genes in bold are associated with the Wnt signalling pathway (signalling by Wnt). Genes associated with the mentioned GO terms were extracted from the Pathcards platform (<https://pathcards.genecards.org/>).

I performed several comparisons to identify common disease-associated DEGs. **A)** comparison of Patient 2-1 versus both CRISPR 2-1 and Control 03, **B)** comparison of Patient 2-1 versus Control 03 and comparison of CRISPR 2-1 versus Control 03 and **C)** comparison of Patient 2-1 versus CRISPR 2-1 and comparison of CRISPR 2-1 versus Control 03. I considered the genes listed in **B)** and **C))** as non-disease associated DEGs most likely due to the same genetic background and subtracted them from **A)** to identify true disease-associated DEGs.

7. 2. 6. 1. Clathrin-Mediated Endocytosis

Analysis of genes associated with *Clathrin-Mediated Endocytosis* revealed a small number of underexpressed genes (**Table 7. 2, Table 7. 3**).

Common underexpressed genes		
A) Pat 2-1 vs CRISPR 2-1 Pat 2-1 vs Ctrl 03	B) Pat 2-1 vs Ctrl 03 CRISPR 2-1 vs Ctrl 03	C) Pat 2-1 vs CRISPR 2-1 CRISPR 2-1 vs Ctrl 03
<i>DNAJC6, TACR1</i>	<i>BTC, DAB2, FZD4, ITSN1, LRP2, NECAP2, STON2, WNT5A</i>	-
Disease-associated underexpressed genes		
<i>DNAJC6, TACR1</i>		

Table 7. 3. List of common underexpressed DEGs and identification of disease-associated DEGs. Genes listed in **B)** and **C)** are considered to be non-disease-associated DEGs due to their common genetic background.

DNAJC6 and *TACR1* (Tachykinin Receptor 1) were identified as disease-associated underexpressed genes. Underexpression of *DNAJC6* is not surprising, given the known protein truncating variant in this gene, leading to loss-of-function. The identification of *TACR1* downregulation is intriguing; this is a G-protein coupled neurokinin 1 receptor, which is selective for the neurotransmitter Substance P. The NK1 receptor is expressed in the CNS, particularly in the locus coeruleus and the ventral striatum³⁵⁵. NK1 has been involved in infection and inflammation³⁵⁵.

7. 2. 6. 2. Dopaminergic Neurogenesis

Analysis of genes associated with *Dopaminergic Neurogenesis* revealed a number of underexpressed genes (**Table 7. 2, Table 7. 4**).

Common underexpressed genes		
A) Pat 2-1 vs CRISPR 2-1 Pat 2-1 vs Ctrl 03	B) Pat 2-1 vs Ctrl 03 CRISPR 2-1 vs Ctrl 03	C) Pat 2-1 vs CRISPR 2-1 CRISPR 2-1 vs Ctrl 03
<i>FOXA2, LMX1A, LMX1B, NEUROD1, NR4A2, SLC18A2</i>	<i>EN1, NKX6-1, SHH, GLI2, ALDH1A1, MSX1</i>	-
Disease-associated underexpressed genes		
<i>FOXA2, LMX1A, LMX1B, NEUROD1, NR4A2, SLC18A2</i>		

Table 7. 4. List of common underexpressed DEGs and identification of disease-associated DEGs. Genes listed in B) and C) are considered to be non-disease-associated DEGs due to their common genetic background.

Disease-associated underexpressed genes in *Dopaminergic Neurogenesis* are mainly involved in midbrain floor specification (*LMX1A, LMX1B*), ventral patterning (*FOXA2*) and mDA identity (*NR4A2*). *NEUROD1* (Neuronal Differentiation 1) is a transcriptional activator that binds to enhancer regulatory elements of neuronal genes to induce the neuronal development program³⁵⁶. *NEUROD1* also regulates several cell differentiation pathways and plays a role in neuronal migration³⁵⁶. *NR4A2* (Nuclear Receptor Subfamily 4 Group A Member 2), also known as *NURR1*, acts as a transcriptional regulator involved in development, differentiation and maintenance of dopaminergic neurons in the substantia nigra. *NR4A2* induces the expression of several dopaminergic genes such as *SLC6A3, SLC18A2, TH* and *DRD2* that are critical for mDA neuron development³⁵⁷. Interestingly, another early-onset parkinsonism called “Intellectual developmental disorder with language impairment and early-onset dopa-responsive dystonia-parkinsonism (IDLDP)” is caused by heterozygous mutations in the *NR4A2* gene^{358,359}. Mutations in *NR4A2* have also been associated with familial PD³⁶⁰. Heterozygous *Nurr1*-deficient (*Nurr1*^{+/-}) mice show decreased levels of dopamine in the striatum and a reduced number of DA neurons in the substantia nigra³⁶¹. *SLC18A2* (Solute Carrier Family 18 Member A2), is located on secretory and synaptic vesicles and involved in the transport of biogenic amines, primarily striatal dopamine, but also adrenaline and noradrenaline, histamine and serotonin into vesicles. Mutations in *SLC18A2* are associated with infantile-onset parkinsonism called “Infantile-Onset and Brain Dopamine-Serotonin Vesicular Transport Disease”^{354,362}.

7. 2. 6. 3. Nervous System Development

Analysis of genes associated with *Nervous System Development* revealed a large number of underexpressed genes (Table 7. 2, Table 7. 5).

Common underexpressed genes		
A) Pat 2-1 vs CRISPR 2-1 Pat 2-1 vs Ctrl 03	B) Pat 2-1 vs Ctrl 03 CRISPR 2-1 vs Ctrl 03	C) Pat 2-1 vs CRISPR 2-1 CRISPR 2-1 vs Ctrl 03
ADGRG6, PAX6, CFC1, COL2A1, COL4A2, EPHA5, EPHA6, FOXA2, FOXP1, HEY2, NEUROD1, POU3F2, PSMB8, MEIS1, SALL4, SCN7A, SLIT1, TRPC5, RGMA, VAV3, ZIC3	ADGRG6, AGRN, AJUBA, ARHGEF28, BOC, CACNA1C, COL3A1, COL4A1, COL5A1, COL5A2, COL5A3, CXCL12, DOCK1, DSP, EFNB2, EFNB3, EPHA4, EPHB4, ERBB2, FOXA1, FURIN, HES1, H3C6, H4C8, HNF4G, ITGA2, ITGAV, ITSN1, KLF5, LAMA2, LAMB1, LYN, MAML2, MMP2, MSI1, MYO10, NKX6-1, NTN1, NTN3, PCK1, PLXNB1, PMP22, POU3F2, RARG, RUNX1, SALL1, SHH, SLIT3, TEAD2, TCF4, TCF7, TLN1, TRPC4, TRPC6	ADGRG6, POU3F2, SCN7A
Disease-associated underexpressed genes		
PAX6, CFC1, COL2A1, COL4A2, EPHA5, EPHA6, FOXA2, FOXP1, HEY2, NEUROD1, PSMB8, MEIS1, SALL4, SLIT1, TRPC5, RGMA, VAV3, ZIC3		

Table 7. 5. List of common underexpressed DEGs and identification of disease-associated DEGs. Genes listed in B) and C) are considered to be non-disease-associated DEGs due to their common genetic background.

Disease-associated underexpressed genes included several transcription factors involved in neural development, in particular in neurogenesis, neuronal migration, axon guidance, dendrite and synapse development and maintenance of embryonic and pluripotent stem cells. Below, I will discuss important functional aspects of these genes that may be associated with altered nervous system development in *DNAJC6* parkinsonism-dystonia.

PAX6 (paired box protein Pax-6) is transcriptional factor involved in central nervous system development. In rodents, *PAX6* controls patterning of the neural tube, neuronal specification, neuronal migration, and axonal projections^{363,364}. *PAX6* has a dual role in neural development. Firstly, *PAX6* is highly expressed in neural stem and progenitor cells of the subventricular zone (SVZ), balancing neural stem cell self-renewal with neurogenesis and determining neuronal cell fate of adult progenitors^{365,366}. Secondly, *PAX6* is expressed in a selective subpopulation of dopaminergic neurons in the olfactory bulb and specifies dopaminergic cell fate in SVZ progenitors^{367–369}. Postmortem studies in PD patients revealed a reduced number of PAX6-positive cells in the substantia nigra compared to age and sex matched controls³⁷⁰. Overexpression of *PAX6* in SH-SY5Y cells treated with common PD-inducing toxins showed

increased survival and reduced apoptosis and oxidative stress³⁷⁰. The authors of the study concluded that *PAX6* may play a role in dopaminergic neurodegeneration in PD³⁷⁰.

MEIS1 (Meis Homeobox 1) is a homeobox gene and a transcriptional regulator of *PAX6*³⁷¹. Together with *MEIS2*, *MEIS1* controls expression of distalless-homeodomain genes that are involved in the regulation of striatal neuron and cortical interneuron generation³⁷². *MEIS1* also regulates genes involved in the Notch signalling pathway³⁷³. *MEIS1* conditional knockout mice show cortical migration defects³⁷⁴.

HEY2 (Hes Related Family BHLH Transcription Factor With YRPW Motif 2) is expressed in the ventricular zone and a direct downstream target of the Notch signalling pathway³⁷⁵. *HEY2* inhibits neuronal basic helix-loop-helix (bHLH) genes, thereby promoting the maintenance of neural progenitor cells³⁷⁵. Misexpression of *HEY1* and *HEY2* at later embryonic stages inhibits neurogenesis in the mouse brain³⁷⁵.

NEUROD1 belongs to the family of neural lineage bHLH transcription factors, which are critical for central nervous system development³⁷⁶. *NEUROD* genes regulate differentiation of neuronal progenitor cells and their specification in the cerebral cortex, the cerebellum, the brainstem, and the spinal cord. *NEUROD1* is activated by Wnt signalling^{377,378}. Overexpression of *NEUROD1* leads to cell cycle exit and induces terminal maturation of neuronal progenitor cells in the subventricular zone and rostral migratory stream³⁷⁷.

SALL4 (Sal-like protein 4) is a transcriptional and epigenetic regulator expressed in embryonic stem cells (ESC)³⁷⁹. In ESCs, *SALL4* is required to maintain pluripotency and early embryonic development by regulating of *POU5F1*³⁷⁹.

FOXP1 (Forkhead Box P1) is a forkhead box transcription factor involved in the regulation of developmental gene expression in various types of tissues and cells³⁸⁰. In the central nervous system, *FOXP1* is mainly expressed in the cerebral cortex, striatum and spinal cord, where it regulates neuronal migration, differentiation and morphogenesis^{380–382}. Mutations in *FOXP1* have been associated with neurodevelopmental disorders and autism^{383,384}. Knockout of *FOXP1* in mice resulted in ectopic localisation of neurons due to radial migration defects and impaired axon outgrowth³⁸¹. In ESC-derived dopaminergic neurons, *FOXP1* regulates *PITX3*, a specific marker of midbrain dopaminergic neurons, thereby promoting midbrain identity³⁸⁵. *FOXP1* is

also a known regulator of Wnt/ β -catenin and Notch signalling, which are both regulated by CME^{386,387}.

EPHA5 (EPH Receptor A5) and *EPHA6* (EPH Receptor A6) are receptor tyrosine kinases (RTK) for ephrins, which are involved in axon guidance and synaptogenesis³⁸⁸. RTK signalling is regulated by CME¹⁷⁰. Internalisation of RTK by endocytosis leads to their down-regulation and localisation to recycling endosomes or lysosomes for subsequent degradation¹⁷⁰. Of note, *EPHA5* and *EPHA6* knockout and double knockout mice show abnormal spine morphology and abnormal Golgi staining with aggregation of neuronal and non-neuronal cells in distinct layers of the cortex³⁸⁹. The *Epha5* receptor is also expressed in the substantia nigra and neostriatum in mice³⁹⁰. *Epha5* transgenic mice expressing a truncated *EPHA5* receptor show decreased striatal dopamine and serotonin concentrations³⁹⁰.

VAV3 (Vav Guanine Nucleotide Exchange Factor 3) belongs to the family of guanine nucleotide exchange factors that control small GTP-hydrolyzing enzymes (GTPases)³⁹¹. *VAV3* becomes phosphorylated by upstream RTK and subsequently activates the small GTPases RhoA, Rac1 and Cdc42³⁹¹. These GTPases are involved in cytoskeletal rearrangement, neural differentiation, synaptogenesis, migration and myelination³⁹¹. The *VAV* small GTPase downstream targets Cdc42 and Rac1 are important for spine formation and neuronal development³⁹². *VAV* family members *VAV2* and *VAV3* also regulate axon guidance through binding of ephrins to their respective RTKs, which leads to VAV-dependent endocytosis of the ligand-receptor complex³⁹³.

SLIT1 (Slit Guidance Ligand 1) is a member of SLIT, a family of secreted glycoproteins. *SLIT1* is expressed in the developing cortex and contributes to neuronal migration, axon guidance and dendrite patterning^{394–396}. In interaction with *ROBO* (Roundabout homolog 1), *SLIT1* strongly induces dendritic growth and branching³⁹⁴. *SLIT1/2* double knockout mice show abnormal ventral location of ascending serotonergic and dopaminergic projections from the SN/VTA but also aberrant corticofugal, callosal, and thalamocortical projections in the forebrain indicating axon guidance errors³⁹⁵.

RGMA (Repulsive Guidance Molecule BMP Co-Receptor A) is a glycosylphosphatidylinositol-anchored membrane protein that acts as a repulsive guidance molecule, thereby inhibiting

neurite outgrowth, cortical neuron branching and development of mature synapses^{397,398}. In a MTPT mouse model of PD, inhibition of *RMGA* protects from loss of dopaminergic neurons³⁹⁹.

ZIC3 (Zic Family Member 3) belongs to the family of C2H2 zinc finger transcription factors, which are involved in early embryonic development, in particular in defining the left-right axis and midline neural patterning⁴⁰⁰. *ZIC3* is able to inhibit β -catenin-mediated transcription of Wnt target genes and is important for the maintenance of embryonic stem cells by activating the Nanog gene promoter^{401,402}.

TRPC5 (Transient Receptor Potential Cation Channel Subfamily C Member 5) is a transient receptor potential channel involved in calcium signalling. Calcium influx through voltage-gated calcium channels is important for the regulation of dendrite morphogenesis and connectivity⁴⁰³. *TRPC5* activates the CaMKII β signalling pathway at the centrosome in neurons and thereby reduces dendrite elaboration and growth⁴⁰⁴.

As outlined in Section 7. 5. 2, *Nervous System Development* appeared among the underexpressed GO terms for biological processes in Patient 2-1 versus CRISPR 2-1, but also among the overexpressed GO terms in CRISPR 2-1 versus Control 03. I extracted the respective set of common genes (**Table 7. 6**). Interestingly, this subset of genes contains many genes associated with the “signalling by Wnt” pathway (highlighted in bold and red in Table 7. 6). As discussed above, this gene expression pattern may result from the correction of the *DNAJC6* mutation, or, possible off-target effects during CRISPR-Cas9 generation.

Underexpressed genes Pat 2-1 vs CRISPR 2-1 Overexpressed genes CRISPR 2-1 vs Control 03
EFNA1, EFNA3, H2AC8, H2AJ, H2BC5, H2BC6, H2BC7, H2BC8, H2BC11, H2BC15, H2BC21 , H3-3B, H4C5 , PKP1, TUBA1A, TUBB2B, TUBB4A

Table 7. 6. List of common DEGs that are underexpressed in Patient 2-1 vs CRISPR 2-1 and overexpressed in CRISPR 2-1 vs Control 03. Genes in bold are associated with the Wnt signalling pathway (signalling by Wnt).

7. 2. 7. GO term enrichment analysis for synaptic location highlights presynaptic locations linked to synaptic vesicle cycling in patient lines compared to control lines

To investigate the effect of auxilin deficiency on synaptic gene expression, I performed synaptic gene enrichment analysis using the SynGO platform. GO analysis of underexpressed DEGs for synaptic location in Patient 2-1 versus CRISPR 2-1 shows a strong enrichment in *Synaptic Vesicle*, in particular *Synaptic Vesicle Membrane*, *Presynaptic Membrane*, *Presynaptic Endocytic Zone* and *Presynaptic Active Zone* (**Fig. 7. 10A left panel, Table 7. 2**). The same presynaptic locations appear in CRISPR 2-1 versus Control 03, but with a lower gene count. The enrichment is most pronounced in Patient 2-1 versus CRISPR 2-1 (**Fig. 7. 10A**), but is evident in Patient 2-1 versus Control 03 and in all Patients versus Control 03 as well (**Fig. 7. 11A/B**).

Common underexpressed genes associated with the compartment *Synaptic Vesicle* in Patient 2-1 versus CRISPR 2-1 and Patient 2-1/all Patients versus Control 03 (**Table 7. 2**) include several SV membrane transporters including (i) *SLC17A7* (Solute Carrier Family 17 Member 7), a sodium-dependent phosphate transporter located on the membrane of SV and involved in glutamate transport, (ii) *SLC17A6* (Solute Carrier Family 17 Member 6), a sodium-dependent inorganic phosphate cotransporter involved in neurotransmitter loading into SV, and (iii) *SLC17A8* (Solute Carrier Family 17 Member 8), a vesicular glutamate transporter. Of note, the gene list associated with *Synaptic Vesicle* in CRISPR 2-1 versus Control 03 was much smaller and did not include the above-mentioned SV membrane transporters possibly indicating that underexpression of these SV membrane transporters may be a true disease-associated gene expression pattern (**Table 7. 2**).

Genes associated with the *Presynaptic Membrane* compartment (**Table 7. 2**) involved several neurotransmitter receptors and receptor subunits located at the presynaptic membrane. *GABRR1* (Gamma-Aminobutyric Acid Type A Receptor Subunit Rho1) and *GLRA1* (glycine receptor alpha 1) are common underexpressed genes in all patients versus both controls. *DRD2* (dopamine receptor D2), *GRM3* (glutamate metabotropic receptor 3), *GRM7* (glutamate metabotropic receptor 7), *KCNA4* (Potassium Voltage-Gated Channel Subfamily A Member 4) and *KCNJ11* (Potassium Inwardly Rectifying Channel Subfamily J Member 1) are only underexpressed in Patient 2-1 versus CRISPR 2-1, but not in CRISPR 2-1 versus Control 03, possibly indicating disease-associated gene expression.

Common underexpressed genes associated with the compartment *Presynaptic Active Zone* (**Table 7. 2**) in all patients versus both controls (and absent in CRISPR 2-1 versus Control 03) include *ADRA2A* (Adrenoceptor Alpha 2A), *GABRB2* (Gamma-Aminobutyric Acid Type A Receptor Subunit Rho2) and *GRM8* (glutamate metabotropic receptor 8).

SYNAPTIC GO TERM HIERARCHICAL STRUCTURE		GENES
PATIENT 2-1 versus CRISPR 2-1		
Presynapse (total 32 genes)		<i>ADRA2A, AMPH, BDNF, DNAJC6, DRD2, ERBB4, GABRR1, GABRB2, GLRA1, GPM6A, GRIK1, GRM3, GRM7, GRM8, GRP, IGF1, KCNA4, KCNJ11, NTNG1, PDYN, PLAT, RPH3A, SEPTIN5, SLC17A7, SLC18A2, TMEM163, SLC17A8, SV2B, SYNPR, SYT7, WLS</i>
Presynaptic active zone Integral component of presynaptic active zone		<i>ADRA2A, GABRB2, GPM6A, GRM7, GRM8</i>
Presynaptic endocytic zone		<i>AMPH, DNAJC6</i>
Synaptic vesicle Synaptic vesicle membrane Integral component of synaptic vesicle membrane		<i>AMPH, PDYN, RPH3A, SLC17A6, SLC17A7, SLC17A8, SLC18A2, SV2B, SYNPR, TMEM163</i>
Neuronal dense core vesicles		<i>BDNF, GRP, IGF1, PDYN, PLAT, SLC18A2</i>
Presynaptic membrane Integral component of presynaptic membrane		<i>DRD2, ERBB4, GABRR1, GLRA1, GRIK1, GRM3, GRM7, KCNA4, KCNJ11, SYT7, WLS</i>
Synaptic cleft		<i>CBLN1, C1QL3, C1QL1, LAMA4, TNR</i>
Postsynapse (total 24 genes)		<i>ACTN2, ADRA2A, ALDOC, ARC, CACNG5, CACNG7, CNTN2, CHRND, DNAJB1, DRD2, ERBB4, GABRB2, GLRA1, GRM1, GRM3, IL1RAPL1, KCNJ2, KCNA4, NRP2, NTRK3, NRG, PLAT, SLC18A, WLS</i>
Postsynaptic specialisation		<i>ACTN2, ADRA2A, ARC, CACNG7, CHRND, DNAJB1, ERBB4, GABRB2, GLRA1, GRM1, IL1RAPL1</i>
Postsynaptic membrane		<i>ADRA2A, CACNG5, CNTN2, DRD2, GRM1, GRM3, KCNA4, KCNJ2, NRG, NRP2, NTRK3</i>
PATIENT 2-1 versus CONTROL 03		
Presynapse (total 57 genes)		<i>ADRA1A, ADRA2A, ANO6, ANXA1, AGRN, APLP2, BCAS1, BDNF, CACNA1C, CACNA1H, CACNA2D1, CACNG4, CACNG5, CADPS2, CALCRL, CALD1, CDH11, CDH6, CDH13, CDH23, C1QL1, CNH2, CNTN6, CRTCL, CSPG5, CTTNBP2, CYFIP1, DLG5, DOCK1, DOCK10, DNAJC6, DRD1, EFN3B, EIF1AY, EFN3B2, EPHA4, ERBB2, ERBB4, FLNA, FZD4, GABRA1, GABRB2, GABRR1, GPC4, GPER1, GRIN3B, GRIK1, GRIK4, GRN, GLRA3, GRIN2A, GRM1, GRM8, HTR2A, IGF1, ITPR1, ITGA2, ITGA5, ITGB3, ITGB4, ITGB5, ITSNI, KCNC3, KCNJ2, LAMA2, LAMA4, LAMC1, LPAR1, LAMB2, LPAR, LRRC4, LRRK2, LYN, MAGI2, MPDZ, NCAM1, NECTIN3, NETO1, NLGN4Y, NPY1R, NSMF, NTRK2, NTRK3, NTNG1, OPRD1, PENK, PLD1, PLAT, PLCXD3, P2RY1, PTN, PTPRO, QKI, RGS9, ROR2, RPH3A, SEPTIN5, SIPA1L1, SNAP23, SLC2A4, SLC6A1, SLC6A6, SLC16A1, SLC17A6, SLC17A8, SLC18A2, SPARCL1, SPARC, SPTB, STON2, SV2B, SYDE1, SYNPO, TACC3, TANC1, TENM2, TDRD6, TMEM163, TNC, WLS</i>
Presynaptic active zone		<i>ADRA2A, CACNA1H, CACNA2D1, GABRB2, GRIN3B, GRM8, LPAR2, NTNG1, P2RY1, SYDE1</i>
Presynaptic endocytic zone		<i>DNAJC6, ITSNI</i>
Synaptic vesicle Synaptic vesicle membrane Integral component of synaptic vesicle membrane		<i>OPRD1, PENK, RPH3A, SLC17A6, SLC17A8, SLC18A2, SV2B, TMEM163</i>
Neuronal dense core vesicles		<i>BDNF, CACNA2D1, CALCRL, IGF1, NPY1R, OPRD1, PENK, PLAT, SLC18A2</i>

Presynaptic membrane Integral component of presynaptic membrane	<i>ADRA1A, CACNA1C, CNTN6, DRD1, EFN2, EFN3, EPHA4, ERBB2, ERBB4, GABRR1, GPER1, GLRA3, GPC4, GRIK1, GRIK4, GRIN2A, HTR2A, KCNC3, LPAR1, NCAM1, NPY1R, OPRD1, RGS9, SLC6A1, WLS</i>
Synaptic cleft	<i>AGRN, C1QL1, LAMA2, LAMA4, LAMB2, LAMC1, SPARCL1</i>
Postsynapse (total 66 genes)	<i>ADRA1A, ADRA2A, APLP2, CACNA1C, CACNA1H, CACNA2D1, CACNG4, CACNG5, CALD1, CNIH2, CRTCI, CSPG5, CYFIP1, CTTNBP2, DLG5, DOCK10, DRD1, EFN2, EFN3, EPHA4, ERBB4, FLNA, GABRA1, GABRB2, GLRA3, GPER1, GRIK4, GRIN2A, GRIN3B, GRM1, HTR2A, ITGA5, ITGB4, ITPRI, ITSNI, KCNC3, KCNJ2, LPAR1, LYN, MPDZ, NCAM1, NECTIN3, NETO1, NLGN4Y, NSMF, NTRK2, NTRK3, MAGI2, OPRD1, PLAT, PTN, PTPRO, LRRC4, RGS9, ROR2, SIPA1L1, SLC6A1, SLC6A, SLC18A2, SNAP23, SPTB, SYNPO, TACC3, TANC1, TENM2, WLS</i>
Postsynaptic specialisation	<i>ADRA2A, CACNG4, CNIH2, CRTCI, DLG5, EFN2, EFN3, ERBB4, GABRA1, GABRB2, GLRA3, GRIN2A, GRIN3B, GRM1, MAGI2, MPDZ, NECTIN3, NETO1, NLGN4Y, LRRC4, LYN, OPRD1, PTPRO, RGS9, TACC3, TANC1</i>
Postsynaptic membrane	<i>ADRA1A, ADRA2A, CACNA1C, CACNA1H, CACNA2D1, CACNG5, CSPG5, DRD1, EPHA4, GPER1, GRIK4, GRM1, HTR2A, ITGA5, ITGB4, KCNC3, KCNJ2, LPAR1, MAGI2, NCAM1, NTRK2, NTRK3, SLC6A1, SLC6A6, TENM2</i>

ALL PATIENTS versus CONTROL 03

Presynapse (total 58 genes)	<i>ADD3, ADRA1A, ADRA2A, BDNF, CACNA1C, CACNA2D1, CACNA1H, CALCRL, CADPS2, CDH10, CHRNA6, CNTN6, DNAJC6, DISC1, DOCK1, DRD1, EFN2, EFN3, EPHA4, ERBB2, ERBB4, GABRB2, GABRR1, GPC4, GPER1, GRIN3B, GRM8, GRIK1, GRIK4, GLRA3, GRIN2A, GRM3, HTR2A, IGF1, ITPRI, ITSNI, ITGA2, LPAR1, LRRC2, OPRD1, PLAT, PENK, PTN, NCAM1, NPY1R, NTNG1, RGS9, RPH3A, SEPTIN5, SLC6A9, SLC17A6, SLC18A2, STON2, SV2B, SYDE1, TMEM163, TRIM9, WLS</i>
Presynaptic active zone	<i>ADRA2A, CACNA2D1, CACNA1H, CDH10, GABRB2, GRIN3B, GRM8, NTNG1, SYDE1</i>
Presynaptic endocytic zone	<i>DNAJC6, ITSNI</i>
Synaptic vesicle Synaptic vesicle membrane Integral component of synaptic vesicle membrane	<i>OPRD1, PENK, RPH3A, SLC6A9, SLC17A6, SLC18A2, SV2B, TMEM163, TRIM9</i>
Neuronal dense core vesicles	<i>BDNF, CACNA2D1, CALCRL, IGF1, NPY1R, OPRD1, PENK, PLAT, SLC18A2</i>
Presynaptic membrane Integral component of presynaptic membrane	<i>ADRA1A, CACNA1C, DRD1, EFN2, EFN3, EPHA4, ERBB2, ERBB4, GABRR, GPER1, GLRA3, GRIK1, GRIK4, GRIN2A, HTR2A, KCNC3, LPAR1, NCAM1, NPY1R, OPRD1, SLC6A1, WLS</i>
Synaptic cleft	<i>AGRN, SPARCL1</i>
Postsynapse (total 74 genes)	<i>ADRA1A, ADRA2A, APLP2, ADD3, CACNA1C, CACNA1H, CACNA2D1, CACNG4, CACNG5, CALD1, CDH10, CNIH2, CHRNA6, CRTCI, CSPG5, CTTNBP2, CYFIP1, DISC1, DLG5, DMD, DOCK10, DRD1, EPHA4, EPHA7, EFN2, EFN3, ERBB4, FLNA, GABRA1, GABRB2, GLRA3, GPER1, GRIN2A, GRIK4, GRIN3B, GRM1, GRM3, HTR2A, ITGA5, ITGA8, ITGB4, ITPRI, ITSNI, KCNJ2, LPAR1, LRRC4, LRRTM3, LYN, MAGI2, MPDZ, NCAM1, NECTIN3, NETO1, NSMF, NTRK2, NTRK3, OPRD1, PLAT, PTN, PTPRO, PTPRZ1, RGS9, ROR2, SIPA1L1, SLC6A9, SLC18A2, SLC30A1, SNAP23, SPTB, SYNPO, TACC3, TANC1, TENM2, WLS</i>
Postsynaptic specialisation	<i>ADRA2A, CACNG4, CDH10, CNIH2, CRTCI, DISC1, DLG5, DMD, EFN2, EFN3, EPHA7, ERBB4, GABRA1, GABRB2, GLRA3, GRIN2A, GRIN3B, GRM1, ITGA8, LYN, LRRC4, LRRTM3, MAGI2, MPDZ, NECTIN3, NETO1, OPRD1, PTPRO, PTPRZ1, RGS9, SLC6A9, SLC30A1, TACC3, TANC1</i>
Postsynaptic membrane	<i>ADRA1A, ADRA2A, CACNA1C, CACNA1H, CACNA2D1, CACNG5, CHRNA6, CSPG5, DRD1, EPHA4, GPER1, GRIK4, GRM1, GRM3, HTR2A, ITGA5, ITGB4, KCNJ2, LPAR1, MAGI2, NCAM1, NTRK2, NTRK3, SLC6A9, TENM2</i>

CRISPR 2-1 versus CONTROL 03	
Presynapse (total 36 genes)	<i>ADRA1A, BDNF, CACNA1C, CALCR, CHRNA6, CNTN6, CPEB2, CTSD, DBNL, DOCK1, DRD1, EFNB2, EFNB3, EPHA4, ERBB2, EXOC3, GLRA3, GPC4, GPER1, GRIK1, GRIN2A, GRIN3B, HTR2A; IGF1, ITGA2, ITPR1, ITSN1, LAMP1, LPAR1, LRRK2, NPY1R, OPRD1, PENK, RNF216; STON2, SYDE1</i>
Presynaptic active zone	<i>GRIN3B, SYDE1</i>
Presynaptic endocytic zone	<i>ITSN1</i>
Synaptic vesicle Synaptic vesicle membrane Integral component of synaptic vesicle membrane	<i>LAMP1, OPRD1, PENK</i>
Neuronal dense core vesicles	<i>BDNF, CALCRL, IGF1, NPY1R, OPRD1; PENK</i>
Presynaptic membrane Integral component of presynaptic membrane	<i>ADRA1A, CACNA1C, CHRNA6, CNTN6, DRD1, EFNB2, EFNB3, EPHA4, ERBB2, EXOC3, OPRD1, GLRA3, GPC4, GPER1, GRIK1, GRIN2A, HTR2A; LPAR1, NPY1R</i>
Synaptic cleft	<i>AGRN, LAMB2, LAMA2, LAMA4, SPARCL1</i>
Postsynapse (total 52 genes)	<i>ADRA1A, APLP2, CACNA1C, CHRNA6, CALD1, CPEB2, CLSTN2, DAG1, DBNL, DGCR8, DLGAP1, DLG5, DRD1, EEF2K, EFNB2, EFNB3, EPHA4, ERBIN, FLNA, FZD9, GABRA1, GABRA4, GLRA3, GPER1, GRIN2A, GRIN3B, HNRNPM, HOMER3, HTR2A, ITGB4, ITSN1, ITGA8, ITPR1, LPAR1, LRRC4, LYN, MAGI2, MPDZ, NECTIN3, NLGN4Y, NTRK2, OPRD1, PTPRT, P2RX6, ROR2; RNF216, SIPA1L1, SNAP23, SNPO, SNX1, TACC3, TANC1</i>
Postsynaptic specialisation	<i>CLSTN2, DGCR8, DLG5, DLGAP1, EEF2K, EFNB2, EFNB3, GABRA1, GABRA4, GLRA3, GRIN2A, GRIN3B, HOMER3, HNRNPM, ITGA8, LRRC4, LYN, MAGI2, MPDZ; NECTIN3, NLGN4Y, OPRD1, P2RX6, PTPRT, RBIN, SNX1, TACC3, TANC1</i>
Postsynaptic membrane	<i>ADRA1A, CACNA1C, CHRNA6, DRD1, EPHA4, GPER1, HTR2A, ITGB4, MAGI2, NTRK2, LPAR1</i>

Table 7. 2. Overview on significantly underexpressed genes associated with synaptic location. Presynaptic GO terms (synaptic location) in hierarchical structure with associated significantly underexpressed genes in Patient 2-1 vs CRISPR 2-1, Patient 2-1 vs Control 1, all Patients vs Control 03 and in CRISPR 2-1 vs Control 03, respectively.

7. 2. 8. GO term enrichment analysis for synaptic function reveals dysregulation of synaptic signalling and synaptic organization in patient lines compared to control lines

GO analysis of underexpressed DEGs for synaptic function shows enrichment in *Presynapse*, *Synaptic Signalling* and *Synaptic Organisation* (Fig. 7. 12, Table 7. 3).

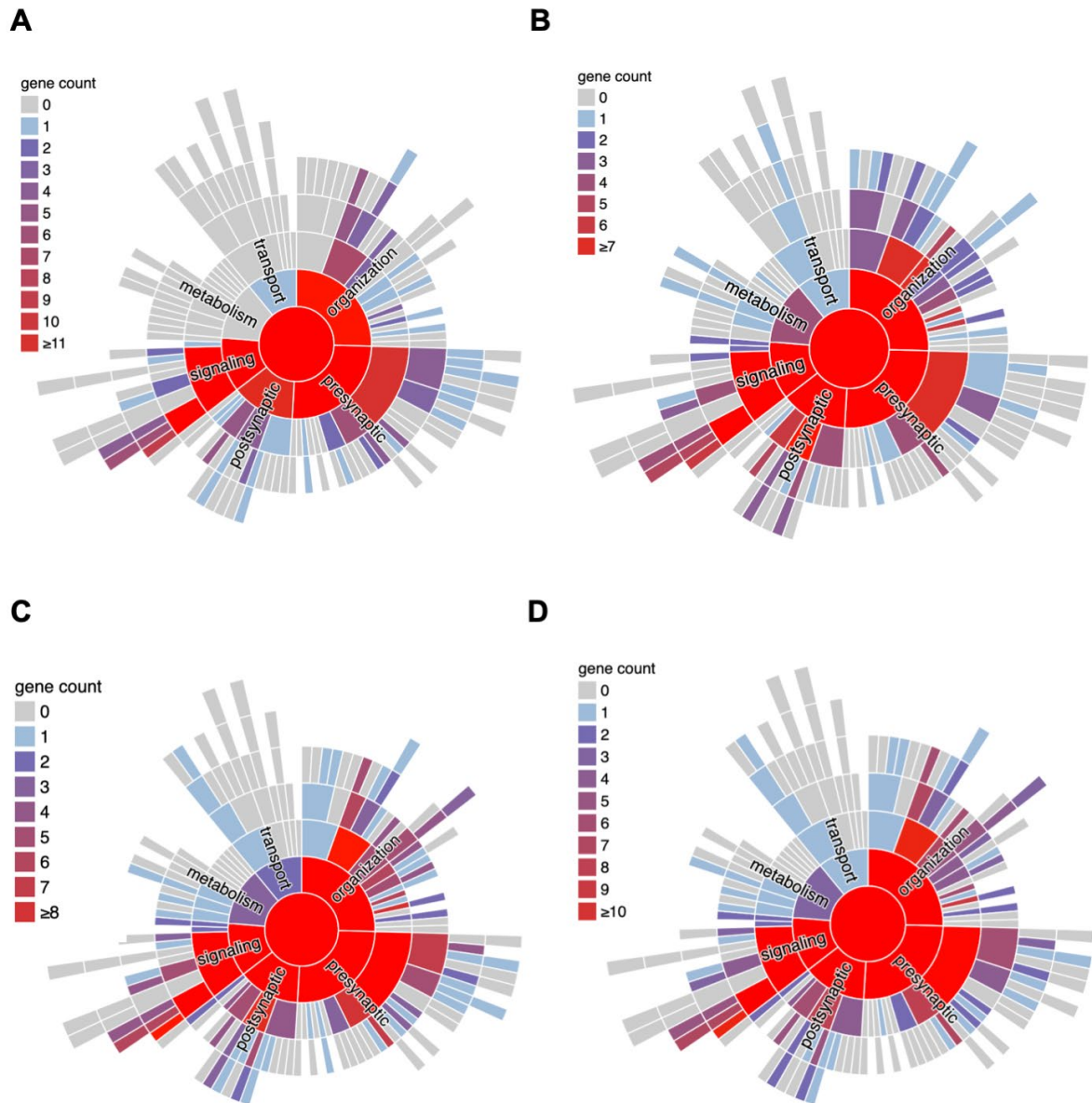


Fig 7.12. Synaptic function enrichment analysis in Patient 2-1 versus Control 03 and in all Patients versus Control 03. A) Pie charts showing synaptic function mapping of underexpressed protein-coding DEGs in Patient 2-1 compared to CRISPR 2-1. B) Pie charts showing synaptic function mapping of underexpressed protein-coding DEGs in CRISPR 2-1 compared to Control 03. C) Pie charts showing synaptic function mapping of underexpressed protein-coding DEGs in Patient 2-1 compared to Control 03. (D) Pie charts showing synaptic function mapping of underexpressed protein-coding DEGs in all Patients compared to Control 03.

Common underexpressed DEGs involved in *Synaptic Signalling*, particularly *Transsynaptic Signalling*, in all patients versus both control lines include several membrane receptors such as *ADRA2A*, *GABRR1* and *GRM8*. The list of common underexpressed genes further contains *NTNG1* (Netrin G1), *CBLN2* (Cerebellin 2 precursor), *TENM1* (Teneurin Transmembrane Protein 1) and *WLS* (Wnt Ligand Secretion Mediator). *NTNG1* plays a role in the regulation of neural circuitry formation, in particular glutamatergic neural circuitry, and is an axon-guidance

pathway molecule involved in both axon and dendrite outgrowth⁴⁰⁵. Interestingly, SNPs in axon-guidance pathway genes such as *NTNG1* have been linked to PD⁴⁰⁶. Aberrant axon guidance might result in developmental dysconnectivity that ultimately contributes to PD pathogenesis⁴⁰⁵. *CBLN2* is a synaptic organiser and binds to presynaptic neuroligins and postsynaptic receptors^{407,408}. *TENM1* is a synaptic cell adhesion molecule, that, in interaction with G protein-coupled receptors, called latrophilins, promotes synapse development⁴⁰⁹. *WLS* regulates the sorting and secretion of Wnt proteins⁴¹⁰.

Common underexpressed DEGs involved in *Synaptic Organization* in all patients versus both controls include *ERBB4* (Erb-B2 Receptor Tyrosine Kinase 4), *CBLN2*, *C1QL1* (Complement C1q Like 1), *NTRK3* (Neurotrophic Receptor Tyrosine Kinase 3), *NTNG1* and *TENM1*. *ERBB4* and *NTRK3* are receptor tyrosine kinases, which are important in nervous system development. They are involved in the regulation and activation of signalling pathways such as phosphatidylinositol 3-kinase/AKT and the MAPK pathway, which promote cell survival and differentiation. *NTRK3* has an important function in the hippocampal region and *NTRK3* deficiency leads to reduced axonal arborization and synaptic plasticity⁴¹¹. *C1QL1* participates in C1ql1-Bai3 signalling, which promotes synapse formation and connectivity in the cerebellum^{412,413}.

SYNAPTIC GO TERM HIERARCHICAL STRUCTURE	GENES
PATIENT 2-1 versus CRISPR 2-1	
Presynapse (total 19 genes)	<i>AMPH, CALB2, DNAJC6, DRD2, GABRR1, GABRB2, GLRA1, GRIK1, KCNA4, KCNJ11, RPH3A, SEPTIN5, SLC17A6, SLC17A7, SLC17A8, SLC18A2, SV2B, SYT7, TMEM163</i>
Regulation of presynaptic membrane potential	<i>GABRR1, GABRB2, GLRA1, GRIK1, KCNA4, KCNJ11</i>
Synaptic vesicle cycle	<i>AMPH, DNAJC6, RPH3A, SEPTIN, SV2B, SYT7, SLC17A6, SLC17A7, SLC17A8, SLC18A2, TMEM163</i>
Postsynapse (total 12 genes)	<i>ARC, CACNG5, CACNG7, C1QL3, CHRND, ERBB4, GABRB2, GLRA1, GLRA2, GRIK1, GRM1, SYT6</i>
Synaptic signalling (total 24 genes)	<i>ADRA2A, ARC, BDNF, CBLN2, CCK, CDH11, CHRNA5, DRD2, GABRR1, GRM3, GRM7, GRM8, IGF1, ILIRAPL1, NRG1, NRN1, NTNG1, PLAT, SYNPR, TENM1, TNR, TUBB2B, UBE3A, WLS</i>
Transsynaptic signalling	<i>ADRA2A, ARC, BDNF, CBLN2, CDH11, CHRNA5, DRD2, GABRR1, GRM3, GRM7, GRM8, IGF1, LIRAPL1, NRN1, NRG1, NTNG1, PLAT, SYNPR, TENM1, TNR, TUBB2B, UBE3A, WLS</i>
Chemical synaptic transmission	<i>ARC, CBLN2, CDH11, GABRR1, NTNG1, SYNPR, TUBB2B, TNR, UBE3A</i>
Synapse organization (total 15 genes)	<i>ERBB4, CBLN1, CBLN2, C1QL3, C1QL1, GPM6A, ILIRAPL1, MDGA1, NRP2, NTRK3, NTNG1, SEMA3F, TENM1, TUBA1A, TUBB</i>
PATIENT 2-1 versus CONTROL 03	
Presynapse (total 30 genes)	<i>BLOC1S1, CADPS2, CSPG5, DNAJC6, DOCK1, GABRA, GABRB2, GABRR1, GRIK1, GRIK4, GRIN2, GRIN3B, ITSN1, KCNMB4, LPAR1, LRRK2, NPY1R, PLD1, P2RX7, P2RY1, RPH3A, SEPTIN5, SLC2A4, SLC6A1, SLC17A6, SLC17A8, SLC18A2, STON2, SV2B, TMEM163</i>
Regulation of presynaptic membrane potential	<i>GABRA1, GABRB2, GABRR1, GRIK1, GRIK4, GRIN2A, GRIN3B, KCNMB4</i>
Synaptic vesicle cycle	<i>ANO6, CACNG4, CACNG5, CNIH2, CRTCI, EFNB2, ERBB2, ERBB4, GABRA1, GABRB2, GPC4, GRIK1, GRM1, GRIN2A, ITGB3, ITPR1, LPAR1, MAGI2, NETO1, NSMF, SNAP23, SYNPO, WNT5A</i>
Postsynapse (total 23 genes)	<i>ANO6, CACNG4, CACNG5, CNIH2, CRTCI, EFNB2, ERBB2, ERBB4, GABRA1, GABRB2, GPC4, GRIK1, GRIN2A, GRM1, ITPR1, ITGB3, LPAR1, MAGI2, NETO1, NSMF, SNAP23, SYNPO, WNT5A</i>
Synaptic signalling (total 30 genes)	<i>ADRA1A, ADRA2A, BDNF, CBLN2, CDH11, DRD1, EFNB3, GABRR1, GLRA3, GPER1, GRM8, HTR2A, IGF1, LRRC4, NCAM1, NPY1R, NTNG1, NTRK2, PENK, PLAT, PTN, ROR2, SLC6A6, SYNPO, TENM1, TENM2, TENM3, TENM4, WLS, WNT5A</i>
Transsynaptic signalling	<i>ADRA1A, ADRA2A, BDNF, CBLN2, CDH11, DRD1, EFNB3, GABRR1, GLRA3, GPER1, GRM8, HTR2A, IGF1, LRRC4, NCAM1, NTNG1, NTRK2, PLAT, PTN, ROR2, SLC6A6, SYNPO, TENM1, TENM2, TENM3, TENM4, WLS, WNT5A</i>
Chemical synaptic transmission	<i>ADRA1A, ADRA2A, CBLN2, CDH11, DRD1, GABRR1, GLRA3, GPER1, GRM8, IGF1, HTR2A, LRRC4, NTNG1, NCAM1, PTN, ROR2, SLC6A6, SYNPO, WNT5A</i>
Synapse organization (total 39 genes)	<i>AGRN, CBLN2, CDH6, C1QL1, CTTNBP2, CYFIP1, DLG5, DRD1, EFNB2, EPHA4, ERBB4, FZD1, GRN, ITGB3, ITSN1, LAMB2, LNA, GPC2, GPC4, LRRC4, MAGI2, MDGA1, NCAM1, NTNG1, NTN1, NTRK3, PTPRO, ROR2, SIPA1L1, SPARC, SPARCL1, SPTB, SYDE1, TANC1, TENM1, TENM2, TENM3, TENM4, WNT5A</i>
ALL PATIENTS versus CONTROL 03	
Presynapse (total 25 genes)	<i>CADPS2, CSPG5, DNAJC6, DOCK1, GABRA1, GABRB2, GRIK1, GRIK4, GRIN2A, GRIN3B, GABRR1, ITSN1, KCNMB4, LPAR1, LRRK2, NPY1R, PLD1, RPH3A, SEPTIN5, SLC6A9, SLC17A6, SLC18A2, STON2, SV2B, TMEM163</i>

	<i>GABRA1, GABRR1, GABRB2, GRIK1, GRIK4, GRIN2A, GRIN3B, KCNMB4</i>
Synaptic vesicle cycle	<i>CADPS2, CSPG5, DNAJC6, DOCK1, ITSN1, LPAR1, LRRK2, NPY1R, PLD1, SEPTIN5, RPH3A, SLC17A6, SLC18A2, STON2, SV2B, TMEM163</i>
Postsynapse (total 23 genes)	<i>ANO6, CACNG4, CACNG5, CNIH2, CRTCI, EFN2, ERBB2, ERBB4, GABRA1, GABRB2, GLRA2, GPC4, GRIN2A, GRM1, GRIK1, ITPR1, LPAR1, MAGI2, NETO1, NSMF, SNAP23, SYNPO, WNT5A</i>
Synaptic signalling (total 32 genes)	<i>ADRA2A, ADRA1A, BDNF, CBLN2, CDH11, CHRNA6, DRD1, EFN3, EPHA7, GABRR1, GLRA3, GPER1, GRM3, GRM8, HTR2A, IGF1, LRRC4, NCAM1, NPY1R, NTNG1, NTRK2, PENK, PLAT, PTN, ROR2, SYNPO, TENM1, TENM2, TENM4, TNR, WNT5A, WLS</i>
Transsynaptic signalling	<i>ADRA1A, ADRA2A, BDNF, CBLN2, CDH11, CHRNA6, DRD1, EFN3, EPHA7, GABRR1, GLRA3, GPER1, GRM, GRM8, HTR2A, IGF1, LRRC4, NCAM1, NTNG1, NTRK2, PLAT, PTN, ROR2, SYNPO, TENM1, TENM2, TENM4, TNR, WNT5A, WLS</i>
Chemical synaptic transmission	<i>ADRA1A, ADRA2A, CBLN2, CDH11, CHRNA6, DRD1, EPHA7, GABRR1, GLRA3, GPER1, GRM3, GRM8, HTR2A, IGF, LRRC4, NCAM1, NTNG1, PTN, ROR2, SYNPO, TNR, WNT5A</i>
Synapse organization (total 40 genes)	<i>AGRN, CBLN2, CDH6, CDH10, C1QL1, CTTNBP2, CYFIP1, DISC1, DRD1, DLG5, EPHA7, EFN2, EPHA4, ERBB4, FLNA, FZD1, GPC4, GRN, ITSN1, LAMB2, LRRC4, LRRTM3, MAGI2, MDGA1, NCAM1, NTN1, NTNG1, NTRK3, PTPRO, ROR2, SIPA1L1, SPARC, SPARCL1, SPTB, SYDE1, TANC1, TENM1, TENM2, TENM4, WNT5A</i>

CRISPR 2-1 versus CONTROL 03

Presynapse (total 12 genes)	<i>DOCK1, GABRA1, GRIK1, GRIN2A, GRIN3B, ITSN1, LPAR1, LRRK2, NPY1R, PLD1, P2RX7, STON2</i>
Regulation of presynaptic membrane potential	<i>GABRA1, GRIK1, GRIN2A, GRIN3B</i>
Synaptic vesicle cycle	<i>DOCK1, ITSN1, LPAR1, LRRK2, NPY1R, PLD1, STON2</i>
Postsynapse (total 20 genes)	<i>ANO6, DAG1, EFN2, ERBIN, ERBB2, FZD9, GABRA1, GABRA4, GABRG3, GPC4, GRIK1, GRIN2A, HOMER3; ITPR1, LPAR1, MAGI2, RNF216, SNAP23, SYNPO, WNT5A</i>
Synaptic signalling (total 21 genes)	<i>ADRA1A, BDNF, CDH11, CHRNA6, DAG1, DLGAP1, DRD1, EFN3, LRRC4, GLRA3, GPER1, HTR2A, IGF1, NPY1R, NTRK2, PENK; ROR2, SYNPO, TENM3, TENM4, WNT5A</i>
Transsynaptic signalling	<i>ADRA1A, BDNF, CDH11, CHRNA6, DAG1, DLGAP1, DRD1, EFN3, LRRC4, GLRA3, GPER1, HTR2A, IGF1, NTRK2, ROR2, SYNPO, TENM3, TENM4, WNT5A</i>
Chemical synaptic transmission	<i>ADRA1A, CDH11; CHRNA6, DLGAP1, DRD1, GPER1; GLRA3, HTR2A; IGF1, LRRC4, ROR2, SYNPO, WNT5A</i>
Synapse organization (total 30 genes)	<i>AGRN, CDH6, DAG1, DBNL, DLG5, DLGAP1, DRD1, EFN2, FLNA, FZD9; EPHA4, GPC4, GRN; ITSN1, HNRNPM; LAMB2, LRRC4, MAGI2, MDGA1, NTN1, PTPRT, ROR2, SIPA1L1, SPARC, SPARCL1, SYDE1, TANC1, TENM3, TENM4, WNT5A</i>

Table 7. 3. Overview on significantly underexpressed genes associated with synaptic function. Presynaptic GO terms (synaptic function) in hierarchical structure with associated significantly underexpressed genes in Patient 2-1 vs CRISPR 2-1, Patient 2-1 vs Control 03, all Patients vs Control 03 and in CRISPR 2-1 vs Control 03, respectively.

7. 3. Discussion

In summary, I have performed transcriptomic analysis of three *DNAJC6* patient lines and two control lines (an isogenic control for Patient 2-1 and a non-isogenic control). GO term enrichment analysis for biological processes revealed common involvement of general neurodevelopmental processes in patient lines. These processes include *Developmental Process*, *Multicellular Organism Development*, *System Development*, and *Anatomical Structure Development*. The GO term *Nervous System Development* particularly emerged in the analysis of Patient 2-1 versus CRISPR 2-1, and had lower ranking in the analysis of Patient 2-1 and all Patients versus Control 03. Differences in genetic background with a higher number of DEGs in the analysis of Patients versus Control 03 may explain this finding.

To further investigate this finding, I extracted underexpressed DEGs associated with *Nervous System Development*. The analysis revealed a large number of underexpressed DEGs in all patient lines compared to control lines. Since the analysis of CRISPR 2-1 versus Control 03 also produced a substantial list of common underexpressed DEGs, I assumed that only a subset of genes may represent true disease-associated DEGs. I compared all patients AND the isogenic control CRISPR 2-1 separately to the non-isogenic Control 03 in order to distinguish between disease-associated DEGs and non-disease-associated DEGs that are likely to be associated with the same genetic background. This analysis resulted in a final list of 18 commonly underexpressed DEGs involved in different neural developmental processes. The same analysis for underexpressed DEGs associated with *Dopaminergic Neurogenesis* produced a list of six common underexpressed DEGs that are involved in midbrain floor plate specification, ventral patterning and mDA identity. Analysis of underexpressed DEGs associated with *Clathrin-Mediated Endocytosis* only produced two genes, among them, not surprisingly, *DNAJC6*. These findings suggest that auxilin deficiency may not directly affect the CME-associated protein machinery as indicated by normal protein levels of direct auxilin-binding proteins clathrin and AP-2 in Western blot studies, but rather may affect CME-associated downstream pathways. CME activates or terminates signalling cascades through the internalisation of various transmembrane receptors and ligands, thereby regulating a variety of synaptic and developmental signalling pathways (e.g. RTK, TGF- β /DPP, Hedgehog, Wnt and Notch)¹⁷⁰. In both developing and mature neurons, CME is involved in neurogenesis, neuronal migration, axon and neurite outgrowth and synaptogenesis. The pattern of underexpressed DEGs linked to *Nervous System Development* and *Dopaminergic Neurogenesis* thus reflects disruption of

CME and associated developmental signalling pathways. Wnt signalling plays a crucial role in midbrain floor plate specification and Wnt dysfunction affects dopaminergic neuron development. A substantial number of underexpressed DEGs linked to *Nervous System Development* in Patient 2-1 versus CRISPR 2-1 was associated with the “signalling by Wnt” pathway, while the same subset of genes was overexpressed in CRISPR 2-1 versus Control 03. This finding may demonstrate the importance of Wnt signalling in dopaminergic neurogenesis and neural development.

SynGO gene enrichment analysis highlighted presynaptic locations that are associated with SV cycling including *Presynaptic Endocytic zone*, *Synaptic Vesicle*, *Presynaptic Membrane* and *Presynaptic Active Zone*. Extraction of associated underexpressed DEGs revealed a variety of transporters involved in the loading of neurotransmitters into SV as well as neurotransmitter receptors located at the presynaptic membrane, in particularly GABA and glutamate receptors and receptor subunits. Glutamate and GABA represent the most important excitatory and inhibitory neurotransmitters in the brain and dysregulation of glutamate and GABA neurotransmitter signalling is likely to disturb the excitation-inhibition balance and contribute to the seizure and neurodevelopmental phenotype seen in patients with *DNAJC6* parkinsonism. Dopamine receptors were only underexpressed in Patient 2-1 versus CRISPR 2-1 (*DRD2*) and versus Control 03 (*DRD1*), but not in CRISPR 2-1 versus Control 03, possibly indicating disease-associated underexpression. Developmental dysregulation of dopamine signalling may therefore contribute to the parkinsonian features in *DNAJC6* patients. Autonomous pacemaker activity is characteristic for dopaminergic neurons. Dopamine receptor dysregulation is likely to affect dopamine homeostasis and neurotransmission and may over time lead to synaptic dysfunction in dopaminergic neurons. Notably, loss-of-function mutations in *DRD1* have recently been described in severe infantile parkinsonism-dystonia⁴¹⁴.

SynGO gene enrichment analysis for synaptic function highlighted *Presynapse*, *Synaptic Signalling* and *Synaptic Organisation*. In addition to the membrane transporters and receptors mentioned above, the analysis of underexpressed DEGS associated with *Synaptic Signalling* and *Synaptic Organisation* revealed genes involved in neural circuit formation, axon guidance, synapse formation and signalling pathways important for neural development.

In summary, transcriptomic analysis highlights both a strong neurodevelopmental and synaptic phenotype in *DNAJC6* mDA neurons. These findings provide further insight into the molecular

mechanisms underlying the neurodevelopmental and neurological symptoms in patients with *DNAJC6* parkinsonism.

CHAPTER 8

***An *in vitro* proof-of-concept gene therapy approach
for *DNAJC6* parkinsonism-dystonia***

8. 1. Introduction

Gene therapy is an emerging and promising tool for the treatment of a broad range of neurological disorders. Viral vectors allow the introduction of a functional copy of a specific gene to replace the impaired function of a defective gene⁴¹⁵. To date, both *in vivo* and *ex vivo* gene therapies have been approved for a number of neurological diseases including spinal muscular atrophy, AADC deficiency, metachromatic leukodystrophy and juvenile cerebral adrenoleukodystrophy^{124,125,132,416–419}. For *in vivo* gene therapy approaches, both lentivirus and adeno-associated viruses have been used⁴²⁰. Lentiviruses are derived from single-stranded RNA retro-viruses HIV-1⁴²¹. They have the capacity to transduce dividing and non-dividing cells and stably integrate into the genome⁴²¹. A great advantage is their large transgene cargo capacity of up to 8 kilobases (kb). Lentiviruses are mostly used for *ex vivo* gene therapy approaches due to the risk of insertional mutagenesis⁴²¹, but have been used in Parkinson Disease trials¹²⁴. AAV viruses are single-stranded DNA parvoviruses that need helper viruses for replication⁴²¹. AAV viruses are not incorporated into the host genome and remain in an epichromosomal state⁴²¹. They have a low pathogenicity and a low immunogenic profile and are able to transduce both dividing and non-dividing cells as well. In contrast to lentiviruses, their transgene capacity is limited to 5 kb⁴²¹. In order to explore gene therapy as a potential precision treatment for *DNAJC6*-related disease, I decided to use a lentiviral vector to deliver a wildtype copy of the *DNAJC6* gene to patient-derived mDA neurons and investigate its effect on cellular phenotype. In this chapter, I describe the generation and validation of a *DNAJC6*-containing lentivirus construct and also report on preliminary effects of *DNAJC6* transgene delivery in patient-derived mDA neurons.

8. 2. Results

8. 2. 1. Generation of lentivirus construct for *DNAJC6* gene delivery

8. 2. 1. 1. Cloning of *DNAJC6* into a DAT lentivirus vector

For the generation of a human *DNAJC6* lentivirus gene construct (**Figure 8. 1**) I used an available lentivirus plasmid construct containing the gene *SCL6A3* (*hDAT*), which was kindly provided by Dr Joanne Ng (UCL, Institute of Women's Health). Generation of the *DNAJC6*-expressing lentivirus is described in Chapter 2, Section 2.9. Dr John Counsell (UCL GOS-ICH) provided technical support and advice for the cloning process. The mock lentivirus plasmid

(pCCL-hSYN- EGFPv2JN) was initially designed with the elements summarised in (Table 8. 1):

Plasmid element	Function
Human cytomegalovirus (CMV) immediate early promoter	Drives transient ubiquitous gene expression
HIV-1 components:	
- Truncated 5' long terminal repeat (5'LTR)	Acts as an RNA polymerase promoter to initiate transcription and facilitate integration into the host genome
- ψ	Packaging signal
- Rev response element (RRE)	Important for post-transcriptional transport of viral mRNA from the nucleus to the cytoplasm
- Central polypurine tract (cPPT)	Increases lentivirus-mediated transduction efficiency
Human synapsin promoter (hSYN)	Neuron-specific promoter for longterm transgene expression
Enhanced green fluorescent protein (EGFP)	Fluorescent marker for gene expression
Woodchuck hepatitis virus posttranscriptional regulatory element (WPRE)	Improves gene expression by RNA modification
HIV-1 self-inactivating 3'long terminal repeat (3'LTR Δ U3)	Important for transcriptional termination and polyadenylation
Simian virus 40 polyadenylation signal (SV40pA)	Facilitates transcriptional termination
NeoR/KanR sequence	Important for antibiotic selection of plasmids by neomycin and kanamycin

Table 8. 1. Elements of the pCCL-hSYN- EGFPv2JN plasmid.

For construction of the *DNAJC6* lentivirus construct, the *hDAT* gene was removed from the plasmid backbone using common restriction enzymes. Subsequently, the human *DNAJC6* gene was cloned between the hSYN promoter and an Internal Ribosome Entry Site (IRES) as a linker between the two genes (*EGFP* and *DNAJC6*) to enhance RNA-translation in a cap-independent manner through recruitment of ribosomes. Following antibiotic selection of the clones, the presence and correct sequence of the human synapsin (hSYN) promoter, the *EGFP* reporter gene in the mock plasmid (pCCL-hSYN- EGFPv2JN), and the *DNAJC6* gene, the IRES and the *EGFP* reporter gene in the *DNAJC6* plasmid (pCCL-hSYN- DNAJC6-IRES-EGFP) (Figure 8. 1) was confirmed by Sanger sequencing.

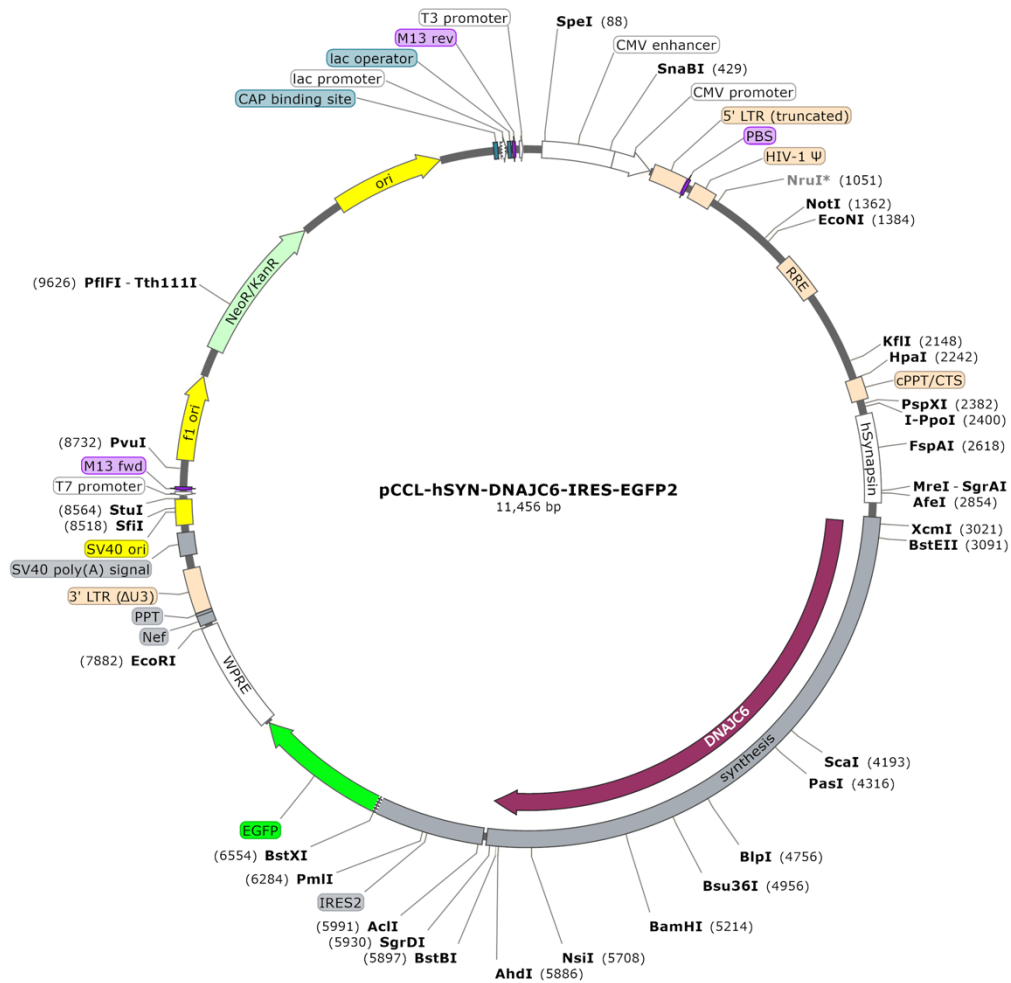


Figure 8. 1. Design of a pCCL-hSYN-DNAJC6-IRES-EGFP2 plasmid. The human DNAJC6 gene sequence (2.9 kb) was cloned between the human synapsin promoter and the IRES sequence linking the DNAJC6 and EGFP gene. CMV= human cytomegalovirus immediate early promoter, 5'LTR= truncated 5' long terminal repeat, ψ = packaging signal, RRE= Rev response element, cPPT= central polypurine tract, hSYN= human synapsin promoter, EGFP= enhanced green fluorescent protein, WPRE= woodchuck hepatitis virus posttranscriptional regulatory element, 3'LTR Δ U3= self-inactivating 3' long terminal repeat, SV40pA= simian virus 40 polyadenylation signal, NeoR/KanR= neomycin and kanamycin antibiotic resistance.

8. 2. 1. 2. Lentivirus production in HEK-293T cells

To confirm successful integration of the DNAJC6-plasmid into the viral capsid, HEK 293T cells were infected with either the pCCL-hSYN-DNAJC6-IRES-EGFP or the pCCL-hSYN-EGFPv2 plasmid (mock plasmid). HEK-293T cells do not endogenously express the neuron-specific auxilin protein and are thus suitable for this analysis. Based on previously established multiplicity of infection (MOI) values for lentivirus transduction in HEK-293T cells in our laboratory, a MOI of 1.5 was used.

8. 2. 2. Transduction of patient-derived mDA neurons and validation of gene transfer

Patient-derived mDA neurons were transfected with the pCCL-hSYN-DNAJC6-IRES-EGFP or the pCCL-hSYN-EGFPv2 mock plasmid at day 28 of differentiation. mDA neurons were subsequently cultured until day 65 of differentiation. Immunofluorescence analysis at day 65 of differentiation showed strong expression of the GFP reporter in both *DNAJC6* lentivirus- and mock-treated mDA neurons. TH and MAP2 expression were similar to non-treated neuronal cultures (**Figure 8. 2**).

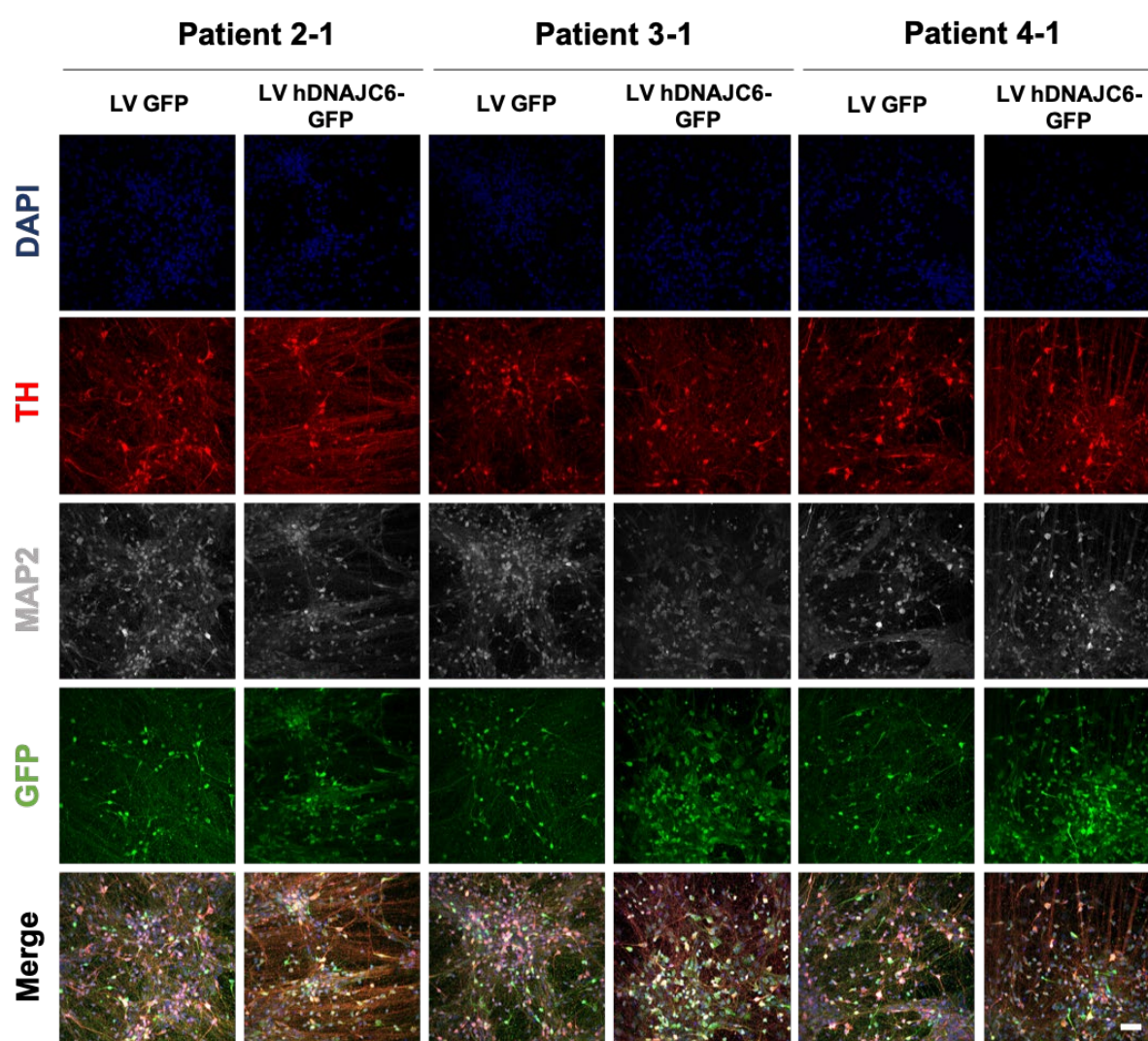


Figure 8. 2. Immunofluorescence analysis of lentivirus-treated patient-derived mDA neurons at day 65 of differentiation. Representative immunofluorescence images for TH, MAP2 and GFP in patient-derived mDA neurons transfected with LV GFP and LV DNAJC6 at day 65 of differentiation. Scale bar = 150 μ m (Figure and legend adapted from Abela et al., 2024)³⁰¹.

To validate *DNAJC6* gene transfer, I performed immunoblotting analysis, which showed strong expression of auxilin protein in *DNAJC6* lentivirus-treated mDA neurons, while mock lentivirus-treated mDA neurons do not express auxilin (**Figure 8. 3**). Healthy controls express high levels of auxilin as shown in **Figure 6.1**. To assess the extent of lentiviral rescue, it would be useful to include an untreated sample to compare levels of auxilin protein expression.

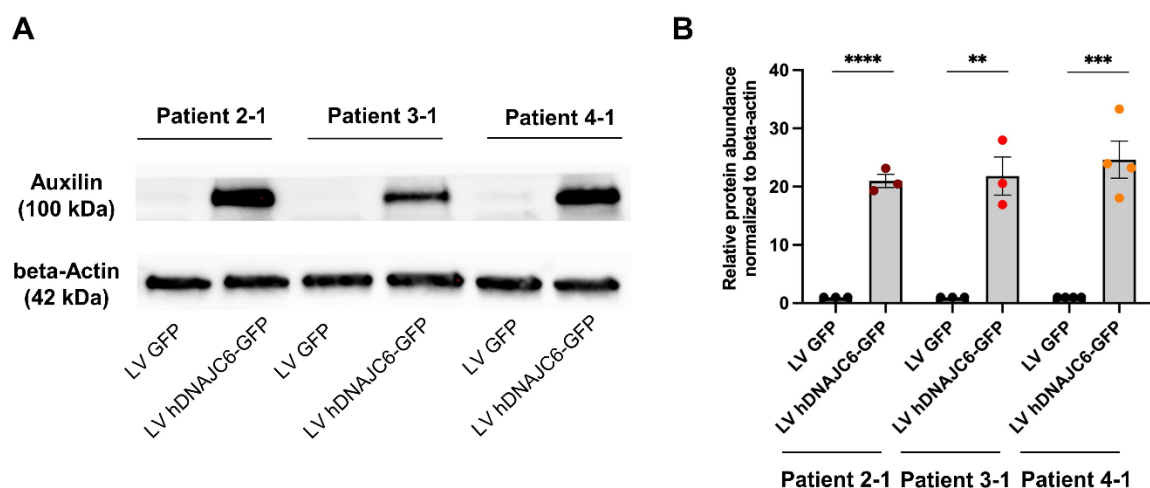


Figure 8. 3. Immunoblot analysis of lentivirus-treated patient-derived mDA neurons at day 65 of differentiation. *A*) Representative immunoblot images for auxilin and loading control (beta-actin) in patient-derived mDA neurons transfected with LV GFP and LV DNAJC6-GFP at day 65 of maturation. *B*) Quantification of relative protein abundance, normalised to the loading control beta-actin. Statistical significance was evaluated using the Student's unpaired, two tailed t-test. Error bars indicate \pm SEM (n = samples from 3-4 independent differentiations). * indicates statistically significant differences: * $p < 0.05$; ** $p < 0.01$, *** $p < 0.001$, **** $p < 0.0001$. (Figure and legend adapted from Abela et al., 2024)³⁰¹.

8. 2. 3. Improvement of clathrin-mediated endocytosis in *DNAJC6* lentivirus-treated patient-derived mDA neurons

I next sought to determine whether restoration of auxilin protein expression in patient-derived mDA neurons improves CME. At day 65 of differentiation, *DNAJC6* lentivirus-treated mDA neurons showed significantly increased FM1-43 dye intensity compared to mock lentivirus-treated mDA neurons indicating increased uptake of FM1-43 dye by CME (**Figure 8. 4/8. 5**). Similar to immunoblotting, the inclusion of an untreated sample would be helpful to estimate the extent of lentiviral rescue of CME.

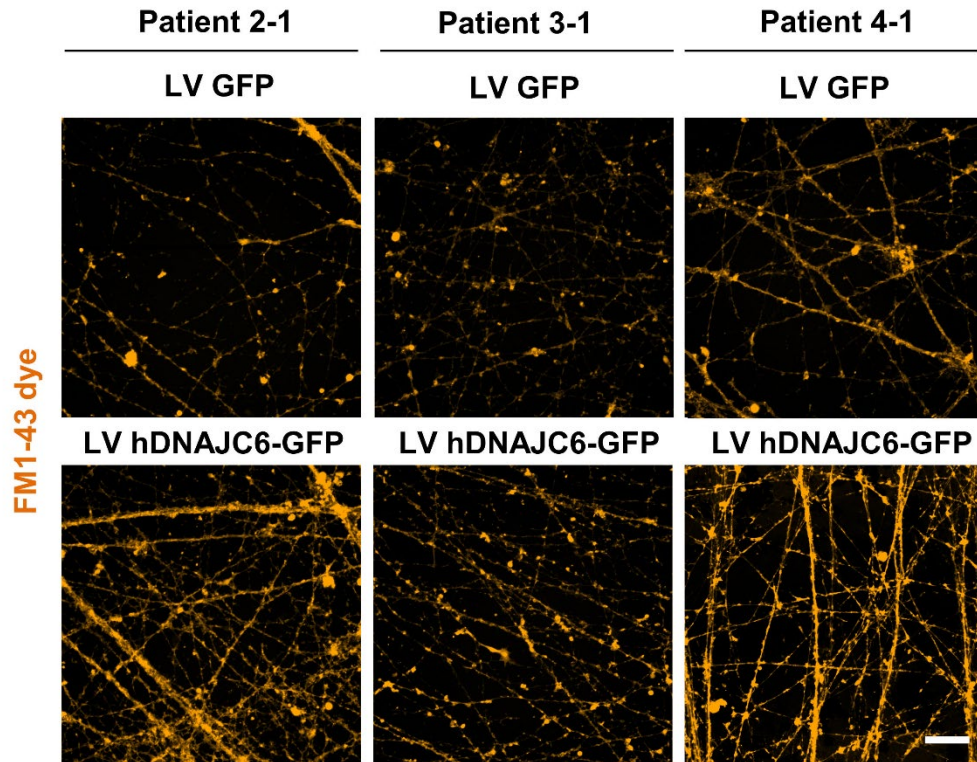


Figure 8. 4. FM1-43 uptake assay in lentivirus-treated patient-derived mDA neurons at day 65 of differentiation. Cells were incubated with FM1-43 dye and stimulated with potassium, subsequently fixed and analysed. Representative immunofluorescence images of FM1-43 uptake in lentivirus-transfected patient-derived mDA neurons at day 65 of differentiation. Upper panel: Patient-derived mDA neurons transfected with LV GFP. Lower panel: Patient-derived mDA neurons transfected with LV DNAJC6. Images were acquired using the LSM710 Zeiss confocal microscope. Scale bar = 20 μ m (Figure and legend adapted from Abela et al., 2024)³⁰¹.

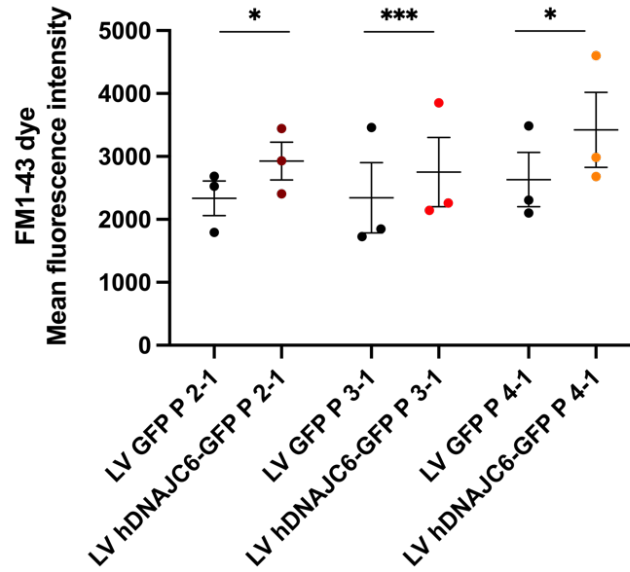


Figure 8. 5. Quantification of the FM1-43 uptake assay. Quantification of FM1-43 mean fluorescence intensity in patient-derived mDA neurons transfected with LV GFP and LV DNAJC6-GFP. Statistical significance was determined using the Student's paired, two tailed t-test. Error bars indicate \pm SEM ($n = 3$ independent differentiations, $N=60$ presynaptic boutons counted per differentiation). *indicates statistically significant differences: * $p<0.05$; ** $p<0.01$, *** $p<0.001$ (Figure and legend adapted from Abela et al., 2024)³⁰¹.

8. 3. Discussion

In this chapter, I describe the generation of a *DNAJC6*-expressing lentivirus construct and successful transduction of patient-derived and control mDA neurons. *DNAJC6* lentivirus-transfected mDA neurons show overexpression of auxilin protein at day 65 of differentiation demonstrating successful *DNAJC6* gene transfer. I have further demonstrated preliminary data regarding improvement in CME post gene transfer. Disruption of CME is a key phenotypic finding in this dopaminergic neuronal cell model and is likely to be responsible for a variety of downstream effects, including impaired SV homeostasis and neurotransmission as well as impaired synaptic and developmental signalling^{186,190}. Transduction of patient mDA neuronal cultures with a *DNAJC6* lentivirus at day 28 of differentiation results in increased FM1-43 uptake at day 65 of differentiation, indicating some rescue of CME. This is a first proof-of concept for a potential gene therapy approach in *DNAJC6* parkinsonism. Correction of one key cellular phenotype is promising; however, further work is required to evaluate and validate the rescue of additional downstream phenotypes.

CHAPTER 9

Discussion

For my PhD project, I have focused my efforts on understanding the clinical and biological basis of *DNAJC6* parkinsonism-dystonia. This is an ultra-rare early-onset movement and neurodevelopmental disorder with less than 50 patients reported worldwide^{61–64,134,135,137,318}. Patients harbouring biallelic *DNAJC6* mutations present with a phenotypic continuum in which three main clinical entities are recognized. The majority of patients suffer from a **juvenile-onset parkinsonism** that manifests with typical parkinsonian symptoms including bradykinesia, tremor, rigidity, hypomimia and postural instability at the end of the first or beginning of the second decade. Many juvenile-onset patients suffer from additional neurological, neurodevelopmental and neuropsychiatric symptoms that commonly precede the movement disorder. With the onset of parkinsonism, the disease usually progresses rapidly and leads to loss of ambulation in the second decade. A small subgroup of patients present with a **predominant dystonic phenotype** with focal cranial dystonia (blepharospasm, jaw opening dystonia, lingual dystonia)¹³⁶, a dystonic gait (“cock walk” gait)¹³⁷ or generalised dystonia¹³⁵, which is rapidly followed by parkinsonian symptoms. Treatment of juvenile-onset parkinsonism remains challenging, with only about one third responding to levodopa therapy, and the treatment is often limited by severe side effects including treatment-related dyskinesia or psychiatric manifestations. A third subgroup of patients with biallelic *DNAJC6* mutations manifest a **milder form of early-onset PD** with onset of symptoms in the third or fourth decade of life, a slower disease progression, a better response to treatment, and in general no additional neurological features. In Chapter 3, Section 3.5.2 and in our *DNAJC6* GeneReviews article⁴²², we speculate on an emerging phenotype-genotype correlation with missense or late splicing variants associated with a milder and later-onset disease phenotype, and nonsense mutations or early splice-site mutations associated with a more severe, juvenile-onset phenotype. Patients harbouring a **monoallelic pathogenic *DNAJC6* variant** are also reported, presenting with **sporadic or familial parkinsonism** with onset between the third to fifth decades of life. Although no detailed clinical information about the disease course in patients with heterozygous *DNAJC6* mutations is available, the disease onset is similar to the third, mildest group harbouring biallelic *DNAJC6* variants. It is conceivable that for these patients, the disease is actually caused by biallelic variants, but the second variant may be difficult to locate, e.g. a short tandem repeat/intronic/promoter or other non-coding/structural variant. Although one patient carried a heterozygous deletion, three patients each had a heterozygous missense mutation, which brings up the possibility of dominant negative effects. Further work will be needed to better understand the genetic mechanisms and functional consequences in recessive and dominant *DNAJC6*-related disease.

Deep phenotyping is important to better define the clinical course of disease, improve diagnosis, better characterise clinical cohorts and understand the natural history of disease for future clinical trials. **The first aim of my PhD was to participate in the endophenotyping of a *DNAJC6* patient cohort**, as demonstrated by the clinical and biochemical characterisation of six patients with biallelic pathogenic *DNAJC6* mutations. *DNAJC6* parkinsonism-dystonia is considered a complex form of parkinsonism. The differential diagnosis includes a number of other early-onset autosomal recessive PDs and juvenile-onset forms of parkinsonism with predominant dystonia including the primary monoamine neurotransmitter disorders, disorders of heavy metal metabolism and inborn errors of metabolisms (including lysosomal and mitochondrial disorders)⁴²². The term “complex” implies that the disease is a ‘parkinsonism-plus’ syndrome with additional neurological symptoms. Indeed, the majority of patients with juvenile-onset *DNAJC6* parkinsonism-dystonia have developmental delay, intellectual disability, cognitive decline, behavioural abnormalities, neuropsychiatric symptoms and additional movement abnormalities such as spasticity, dystonia or myoclonus. The complex clinical phenotype suggests that *DNAJC6* mutations have widespread effects on brain function, particularly on circuitries that control movement, development and neuronal excitation. In our study cohort, all six patients had a complex disease: all manifested early developmental delay and cognitive impairment from early childhood, two patients suffered from seizures and four patients had dystonia.

My clinical study of this patient cohort also confirms that the complex neurological manifestation and progressive disease course in *DNAJC6* parkinsonism-dystonia leads to increased morbidity and mortality, requiring a multimodal treatment approach and specialised multidisciplinary care. Neurologists are commonly involved in the treatment of the movement disorder, predominantly parkinsonism and dystonia. Only about a third of patients respond to levodopa, and other symptomatic medications need to be trialled. Dopamine receptor agonists and anticholinergic agents have shown some clinical benefit^{65,136}. Patients often suffer from levodopa-related side effects including wearing-off symptoms and dyskinesias. The use of pump-based PD therapies (e.g. levodopa-carbidopa intestinal gel) with continuous levodopa delivery may reduce these side effects. According to the current literature, only three patients have been treated with neurosurgical procedures such as STN-DBS and pallidotomy^{63,134}, and interestingly all of them have reported a good effect. DBS could therefore be considered early in the disease course, particularly if there is levodopa resistance. Orthopaedic complications including hip dislocation, kyphoscoliosis and severe contractures should be monitored and

treated by orthopaedic surgeons, rehabilitation specialists and physiotherapists. Developmental and behavioural problems may require the involvement of developmental specialists, occupational therapists, psychologists and psychiatrists.

The advent of next-generation sequencing has greatly accelerated the discovery of new genes causing early-onset, Mendelian forms of PD, which has provided new insights into common disease mechanisms. In our study cohort, exome sequencing identified two different novel *DNAJC6* mutations in three unrelated families. Identification of the same mutation in two unrelated families originating from the same region of Pakistan is highly suggestive of a founder mutation in this population. *DNAJC6* encodes auxilin, a neuronal-specific co-chaperone protein involved in CME. Dysfunction of SV endocytosis and cellular trafficking has recently been postulated as another key pathogenic driver in monogenic and sporadic PD⁸², along with mitochondrial and lysosomal dysfunction. A better understanding of the underlying disease mechanisms is essential for the development of novel, targeted and effective treatments. As I have alluded to above, though numerous antiparkinsonian drugs are available on the market, they only provide symptomatic relief of motor symptoms and do not modify the disease course. Personalised treatments based on a patient's individual genotype are therefore urgently needed to target specific molecular pathways, modify the disease course and provide long-term clinical benefit to affected individuals. For this to become a reality, we need better disease models to elucidate disease mechanisms and test new targeted therapies.

With this in mind, the second aim of my PhD was the development of a patient-derived midbrain dopaminergic neuronal cell model for *DNAJC6* parkinsonism-dystonia. I chose a mDA model because there is evidence from our patient cohort that there is significant disruption of the dopaminergic system in *DNAJC6*-related disease: Firstly, biochemical analysis of CSF neurotransmitters revealed disturbance of dopaminergic homeostasis with reduced levels of HVA, a dopamine catabolite. Secondly, involvement of the dopaminergic system was also evident on DaTScanTM imaging in two patients with reduced tracer uptake in the basal ganglia suggesting striatonigral degeneration. Whilst a number of animal models has been developed for *DNAJC6* deficiency^{141,162,189}, only one stem cell model has been published so far¹⁹⁰. Animal models including neurotoxin-induced or transgenic mouse models have been the mainstay of PD research in recent decades and have contributed enormously to the elucidation of basic pathomechanisms. However, they often do not fully recapitulate the human disease phenotype and are therefore poorly predictive of drug efficacy in human clinical

trials⁴²³. The discovery of human induced pluripotent stem cell (iPSC) technology from 2007 onwards, has opened up new avenues for disease modelling in PD and other neurological disorders³²⁵. Neuronal stem cell-based models can be generated from easily accessible tissues such as skin or blood and arguably offer a more robust system for disease modelling than primary neuronal cultures. Compared to traditional cell models, they are not dependent on genetic overexpression strategies or immortalisation. In addition, humanised stem-cell models preserve the patient's individual genotype, making them an attractive tool to develop personalised treatment approaches. From drug discovery, to preclinical and clinical phase studies and regulatory approval takes on average 10-15 years with costs of around US \$2.8 billion⁴²⁴. iPSC-based models have the potential to greatly accelerate this process, enabling high-throughput drug screening assays with subsequently more focused *in vivo* testing. iPSC-derived cell models can also be used for the investigation of classical gene therapy approaches using a viral or non-viral vector, or, CRISPR-Cas9 gene editing approaches⁴²⁵.

From undertaking my PhD, I am acutely aware that despite many advantages, stem-cell derived models still face a number of hurdles and limitations.

Variability. Line-to-line and interline variability constitutes a major challenge when dissecting molecular disease phenotypes, particularly if they are subtle. The use of genome-editing techniques to correct a mutation in a patient line or to introduce a pathogenic mutation in a control line has become a prerequisite to minimise the impact of such variability and confidently identify disease-relevant phenotypes⁴²⁶. In my PhD, I addressed line variability by 1) using multiple patient and control lines, 2) using two clones per line for differentiation and characterisation at a progenitor and at a mature state, 3) generating an isogenic control for Patient 2-1. Except clone 1-1, I did not observe major differences between the clones with regard to their differentiation ability and maturation characteristics. Reprogramming of individual patient lines is a lengthy and laborious process. Recently, new methods have emerged that enable generation of iPSC from multiple donor or isogenic lines. Cederquist et al. developed an hPSC-based multiplex platform with construction of an isogenic hPSC library⁴²⁷. Multiple disease lines are then pooled and differentiated into the disease-relevant cell type with subsequent parallel phenotypic screening⁴²⁷. Smullen et al. developed a similar approach called induction of pluripotency from pooled cells (iPPC) that enables the multiplex generation of iPSC from multiple different donors in a single experiment⁴²⁸. A multiplex approach provides consistent extracellular environment for all the lines and thus minimises inter-line variability and reduces both time and resources^{427,428}.

Maturation. iPSC-derived cellular models retain fetal-like cellular characteristics even with derived maturity due to epigenetic resetting during the process of reprogramming. The relative “immaturity” of iPSC-derived neuronal models can be challenging for the modelling of late-onset neurodegenerative disorders such as PD. Aging strategies may help to overcome this problem. In juvenile-onset *DNAJC6* parkinsonism, the presence of neurodevelopmental symptoms in infancy/childhood indicates that the disease most likely starts earlier than with the manifestation of parkinsonism. We therefore hypothesised that an iPSC-based neuronal model would be useful in identifying early disease pathomechanisms. Similarly, iPSC-derived disease models of other early-onset complex parkinsonism in my host laboratory have revealed robust cellular disease phenotypes^{94,258}.

After establishing the model, the third aim of my PhD was the molecular characterisation of my patient-derived dopaminergic neuronal cell model for *DNAJC6* parkinsonism-dystonia. The reasons for this choice of a 2D iPSC-derived mDA system are described above. Notably, dopaminergic neurons are highly vulnerable due to their high metabolic turnover and pacemaker activity. However, given that CME is a ubiquitous cellular process, other types of neurons are also affected in this disease. Indeed, in our cohort, MR imaging showed mild to moderate cerebral atrophy in four patients, and additional cerebellar atrophy in two patients, suggesting involvement of other neuronal populations. Whilst it would not have been possible to develop multiple iPSC-derived cultures from different brain regions of interest in this disease due to time constraints, future work focusing on cortical/striatal/cerebellar iPSC-derived models will no doubt further advance our understanding of loss of *DNAJC6* function more widely in the brain.

Patient-derived mDA neurons show aberrant ventral midbrain patterning at a dopaminergic progenitor state. At day 11 of differentiation, all patient lines exhibited reduced LMX1A staining. In addition, transcriptomic analysis at day 65 of differentiation showed underexpression of additional dopaminergic transcription factors including *FOXA2*, *LMX1B*, *NR4A2* (*NURR1*) and *NEUROD1* (compared to the isogenic control) as well as *MSX1* and *SHH* (compared to the non-isogenic control). These results indicate that auxilin deficiency affects several aspects of dopaminergic neurogenesis, in particular the specification of mDA neurons (*LMX1A*, *LMX1B*), ventral patterning (*FOXA2*) and mDA identity (*NR4A2*). Transcriptional regulation of mDA specification involves two major gene networks: 1) the *SHH-FOXA2* and the *OTX2-WNT1-LMX1A/MSX1* network, as well as 2) the *LMX1A/B-WNT1/β-catenin*

autoregulatory loop²⁰³. *LMX1A* is under the direct control of *FOXA2* and *WNT/β-catenin*, and, together with *LMX1B*, initiates midbrain floor plate specification. *LMX1A* further interacts with *LMX1B*, *MSX1* and *NURR1 (NR4A2)*²⁰³. In *DNAJC6*-mutant hMLOs, Wulansari et al. showed disruption of the *LMX1A-WNT* positive feedback loop with reduced protein levels of β-catenin and reduced mRNA levels of *LMX1A* and *EN1*, which are under transcriptional control of *WNT-β-catenin*¹⁹⁰. My own findings with reduced expression of *LMX1A*, *LMX1B* and *NURR1* confirm disruption of upstream regulation by Wnt/β-catenin signalling and further highlight aberrant mDA identity. Of note, components of the Shh signalling pathway are internalised via CME as well⁴²⁹. Further studies investigating Shh-associated signalling may unravel involvement of additional developmental pathways.

Patient-derived mDA neurons shows impaired SV endocytosis at presynaptic terminals.

The FM1-43 styryl dye uptake assay demonstrated reduced uptake of FM1-43 dye in all patient lines compared to controls lines indicating impaired CME. These results are in line with the findings in the auxilin knockout mouse and the R857G mouse model, which showed impaired endocytosis with sequestration of clathrin coat components and accumulation of CCVs and empty clathrin cages^{141,162}. Rapid recycling of SV is not only essential for proper and sustained neurotransmission, but also for the regulation of synaptic and developmental signalling as discussed below.

As a consequence of impaired CME, patient-derived mDA neurons show reduced numbers of SVs at the presynaptic terminal. Electron microscopy analysis demonstrated significantly reduced SV density at presynaptic terminals. According to the three-pool model, SVs at the presynaptic terminal are located within three pools: 1) the readily releasable pool (5%), 2) the recycling pool (10%) and 3) the reserve pool (85%)⁴³⁰. SVs in these pools are accessed in sequential order. Once the readily releasable pool is depleted, SVs can be released from the recycling pool, while the reserve pool is only accessed during intense stimulation⁴³⁰. We observed a significant reduction of docked SVs/AZ length in Patient 2-1 and Patient 3-1 possibly indicating depletion of the readily releasable pool and the recycling pool with subsequently impaired release capacity. Recycling pool homeostasis is vital in the regulation of neurotransmitter release and the release-probability is strongly correlated with the size of the recycling pool⁴³¹. There is a growing body of evidence that impaired SV recycling is an important causative factor in PD. Defective SV endocytosis has also been observed in other early-onset, autosomal recessive PD caused by mutations in the gene *SYN1* encoding the

endocytic synaptic protein synaptojanin-1, and by mutations in *DJ-1*, encoding a synaptic protein that associates with synaptic membranes^{68,432,433}. In addition, alpha-synuclein has been shown to regulate recycling pool homeostasis further highlighting the role of defective SV homeostasis in PD⁴³⁴.

Patch clamp analysis of sEPSCs shows decreased amplitude of events in Patient 2-1 compared to CRISPR 2-1. A progressively smaller postsynaptic response in response to repetitive stimuli is known as depression⁴³⁵. In animal models with genetically induced impairment or knockout of endocytic proteins, enhanced depression is typically observed indicating progressive depletion of SVs that are ready to be released⁸⁸. Decreased amplitude of events in Patient 2-1 thus reflects depletion of the readily releasable SV pool, although analysis in the remaining patients is required to confirm this phenotypic finding. Further electrophysiological analysis such as amperometric detection of dopamine would be needed to assess the effect of SV depletion on dopaminergic neurotransmission. A reduction in the rate of synaptic currents was a common pathophysiological feature of iPSC-derived neurons from patients with sporadic PD and from patients harbouring PD-disease causing mutations, possibly indicating a convergent pathway in monogenic and sporadic PD⁴³⁶. Decreased synaptic activity is one of the factors contributing to synaptic pathology that precedes neuronal death and neurodegeneration¹¹⁴.

Patient-derived mDA neurons show no signs of neurodegeneration at day 65 of differentiation. Patient lines manifested similar levels of TH/MAP2-positive mDA neurons and cleaved CASP3-positive mDA neurons when compared to control lines. It may be that a longer culture time or more 3-dimensional model is required to show neurodegeneration for this disease. Indeed, Wulansari et al. observed decreased numbers of TH-positive mDA neurons and increased numbers of cleaved CASP3-positive mDA neurons in *DNAJC6*-mutant hMLOs at day 80 of differentiation¹⁹⁰. In *LMX1A* mutant mouse embryos, the number of mDA neurons is only moderately reduced, while *LMX1B*^{ff} double mutants exhibit a severe loss of mDA neurons⁴³⁷. These findings support the “multiple hit hypothesis” introduced by Schwamborn, where not only mutations in PD-causing genes, but also SNPs and mutations in PD risk genes, can cause alterations that result in a cumulative susceptibility to developing PD later in life⁴³⁸.

Transcriptomic analysis revealed alterations of neurodevelopmental processes in patient-derived mDA neurons. GO term enrichment analysis for biological processes showed

underexpressed DEGs associated with general developmental processes in all patients versus both the non-isogenic and isogenic control, and undexpressed DEGs associated with Nervous System Development in the analysis of Patient 2-1 versus CRISPR 2-1. Extraction of common, disease-related, underexpressed DEGs associated with Nervous System Development highlighted several neurodevelopmental processes including: 1) dopaminergic neurogenesis (*FOXA2, LMX1A, LMX1B, NEUROD1, NR4A2, SLC18A2*), 2) neurogenesis and maintenance of stem and neural precursor cells (*PAX6, MEIS1, HEY2*), 3) neuronal specification and differentiation (*NEUROD1, FOXP1*), 4) axon guidance and dendritogenesis (*EPHA5, EPHA6, VAV3, SLIT1, RGMA, TRPC5*) and 5) maintenance of embryonic stem cells (*ZIC3, SALL4*).

Several genes are associated with signalling pathways that are regulated by CME, in particular Wnt signalling, Notch signalling and receptor tyrosine kinase (Eph) signalling¹⁷⁰. In addition to dopaminergic neurogenesis, Wnt- β -catenin signalling also regulates neurite outgrowth, axon guidance, dendrite development and branching, synaptic function, and neuronal plasticity^{337,439}. Wnt-signalling regulated neurite outgrowth is mediated by several downstream effectors including GSK-3, the small GTPase Rac with subsequent activation of JNK signalling pathway as well as the small GTPases Rho and Rac/Cdc42 that ultimately induce actin polymerisation and microtubule stability⁴³⁹. Upon binding of Wnt to specific transmembrane receptors, the receptor-ligand complex is endocytosed by CME and becomes activated upon clathrin coat disassembly in order to regulate transcription of Wnt target genes⁴⁴⁰. Notch is another important neurodevelopmental signalling pathway, which regulates neural stem cell proliferation and differentiation as well as neurogenesis, axon outgrowth, dendritogenesis and synaptic plasticity¹⁶⁴. Notch transmembrane receptor-ligand complexes are internalised by CME with subsequent activation of the Notch signalling pathway. The Eph/ephrin receptor tyrosine kinase signalling pathway is important for axon guidance, synapse formation and maturation⁴⁴¹. Eph/ephrin signalling interactions generates repulsive signals required for axon guidance and cell migration. Internalisation of the Eph receptor/ligand complex by CME terminates Eph signalling at the postsynaptic membrane and leads to cell retraction⁴⁴¹. It is likely that in *DNAJC6* parkinsonism-dystonia, impaired CME leads to dysfunction of developmental signalling pathways with subsequent downstream transcriptional dysregulation as reflected in my transcriptomic analysis.

The RNA-seq findings also support the hypothesis that developmental defects may increase the vulnerability of mDA neurons and may contribute to or even cause development of PD⁴³⁸. In

complex, juvenile-onset PD with neurodevelopmental features, mutations are found in the genes *ATP13A2*, *PLA2G6*, *FBXO7*, *SYNJ1*, *PINK1* and *PRKN*⁴⁴². These genes are involved in the autophagy lysosomal pathway (*ATP13A2*), mitochondrial homeostasis (*PINK1*, *PRKN*), plasma lipid homeostasis (*PLA2G6*) and SV recycling (*SYNJ1*, *DNAJC6*). Disruption of these cellular processes renders dopaminergic neurons susceptible to impaired protein clearance, reduced energy metabolism and defective synaptic function. Interestingly, more than half of all familial PD disease-causing genes have a synaptic function¹¹⁴. Further evidence for the role of developmental dysfunction in PD comes from genetic neurodevelopmental disorders that present with parkinsonism, notably 22q11.2 deletion syndrome, beta-propeller protein-associated neurodegeneration, Down syndrome, cerebrotendinous xanthomatosis, and Rett syndrome³⁵⁹. In these neurodevelopmental disorders, common disease mechanisms include mitochondrial dysfunction, defective autophagy lysosomal pathway and ubiquitin-proteasome system as well as impaired endosomal trafficking. At presynaptic terminals, dysfunction of these cellular processes is thought to disturb synaptic homeostasis and cumulate over time into synaptic pathology and ultimately neurodegeneration¹¹⁴.

In addition to the observed transcriptional dysregulation of neurodevelopmental processes, patient-derived mDA neurons show defects in neuronal maturity and neurite outgrowth at day 65 of differentiation. All patient lines manifested reduced expression of NeuN, a highly specific neuronal marker in the human fetal brain⁴⁴³. NeuN is a marker of late stage neuronal maturation. MAP2 in contrast, is expressed earlier and stains both undifferentiated neuroepithelial cells and mature neurons⁴⁴⁴. While MAP2 is found from gestational week 14 on in the fetal cortical plate, NeuN shows strong immunoreactivity from gestational week 24 on⁴⁴³. Decreased NeuN staining along with normal TH/MAP2 staining in patient-derived mDA neurons may indicate delayed acquisition of late neuronal maturity. At day 65 of differentiation, patient-derived mDA neurons showed reduced sprouting of primary neurites. Neurite outgrowth is a complex neuronal differentiation process and its regulation involves a variety of different factors including ECM-associated factors, CAMs, neurotrophic factors, inhibitory factors and guidance factors³⁹⁶. The trafficking of their corresponding receptors to axons and growth cones involves different vesicular compartments including early and late endosomes, recycling endosomes and lysosomes⁴⁴⁵. The correct spatial and temporal positioning of these receptors is regulated by various forms of endocytosis, including CME⁴⁴⁶. Defects in endocytic membrane trafficking and vesicular transport have been associated with a variety of neurodegenerative disorders including Alzheimer's disease, PD, polyQ diseases,

peripheral neuropathies, and lysosomal storage disorders⁴⁴⁷. In familial PD, a high number of disease-causing genes is involved in intracellular trafficking, notably in CME (*SNCA*, *LRRK2*, *PRKN*, *DNAJC6*, *SYNJ1*, *DNAJC13*), endo-lysosomal trafficking (*LRRK2*, *VPS35*, *ATP13A2*, *DNAJC13*) and membrane trafficking (*PLA2G6*).

Given the defects in neurite outgrowth, it would be interesting to investigate whether auxilin deficiency affects other intracellular trafficking systems such as endosomes and lysosomes. Studies in the R857G auxilin mouse model have shown that auxilin is involved in the trafficking of trans-Golgi-derived CCVs¹⁶². The authors also generated an auxilin interactom that demonstrated interaction of auxilin with a subset of synaptic and Golgi-resident clathrin adaptor proteins. Additional experiments investigating the co-localisation of auxilin with endosomal and lysosomal markers and co-immunoprecipitation analysis may lead to the identification of novel interaction partners.

As a clinician, an important fourth aim of my PhD was to develop a gene therapy approach for this drug-resistant disorder. To date, there is no curative treatment available for *DNAJC6* parkinsonism-dystonia. To provide a first proof-of-concept for a future gene therapy approach in *DNAJC6* parkinsonism-dystonia, I cloned a wildtype *DNAJC6* gene into a lentiviral vector and transfected mDA neurons at day 28 of differentiation. At day 65 of differentiation, patient-derived mDA neurons expressed high levels of auxilin protein and showed some rescue of CME. Rescuing CME is likely to be key to restoring downstream phenotypes including neuronal maturation, aberrant ventral midbrain patterning and decreased neurite outgrowth that are associated with defective endocytosis. Future experimental validation of these downstream phenotype correction will be mandatory in order to take this therapy approach a step forward.

I recognise that there are a number of limitations to this work presented here.

Firstly, this project was undertaken before CRISPR-Cas9 technology was established in my host lab and hence generation of the isogenic control was outsourced to a company, and I had sufficient funding to generate one isogenic line. I therefore used three patient lines, two non-isogenic age-matched control lines and one isogenic control line for Patient 2-1. In general, the main phenotypic findings showed similar results between both the non-isogenic and isogenic controls, though transcriptomics analysis clearly revealed differences in gene expression patterns, likely related to genetic background. The availability of isogenic controls for all

patient lines would indeed be helpful to validate the results and to further unravel mutation-specific phenotypic findings.

Secondly, given the predominant parkinsonian movement disorder phenotype, I developed a dopaminergic neuronal cell model using a well-established 2D dopaminergic differentiation protocol. Development of advanced, 3D neuronal stem cell models with a more complex cellular cytoarchitecture and connectivity, e.g. midbrain-like or cortical organoids and fusion models²⁴⁹ may provide additional information about the effects of auxilin deficiency on neuronal development, morphogenesis and neural connectivity more broadly in the brain.

In addition, I performed RNA-seq analysis relatively late in my PhD project. Whilst transcriptomic analysis corroborated other experimental findings (in particular impaired neuronal maturation and neurite outgrowth), I believe that RNA-seq analysis, performed at an early stage of the project, may be of great value to get a global impression of dysregulated pathways in disease. This unbiased approach may unravel previously unanticipated molecular pathways that can be subsequently investigated in more detail. In the future, single-cell and spatial RNA-seq analysis in a 3D-organoid model might be useful to unravel cell-specific effects of auxilin deficiency.

Finally, with more time, the gene therapy approach could be better optimised. Based on a previously established protocol in my host laboratory, I transduced neurons at day 28 of differentiation. Given that ventral midbrain patterning defects are evident as early as day 11 of differentiation, it would be interesting to transduce the neurons at an earlier time point. CME is involved in the regulation of developmental signalling pathways that are important in neural stem and precursor cells. Earlier transfection and use of a neural promotor that is active early in neural stem/progenitor cells and developing synapses may help to target some of these neurodevelopmental abnormalities. In the future, additional functional assays including RNA seq analysis and neuronal maturation assays are needed to evaluate the effect of the gene therapy on developmental processes. With regard to patients, an early diagnosis of neurodevelopmental features may allow treatment of patients with a therapeutic window, before the disease burden becomes severe, in particular before the onset of parkinsonian symptoms. Optimisation of an *in vitro* approach might therefore help us understand the timing for optimal treatment, in tandem with work in an animal model and human natural history studies.

There are several future directions of research that I think would be worth exploring. Firstly, it would be important to further elucidate downstream phenotypic effects of impaired CME. To better understand the effects of auxilin deficiency on neurodevelopmental processes, future work should focus on the main signalling pathways regulated by CME, in particular Wnt, Notch and RTK signalling. Immunofluorescence and western blot analysis for signalling-associated membrane receptors and downstream proteins may provide information about the activation of the corresponding signalling pathway. As mentioned above, use of more advanced 3D models may unravel additional phenotypes with regard to morphology, growth, and other neural populations. To study the effects of auxilin deficiency on a synaptic level, iPSC-derived, engineered microfluidic systems such as “synapse-on-a-chip” may be developed⁴⁴⁸. These systems will allow high-resolution imaging, e.g. synaptic vesicle cycling, and drug screening approaches, e.g. restoration of CME at presynaptic terminals.

Secondly, it would be very important to now work towards clinical translation of a gene therapy approach. Following completion of the lentiviral gene therapy studies *in vitro*, additional studies in a *DNAJC6* knockout mouse model using an AAV vector will help to accelerate development and clinical translation, which will potentially identify a new precision therapy strategy for this disorder. In the field of inherited monogenic neurodegenerative diseases, gene therapies hold great promise because they directly target the underlying etiology and aim to achieve long-lasting correction. However, there are still a number of challenges that need to be addressed including: 1) choice of viral vector, 2) route of vector administration, 3) gene expression efficacy using cell-specific promoters, 4) evaluation of gene therapy effect and clinical outcome measures, and 5) timing of therapy. Over the last few years, AAV vectors have become the most popular viral vectors for human delivery due to their widespread distribution, serotype-dependent neurotropism, transduction efficiency and safety profile^{420,449}. The most frequently used capsids are AAV1, AAV2, AAV5, AAV9 and AAVrh.10⁴²⁰. Nevertheless, activation of host immune responses and development of neutralising antibodies is an issue in clinical studies. The route of administration depends on the target region. The specific pathogenesis of the disease and the anatomical structures involved must be taken into account when designing a gene therapy for a specific disease. Stereotactic intraputaminial delivery achieves a high local concentration and is potentially suitable for neurodegenerative diseases primarily affecting the nigrostriatal pathway. Although highly relevant for *DNAJC6* parkinsonism-dystonia, this route of delivery would probably not target other disease-relevant neuronal cell populations that are responsible for non-motor symptoms. The choice of a

promotor or enhancer is equally important to drive transgene expression in disease-affected brain cells and limit expression in off-target cells⁴²⁰. Promoter optimisation, efficacy and toxicology studies may be conducted in complementary animal models when available. The optimal therapeutic window for gene therapy also needs to be evaluated. In general, pre-symptomatic treatment would be ideal; in the future, programs focused on newborn screening may facilitate this for diseases where there are targeted precision therapies and where earlier intervention is proven to result in better patient outcomes. Nevertheless, treatment of symptomatic patients can also result in clinical benefit. Indeed, gene therapy trials in AADC deficiency have shown that even older patients with a higher disease burden may benefit from gene therapy with improvements in motor and mental function¹³². In *DNAJC6* parkinsonism-dystonia, patients may benefit from a therapeutic time window with treatment in the first decade and before the onset of progressive parkinsonian symptoms.

For the design of clinical gene therapy trials, well-defined natural history cohorts, meaningful clinical disease rating scales and robust radiological/biochemical biomarkers are necessary clinical outcome parameters. Advancement of clinical trials is often hindered by differences in the regulatory framework between different countries⁴⁵⁰. Accelerated pathways for approval, adaptive licensing and innovative clinical trial designs for rare diseases should be promoted to develop global regulatory convergence and networks for the benefit of patients with rare and ultra-rare disorders⁴⁵⁰.

Finally, adoption of new AI-technologies and automated systems will be important to explore in the future. Machine-learning strategies are increasingly used in the analysis of complex and large datasets⁴⁵¹. Integrated transcriptomics, proteomics, lipidomics and metabolomics may be used for additional molecular characterisation of iPSC-derived 3D cultures or single-cells⁴⁵². Deep phenotyping of iPSC-derived neuronal cell models using multiomic strategies combined with clinical data has the potential to identify novel biomarkers and novel disease-relevant molecular pathways that may serve as novel drug targets and also refine patient stratification for future precision medicine approaches^{453,454}.

In conclusion, I have contributed to the clinical characterisation of a *DNAJC6* patient cohort and provided clinical, biochemical and imaging characteristics of a rare neurogenetic movement disorder. I was able to efficiently reprogram three patient-derived fibroblast lines, and differentiate them into midbrain dopaminergic neurons together with two non-isogenic controls

and one isogenic control. In this dopaminergic neuronal cell model, I was able to demonstrate auxilin deficiency and impaired CME, which further revealed defects in synaptic vesicle homeostasis and synaptic transmission. I also identified aberrant ventral midbrain patterning and defects in neuronal maturation and neurite outgrowth. Transcriptomics analysis confirmed defects in synaptic vesicle cycling and highlighted disturbance of a variety of neurodevelopmental processes. Finally, I was able to develop a lentiviral vector for *DNAJC6* transgene delivery and restore auxilin deficiency and CME in patient-derived mDA neurons. Better understanding of this rare neurodegenerative disorder will hopefully soon lead to precision therapies for this condition, that can be delivered within a therapeutic window for better patient outcomes.

References

1. Clark LN, Louis ED. Essential tremor [Internet]. In: Handbook of Clinical Neurology. Elsevier B.V.; 2018 p. 229–239.[cited 2020 May 4] Available from: <https://linkinghub.elsevier.com/retrieve/pii/B9780444632333000154>
2. Lebouvier T, Chaumette T, Paillusson S, et al. The second brain and Parkinson's disease. *Eur. J. Neurosci.* 2009;30(5):735–741.
3. Pringsheim T, Jette N, Frolkis A, Steeves TDL. The prevalence of Parkinson's disease: a systematic review and meta-analysis. [Internet]. *Mov. Disord.* 2014;29(13):1583–90.[cited 2016 Jul 22] Available from: <http://www.ncbi.nlm.nih.gov/pubmed/24976103>
4. Ray Dorsey E, Elbaz A, Nichols E, et al. Global, regional, and national burden of Parkinson's disease, 1990-2016: a systematic analysis for the Global Burden of Disease Study 2016 [Internet]. *Lancet. Neurol.* 2018;17(11):939–953.[cited 2023 Mar 17] Available from: <https://pubmed.ncbi.nlm.nih.gov/30287051/>
5. Poewe W, Seppi K, Tanner CM, et al. Parkinson disease [Internet]. *Nat. Rev. Dis. Prim.* 2017;3(1):1–21.[cited 2020 May 4] Available from: <http://www.nature.com/articles/nrdp201713>
6. Parkinson J. An essay on the shaking palsy. 1817 [Internet]. *J. Neuropsychiatry Clin. Neurosci.* 2002;14(2)[cited 2022 Nov 12] Available from: <https://pubmed.ncbi.nlm.nih.gov/11983801/>
7. Lang AE, Lozano AM. Parkinson's disease. First of two parts [Internet]. *N. Engl. J. Med.* 1998;339(15):1044–53.[cited 2023 Mar 15] Available from: <https://pubmed.ncbi.nlm.nih.gov/9761807/>
8. Giguère N, Nanni SB, Trudeau LE. On Cell Loss and Selective Vulnerability of Neuronal Populations in Parkinson's Disease [Internet]. *Front. Neurol.* 2018;9(JUN)[cited 2023 Mar 22] Available from: <https://pubmed.ncbi.nlm.nih.gov/29971039/>
9. Jankovic J, Tan EK. Parkinson's disease: etiopathogenesis and treatment [Internet]. *J. Neurol. Neurosurg. Psychiatry* 2020;91(8):795–808.[cited 2023 Mar 17] Available from: <https://pubmed.ncbi.nlm.nih.gov/32576618/>
10. Fahn S. The 200-year journey of Parkinson disease: Reflecting on the past and looking towards the future [Internet]. *Parkinsonism Relat. Disord.* 2018;46 Suppl 1:S1–S5.[cited 2023 Mar 17] Available from: <https://pubmed.ncbi.nlm.nih.gov/28784297/>
11. Langston JW. The MPTP Story [Internet]. *J. Parkinsons. Dis.* 2017;7(s1):S11–S19.[cited 2023 Mar 17] Available from: <https://pubmed.ncbi.nlm.nih.gov/28282815/>
12. Postuma RB, Berg D, Stern M, et al. MDS clinical diagnostic criteria for Parkinson's disease [Internet]. *Mov. Disord.* 2015;30(12):1591–1601.[cited 2023 Mar 17] Available from: <https://pubmed.ncbi.nlm.nih.gov/26474316/>
13. Groenewegen HJ. The basal ganglia and motor control [Internet]. *Neural Plast.* 2003;10(1–2):107–120.[cited 2023 Jan 6] Available from: <https://pubmed.ncbi.nlm.nih.gov/14640312/>
14. Fisone G, Håkansson K, Borgkvist A, Santini E. Signaling in the basal ganglia: Postsynaptic and presynaptic mechanisms [Internet]. *Physiol. Behav.* 2007;92(1–2):8–14.[cited 2017 Nov 21] Available from: <http://www.ncbi.nlm.nih.gov/pubmed/17585965>
15. Chuhma N, Tanaka KF, Hen R, Rayport S. Functional connectome of the striatal medium spiny neuron. [Internet]. *J. Neurosci.* 2011;31(4):1183–92.[cited 2018 Feb 28] Available from: <http://www.jneurosci.org/cgi/doi/10.1523/JNEUROSCI.3833-10.2011>

16. DeLong MR, Wichmann T, V D, et al. Circuits and Circuit Disorders of the Basal Ganglia [Internet]. *Arch. Neurol.* 2007;64(1):20.[cited 2017 Jul 25] Available from: <http://archneur.jamanetwork.com/article.aspx?doi=10.1001/archneur.64.1.20>
17. McGregor MM, Nelson AB. Circuit Mechanisms of Parkinson's Disease [Internet]. *Neuron* 2019;101(6):1042–1056.[cited 2023 Mar 17] Available from: <https://pubmed.ncbi.nlm.nih.gov/30897356/>
18. Lanciego JL, Luquin N, Obeso JA. Functional neuroanatomy of the basal ganglia. [Internet]. *Cold Spring Harb. Perspect. Med.* 2012;2(12):a009621.[cited 2017 Sep 8] Available from: <http://www.ncbi.nlm.nih.gov/pubmed/23071379>
19. Obeso JA, Marin C, Rodriguez-Oroz C, et al. The basal ganglia in Parkinson's disease: current concepts and unexplained observations [Internet]. *Ann. Neurol.* 2008;64 Suppl 2(SUPPL. 2)[cited 2023 Jan 20] Available from: <https://pubmed.ncbi.nlm.nih.gov/19127584/>
20. Wichmann T, Bergman H, DeLong MR. Basal ganglia, movement disorders and deep brain stimulation: advances made through non-human primate research [Internet]. *J. Neural Transm.* 2018;125(3):419–430.[cited 2023 Jun 3] Available from: <https://pubmed.ncbi.nlm.nih.gov/28601961/>
21. Bloem BR, Okun MS, Klein C. Parkinson's disease [Internet]. *Lancet (London, England)* 2021;397(10291):2284–2303.[cited 2022 Nov 12] Available from: <https://pubmed.ncbi.nlm.nih.gov/33848468/>
22. Mackay DF, Russell ER, Stewart K, et al. Neurodegenerative Disease Mortality among Former Professional Soccer Players [Internet]. *N. Engl. J. Med.* 2019;381(19):1801–1808.[cited 2023 Mar 18] Available from: <https://pubmed.ncbi.nlm.nih.gov/31633894/>
23. Blauwendraat C, Nalls MA, Singleton AB. The genetic architecture of Parkinson's disease [Internet]. *Lancet Neurol.* 2020;19(2):170–178.[cited 2020 Apr 16] Available from: <http://www.ncbi.nlm.nih.gov/pubmed/31521533>
24. Nalls MA, Blauwendraat C, Vallerga CL, et al. Identification of novel risk loci, causal insights, and heritable risk for Parkinson's disease: a meta-analysis of genome-wide association studies [Internet]. *Lancet. Neurol.* 2019;18(12):1091–1102.[cited 2022 Nov 14] Available from: <https://pubmed.ncbi.nlm.nih.gov/31701892/>
25. Hall A, Bandres-Ciga S, Diez-Fairen M, et al. Genetic Risk Profiling in Parkinson's Disease and Utilizing Genetics to Gain Insight into Disease-Related Biological Pathways [Internet]. *Int. J. Mol. Sci.* 2020;21(19):1–15.[cited 2022 Nov 14] Available from: <https://pubmed.ncbi.nlm.nih.gov/33020390/>
26. Reed X, Bandrés-Ciga S, Blauwendraat C, Cookson MR. The role of monogenic genes in idiopathic Parkinson's disease [Internet]. *Neurobiol. Dis.* 2019;124:230–239.[cited 2020 Mar 4] Available from: <http://www.ncbi.nlm.nih.gov/pubmed/30448284>
27. Lill CM. Genetics of Parkinson's disease. *Mol. Cell. Probes* 2016;
28. Balestrino R, Schapira AHV. Parkinson disease. *Eur. J. Neurol.* 2020;
29. Rizek P, Kumar N, Jog MS. An update on the diagnosis and treatment of Parkinson disease. *CMAJ* 2016;188(16):1157–1165.
30. Domingo A, Klein C. Genetics of Parkinson disease [Internet]. In: *Handbook of Clinical Neurology*. Elsevier B.V.; 2018 p. 211–227.[cited 2020 Mar 25] Available from: <https://linkinghub.elsevier.com/retrieve/pii/B9780444632333000142>
31. Polymeropoulos MH, Lavedan C, Leroy E, et al. Mutation in the α -synuclein gene identified in families with Parkinson's disease. *Science* (80-.). 1997;
32. Puschmann A. New Genes Causing Hereditary Parkinson's Disease or Parkinsonism [Internet]. *Curr. Neurol. Neurosci. Rep.* 2017;17(9):66.[cited 2018 Jun 27] Available from: <http://link.springer.com/10.1007/s11910-017-0780-8>
33. Mehanna R, Moore S, Hou JG, et al. Comparing clinical features of young onset, middle onset and late onset Parkinson's disease [Internet]. *Parkinsonism Relat. Disord.*

- 2014;20(5):530–534.[cited 2023 May 30] Available from:
<https://pubmed.ncbi.nlm.nih.gov/24631501/>
34. Morales-Briceño H, Mohammad SS, Post B, et al. Clinical and neuroimaging phenotypes of genetic parkinsonism from infancy to adolescence [Internet]. *Brain* 2020;143(3):751–770.[cited 2023 Jun 16] Available from:
<https://pubmed.ncbi.nlm.nih.gov/31800013/>
 35. Ferguson LW, Rajput AH, Rajput A. Early-onset vs. Late-onset Parkinson’s disease: A Clinical-pathological Study [Internet]. *Can. J. Neurol. Sci.* 2016;43(1):113–119.[cited 2023 May 30] Available from: <https://pubmed.ncbi.nlm.nih.gov/26189779/>
 36. Leuzzi V, Nardecchia F, Pons R, Galosi S. Parkinsonism in children: Clinical classification and etiological spectrum [Internet]. *Parkinsonism Relat. Disord.* 2021;82:150–157.[cited 2023 May 29] Available from:
<https://pubmed.ncbi.nlm.nih.gov/33109474/>
 37. Garcia-Cazorla A, Duarte ST. Parkinsonism and inborn errors of metabolism [Internet]. In: *Journal of Inherited Metabolic Disease*. 2014 p. 627–642.[cited 2018 Apr 2] Available from: <http://www.ncbi.nlm.nih.gov/pubmed/24906253>
 38. Malkus KA, Tsika E, Ischiropoulos H. Oxidative modifications, mitochondrial dysfunction, and impaired protein degradation in Parkinson’s disease: how neurons are lost in the Bermuda triangle. [Internet]. *Mol. Neurodegener.* 2009;4(1):24.[cited 2020 Mar 25] Available from: <http://www.ncbi.nlm.nih.gov/pubmed/19500376>
 39. Kramer ML, Schulz-Schaeffer WJ. Presynaptic alpha-synuclein aggregates, not Lewy bodies, cause neurodegeneration in dementia with Lewy bodies [Internet]. *J. Neurosci.* 2007;27(6):1405–1410.[cited 2023 Mar 18] Available from:
<https://pubmed.ncbi.nlm.nih.gov/17287515/>
 40. Braak H, Sandmann-Keil D, Gai W, Braak E. Extensive axonal Lewy neurites in Parkinson’s disease: a novel pathological feature revealed by alpha-synuclein immunocytochemistry [Internet]. *Neurosci. Lett.* 1999;265(1):67–69.[cited 2023 Mar 18] Available from: <https://pubmed.ncbi.nlm.nih.gov/10327208/>
 41. Masliah E, Rockenstein E, Veinbergs I, et al. Dopaminergic loss and inclusion body formation in alpha-synuclein mice: implications for neurodegenerative disorders [Internet]. *Science* 2000;287(5456):1265–1269.[cited 2023 Mar 18] Available from:
<https://pubmed.ncbi.nlm.nih.gov/10678833/>
 42. Janezic S, Threlfell S, Dodson PD, et al. Deficits in dopaminergic transmission precede neuron loss and dysfunction in a new Parkinson model [Internet]. *Proc. Natl. Acad. Sci. U. S. A.* 2013;110(42)[cited 2023 Mar 18] Available from:
<https://pubmed.ncbi.nlm.nih.gov/24082145/>
 43. West AB, Moore DJ, Biskup S, et al. Parkinson’s disease-associated mutations in leucine-rich repeat kinase 2 augment kinase activity [Internet]. *Proc. Natl. Acad. Sci. U. S. A.* 2005;102(46):16842–16847.[cited 2023 Feb 13] Available from:
<https://pubmed.ncbi.nlm.nih.gov/16269541/>
 44. Mazzulli JR, Zunke F, Tsunemi T, et al. Activation of β -Glucocerebrosidase Reduces Pathological α -Synuclein and Restores Lysosomal Function in Parkinson’s Patient Midbrain Neurons [Internet]. *J. Neurosci.* 2016;36(29):7693–7706.[cited 2023 Mar 18] Available from: <https://pubmed.ncbi.nlm.nih.gov/27445146/>
 45. Zunke F, Moise AC, Belur NR, et al. Reversible Conformational Conversion of α -Synuclein into Toxic Assemblies by Glucosylceramide [Internet]. *Neuron* 2018;97(1):92-107.e10.[cited 2023 Mar 18] Available from:
<https://pubmed.ncbi.nlm.nih.gov/29290548/>
 46. Seaman MN, Freeman CL. Analysis of the Retromer complex-WASH complex interaction illuminates new avenues to explore in Parkinson disease [Internet]. *Commun. Integr. Biol.* 2014;7(4):e29483.[cited 2023 Feb 13] Available from:

- <https://pubmed.ncbi.nlm.nih.gov/25067992/>
47. Tang FL, Erion JR, Tian Y, et al. VPS35 in Dopamine Neurons Is Required for Endosome-to-Golgi Retrieval of Lamp2a, a Receptor of Chaperone-Mediated Autophagy That Is Critical for α -Synuclein Degradation and Prevention of Pathogenesis of Parkinson's Disease [Internet]. *J. Neurosci.* 2015;35(29):10613–10628.[cited 2023 Feb 13] Available from: <https://pubmed.ncbi.nlm.nih.gov/26203154/>
 48. Ramirez A, Heimbach A, Gründemann J, et al. Hereditary parkinsonism with dementia is caused by mutations in ATP13A2, encoding a lysosomal type 5 P-type ATPase [Internet]. *Nat. Genet.* 2006;38(10):1184–1191.[cited 2018 Jul 12] Available from: <https://pubmed.ncbi.nlm.nih.gov/16964263/>
 49. Tsunemi T, Hamada K, Krainc D. ATP13A2/PARK9 regulates secretion of exosomes and α -synuclein [Internet]. *J. Neurosci.* 2014;34(46):15281–15287.[cited 2023 Mar 18] Available from: <https://pubmed.ncbi.nlm.nih.gov/25392495/>
 50. Burbulla LF, Song P, Mazzulli JR, et al. Dopamine oxidation mediates mitochondrial and lysosomal dysfunction in Parkinson's disease [Internet]. *Science* 2017;357(6357):1255–1261.[cited 2019 Apr 2] Available from: <https://pubmed.ncbi.nlm.nih.gov/28882997/>
 51. Conway KA, Rochet JC, Bieganski RM, Lansbury J. Kinetic stabilization of the alpha-synuclein protofibril by a dopamine-alpha-synuclein adduct [Internet]. *Science* 2001;294(5545):1346–1349.[cited 2023 Mar 18] Available from: <https://pubmed.ncbi.nlm.nih.gov/11701929/>
 52. William Langston J, Ballard P, Tetrud JW, Irwin I. Chronic Parkinsonism in humans due to a product of meperidine-analog synthesis [Internet]. *Science* 1983;219(4587):979–980.[cited 2022 Nov 12] Available from: <https://pubmed.ncbi.nlm.nih.gov/6823561/>
 53. Rangaraju V, Calloway N, Ryan TA. Activity-driven local ATP synthesis is required for synaptic function [Internet]. *Cell* 2014;156(4):825–835.[cited 2023 Mar 19] Available from: <https://pubmed.ncbi.nlm.nih.gov/24529383/>
 54. Heger LM, Wise RM, Hees JT, et al. Mitochondrial Phenotypes in Parkinson's Diseases-A Focus on Human iPSC-Derived Dopaminergic Neurons [Internet]. *Cells* 2021;10(12)[cited 2023 Mar 18] Available from: <https://pubmed.ncbi.nlm.nih.gov/34943944/>
 55. Noda S, Sato S, Fukuda T, et al. Loss of Parkin contributes to mitochondrial turnover and dopaminergic neuronal loss in aged mice [Internet]. *Neurobiol. Dis.* 2020;136:104717.[cited 2020 Apr 24] Available from: <http://www.ncbi.nlm.nih.gov/pubmed/31846738>
 56. Zhi L, Qin Q, Muqeem T, et al. Loss of PINK1 causes age-dependent decrease of dopamine release and mitochondrial dysfunction [Internet]. *Neurobiol. Aging* 2019;75:1–10.[cited 2020 Apr 24] Available from: <http://www.ncbi.nlm.nih.gov/pubmed/30504091>
 57. Pickrell AM, Youle RJ. The Roles of PINK1, Parkin, and Mitochondrial Fidelity in Parkinson's Disease [Internet]. *Neuron* 2015;85(2):257–273.[cited 2017 Nov 7] Available from: <https://linkinghub.elsevier.com/retrieve/pii/S0896627314010885>
 58. Bose A, Beal MF. Mitochondrial dysfunction in Parkinson's disease [Internet]. *J. Neurochem.* 2016;139 Suppl:216–231.[cited 2023 Jun 14] Available from: <https://pubmed.ncbi.nlm.nih.gov/27546335/>
 59. Li JL, Lin TY, Chen PL, et al. Mitochondrial Function and Parkinson's Disease: From the Perspective of the Electron Transport Chain [Internet]. *Front. Mol. Neurosci.* 2021;14[cited 2023 Jun 14] Available from: <https://pubmed.ncbi.nlm.nih.gov/34955747/>

60. Jia F, Fellner A, Kumar KR. Monogenic Parkinson's Disease: Genotype, Phenotype, Pathophysiology, and Genetic Testing [Internet]. *Genes (Basel)*. 2022;13(3)[cited 2022 Nov 12] Available from: <https://pubmed.ncbi.nlm.nih.gov/35328025/>
61. Edvardson S, Cinnamon Y, Ta-Shma A, et al. A deleterious mutation in DNAJC6 encoding the neuronal-specific clathrin-uncoating co-chaperone auxilin, is associated with juvenile parkinsonism. [Internet]. *PLoS One* 2012;7(5):e36458.[cited 2016 Jul 22] Available from: <http://www.ncbi.nlm.nih.gov/pubmed/22563501>
62. Köroğlu Ç, Baysal L, Cetinkaya M, et al. DNAJC6 is responsible for juvenile parkinsonism with phenotypic variability. *Park. Relat. Disord.* 2013;19(3):320–324.
63. Olgiati S, Quadri M, Fang M, et al. DNAJC6 mutations associated with early-onset Parkinson's disease. *Ann. Neurol.* 2015;79(2):244–56.
64. Elsayed LEO, Drouet V, Usenko T, et al. A Novel Nonsense Mutation in DNAJC6 Expands the Phenotype of Autosomal-Recessive Juvenile-Onset Parkinson's Disease. [Internet]. *Ann. Neurol.* 2016;79(2):335–337.[cited 2023 Jan 13] Available from: <https://pubmed.ncbi.nlm.nih.gov/26703368/>
65. Ng J, Cortès-Saladelafont E, Abela L, et al. DNAJC6 Mutations Disrupt Dopamine Homeostasis in Juvenile Parkinsonism-Dystonia [Internet]. *Mov. Disord.* 2020;35(8):1357–1368.[cited 2022 Feb 24] Available from: <https://pubmed.ncbi.nlm.nih.gov/32472658/>
66. Vilariño-Güell C, Rajput A, Milnerwood AJ, et al. DNAJC13 mutations in Parkinson disease [Internet]. *Hum. Mol. Genet.* 2014;23(7):1794–1801.[cited 2020 Apr 22] Available from: <http://www.ncbi.nlm.nih.gov/pubmed/24218364>
67. Dymant DA, Smith AC, Humphreys P, et al. Homozygous nonsense mutation in SYNJ1 associated with intractable epilepsy and tau pathology. *Neurobiol. Aging* 2015;36(2):1222.e1-1222.e5.
68. Quadri M, Fang M, Picillo M, et al. Mutation in the *SYNJ1* Gene Associated with Autosomal Recessive, Early-Onset Parkinsonism. *Hum. Mutat.* 2013;34(9):1208–1215.
69. Krebs CE, Karkheiran S, Powell JC, et al. The Sac1 domain of SYNJ1 identified mutated in a family with early-onset progressive Parkinsonism with generalized seizures [Internet]. *Hum. Mutat.* 2013;34(9):1200–1207.[cited 2020 Apr 30] Available from: <https://pubmed.ncbi.nlm.nih.gov/23804563/>
70. Hunn BHMM, Cragg SJ, Bolam JP, et al. Impaired intracellular trafficking defines early Parkinson's disease [Internet]. *Trends Neurosci.* 2015;38(3):178–188.[cited 2017 Nov 7] Available from: <http://linkinghub.elsevier.com/retrieve/pii/S0166223614002380>
71. Abeliovich A, Gitler AD. Defects in trafficking bridge Parkinson's disease pathology and genetics [Internet]. *Nature* 2016;539(7628):207–216.[cited 2023 Mar 15] Available from: <https://pubmed.ncbi.nlm.nih.gov/27830778/>
72. Vidyadhara DJ, Lee JE, Chandra SS. Role of the endolysosomal system in Parkinson's disease [Internet]. *J. Neurochem.* 2019;150(5):487–506.[cited 2020 Mar 26] Available from: <http://www.ncbi.nlm.nih.gov/pubmed/31287913>
73. Hasegawa T, Sugeno N, Kikuchi A, et al. Membrane Trafficking Illuminates a Path to Parkinson's Disease [Internet]. *Tohoku J. Exp. Med.* 2017;242(1):63–76.[cited 2023 Mar 15] Available from: <https://pubmed.ncbi.nlm.nih.gov/28539529/>
74. Williams ET, Chen X, Moore DJ. VPS35, the Retromer Complex and Parkinson's Disease [Internet]. *J. Parkinsons. Dis.* 2017;7(2):219–233.[cited 2022 Nov 15] Available from: <https://pubmed.ncbi.nlm.nih.gov/28222538/>
75. Lesage S, Drouet V, Majounie E, et al. Loss of VPS13C Function in Autosomal-Recessive Parkinsonism Causes Mitochondrial Dysfunction and Increases PINK1/Parkin-Dependent Mitophagy [Internet]. *Am. J. Hum. Genet.* 2016;98(3):500–513.[cited 2022 Nov 15] Available from: <https://pubmed.ncbi.nlm.nih.gov/26942284/>

76. Nguyen M, Wong YC, Ysselstein D, et al. Synaptic, Mitochondrial, and Lysosomal Dysfunction in Parkinson's Disease [Internet]. *Trends Neurosci.* 2019;42(2):140–149.[cited 2020 Mar 27] Available from: <http://www.ncbi.nlm.nih.gov/pubmed/30509690>
77. Follett J, Norwood SJ, Hamilton NA, et al. The Vps35 D620N mutation linked to Parkinson's disease disrupts the cargo sorting function of retromer. [Internet]. *Traffic* 2014;15(2):230–44.[cited 2020 Apr 10] Available from: <http://www.ncbi.nlm.nih.gov/pubmed/24152121>
78. Kett LR, Stiller B, Bernath MM, et al. α -Synuclein-independent histopathological and motor deficits in mice lacking the endolysosomal Parkinsonism protein Atp13a2 [Internet]. *J. Neurosci.* 2015;35(14):5724–5742.[cited 2022 Nov 15] Available from: <https://pubmed.ncbi.nlm.nih.gov/25855184/>
79. Grünewald A, Arns B, Seibler P, et al. ATP13A2 mutations impair mitochondrial function in fibroblasts from patients with Kufor-Rakeb syndrome [Internet]. *Neurobiol. Aging* 2012;33(8):1843.e1-1843.e7.[cited 2023 Mar 19] Available from: <https://pubmed.ncbi.nlm.nih.gov/22296644/>
80. Usenovic M, Tresse E, Mazzulli JR, et al. Deficiency of ATP13A2 leads to lysosomal dysfunction, α -synuclein accumulation, and neurotoxicity [Internet]. *J. Neurosci.* 2012;32(12):4240–4246.[cited 2023 Mar 19] Available from: <https://pubmed.ncbi.nlm.nih.gov/22442086/>
81. Besemer AS, Maus J, Ax MDA, et al. Receptor-mediated endocytosis 8 (RME-8)/DNAJC13 is a novel positive modulator of autophagy and stabilizes cellular protein homeostasis [Internet]. *Cell. Mol. Life Sci.* 2021;78(2):645–660.[cited 2023 Mar 19] Available from: <https://pubmed.ncbi.nlm.nih.gov/32322926/>
82. Zou L, Tian Y, Zhang Z. Dysfunction of Synaptic Vesicle Endocytosis in Parkinson's Disease [Internet]. *Front. Integr. Neurosci.* 2021;15[cited 2022 May 27] Available from: <https://pmc/articles/PMC8172812/>
83. Kaksonen M, Roux A. Mechanisms of clathrin-mediated endocytosis [Internet]. *Nat. Rev. Mol. Cell Biol.* 2018;19(5):313–326.[cited 2020 Mar 12] Available from: <http://www.ncbi.nlm.nih.gov/pubmed/29410531>
84. Milosevic I. Revisiting the role of clathrin-mediated endocytosis in synaptic vesicle recycling. *Front. Cell. Neurosci.* 2018;12
85. Chang D, Nalls MA, Hallgrímsdóttir IB, et al. A meta-analysis of genome-wide association studies identifies 17 new Parkinson's disease risk loci [Internet]. *Nat. Genet.* 2017;49(10):1511–1516.[cited 2020 Mar 27] Available from: <https://pubmed.ncbi.nlm.nih.gov/28892059/>
86. Bai J, Hu Z, Dittman JS, et al. Endophilin functions as a membrane-bending molecule and is delivered to endocytic zones by exocytosis [Internet]. *Cell* 2010;143(3):430–441.[cited 2022 Nov 18] Available from: <https://pubmed.ncbi.nlm.nih.gov/21029864/>
87. Murdoch JD, Rostovsky CM, Gowrisankaran S, et al. Endophilin-A Deficiency Induces the Foxo3a-Fbxo32 Network in the Brain and Causes Dysregulation of Autophagy and the Ubiquitin-Proteasome System [Internet]. *Cell Rep.* 2016;17(4):1071–1086.[cited 2022 Nov 18] Available from: <https://pubmed.ncbi.nlm.nih.gov/27720640/>
88. Milosevic I, Giovedi S, Lou X, et al. Recruitment of endophilin to clathrin-coated pit necks is required for efficient vesicle uncoating after fission. [Internet]. *Neuron* 2011;72(4):587–601.[cited 2020 Apr 10] Available from: <http://www.ncbi.nlm.nih.gov/pubmed/22099461>
89. Arranz AM, Delbroek L, van Kolen K, et al. LRRK2 functions in synaptic vesicle endocytosis through a kinasedependent mechanism. *J. Cell Sci.* 2015;128(3):541–552.
90. Nguyen M, Krainc D. LRRK2 phosphorylation of auxilin mediates synaptic defects in dopaminergic neurons from patients with Parkinson's disease [Internet]. *Proc. Natl.*

- Acad. Sci. 2018;115(21):5576–5581.[cited 2018 Jun 27] Available from:
<http://www.pnas.org/lookup/doi/10.1073/pnas.1717590115>
91. Xiong Y, Neifert S, Karuppagounder SS, et al. Robust kinase- and age-dependent dopaminergic and norepinephrine neurodegeneration in LRRK2 G2019S transgenic mice [Internet]. *Proc. Natl. Acad. Sci. U. S. A.* 2018;115(7):1635–1640.[cited 2020 Apr 22] Available from: <https://pubmed.ncbi.nlm.nih.gov/29386392/>
 92. Ng J, Papandreou A, Heales SJ, Kurian MA. Monoamine neurotransmitter disorders—clinical advances and future perspectives [Internet]. *Nat. Rev. Neurol.* 2015;11(10):567–584.Available from:
<http://www.nature.com/nrneurol/journal/v11/n10/full/nrneurol.2015.172.html%5Cnhttp://www.nature.com/nrneurol/journal/v11/n10/pdf/nrneurol.2015.172.pdf>
 93. Mencacci NE, Isaias IU, Reich MM, et al. Parkinson’s disease in GTP cyclohydrolase 1 mutation carriers [Internet]. *Brain* 2014;137(Pt 9):2480–2492.[cited 2023 Jun 15] Available from: <https://pubmed.ncbi.nlm.nih.gov/24993959/>
 94. Ng J, Barral S, de la Fuente Barrigon C, et al. Gene therapy restores dopamine transporter expression and ameliorates pathology in iPSC and mouse models of infantile parkinsonism [Internet]. *Sci. Transl. Med.* 2021;13(594)[cited 2021 Sep 26] Available from: <https://pubmed.ncbi.nlm.nih.gov/34011628/>
 95. Masato A, Plotegher N, Boassa D, Bubacco L. Impaired dopamine metabolism in Parkinson’s disease pathogenesis [Internet]. *Mol. Neurodegener.* 2019;14(1)[cited 2023 Jun 14] Available from: <https://pubmed.ncbi.nlm.nih.gov/31488222/>
 96. Wise RM, Wagener A, Fietzek UM, et al. Interactions of dopamine, iron, and alpha-synuclein linked to dopaminergic neuron vulnerability in Parkinson’s disease and Neurodegeneration with Brain Iron Accumulation disorders [Internet]. *Neurobiol. Dis.* 2022;175[cited 2023 Jun 14] Available from:
<https://pubmed.ncbi.nlm.nih.gov/36351559/>
 97. Chakrabarti S, Bisaglia M. Oxidative Stress and Neuroinflammation in Parkinson’s Disease: The Role of Dopamine Oxidation Products [Internet]. *Antioxidants (Basel, Switzerland)* 2023;12(4)[cited 2023 Jun 14] Available from:
<https://pubmed.ncbi.nlm.nih.gov/37107329/>
 98. Bolam JP, Pissadaki EK. Living on the edge with too many mouths to feed: why dopamine neurons die [Internet]. *Mov. Disord.* 2012;27(12):1478–1483.[cited 2022 Nov 19] Available from: <https://pubmed.ncbi.nlm.nih.gov/23008164/>
 99. Guzman JN, Sanchez-Padilla J, Chan CS, Surmeier DJ. Robust Pacemaking in Substantia Nigra Dopaminergic Neurons [Internet]. *J. Neurosci.* 2009;29(35):11011–11019.[cited 2020 Apr 10] Available from:
<http://www.jneurosci.org/cgi/doi/10.1523/JNEUROSCI.2519-09.2009>
 100. Sulzer D, Zecca L. Intraneuronal dopamine-quinone synthesis: a review [Internet]. *Neurotox. Res.* 2000;1(3):181–195.[cited 2022 Nov 19] Available from:
<https://pubmed.ncbi.nlm.nih.gov/12835101/>
 101. Pacelli C, Giguère N, Bourque MJ, et al. Elevated Mitochondrial Bioenergetics and Axonal Arborization Size Are Key Contributors to the Vulnerability of Dopamine Neurons. *Curr. Biol.* 2015;25(18):2349–2360.
 102. Surmeier DJ, Schumacker PT. Calcium, bioenergetics, and neuronal vulnerability in Parkinson’s disease [Internet]. *J. Biol. Chem.* 2013;288(15):10736–10741.[cited 2022 Dec 2] Available from: <https://pubmed.ncbi.nlm.nih.gov/23086948/>
 103. Guzman JN, Sanchez-Padilla J, Wokosin D, et al. Oxidant stress evoked by pacemaking in dopaminergic neurons is attenuated by DJ-1 [Internet]. *Nature* 2010;468(7324):696–700.[cited 2022 Dec 4] Available from:
<https://pubmed.ncbi.nlm.nih.gov/21068725/>
 104. Goodwin J, Nath S, Engelborghs Y, Pountney DL. Raised calcium and oxidative stress

- cooperatively promote alpha-synuclein aggregate formation [Internet]. *Neurochem. Int.* 2013;62(5):703–711.[cited 2022 Nov 25] Available from: <https://pubmed.ncbi.nlm.nih.gov/23159813/>
105. Minakaki G, Krainc D, Burbulla LF. The Convergence of Alpha-Synuclein, Mitochondrial, and Lysosomal Pathways in Vulnerability of Midbrain Dopaminergic Neurons in Parkinson's Disease [Internet]. *Front. cell Dev. Biol.* 2020;8[cited 2022 Nov 19] Available from: <https://pubmed.ncbi.nlm.nih.gov/33381501/>
 106. Gwensa NZ, Russell DL, Cowell RM, Volpicelli-Daley LA. Molecular Mechanisms Underlying Synaptic and Axon Degeneration in Parkinson's Disease [Internet]. *Front. Cell. Neurosci.* 2021;15[cited 2022 Nov 19] Available from: <https://pubmed.ncbi.nlm.nih.gov/33737866/>
 107. Schirinzi T, Madeo G, Martella G, et al. Early synaptic dysfunction in Parkinson's disease: Insights from animal models [Internet]. *Mov. Disord.* 2016;31(6):802–813.[cited 2017 Aug 21] Available from: <http://www.ncbi.nlm.nih.gov/pubmed/27193205>
 108. Jennings D, Siderowf A, Stern M, et al. Conversion to Parkinson Disease in the PARS Hypothesis and Dopamine Transporter-Deficit Prodromal Cohort [Internet]. *JAMA Neurol.* 2017;74(8):933–940.[cited 2022 Nov 25] Available from: <https://pubmed.ncbi.nlm.nih.gov/28595287/>
 109. Delva A, Van Weehaeghe D, Koole M, et al. Loss of Presynaptic Terminal Integrity in the Substantia Nigra in Early Parkinson's Disease [Internet]. *Mov. Disord.* 2020;35(11):1977–1986.[cited 2022 Nov 25] Available from: <https://pubmed.ncbi.nlm.nih.gov/32767618/>
 110. Chu Y, Morfini GA, Langhamer LB, et al. Alterations in axonal transport motor proteins in sporadic and experimental Parkinson's disease [Internet]. *Brain* 2012;135(Pt 7):2058–2073.[cited 2022 Nov 25] Available from: <https://pubmed.ncbi.nlm.nih.gov/22719003/>
 111. Oliveira LMA, Falomir-Lockhart LJ, Botelho MG, et al. Elevated α -synuclein caused by SNCA gene triplication impairs neuronal differentiation and maturation in Parkinson's patient-derived induced pluripotent stem cells [Internet]. *Cell Death Dis.* 2015;6(11)[cited 2022 Nov 28] Available from: <https://pubmed.ncbi.nlm.nih.gov/26610207/>
 112. Lin L, Göke J, Cukuroglu E, et al. Molecular Features Underlying Neurodegeneration Identified through In Vitro Modeling of Genetically Diverse Parkinson's Disease Patients [Internet]. *Cell Rep.* 2016;15(11):2411–2426.[cited 2022 Nov 28] Available from: <https://pubmed.ncbi.nlm.nih.gov/27264186/>
 113. Garcia-Reitböck P, Anichtchik O, Bellucci A, et al. SNARE protein redistribution and synaptic failure in a transgenic mouse model of Parkinson's disease [Internet]. *Brain* 2010;133(Pt 7):2032–2044.[cited 2022 Nov 28] Available from: <https://pubmed.ncbi.nlm.nih.gov/20534649/>
 114. Soukup S, Vanhauwaert R, Verstreken P. Parkinson's disease: convergence on synaptic homeostasis [Internet]. *EMBO J.* 2018;37(18)[cited 2023 Mar 25] Available from: <https://pubmed.ncbi.nlm.nih.gov/30065071/>
 115. Villalba RM, Smith Y. Loss and remodeling of striatal dendritic spines in Parkinson's disease: from homeostasis to maladaptive plasticity? [Internet]. *J. Neural Transm.* 2018;125(3):431–447.[cited 2022 Nov 25] Available from: <https://pubmed.ncbi.nlm.nih.gov/28540422/>
 116. Nyholm D. Enteral levodopa/carbidopa gel infusion for the treatment of motor fluctuations and dyskinesias in advanced Parkinson's disease [Internet]. *Expert Rev. Neurother.* 2006;6(10):1403–1411.[cited 2023 Aug 28] Available from: <https://pubmed.ncbi.nlm.nih.gov/17078781/>

117. Straccia G, Colucci F, Eleopra R, Cilia R. Precision Medicine in Parkinson's Disease: From Genetic Risk Signals to Personalized Therapy [Internet]. *Brain Sci.* 2022;12(10)[cited 2022 Dec 2] Available from: <https://pubmed.ncbi.nlm.nih.gov/36291241/>
118. Fox SH, Katzenschlager R, Lim SY, et al. International Parkinson and movement disorder society evidence-based medicine review: Update on treatments for the motor symptoms of Parkinson's disease [Internet]. *Mov. Disord.* 2018;33(8):1248–1266.[cited 2023 Mar 25] Available from: <https://pubmed.ncbi.nlm.nih.gov/29570866/>
119. Axelsen TM, Woldbye DPD. Gene Therapy for Parkinson's Disease, An Update [Internet]. *J. Parkinsons. Dis.* 2018;8(2):195–215.[cited 2022 Nov 28] Available from: <https://pubmed.ncbi.nlm.nih.gov/29710735/>
120. Elkouzi A, Vedam-Mai V, Eisinger RS, Okun MS. Emerging therapies in Parkinson disease - repurposed drugs and new approaches [Internet]. *Nat. Rev. Neurol.* 2019;15(4):204–223.[cited 2022 Nov 28] Available from: <https://pubmed.ncbi.nlm.nih.gov/30867588/>
121. Hitti FL, Yang AI, Gonzalez-Alegre P, Baltuch GH. Human gene therapy approaches for the treatment of Parkinson's disease: An overview of current and completed clinical trials [Internet]. *Parkinsonism Relat. Disord.* 2019;66:16–24.[cited 2022 Dec 2] Available from: <https://pubmed.ncbi.nlm.nih.gov/31324556/>
122. Muramatsu SI, Fujimoto KI, Kato S, et al. A phase I study of aromatic L-amino acid decarboxylase gene therapy for Parkinson's disease [Internet]. *Mol. Ther.* 2010;18(9):1731–1735.[cited 2022 Dec 4] Available from: <https://pubmed.ncbi.nlm.nih.gov/20606642/>
123. Christine CW, Starr PA, Larson PS, et al. Safety and tolerability of putaminal AADC gene therapy for Parkinson disease [Internet]. *Neurology* 2009;73(20):1662–1669.[cited 2022 Dec 4] Available from: <https://pubmed.ncbi.nlm.nih.gov/19828868/>
124. Palfi S, Gurruchaga JM, Scott Ralph G, et al. Long-term safety and tolerability of ProSavin, a lentiviral vector-based gene therapy for Parkinson's disease: a dose escalation, open-label, phase 1/2 trial [Internet]. *Lancet (London, England)* 2014;383(9923):1138–1146.[cited 2023 Mar 26] Available from: <https://pubmed.ncbi.nlm.nih.gov/24412048/>
125. Serva SN, Bernstein J, Thompson JA, et al. An update on advanced therapies for Parkinson's disease: From gene therapy to neuromodulation [Internet]. *Front. Surg.* 2022;9[cited 2023 Mar 26] Available from: <https://pubmed.ncbi.nlm.nih.gov/36211256/>
126. Jankovic J, Chen S, Le WD. The role of Nurr1 in the development of dopaminergic neurons and Parkinson's disease [Internet]. *Prog. Neurobiol.* 2005;77(1–2):128–138.[cited 2023 Jan 4] Available from: <https://pubmed.ncbi.nlm.nih.gov/16243425/>
127. Warren Olanow C, Bartus RT, Baumann TL, et al. Gene delivery of neurturin to putamen and substantia nigra in Parkinson disease: A double-blind, randomized, controlled trial [Internet]. *Ann. Neurol.* 2015;78(2):248–257.[cited 2022 Dec 4] Available from: <https://pubmed.ncbi.nlm.nih.gov/26061140/>
128. Bartus RT, Baumann TL, Siffert J, et al. Safety/feasibility of targeting the substantia nigra with AAV2-neurturin in Parkinson patients [Internet]. *Neurology* 2013;80(18):1698–1701.[cited 2022 Dec 4] Available from: <https://pubmed.ncbi.nlm.nih.gov/23576625/>
129. Erlander MG, Tillakaratne NJK, Feldblum S, et al. Two genes encode distinct glutamate decarboxylases [Internet]. *Neuron* 1991;7(1):91–100.[cited 2022 Dec 4] Available from: <https://pubmed.ncbi.nlm.nih.gov/2069816/>
130. Kaplitt MG, Feigin A, Tang C, et al. Safety and tolerability of gene therapy with an adeno-associated virus (AAV) borne GAD gene for Parkinson's disease: an open label,

- phase I trial [Internet]. *Lancet* (London, England) 2007;369(9579):2097–2105.[cited 2022 Dec 4] Available from: <https://pubmed.ncbi.nlm.nih.gov/17586305/>
131. Niethammer M, Tang CC, LeWitt PA, et al. Long-term follow-up of a randomized AAV2- GAD gene therapy trial for Parkinson’s disease [Internet]. *JCI insight* 2017;2(7)[cited 2022 Dec 4] Available from: <https://pubmed.ncbi.nlm.nih.gov/28405611/>
 132. Pearson TS, Gupta N, San Sebastian W, et al. Gene therapy for aromatic L-amino acid decarboxylase deficiency by MR-guided direct delivery of AAV2-AADC to midbrain dopaminergic neurons [Internet]. *Nat. Commun.* 2021;12(1)[cited 2022 Sep 25] Available from: <https://pubmed.ncbi.nlm.nih.gov/34253733/>
 133. Kojima K, Nakajima T, Taga N, et al. Gene therapy improves motor and mental function of aromatic l-amino acid decarboxylase deficiency [Internet]. *Brain* 2019;142(2):322–333.[cited 2022 Dec 16] Available from: <https://pubmed.ncbi.nlm.nih.gov/30689738/>
 134. Li CY, Ou RW, Chen YP, et al. Mutation Analysis of DNAJC Family for Early-Onset Parkinson’s Disease in a Chinese Cohort [Internet]. *Mov. Disord.* 2020;35(11):2068–2076.[cited 2023 Jun 19] Available from: <https://pubmed.ncbi.nlm.nih.gov/32662538/>
 135. Mittal SO. Levodopa responsive-generalized dystonic spells and moaning in DNAJC6 related Juvenile Parkinson’s disease [Internet]. *Parkinsonism Relat. Disord.* 2020;81:188–189.[cited 2023 Jun 23] Available from: <https://pubmed.ncbi.nlm.nih.gov/33181391/>
 136. Ray S, Padmanabha H, Mahale R, et al. DNAJC6 mutation causing cranial-onset dystonia with tremor dominant levodopa non-responsive parkinsonism: A novel phenotype [Internet]. *Parkinsonism Relat. Disord.* 2021;89:1–3.[cited 2023 Jun 16] Available from: <https://pubmed.ncbi.nlm.nih.gov/34175496/>
 137. Garza-Brambila D, Esparza-Hernández CN, Ramirez-Zenteno J, Martinez-Ramirez D. Juvenile Dystonia-Parkinsonism Due to DNAJC6 Mutation [Internet]. *Mov. Disord. Clin. Pract.* 2021;8(Suppl 1):S26–S28.[cited 2023 Jun 19] Available from: <https://pubmed.ncbi.nlm.nih.gov/34514042/>
 138. Eisenberg E, Greene LE. Multiple Roles of Auxilin and Hsc70 in Clathrin-Mediated Endocytosis [Internet]. *Traffic* 2007;8(6):640–646.[cited 2018 Jul 12] Available from: <http://www.ncbi.nlm.nih.gov/pubmed/17488288>
 139. Guan R, Dai H, Han D, et al. Structure of the PTEN-like region of auxilin, a detector of clathrin-coated vesicle budding. [Internet]. *Structure* 2010;18(9):1191–8.[cited 2020 Apr 11] Available from: <http://www.ncbi.nlm.nih.gov/pubmed/20826345>
 140. He K, Song E, Upadhyayula S, et al. Dynamics of Auxilin 1 and GAK in clathrin-mediated traffic [Internet]. *J. Cell Biol.* 2020;219(3)[cited 2020 Mar 12] Available from: <http://www.ncbi.nlm.nih.gov/pubmed/31962345>
 141. Yim Y-IY-I, Sun T, Wu L-GL-GL-G, et al. Endocytosis and clathrin-uncoating defects at synapses of auxilin knockout mice [Internet]. *Proc. Natl. Acad. Sci. U. S. A.* 2010;107(9):4412–4417.[cited 2018 Apr 2] Available from: <http://www.ncbi.nlm.nih.gov/pubmed/20160091>
 142. Ungewickell E, Ungewickell H, Holstein SE, et al. Role of auxilin in uncoating clathrin-coated vesicles. [Internet]. *Nature* 1995;378(6557):632–5.Available from: <http://www.nature.com/nature/journal/v378/n6557/pdf/378632a0.pdf%5Cnhttp://www.nature.com/nature/journal/v378/n6557/abs/378632a0.html%5Cnhttp://www.ncbi.nlm.nih.gov/pubmed/8524399>
 143. Traub LM. Regarding the amazing choreography of clathrin coats. [Internet]. *PLoS Biol.* 2011;9(3):e1001037.[cited 2020 Mar 12] Available from: <http://www.ncbi.nlm.nih.gov/pubmed/21445329>
 144. McMahon HT, Boucrot E. Molecular mechanism and physiological functions of

- clathrin-mediated endocytosis [Internet]. *Nat. Rev. Mol. Cell Biol.* 2011;12(8):517–533.[cited 2020 Apr 13] Available from: <http://www.nature.com/articles/nrm3151>
145. Prichard KL, O'Brien NS, Murcia SR, et al. Role of Clathrin and Dynamin in Clathrin Mediated Endocytosis/Synaptic Vesicle Recycling and Implications in Neurological Diseases [Internet]. *Front. Cell. Neurosci.* 2021;15[cited 2022 Mar 3] Available from: [/pmc/articles/PMC8805674/](https://pubmed.ncbi.nlm.nih.gov/38805674/)
 146. Massol RH, Boll W, Griffin AM, Kirchhausen T. A burst of auxilin recruitment determines the onset of clathrin-coated vesicle uncoating [Internet]. *Proc. Natl. Acad. Sci. U. S. A.* 2006;103(27):10265–10270.[cited 2023 Feb 14] Available from: <https://pubmed.ncbi.nlm.nih.gov/16798879/>
 147. Xing Y, Böcking T, Wolf M, et al. Structure of clathrin coat with bound Hsc70 and auxilin: mechanism of Hsc70-facilitated disassembly [Internet]. *EMBO J.* 2010;29(3):655–665.[cited 2023 Feb 14] Available from: <https://pubmed.ncbi.nlm.nih.gov/20033059/>
 148. Sousa R, Lafer EM. The role of molecular chaperones in clathrin mediated vesicular trafficking [Internet]. *Front. Mol. Biosci.* 2015;2(MAY)[cited 2023 Feb 14] Available from: <https://pubmed.ncbi.nlm.nih.gov/26042225/>
 149. De Los Rios P, Ben-Zvi A, Slutsky O, et al. Hsp70 chaperones accelerate protein translocation and the unfolding of stable protein aggregates by entropic pulling [Internet]. *Proc. Natl. Acad. Sci. U. S. A.* 2006;103(16):6166–6171.[cited 2023 Feb 14] Available from: <https://pubmed.ncbi.nlm.nih.gov/16606842/>
 150. Gorenberg EL, Chandra SS. The Role of Co-chaperones in Synaptic Proteostasis and Neurodegenerative Disease [Internet]. *Front. Neurosci.* 2017;11(MAY)[cited 2023 Mar 27] Available from: <https://pubmed.ncbi.nlm.nih.gov/28579939/>
 151. Roosen DA, Blauwendraat C, Cookson MR, Lewis PA. DNAJC proteins and pathways to parkinsonism [Internet]. *FEBS J.* 2019;286(16):3080–3094.[cited 2023 Mar 27] Available from: <https://pubmed.ncbi.nlm.nih.gov/31120186/>
 152. Nosková L, Stránecký V, Hartmannová H, et al. Mutations in DNAJC5, encoding cysteine-string protein alpha, cause autosomal-dominant adult-onset neuronal ceroid lipofuscinosis [Internet]. *Am. J. Hum. Genet.* 2011;89(2):241–252.[cited 2023 Mar 27] Available from: <https://pubmed.ncbi.nlm.nih.gov/21820099/>
 153. Benitez BA, Alvarado D, Cai Y, et al. Exome-sequencing confirms DNAJC5 mutations as cause of adult neuronal ceroid-lipofuscinosis [Internet]. *PLoS One* 2011;6(11)[cited 2023 Mar 27] Available from: <https://pubmed.ncbi.nlm.nih.gov/22073189/>
 154. Cadieux-Dion M, Andermann E, Lachance-Touchette P, et al. Recurrent mutations in DNAJC5 cause autosomal dominant Kufs disease [Internet]. *Clin. Genet.* 2013;83(6):571–575.[cited 2023 Mar 27] Available from: <https://pubmed.ncbi.nlm.nih.gov/22978711/>
 155. Lorenzo-Betancor O, Ogaki K, Soto-Ortolaza AI, et al. DNAJC13 p.Asn855Ser mutation screening in Parkinson's disease and pathologically confirmed Lewy body disease patients [Internet]. *Eur. J. Neurol.* 2015;22(9):1323–1325.[cited 2023 Mar 27] Available from: <https://pubmed.ncbi.nlm.nih.gov/26278106/>
 156. Yuan L, Song Z, Deng X, et al. Systematic analysis of genetic variants in Han Chinese patients with sporadic Parkinson's disease [Internet]. *Sci. Rep.* 2016;6[cited 2023 Mar 27] Available from: <https://pubmed.ncbi.nlm.nih.gov/27653456/>
 157. Anikster Y, Haack TB, Vilboux T, et al. Biallelic Mutations in DNAJC12 Cause Hyperphenylalaninemia, Dystonia, and Intellectual Disability [Internet]. *Am. J. Hum. Genet.* 2017;100(2):257–266.[cited 2018 Jul 13] Available from: <https://pubmed.ncbi.nlm.nih.gov/28132689/>
 158. Straniero L, Guella I, Cilia R, et al. DNAJC12 and dopa-responsive nonprogressive parkinsonism [Internet]. *Ann. Neurol.* 2017;82(4):640–646.[cited 2023 Mar 27]

- Available from: <https://pubmed.ncbi.nlm.nih.gov/28892570/>
159. Ding J, Segarra VA, Chen S, et al. Auxilin facilitates membrane traffic in the early secretory pathway [Internet]. *Mol. Biol. Cell* 2016;27(1):127–136.[cited 2020 Mar 26] Available from: <http://www.ncbi.nlm.nih.gov/pubmed/26538028>
 160. Beck R, Ravet M, Wieland FT, Cassel D. The COPI system: molecular mechanisms and function [Internet]. *FEBS Lett.* 2009;583(17):2701–2709.[cited 2023 Feb 15] Available from: <https://pubmed.ncbi.nlm.nih.gov/19631211/>
 161. Jensen D, Schekman R. COPII-mediated vesicle formation at a glance [Internet]. *J. Cell Sci.* 2011;124(Pt 1):1–4.[cited 2023 Feb 15] Available from: <https://pubmed.ncbi.nlm.nih.gov/21172817/>
 162. Roosen DA, Landeck N, Bonet LP, et al. Mutations in Auxilin cause parkinsonism via impaired clathrin-mediated trafficking at the Golgi apparatus and synapse [Internet]. *bioRxiv* 2019;830802.[cited 2022 Feb 13] Available from: <https://www.biorxiv.org/content/10.1101/830802v3>
 163. Eun SH, Banks SML, Fischer JA. Auxilin is essential for Delta signaling. *Development* 2008;
 164. Lathia JD, Mattson MP, Cheng A. Notch: From neural development to neurological disorders [Internet]. *J Neurochem*; 2008.[cited 2024 Jan 25] Available from: <https://pubmed.ncbi.nlm.nih.gov/19094054/>
 165. Tio M, Toh J, Fang W, et al. Asymmetric cell division and notch signaling specify dopaminergic neurons in *Drosophila*. *PLoS One* 2011;
 166. Sorkin A, Von Zastrow M. Endocytosis and signalling: intertwining molecular networks [Internet]. *Nat. Rev. Mol. Cell Biol.* 2009;10(9):609–622.[cited 2023 Feb 15] Available from: <https://pubmed.ncbi.nlm.nih.gov/19696798/>
 167. Farsi Z, Gowrisankaran S, Krunic M, et al. Clathrin coat controls synaptic vesicle acidification by blocking vacuolar ATPase activity [Internet]. *Elife* 2018;7[cited 2022 Feb 24] Available from: <https://pubmed.ncbi.nlm.nih.gov/29652249/>
 168. Mitsunari T, Nakatsu F, Shioda N, et al. Clathrin adaptor AP-2 is essential for early embryonal development [Internet]. *Mol. Cell. Biol.* 2005;25(21):9318–9323.[cited 2023 Feb 15] Available from: <https://pubmed.ncbi.nlm.nih.gov/16227583/>
 169. Chen H, Ko G, Zatti A, et al. Embryonic arrest at midgestation and disruption of Notch signaling produced by the absence of both epsin 1 and epsin 2 in mice [Internet]. *Proc. Natl. Acad. Sci. U. S. A.* 2009;106(33):13838–13843.[cited 2023 Feb 15] Available from: <https://pubmed.ncbi.nlm.nih.gov/19666558/>
 170. Seto ES, Bellen HJ, Lloyd TE. When cell biology meets development: endocytic regulation of signaling pathways [Internet]. *Genes Dev.* 2002;16(11):1314–1336.[cited 2022 Mar 12] Available from: <https://pubmed.ncbi.nlm.nih.gov/12050111/>
 171. Camblor-Perujo S, Kononenko NL. Brain-specific functions of the endocytic machinery [Internet]. *FEBS J.* 2022;289(8):2219–2246.[cited 2022 Jun 26] Available from: <https://onlinelibrary.wiley.com/doi/full/10.1111/febs.15897>
 172. Baker K, Gordon SL, Grozeva D, et al. Identification of a human synaptotagmin-1 mutation that perturbs synaptic vesicle cycling [Internet]. *J. Clin. Invest.* 2015;125(4):1670–1678.[cited 2023 Mar 27] Available from: <https://pubmed.ncbi.nlm.nih.gov/25705886/>
 173. Melland H, Bumbak F, Kolesnik-Taylor A, et al. Expanding the genotype and phenotype spectrum of SYT1-associated neurodevelopmental disorder. *Genet. Med.* 2022;24(4):880–893.
 174. Appenzeller S, Balling R, Barisic N, et al. De novo mutations in synaptic transmission genes including *DNM1* cause epileptic encephalopathies [Internet]. *Am. J. Hum. Genet.* 2014;95(4):360–370.[cited 2017 Jul 31] Available from: <http://www.ncbi.nlm.nih.gov/pubmed/25262651>

175. Von Spiczak S, Helbig KL, Shinde DN, et al. DNMT1 encephalopathy. *Neurology* 2017;89(4):385–394.
176. Fasano D, Parisi S, Pierantoni GM, et al. DNMT1 Mutation in a child associated with progressive bilateral mesial temporal sclerosis. *Clin. Case Reports* 2015;125(2):1200–1207.
177. Yigit G, Sheffer R, Daana M, et al. Loss-of-function variants in DNMT1 cause a specific form of developmental and epileptic encephalopathy only in biallelic state [Internet]. *J. Med. Genet.* 2022;59(6):549–553.[cited 2022 Jun 10] Available from: <https://pubmed.ncbi.nlm.nih.gov/34172529/>
178. Durieux AC, Prudhon B, Guicheney P, Bitoun M. Dynamin 2 and human diseases [Internet]. *J. Mol. Med. (Berl)*. 2010;88(4):339–350.[cited 2023 Feb 15] Available from: <https://pubmed.ncbi.nlm.nih.gov/20127478/>
179. Herrmann DN, Horvath R, Sowden JE, et al. Synaptotagmin 2 mutations cause an autosomal-dominant form of lambert-eaton myasthenic syndrome and nonprogressive motor neuropathy [Internet]. *Am. J. Hum. Genet.* 2014;95(3):332–339.[cited 2023 Mar 27] Available from: <https://pubmed.ncbi.nlm.nih.gov/25192047/>
180. Sahly AN, Krochmalnek E, St-Onge J, et al. Severe DNMT1 encephalopathy with dysmyelination due to recurrent splice site pathogenic variant [Internet]. *Hum. Genet.* 2020;139(12):1575–1578.[cited 2023 Jun 26] Available from: <https://pubmed.ncbi.nlm.nih.gov/32909139/>
181. Kolnikova M, Skopkova M, Ilencikova D, et al. DNMT1 encephalopathy - atypical phenotype with hypomyelination due to a novel de novo variant in the DNMT1 gene [Internet]. *Seizure* 2018;56:31–33.[cited 2023 Jun 26] Available from: <https://pubmed.ncbi.nlm.nih.gov/29427836/>
182. Mei D, Parrini E, Bianchini C, et al. Autism and mild epilepsy associated with a de novo missense pathogenic variant in the GTPase effector domain of DNMT1 [Internet]. *Am. J. Med. Genet. C. Semin. Med. Genet.* 2023;[cited 2023 Jun 26] Available from: <https://pubmed.ncbi.nlm.nih.gov/37132416/>
183. Yu A, Shibata Y, Shah B, et al. Protein aggregation can inhibit clathrin-mediated endocytosis by chaperone competition [Internet]. *Proc. Natl. Acad. Sci. U. S. A.* 2014;111(15)[cited 2023 Feb 15] Available from: <https://pubmed.ncbi.nlm.nih.gov/24706768/>
184. Kumaran R, Cookson MR. Pathways to Parkinsonism Redux: convergent pathobiological mechanisms in genetics of Parkinson’s disease [Internet]. *Hum. Mol. Genet.* 2015;24(R1):R32–R44.[cited 2023 Jun 22] Available from: <https://pubmed.ncbi.nlm.nih.gov/26101198/>
185. Jacquemyn J, Kuenen S, Swerts J, et al. Parkinsonism mutations in DNAJC6 cause lipid defects and neurodegeneration that are rescued by Synj1 [Internet]. *NPJ Park. Dis.* 2023;9(1)[cited 2023 Jun 22] Available from: <https://pubmed.ncbi.nlm.nih.gov/36739293/>
186. Ng XY, Wu Y, Lin Y, et al. Mutations in Parkinsonism-linked endocytic proteins synaptotagmin1 and auxilin have synergistic effects on dopaminergic axonal pathology [Internet]. *NPJ Park. Dis.* 2023;9(1)[cited 2023 Jun 14] Available from: <https://pubmed.ncbi.nlm.nih.gov/36792618/>
187. Cao M, Wu Y, Ashrafi G, et al. Parkinson Sac Domain Mutation in Synaptotagmin 1 Impairs Clathrin Uncoating at Synapses and Triggers Dystrophic Changes in Dopaminergic Axons [Internet]. *Neuron* 2017;93(4):882–896.e5.[cited 2018 Jun 27] Available from: <https://pubmed.ncbi.nlm.nih.gov/28231468/>
188. Vidyadhara DJ, Somayaji M, Wade N, et al. Dopamine transporter and synaptic vesicle sorting defects underlie auxilin-associated Parkinson’s disease [Internet]. *Cell Rep.* 2023;42(3):112231.[cited 2023 Jun 20] Available from:

- <https://pubmed.ncbi.nlm.nih.gov/36920906/>
189. Song L, He Y, Ou J, et al. Auxilin Underlies Progressive Locomotor Deficits and Dopaminergic Neuron Loss in a Drosophila Model of Parkinson's Disease [Internet]. *Cell Rep.* 2017;18(5):1132–1143.[cited 2018 Apr 2] Available from: <http://linkinghub.elsevier.com/retrieve/pii/S2211124717300232>
 190. Wulansari N, Darsono WHW, Woo HJ, et al. Neurodevelopmental defects and neurodegenerative phenotypes in human brain organoids carrying Parkinson's disease-linked DNAJC6 mutations [Internet]. *Sci. Adv.* 2021;7(8)[cited 2022 Feb 10] Available from: <https://pubmed.ncbi.nlm.nih.gov/33597231/>
 191. Till JE, McCulloch EA. A direct measurement of the radiation sensitivity of normal mouse bone marrow cells. 1961 [Internet]. *Radiat. Res.* 2012;178(2)[cited 2022 Dec 20] Available from: <https://pubmed.ncbi.nlm.nih.gov/22870977/>
 192. JA T, J I-E, SS S, et al. Embryonic stem cell lines derived from human blastocysts [Internet]. *Science* 1998;282(5391):1145–1147.[cited 2022 Dec 20] Available from: <https://pubmed.ncbi.nlm.nih.gov/9804556/>
 193. Takahashi K, Yamanaka S. Induction of Pluripotent Stem Cells from Mouse Embryonic and Adult Fibroblast Cultures by Defined Factors. *Cell* 2006;126(4):663–676.
 194. Doss MX, Sachinidis A. Current Challenges of iPSC-Based Disease Modeling and Therapeutic Implications. [Internet]. *Cells* 2019;8(5):403.[cited 2020 Mar 31] Available from: <http://www.ncbi.nlm.nih.gov/pubmed/31052294>
 195. Chang CY, Ting HC, Su HL, Jeng JR. Combining Induced Pluripotent Stem Cells and Genome Editing Technologies for Clinical Applications [Internet]. *Cell Transplant.* 2018;27(3):379–392.[cited 2023 Jan 2] Available from: <https://pubmed.ncbi.nlm.nih.gov/29806481/>
 196. Nidhi S, Anand U, Oleksak P, et al. Novel CRISPR–Cas Systems: An Updated Review of the Current Achievements, Applications, and Future Research Perspectives [Internet]. *Int. J. Mol. Sci.* 2021;22(7)[cited 2023 Mar 11] Available from: </pmc/articles/PMC8036902/>
 197. Li L, Chao J, Shi Y. Modeling neurological diseases using iPSC-derived neural cells : iPSC modeling of neurological diseases [Internet]. *Cell Tissue Res.* 2018;371(1):143–151.[cited 2021 Sep 29] Available from: <https://pubmed.ncbi.nlm.nih.gov/29079884/>
 198. Kilpinen H, Goncalves A, Leha A, et al. Common genetic variation drives molecular heterogeneity in human iPSCs [Internet]. *Nature* 2017;546(7658):370–375.[cited 2023 Mar 5] Available from: <https://pubmed.ncbi.nlm.nih.gov/28489815/>
 199. Okita K, Ichisaka T, Yamanaka S. Generation of germline-competent induced pluripotent stem cells [Internet]. *Nature* 2007;448(7151):313–317.[cited 2022 Dec 23] Available from: <https://pubmed.ncbi.nlm.nih.gov/17554338/>
 200. Liu G, David BT, Trawczynski M, Fessler RG. Advances in Pluripotent Stem Cells: History, Mechanisms, Technologies, and Applications [Internet]. *Stem cell Rev. reports* 2020;16(1):3–32.[cited 2022 Dec 23] Available from: <https://pubmed.ncbi.nlm.nih.gov/31760627/>
 201. Ghimire S, Mantziou V, Moris N, Martinez Arias A. Human gastrulation: The embryo and its models [Internet]. *Dev. Biol.* 2021;474:100–108.[cited 2023 Jan 3] Available from: <https://pubmed.ncbi.nlm.nih.gov/33484705/>
 202. Tao Y, Zhang SC. Neural Subtype Specification from Human Pluripotent Stem Cells [Internet]. *Cell Stem Cell* 2016;19(5):573–586.[cited 2021 Sep 30] Available from: <https://pubmed.ncbi.nlm.nih.gov/27814479/>
 203. Arenas E, Denham M, Villaescusa JC. How to make a midbrain dopaminergic neuron. *Dev.* 2015;142(11):1918–1936.
 204. Pakkenberg B, Moller A, Gundersen HJG, et al. The absolute number of nerve cells in

- substantia nigra in normal subjects and in patients with Parkinson's disease estimated with an unbiased stereological method. *J. Neurol. Neurosurg. Psychiatry* 1991;54(1):30–33.
205. Studer L. Derivation of dopaminergic neurons from pluripotent stem cells [Internet]. *Prog. Brain Res.* 2012;200:243–263.[cited 2023 Mar 29] Available from: <https://pubmed.ncbi.nlm.nih.gov/23195422/>
 206. Broccoli V, Boncinelli E, Wurst W. The caudal limit of Otx2 expression positions the isthmus organizer [Internet]. *Nature* 1999;401(6749):164–168.[cited 2020 Jun 11] Available from: <https://pubmed.ncbi.nlm.nih.gov/10490025/>
 207. Millet S, Campbell K, Epstein DJ, et al. A role for Gbx2 in repression of Otx2 and positioning the mid/hindbrain organizer [Internet]. *Nature* 1999;401(6749):161–164.[cited 2020 Jun 11] Available from: <https://pubmed.ncbi.nlm.nih.gov/10490024/>
 208. Wassarman KM, Lewandoski M, Campbell K, et al. Specification of the anterior hindbrain and establishment of a normal mid/hindbrain organizer is dependent on Gbx2 gene function [Internet]. *Development* 1997;124(15):2923–2934.[cited 2023 Jan 3] Available from: <https://pubmed.ncbi.nlm.nih.gov/9247335/>
 209. Metzakopian E, Lin W, Salmon-Divon M, et al. Genome-wide characterization of Foxa2 targets reveals upregulation of floor plate genes and repression of ventrolateral genes in midbrain dopaminergic progenitors [Internet]. *Dev.* 2012;139(14):2625–2634.[cited 2023 Jan 6] Available from: <https://pubmed.ncbi.nlm.nih.gov/22696295/>
 210. Chung S, Leung A, Han BS, et al. Wnt1-lmx1a forms a novel autoregulatory loop and controls midbrain dopaminergic differentiation synergistically with the SHH-FoxA2 pathway [Internet]. *Cell Stem Cell* 2009;5(6):646–658.[cited 2023 Jan 3] Available from: <https://pubmed.ncbi.nlm.nih.gov/19951692/>
 211. McMahon AP, Bradley A. The Wnt-1 (int-1) proto-oncogene is required for development of a large region of the mouse brain [Internet]. *Cell* 1990;62(6):1073–1085.[cited 2020 Jun 11] Available from: <https://pubmed.ncbi.nlm.nih.gov/2205396/>
 212. McMahon AP, Joyner AL, Bradley A, McMahon JA. The midbrain-hindbrain phenotype of Wnt-1-/Wnt-1- mice results from stepwise deletion of engrailed-expressing cells by 9.5 days postcoitum [Internet]. *Cell* 1992;69(4):581–595.[cited 2020 Jun 11] Available from: <https://pubmed.ncbi.nlm.nih.gov/1534034/>
 213. Thomas KR, Capecchi MR. Targeted disruption of the murine int-1 proto-oncogene resulting in severe abnormalities in midbrain and cerebellar development [Internet]. *Nature* 1990;346(6287):847–850.[cited 2023 Jan 6] Available from: <https://pubmed.ncbi.nlm.nih.gov/2202907/>
 214. Arenas E. Wnt signaling in midbrain dopaminergic neuron development and regenerative medicine for Parkinson's disease [Internet]. *J. Mol. Cell Biol.* 2014;6(1):42–53.[cited 2023 Jan 6] Available from: <https://pubmed.ncbi.nlm.nih.gov/24431302/>
 215. Andersson E, Tryggvason U, Deng Q, et al. Identification of intrinsic determinants of midbrain dopamine neurons [Internet]. *Cell* 2006;124(2):393–405.[cited 2020 Jun 11] Available from: <https://pubmed.ncbi.nlm.nih.gov/16439212/>
 216. Deng Q, Andersson E, Hedlund E, et al. Specific and integrated roles of Lmx1a, Lmx1b and Phox2a in ventral midbrain development [Internet]. *Development* 2011;138(16):3399–3408.[cited 2020 Jun 11] Available from: <https://pubmed.ncbi.nlm.nih.gov/21752929/>
 217. Smidt MP, Asbreuk CHJ, Cox JJ, et al. A second independent pathway for development of mesencephalic dopaminergic neurons requires Lmx1b. *Nat. Neurosci.* 2000;3(4):337–341.
 218. Andersson ER, Prakash N, Cajanek L, et al. Wnt5a regulates ventral midbrain morphogenesis and the development of A9-A10 dopaminergic cells in vivo [Internet].

- PLoS One 2008;3(10)[cited 2020 Jun 11] Available from:
<https://pubmed.ncbi.nlm.nih.gov/18953410/>
219. Zetterström RH, Solomin L, Jansson L, et al. Dopamine neuron agenesis in Nurr1-deficient mice [Internet]. *Science* 1997;276(5310):248–250.[cited 2023 Jan 3] Available from: <https://pubmed.ncbi.nlm.nih.gov/9092472/>
 220. Maxwell SL, Ho HY, Kuehner E, et al. Pitx3 regulates tyrosine hydroxylase expression in the substantia nigra and identifies a subgroup of mesencephalic dopaminergic progenitor neurons during mouse development [Internet]. *Dev. Biol.* 2005;282(2):467–479.[cited 2023 Jan 3] Available from: <https://pubmed.ncbi.nlm.nih.gov/15950611/>
 221. Gil M, McKinney C, Lee MK, et al. Regulation of GTP cyclohydrolase I expression by orphan receptor Nurr1 in cell culture and in vivo [Internet]. *J. Neurochem.* 2007;101(1):142–150.[cited 2023 Jan 4] Available from: <https://pubmed.ncbi.nlm.nih.gov/17394463/>
 222. Saucedo-Cardenas O, Quintana-Hau JD, Le WD, et al. Nurr1 is essential for the induction of the dopaminergic phenotype and the survival of ventral mesencephalic late dopaminergic precursor neurons [Internet]. *Proc. Natl. Acad. Sci. U. S. A.* 1998;95(7):4013–4018.[cited 2023 Jan 4] Available from: <https://pubmed.ncbi.nlm.nih.gov/9520484/>
 223. Smits SM, Ponnio T, Conneely OM, et al. Involvement of Nurr1 in specifying the neurotransmitter identity of ventral midbrain dopaminergic neurons [Internet]. *Eur. J. Neurosci.* 2003;18(7):1731–1738.[cited 2023 Jan 4] Available from: <https://pubmed.ncbi.nlm.nih.gov/14622207/>
 224. Wallén Å, Castro DS, Zetterström RH, et al. Orphan nuclear receptor Nurr1 is essential for Ret expression in midbrain dopamine neurons and in the brain stem [Internet]. *Mol. Cell. Neurosci.* 2001;18(6):649–663.[cited 2023 Jan 4] Available from: <https://pubmed.ncbi.nlm.nih.gov/11749040/>
 225. Stott SRW, Metzakopian E, Lin W, et al. Foxa1 and foxa2 are required for the maintenance of dopaminergic properties in ventral midbrain neurons at late embryonic stages [Internet]. *J. Neurosci.* 2013;33(18):8022–8034.[cited 2023 Mar 28] Available from: <https://pubmed.ncbi.nlm.nih.gov/23637192/>
 226. Dawson TM, Golde TE, Lagier-Tourenne C. Animal models of neurodegenerative diseases [Internet]. *Nat. Neurosci.* 2018;21(10):1370–1379.[cited 2023 Mar 18] Available from: <https://pubmed.ncbi.nlm.nih.gov/30250265/>
 227. Slanzi A, Iannoto G, Rossi B, et al. In vitro Models of Neurodegenerative Diseases [Internet]. *Front. cell Dev. Biol.* 2020;8[cited 2023 Jun 27] Available from: <https://pubmed.ncbi.nlm.nih.gov/32528949/>
 228. Shi Y, Kirwan P, Livesey FJ. Directed differentiation of human pluripotent stem cells to cerebral cortex neurons and neural networks [Internet]. *Nat. Protoc.* 2012;7(10):1836–1846.[cited 2021 Oct 17] Available from: <https://pubmed.ncbi.nlm.nih.gov/22976355/>
 229. Qi Y, Zhang XJ, Renier N, et al. Combined small-molecule inhibition accelerates the derivation of functional cortical neurons from human pluripotent stem cells [Internet]. *Nat. Biotechnol.* 2017;35(2):154–163.[cited 2023 Jun 28] Available from: <https://pubmed.ncbi.nlm.nih.gov/28112759/>
 230. Nicholas CR, Chen J, Tang Y, et al. Functional maturation of hPSC-derived forebrain interneurons requires an extended timeline and mimics human neural development [Internet]. *Cell Stem Cell* 2013;12(5):573–586.[cited 2023 Jun 28] Available from: <https://pubmed.ncbi.nlm.nih.gov/23642366/>
 231. Arber C, Precious S V., Cambray S, et al. Activin A directs striatal projection neuron differentiation of human pluripotent stem cells [Internet]. *Development* 2015;142(7):1375–1386.[cited 2023 Jun 28] Available from:

- <https://pubmed.ncbi.nlm.nih.gov/25804741/>
232. Kirkeby A, Grealish S, Wolf DA, et al. Generation of Regionally Specified Neural Progenitors and Functional Neurons from Human Embryonic Stem Cells under Defined Conditions. *Cell Rep.* 2012;1(6):703–714.
 233. Kriks S, Shim J-W, Piao J, et al. Dopamine neurons derived from human ES cells efficiently engraft in animal models of Parkinson’s disease. [Internet]. *Nature* 2011;480(7378):547–51. Available from: <http://dx.doi.org/10.1038/nature10648>
 234. Devine MJ, Ryten M, Vodicka P, et al. Parkinson’s disease induced pluripotent stem cells with triplication of the α -synuclein locus [Internet]. *Nat Commun* 2011;2(1):440.[cited 2023 Mar 30] Available from: <http://www.ncbi.nlm.nih.gov/pubmed/21863007> <http://www.ncbi.nlm.nih.gov/pmc/articles/PMC3265381/pdf/ncomms1453.pdf>
 235. Shaltouki A, Peng J, Liu Q, et al. Efficient generation of astrocytes from human pluripotent stem cells in defined conditions [Internet]. *Stem Cells* 2013;31(5):941–952.[cited 2023 Jun 28] Available from: <https://pubmed.ncbi.nlm.nih.gov/23341249/>
 236. Serio A, Bilican B, Barmada SJ, et al. Astrocyte pathology and the absence of non-cell autonomy in an induced pluripotent stem cell model of TDP-43 proteinopathy [Internet]. *Proc. Natl. Acad. Sci. U. S. A.* 2013;110(12):4697–4702.[cited 2023 Jun 28] Available from: <https://pubmed.ncbi.nlm.nih.gov/23401527/>
 237. Emdad L, D’Souza SL, Kothari HP, et al. Efficient differentiation of human embryonic and induced pluripotent stem cells into functional astrocytes [Internet]. *Stem Cells Dev.* 2012;21(3):404–410.[cited 2023 Jun 28] Available from: <https://pubmed.ncbi.nlm.nih.gov/21631388/>
 238. Wang S, Bates J, Li X, et al. Human iPSC-derived oligodendrocyte progenitor cells can myelinate and rescue a mouse model of congenital hypomyelination [Internet]. *Cell Stem Cell* 2013;12(2):252–264.[cited 2023 Jun 28] Available from: <https://pubmed.ncbi.nlm.nih.gov/23395447/>
 239. Douvaras P, Wang J, Zimmer M, et al. Efficient generation of myelinating oligodendrocytes from primary progressive multiple sclerosis patients by induced pluripotent stem cells [Internet]. *Stem cell reports* 2014;3(2):250–259.[cited 2023 Jun 28] Available from: <https://pubmed.ncbi.nlm.nih.gov/25254339/>
 240. Abud EM, Ramirez RN, Martinez ES, et al. iPSC-Derived Human Microglia-like Cells to Study Neurological Diseases [Internet]. *Neuron* 2017;94(2):278–293.e9.[cited 2023 Jun 28] Available from: <https://pubmed.ncbi.nlm.nih.gov/28426964/>
 241. Douvaras P, Sun B, Wang M, et al. Directed Differentiation of Human Pluripotent Stem Cells to Microglia [Internet]. *Stem cell reports* 2017;8(6):1516–1524.[cited 2023 Jun 28] Available from: <https://pubmed.ncbi.nlm.nih.gov/28528700/>
 242. McComish SF, Caldwell MA. Generation of defined neural populations from pluripotent stem cells [Internet]. *Philos. Trans. R. Soc. Lond. B. Biol. Sci.* 2018;373(1750)[cited 2023 Jun 29] Available from: <https://pubmed.ncbi.nlm.nih.gov/29786550/>
 243. Pas SP. The rise of three-dimensional human brain cultures [Internet]. *Nature* 2018;553(7689):437–445.[cited 2023 Mar 5] Available from: <https://pubmed.ncbi.nlm.nih.gov/29364288/>
 244. Lancaster MA, Renner M, Martin C-AA, et al. Cerebral organoids model human brain development and microcephaly [Internet]. *Nature* 2013;501(7467):373–379.[cited 2018 Jul 16] Available from: <http://www.ncbi.nlm.nih.gov/pubmed/23995685>
 245. Qian X, Jacob F, Song MM, et al. Generation of human brain region-specific organoids using a miniaturized spinning bioreactor [Internet]. *Nat. Protoc.* 2018;13(3):565–580.[cited 2023 Jun 29] Available from: <https://pubmed.ncbi.nlm.nih.gov/29470464/>
 246. Jo J, Xiao Y, Sun AX, et al. Midbrain-like Organoids from Human Pluripotent Stem

- Cells Contain Functional Dopaminergic and Neuromelanin-Producing Neurons [Internet]. *Cell Stem Cell* 2016;19(2):248–257.[cited 2019 Apr 2] Available from: <https://pubmed.ncbi.nlm.nih.gov/27476966/>
247. Muguruma K, Nishiyama A, Kawakami H, et al. Self-organization of polarized cerebellar tissue in 3D culture of human pluripotent stem cells [Internet]. *Cell Rep.* 2015;10(4):537–550.[cited 2023 Jun 29] Available from: <https://pubmed.ncbi.nlm.nih.gov/25640179/>
 248. Birey F, Andersen J, Makinson CD, et al. Assembly of functionally integrated human forebrain spheroids [Internet]. *Nature* 2017;545(7652):54–59.[cited 2023 Jun 29] Available from: <https://pubmed.ncbi.nlm.nih.gov/28445465/>
 249. Miura Y, Li MY, Birey F, et al. Generation of human striatal organoids and cortico-striatal assembloids from human pluripotent stem cells [Internet]. *Nat. Biotechnol.* 2020;38(12):1421–1430.[cited 2021 Sep 30] Available from: <https://pubmed.ncbi.nlm.nih.gov/33273741/>
 250. Koo B, Choi B, Park H, Yoon KJ. Past, Present, and Future of Brain Organoid Technology [Internet]. *Mol. Cells* 2019;42(9):617–627.[cited 2023 Jun 29] Available from: <https://pubmed.ncbi.nlm.nih.gov/31564073/>
 251. Ono Y, Nakatani T, Sakamoto Y, et al. Differences in neurogenic potential in floor plate cells along an anteroposterior location: midbrain dopaminergic neurons originate from mesencephalic floor plate cells. *Development* 2007;134(17):3213–3225.
 252. Chambers SM, Fasano CA, Papapetrou EP, et al. Highly efficient neural conversion of human ES and iPS cells by dual inhibition of SMAD signaling [Internet]. *Nat. Biotechnol.* 2009;27(3):275–280.[cited 2015 Oct 11] Available from: <http://www.pubmedcentral.nih.gov/articlerender.fcgi?artid=2756723&tool=pmcentrez&rendertype=abstract>
 253. Smits LM, Schwamborn JC. Midbrain Organoids: A New Tool to Investigate Parkinson's Disease [Internet]. *Front. cell Dev. Biol.* 2020;8[cited 2023 Mar 30] Available from: <https://pubmed.ncbi.nlm.nih.gov/32509785/>
 254. Ardhanareeswaran K, Mariani J, Coppola G, et al. Human induced pluripotent stem cells for modelling neurodevelopmental disorders [Internet]. *Nat. Rev. Neurol.* 2017;13(5):265–278.[cited 2023 Feb 25] Available from: <https://pubmed.ncbi.nlm.nih.gov/28418023/>
 255. Taoufik E, Kouroupi G, Zygogianni O, Matsas R. Synaptic dysfunction in neurodegenerative and neurodevelopmental diseases: an overview of induced pluripotent stem-cell-based disease models [Internet]. *Open Biol.* 2018;8(9)[cited 2023 Feb 26] Available from: <https://pubmed.ncbi.nlm.nih.gov/30185603/>
 256. Studer L, Vera E, Cornacchia D. Programming and Reprogramming Cellular Age in the Era of Induced Pluripotency [Internet]. *Cell Stem Cell* 2015;16(6):591–600.[cited 2020 Apr 16] Available from: <https://linkinghub.elsevier.com/retrieve/pii/S1934590915002131>
 257. Linda K, Fiuza C, Nadif Kasri N. The promise of induced pluripotent stem cells for neurodevelopmental disorders [Internet]. *Prog. Neuropsychopharmacol. Biol. Psychiatry* 2018;84(Pt B):382–391.[cited 2023 Feb 26] Available from: <https://pubmed.ncbi.nlm.nih.gov/29128445/>
 258. Rossignoli G, Krämer K, Lugarà E, et al. Aromatic l -amino acid decarboxylase deficiency: a patient-derived neuronal model for precision therapies [Internet]. *Brain* 2021;144(8):2443–2456.[cited 2021 Sep 26] Available from: <https://pubmed.ncbi.nlm.nih.gov/33734312/>
 259. Shen X, Yeung HT, Lai KO. Application of Human-Induced Pluripotent Stem Cells (hiPSCs) to Study Synaptopathy of Neurodevelopmental Disorders [Internet]. *Dev. Neurobiol.* 2019;79(1):20–35.[cited 2021 Sep 29] Available from:

- <https://pubmed.ncbi.nlm.nih.gov/30304570/>
260. Krey JF, Paşca SP, Shcheglovitov A, et al. Timothy syndrome is associated with activity-dependent dendritic retraction in rodent and human neurons [Internet]. *Nat. Neurosci.* 2013;16(2):201–209.[cited 2023 Mar 30] Available from: <https://pubmed.ncbi.nlm.nih.gov/23313911/>
 261. Zhang Z, Marro SG, Zhang Y, et al. The fragile X mutation impairs homeostatic plasticity in human neurons by blocking synaptic retinoic acid signaling [Internet]. *Sci. Transl. Med.* 2018;10(452)[cited 2023 Mar 30] Available from: <https://pubmed.ncbi.nlm.nih.gov/30068571/>
 262. Boland MJ, Nazor KL, Tran HT, et al. Molecular analyses of neurogenic defects in a human pluripotent stem cell model of fragile X syndrome [Internet]. *Brain* 2017;140(3):582–598.[cited 2023 Mar 30] Available from: <https://pubmed.ncbi.nlm.nih.gov/28137726/>
 263. Marchetto MCN, Carroneu C, Acab A, et al. A model for neural development and treatment of Rett syndrome using human induced pluripotent stem cells [Internet]. *Cell* 2010;143(4):527–539.[cited 2023 Mar 30] Available from: <https://pubmed.ncbi.nlm.nih.gov/21074045/>
 264. Yamashita S, Chiyonobu T, Yoshida M, et al. Mislocalization of syntaxin-1 and impaired neurite growth observed in a human iPSC model for STXBP1-related epileptic encephalopathy [Internet]. *Epilepsia* 2016;57(4):e81–e86.[cited 2023 Mar 30] Available from: <https://pubmed.ncbi.nlm.nih.gov/26918652/>
 265. Shcheglovitov A, Shcheglovitova O, Yazawa M, et al. SHANK3 and IGF1 restore synaptic deficits in neurons from 22q13 deletion syndrome patients [Internet]. *Nature* 2013;503(7475):267–271.[cited 2023 Mar 30] Available from: <https://pubmed.ncbi.nlm.nih.gov/24132240/>
 266. Fink JJ, Robinson TM, Germain ND, et al. Disrupted neuronal maturation in Angelman syndrome-derived induced pluripotent stem cells [Internet]. *Nat. Commun.* 2017;8[cited 2023 Mar 30] Available from: <https://pubmed.ncbi.nlm.nih.gov/28436452/>
 267. Giacomelli E, Vahsen BF, Calder EL, et al. Human stem cell models of neurodegeneration: From basic science of amyotrophic lateral sclerosis to clinical translation [Internet]. *Cell Stem Cell* 2022;29(1):11–35.[cited 2023 Mar 5] Available from: <https://pubmed.ncbi.nlm.nih.gov/34995492/>
 268. Radke J, Stenzel W, Goebel HH. Neurometabolic and neurodegenerative diseases in children [Internet]. *Handb. Clin. Neurol.* 2017;145:133–146.[cited 2023 Jun 27] Available from: <https://pubmed.ncbi.nlm.nih.gov/28987164/>
 269. Li L, Kim HJ, Roh JH, et al. Pathological manifestation of the induced pluripotent stem cell-derived cortical neurons from an early-onset Alzheimer’s disease patient carrying a presenilin-1 mutation (S170F) [Internet]. *Cell Prolif.* 2020;e12798.[cited 2020 Apr 1] Available from: <http://www.ncbi.nlm.nih.gov/pubmed/32216003>
 270. Iwasawa C, Kuzumaki N, Suda Y, et al. Reduced expression of somatostatin in GABAergic interneurons derived from induced pluripotent stem cells of patients with parkin mutations [Internet]. *Mol. Brain* 2019;12(1):5.[cited 2020 Apr 1] Available from: <https://molecularbrain.biomedcentral.com/articles/10.1186/s13041-019-0426-7>
 271. Kim BW, Jeong YE, Wong M, Martin LJ. DNA damage accumulates and responses are engaged in human ALS brain and spinal motor neurons and DNA repair is activatable in iPSC-derived motor neurons with SOD1 mutations [Internet]. *Acta Neuropathol. Commun.* 2020;8(1):7.[cited 2020 Apr 1] Available from: <https://actaneurocomms.biomedcentral.com/articles/10.1186/s40478-019-0874-4>
 272. Stanslowsky N, Reinhardt P, Glass H, et al. Neuronal dysfunction in iPSC-derived medium spiny neurons from chorea-acanthocytosis patients is reversed by Src kinase

- inhibition and F-actin stabilization. *J. Neurosci.* 2016;36(47):12027–12043.
273. Lang C, Campbell KR, Ryan BJ, et al. Single-Cell Sequencing of iPSC-Dopamine Neurons Reconstructs Disease Progression and Identifies HDAC4 as a Regulator of Parkinson Cell Phenotypes. *Cell Stem Cell* 2019;24(1):93-106.e6.
 274. di Domenico A, Carola G, Calatayud C, et al. Patient-Specific iPSC-Derived Astrocytes Contribute to Non-Cell-Autonomous Neurodegeneration in Parkinson's Disease [Internet]. *Stem Cell Reports* 2019;12(2):213–229.[cited 2020 Apr 1] Available from: <http://www.ncbi.nlm.nih.gov/pubmed/30639209>
 275. Juopperi TA, Kim WR, Chiang C-H, et al. Astrocytes generated from patient induced pluripotent stem cells recapitulate features of Huntington's disease patient cells. [Internet]. *Mol. Brain* 2012;5(1):17.[cited 2020 Apr 1] Available from: <http://www.ncbi.nlm.nih.gov/pubmed/22613578>
 276. Borger DK, McMahon B, Lal TR, et al. Induced pluripotent stem cell models of lysosomal storage disorders [Internet]. *Dis. Model. Mech.* 2017;10(6):691.[cited 2023 Jun 27] Available from: [/pmc/articles/PMC5483008/](https://pubmed.ncbi.nlm.nih.gov/34299348/)
 277. McKnight CL, Low YC, Elliott DA, et al. Modelling Mitochondrial Disease in Human Pluripotent Stem Cells: What Have We Learned? [Internet]. *Int. J. Mol. Sci.* 2021;22(14)[cited 2023 Jun 27] Available from: <https://pubmed.ncbi.nlm.nih.gov/34299348/>
 278. Miller JD, Ganat YM, Kishinevsky S, et al. Human iPSC-based modeling of late-onset disease via progerin-induced aging [Internet]. *Cell Stem Cell* 2013;13(6):691–705.[cited 2022 May 31] Available from: <https://pubmed.ncbi.nlm.nih.gov/24315443/>
 279. Zhu L, Sun C, Ren J, et al. Stress-induced precocious aging in PD-patient iPSC-derived NSCs may underlie the pathophysiology of Parkinson's disease [Internet]. *Cell Death Dis.* 2019;10(2)[cited 2023 Mar 11] Available from: <https://pubmed.ncbi.nlm.nih.gov/30718471/>
 280. Vera E, Bosco N, Studer L. Generating Late-Onset Human iPSC-Based Disease Models by Inducing Neuronal Age-Related Phenotypes through Telomerase Manipulation [Internet]. *Cell Rep.* 2016;17(4):1184–1192.[cited 2022 May 31] Available from: <https://pubmed.ncbi.nlm.nih.gov/27760320/>
 281. Mertens J, Herdy JR, Traxler L, et al. Age-dependent instability of mature neuronal fate in induced neurons from Alzheimer's patients [Internet]. *Cell Stem Cell* 2021;28(9)[cited 2023 Mar 11] Available from: <https://pubmed.ncbi.nlm.nih.gov/33910058/>
 282. Vierbuchen T, Ostermeier A, Pang ZP, et al. Direct conversion of fibroblasts to functional neurons by defined factors [Internet]. *Nature* 2010;463(7284):1035–1041.[cited 2023 Mar 11] Available from: <https://pubmed.ncbi.nlm.nih.gov/20107439/>
 283. Richner M, Victor MB, Liu Y, et al. MicroRNA-based conversion of human fibroblasts into striatal medium spiny neurons [Internet]. *Nat. Protoc.* 2015;10(10):1543–1555.[cited 2023 Mar 11] Available from: <https://pubmed.ncbi.nlm.nih.gov/26379228/>
 284. Mertens J, Paquola ACM, Ku M, et al. Directly Reprogrammed Human Neurons Retain Aging-Associated Transcriptomic Signatures and Reveal Age-Related Nucleocytoplasmic Defects [Internet]. *Cell Stem Cell* 2015;17(6):705–718.[cited 2023 Mar 11] Available from: <https://pubmed.ncbi.nlm.nih.gov/26456686/>
 285. Gordon A, Yoon SJ, Tran SS, et al. Long-term maturation of human cortical organoids matches key early postnatal transitions [Internet]. *Nat. Neurosci.* 2021;24(3):331–342.[cited 2023 Mar 5] Available from: <https://pubmed.ncbi.nlm.nih.gov/33619405/>
 286. Okano H, Morimoto S. iPSC-based disease modeling and drug discovery in cardinal neurodegenerative disorders [Internet]. *Cell Stem Cell* 2022;29(2):189–208.[cited 2023 Mar 11] Available from: <https://pubmed.ncbi.nlm.nih.gov/35120619/>
 287. Byers B, Cord B, Nguyen HN, et al. SNCA triplication Parkinson's patient's iPSC-

- derived DA neurons accumulate α -synuclein and are susceptible to oxidative stress [Internet]. *PLoS One* 2011;6(11)[cited 2023 Mar 30] Available from: <https://pubmed.ncbi.nlm.nih.gov/22110584/>
288. Ludtmann MHR, Angelova PR, Horrocks MH, et al. α -synuclein oligomers interact with ATP synthase and open the permeability transition pore in Parkinson's disease [Internet]. *Nat. Commun.* 2018;9(1)[cited 2023 Mar 30] Available from: <https://pubmed.ncbi.nlm.nih.gov/29895861/>
 289. Cooper O, Seo H, Andrabi S, et al. Pharmacological rescue of mitochondrial deficits in iPSC-derived neural cells from patients with familial Parkinson's disease [Internet]. *Sci. Transl. Med.* 2012;4(141)[cited 2023 Mar 30] Available from: <https://pubmed.ncbi.nlm.nih.gov/22764206/>
 290. Nguyen HN, Byers B, Cord B, et al. LRRK2 mutant iPSC-derived DA neurons demonstrate increased susceptibility to oxidative stress [Internet]. *Cell Stem Cell* 2011;8(3):267–280.[cited 2023 Mar 30] Available from: <https://pubmed.ncbi.nlm.nih.gov/21362567/>
 291. Reinhardt P, Schmid B, Burbulla LF, et al. Genetic correction of a LRRK2 mutation in human iPSCs links parkinsonian neurodegeneration to ERK-dependent changes in gene expression [Internet]. *Cell Stem Cell* 2013;12(3):354–367.[cited 2023 Mar 30] Available from: <https://pubmed.ncbi.nlm.nih.gov/23472874/>
 292. Sanders LH, Laganière J, Cooper O, et al. LRRK2 mutations cause mitochondrial DNA damage in iPSC-derived neural cells from Parkinson's disease patients: reversal by gene correction [Internet]. *Neurobiol. Dis.* 2014;62:381–386.[cited 2023 Mar 30] Available from: <https://pubmed.ncbi.nlm.nih.gov/24148854/>
 293. Hsieh CH, Shaltouki A, Gonzalez AE, et al. Functional Impairment in Miro Degradation and Mitophagy Is a Shared Feature in Familial and Sporadic Parkinson's Disease [Internet]. *Cell Stem Cell* 2016;19(6):709–724.[cited 2023 Mar 30] Available from: <https://pubmed.ncbi.nlm.nih.gov/27618216/>
 294. Burbulla LF, Jeon S, Zheng J, et al. A modulator of wild-type glucocerebrosidase improves pathogenic phenotypes in dopaminergic neuronal models of Parkinson's disease [Internet]. *Sci. Transl. Med.* 2019;11(514)[cited 2023 Mar 31] Available from: <https://pubmed.ncbi.nlm.nih.gov/31619543/>
 295. Imaizumi Y, Okada Y, Akamatsu W, et al. Mitochondrial dysfunction associated with increased oxidative stress and α -synuclein accumulation in PARK2 iPSC-derived neurons and postmortem brain tissue [Internet]. *Mol. Brain* 2012;5(1)[cited 2023 Mar 30] Available from: <https://pubmed.ncbi.nlm.nih.gov/23039195/>
 296. Chung SY, Kishinevsky S, Mazzulli JR, et al. Parkin and PINK1 Patient iPSC-Derived Midbrain Dopamine Neurons Exhibit Mitochondrial Dysfunction and α -Synuclein Accumulation [Internet]. *Stem cell reports* 2016;7(4):664–677.[cited 2023 Mar 30] Available from: <https://pubmed.ncbi.nlm.nih.gov/27641647/>
 297. Oh CK, Sultan A, Platzer J, et al. S-Nitrosylation of PINK1 Attenuates PINK1/Parkin-Dependent Mitophagy in hiPSC-Based Parkinson's Disease Models [Internet]. *Cell Rep.* 2017;21(8):2171–2182.[cited 2023 Mar 30] Available from: <https://pubmed.ncbi.nlm.nih.gov/29166608/>
 298. Seibler P, Graziotto J, Jeong H, et al. Mitochondrial Parkin recruitment is impaired in neurons derived from mutant PINK1 induced pluripotent stem cells [Internet]. *J. Neurosci.* 2011;31(16):5970–5976.[cited 2023 Mar 31] Available from: <https://pubmed.ncbi.nlm.nih.gov/21508222/>
 299. Munsie LN, Milnerwood AJ, Seibler P, et al. Retromer-dependent neurotransmitter receptor trafficking to synapses is altered by the Parkinson's disease VPS35 mutation p.D620N [Internet]. *Hum. Mol. Genet.* 2015;24(6):1691–1703.[cited 2023 Mar 31] Available from: <https://pubmed.ncbi.nlm.nih.gov/25416282/>

300. Bose A, Petsko GA, Studer L. Induced pluripotent stem cells: a tool for modeling Parkinson's disease [Internet]. *Trends Neurosci.* 2022;45(8):608–620.[cited 2023 Mar 11] Available from: <https://pubmed.ncbi.nlm.nih.gov/35667922/>
301. Abela L, Gianfrancesco L, Tagliatti E, et al. Neurodevelopmental and synaptic defects in DNAJC6 parkinsonism, amenable to gene therapy [Internet]. *Brain* 2024;[cited 2024 May 1] Available from: <https://pubmed.ncbi.nlm.nih.gov/38242634/>
302. Quinlan AR, Hall IM. BEDTools: a flexible suite of utilities for comparing genomic features. [Internet]. *Bioinformatics* 2010;26(6):841–2.[cited 2018 Jul 12] Available from: <https://academic.oup.com/bioinformatics/article-lookup/doi/10.1093/bioinformatics/btq033>
303. Meyer E, Carss KJ, Rankin J, et al. Mutations in the histone methyltransferase gene KMT2B cause complex early-onset dystonia [Internet]. *Nat. Genet.* 2017;49(2):223–237.[cited 2018 Jul 13] Available from: <http://www.ncbi.nlm.nih.gov/pubmed/27992417>
304. Hyland K, Surtees RA, Heales SJ, et al. Cerebrospinal fluid concentrations of pterins and metabolites of serotonin and dopamine in a pediatric reference population. [Internet]. *Pediatr. Res.* 1993;34(1):10–4.[cited 2018 Jul 12] Available from: <http://www.nature.com/doifinder/10.1203/00006450-199307000-00003>
305. Orteza C, Duarte ST, Ormazábal A, et al. Cerebrospinal fluid synaptic proteins as useful biomarkers in tyrosine hydroxylase deficiency [Internet]. *Mol. Genet. Metab.* 2015;114(1):34–40.[cited 2018 Jul 12] Available from: <http://linkinghub.elsevier.com/retrieve/pii/S1096719214003400>
306. Afgan E, Baker D, Batut B, et al. The Galaxy platform for accessible, reproducible and collaborative biomedical analyses: 2018 update [Internet]. *Nucleic Acids Res.* 2018;46(W1):W537–W544.[cited 2022 Jun 6] Available from: <https://pubmed.ncbi.nlm.nih.gov/29790989/>
307. Chen S, Zhou Y, Chen Y, Gu J. fastp: an ultra-fast all-in-one FASTQ preprocessor [Internet]. *Bioinformatics* 2018;34(17):i884–i890.[cited 2022 Jun 6] Available from: <https://pubmed.ncbi.nlm.nih.gov/30423086/>
308. Kim D, Langmead B, Salzberg SL. HISAT: a fast spliced aligner with low memory requirements [Internet]. *Nat. Methods* 2015;12(4):357–360.[cited 2022 Jun 6] Available from: <https://pubmed.ncbi.nlm.nih.gov/25751142/>
309. Liao Y, Smyth GK, Shi W. featureCounts: an efficient general purpose program for assigning sequence reads to genomic features [Internet]. *Bioinformatics* 2014;30(7):923–930.[cited 2022 Jun 6] Available from: <https://pubmed.ncbi.nlm.nih.gov/24227677/>
310. Robinson MD, McCarthy DJ, Smyth GK. edgeR: a Bioconductor package for differential expression analysis of digital gene expression data [Internet]. *Bioinformatics* 2010;26(1):139–140.[cited 2022 Jun 6] Available from: <https://pubmed.ncbi.nlm.nih.gov/19910308/>
311. Liu R, Holik AZ, Su S, et al. Why weight? Modelling sample and observational level variability improves power in RNA-seq analyses [Internet]. *Nucleic Acids Res.* 2015;43(15)[cited 2022 Jun 6] Available from: <https://pubmed.ncbi.nlm.nih.gov/25925576/>
312. Mi H, Muruganujan A, Ebert D, et al. PANTHER version 14: more genomes, a new PANTHER GO-slim and improvements in enrichment analysis tools [Internet]. *Nucleic Acids Res.* 2019;47(D1):D419–D426.[cited 2022 Jun 6] Available from: <https://pubmed.ncbi.nlm.nih.gov/30407594/>
313. Koopmans F, van Nierop P, Andres-Alonso M, et al. SynGO: An Evidence-Based, Expert-Curated Knowledge Base for the Synapse [Internet]. *Neuron* 2019;103(2):217–234.e4.[cited 2022 Jun 6] Available from: <https://pubmed.ncbi.nlm.nih.gov/31171447/>

314. Barczak W, Suchorska W, Rubiś B, Kulcenty K. Universal real-time PCR-based assay for lentiviral titration [Internet]. *Mol. Biotechnol.* 2015;57(2):195–200.[cited 2022 Feb 13] Available from: <https://pubmed.ncbi.nlm.nih.gov/25370825/>
315. Cordeiro D, Bullivant G, Siriwardena K, et al. Genetic landscape of pediatric movement disorders and management implications [Internet]. *Neurol. Genet.* 2018;4(5):e265.[cited 2023 Jun 18] Available from: <https://pubmed.ncbi.nlm.nih.gov/30283815/>
316. Kim MJ, Yum MS, Seo GH, et al. Phenotypic and Genetic Complexity in Pediatric Movement Disorders [Internet]. *Front. Genet.* 2022;13[cited 2023 Jun 18] Available from: <https://pubmed.ncbi.nlm.nih.gov/35719373/>
317. Kwong AKY, Tsang MHY, Fung JLF, et al. Exome sequencing in paediatric patients with movement disorders [Internet]. *Orphanet J. Rare Dis.* 2021;16(1)[cited 2021 Sep 26] Available from: <https://pubmed.ncbi.nlm.nih.gov/33446253/>
318. Vauthier V, Jaillard S, Journal H, et al. Homozygous deletion of an 80kb region comprising part of DNAJC6 and LEPR genes on chromosome 1P31.3 is associated with early onset obesity, mental retardation and epilepsy. *Mol. Genet. Metab.* 2012;106(3):345–350.
319. Fasano A, Bloem BR. Gait disorders [Internet]. *Continuum (Minneap. Minn).* 2013;19(5 Movement Disorders):1344–1382.[cited 2023 Jun 19] Available from: <https://pubmed.ncbi.nlm.nih.gov/24092293/>
320. Avelino MA, Fusão EF, Pedroso JL, et al. Inherited manganism: the “cock-walk” gait and typical neuroimaging features [Internet]. *J. Neurol. Sci.* 2014;341(1–2):150–152.[cited 2023 Jun 19] Available from: <https://pubmed.ncbi.nlm.nih.gov/24746291/>
321. Rocha E, Vale TC, Kok F, et al. Teaching Neuro Images: Spinocerebellar ataxia type 3 presenting with a cock-walk gait phenotype [Internet]. *Neurology* 2017;89(15):e192.[cited 2023 Jun 19] Available from: <https://pubmed.ncbi.nlm.nih.gov/28993536/>
322. Dolgan A, Budrewicz S, Koszewicz M, et al. Acute hyperkinetic syndrome due to ephedrone abuse [Internet]. *J. Addict. Med.* 2015;9(3):244–245.[cited 2023 Jun 19] Available from: <https://pubmed.ncbi.nlm.nih.gov/25835774/>
323. Liang G, Zhang Y. Genetic and epigenetic variations in iPSCs: potential causes and implications for application [Internet]. *Cell Stem Cell* 2013;13(2):149–159.[cited 2020 Apr 21] Available from: <https://pubmed.ncbi.nlm.nih.gov/23910082/>
324. Steichen C, Hannoun Z, Luce E, et al. Genomic integrity of human induced pluripotent stem cells: Reprogramming, differentiation and applications [Internet]. *World J. Stem Cells* 2019;11(10):729–747.[cited 2023 May 13] Available from: <https://pubmed.ncbi.nlm.nih.gov/31692979/>
325. Takahashi K, Tanabe K, Ohnuki M, et al. Induction of Pluripotent Stem Cells from Adult Human Fibroblasts by Defined Factors [Internet]. *Cell* 2007;131(5):861–872.[cited 2021 Oct 21] Available from: <https://pubmed.ncbi.nlm.nih.gov/18035408/>
326. Lenz M, Goetzke R, Schenk A, et al. Epigenetic biomarker to support classification into pluripotent and non-pluripotent cells [Internet]. *Sci. Rep.* 2015;5(1):8973.[cited 2020 Mar 25] Available from: <https://www.ncbi.nlm.nih.gov/pubmed/?term=lenz+M+and+epigenetic+and+2015>
327. Wesselschmidt RL. The teratoma assay: an in vivo assessment of pluripotency [Internet]. *Methods Mol. Biol.* 2011;767:231–241.[cited 2023 May 15] Available from: <https://pubmed.ncbi.nlm.nih.gov/21822879/>
328. Hubrecht RC, Carter E. The 3Rs and Humane Experimental Technique: Implementing Change [Internet]. *Anim. an Open Access J. from MDPI* 2019;9(10)[cited 2024 Apr 4] Available from: [/pmc/articles/PMC6826930/](https://pmc/articles/PMC6826930/)
329. Itskovitz-Eldor J, Schuldiner M, Karsenti D, et al. Differentiation of human embryonic

- stem cells into embryoid bodies compromising the three embryonic germ layers [Internet]. *Mol. Med.* 2000;6(2):88–95.[cited 2023 May 17] Available from: <https://pubmed.ncbi.nlm.nih.gov/10859025/>
330. Kogut I, McCarthy SM, Pavlova M, et al. High-efficiency RNA-based reprogramming of human primary fibroblasts [Internet]. *Nat. Commun.* 2018;9(1)[cited 2023 Jul 10] Available from: <https://pubmed.ncbi.nlm.nih.gov/29467427/>
 331. Luni C, Giulitti S, Serena E, et al. High-efficiency cellular reprogramming with microfluidics [Internet]. *Nat. Methods* 2016;13(5):446–452.[cited 2023 Jul 10] Available from: <https://pubmed.ncbi.nlm.nih.gov/27088312/>
 332. Beers J, Linask KL, Chen JA, et al. A cost-effective and efficient reprogramming platform for large-scale production of integration-free human induced pluripotent stem cells in chemically defined culture [Internet]. *Sci. Rep.* 2015;5[cited 2023 Jul 10] Available from: <https://pubmed.ncbi.nlm.nih.gov/26066579/>
 333. Placzek M, Briscoe J. The floor plate: multiple cells, multiple signals [Internet]. *Nat. Rev. Neurosci.* 2005;6(3):230–240.[cited 2023 Jun 2] Available from: <https://pubmed.ncbi.nlm.nih.gov/15738958/>
 334. Dehmelt L, Halpain S. The MAP2/Tau family of microtubule-associated proteins [Internet]. *Genome Biol.* 2005;6(1)[cited 2023 Jun 1] Available from: <https://pubmed.ncbi.nlm.nih.gov/15642108/>
 335. Gusel'nikova V V., Korzhevskiy DE. NeuN As a Neuronal Nuclear Antigen and Neuron Differentiation Marker [Internet]. *Acta Naturae* 2015;7(2):42.[cited 2023 Jun 1] Available from: [/pmc/articles/PMC4463411/](https://pubmed.ncbi.nlm.nih.gov/26066579/)
 336. Blitzer JT, Nusse R. A critical role for endocytosis in Wnt signaling [Internet]. *BMC Cell Biol.* 2006;7[cited 2022 Mar 3] Available from: <https://pubmed.ncbi.nlm.nih.gov/16824228/>
 337. Rosso SB, Inestrosa NC. WNT signaling in neuronal maturation and synaptogenesis [Internet]. *Front. Cell. Neurosci.* 2013;7(JUNE)[cited 2023 Jun 4] Available from: <https://pubmed.ncbi.nlm.nih.gov/23847469/>
 338. Colozza G, Koo BK. Wnt/ β -catenin signaling: Structure, assembly and endocytosis of the signalosome [Internet]. *Dev. Growth Differ.* 2021;63(3):199–218.[cited 2023 Jun 4] Available from: <https://pubmed.ncbi.nlm.nih.gov/33619734/>
 339. DeGiosio RA, Grubisha MJ, MacDonald ML, et al. More than a marker: potential pathogenic functions of MAP2 [Internet]. *Front. Mol. Neurosci.* 2022;15[cited 2023 Jun 3] Available from: [/pmc/articles/PMC9525131/](https://pubmed.ncbi.nlm.nih.gov/33619734/)
 340. Mullen RJ, Buck CR, Smith AM. NeuN, a neuronal specific nuclear protein in vertebrates [Internet]. *Development* 1992;116(1):201–211.[cited 2023 Jun 3] Available from: <https://pubmed.ncbi.nlm.nih.gov/1483388/>
 341. Krug AK, Balmer N V., Matt F, et al. Evaluation of a human neurite growth assay as specific screen for developmental neurotoxicants [Internet]. *Arch. Toxicol.* 2013;87(12):2215–2231.[cited 2024 Apr 4] Available from: <https://pubmed.ncbi.nlm.nih.gov/23670202/>
 342. Radio NM, Mundy WR. Developmental neurotoxicity testing in vitro: models for assessing chemical effects on neurite outgrowth [Internet]. *Neurotoxicology* 2008;29(3):361–376.[cited 2024 Apr 4] Available from: <https://pubmed.ncbi.nlm.nih.gov/18403021/>
 343. Kamiguchi H, Long KE, Pendergast M, et al. The neural cell adhesion molecule L1 interacts with the AP-2 adaptor and is endocytosed via the clathrin-mediated pathway [Internet]. *J. Neurosci.* 1998;18(14):5311–5321.[cited 2023 Jul 22] Available from: <https://pubmed.ncbi.nlm.nih.gov/9651214/>
 344. Chen YT, Tai CY. μ 2-Dependent endocytosis of N-cadherin is regulated by β -catenin to facilitate neurite outgrowth [Internet]. *Traffic* 2017;18(5):287–303.[cited 2023 Jul 22]

-] Available from: <https://pubmed.ncbi.nlm.nih.gov/28224728/>
345. Schwartz CM, Cheng A, Mughal MR, et al. Clathrin assembly proteins AP180 and CALM in the embryonic rat brain [Internet]. *J. Comp. Neurol.* 2010;518(18):3803–3818.[cited 2023 Jul 22] Available from: <https://pubmed.ncbi.nlm.nih.gov/20653035/>
 346. Suzuki M, Tanaka H, Tanimura A, et al. The clathrin assembly protein PICALM is required for erythroid maturation and transferrin internalization in mice [Internet]. *PLoS One* 2012;7(2)[cited 2023 Jul 22] Available from: <https://pubmed.ncbi.nlm.nih.gov/22363754/>
 347. Ma Y, Greener T, Pacold ME, et al. Identification of domain required for catalytic activity of auxilin in supporting clathrin uncoating by Hsc70 [Internet]. *J. Biol. Chem.* 2002;277(51):49267–49274.[cited 2022 Feb 24] Available from: <https://pubmed.ncbi.nlm.nih.gov/12377777/>
 348. Scheele U, Kalthoff C, Ungewickell E. Multiple interactions of auxilin 1 with clathrin and the AP-2 adaptor complex. [Internet]. *J. Biol. Chem.* 2001;276(39):36131–8.[cited 2016 May 21] Available from: <http://www.ncbi.nlm.nih.gov/pubmed/11470803>
 349. Cochilla AJ, Angleson JK, Betz WJ. Monitoring secretory membrane with FM1-43 fluorescence [Internet]. *Annu. Rev. Neurosci.* 1999;22:1–10.[cited 2023 Sep 5] Available from: <https://pubmed.ncbi.nlm.nih.gov/10202529/>
 350. Gaffield MA, Betz WJ. Imaging synaptic vesicle exocytosis and endocytosis with FM dyes. *Nat. Protoc.* 2007;1(6):2916–2921.
 351. Hoopmann P, Rizzoli SO, Betz WJ. Imaging synaptic vesicle recycling by staining and destaining vesicles with FM dyes [Internet]. *Cold Spring Harb. Protoc.* 2012;2012(1):77–83.[cited 2023 Jun 6] Available from: <https://pubmed.ncbi.nlm.nih.gov/22194270/>
 352. Wang Z, Gerstein M, Snyder M. RNA-Seq: a revolutionary tool for transcriptomics [Internet]. *Nat. Rev. Genet.* 2009;10(1):57–63.[cited 2023 Oct 14] Available from: <https://pubmed.ncbi.nlm.nih.gov/19015660/>
 353. Stark R, Grzelak M, Hadfield J. RNA sequencing: the teenage years [Internet]. *Nat. Rev. Genet.* 2019;20(11):631–656.[cited 2023 Oct 14] Available from: <https://pubmed.ncbi.nlm.nih.gov/31341269/>
 354. Rilstone JJ, Alkhatir RA, Minassian BA. Brain Dopamine–Serotonin Vesicular Transport Disease and Its Treatment [Internet]. *N. Engl. J. Med.* 2013;368(6):543–550.Available from: <http://www.nejm.org/doi/abs/10.1056/NEJMoa1207281>
 355. Douglas SD, Leeman SE. Neurokinin-1 receptor: functional significance in the immune system in reference to selected infections and inflammation [Internet]. *Ann. N. Y. Acad. Sci.* 2011;1217(1):83.[cited 2023 Nov 29] Available from: </pmc/articles/PMC3058850/>
 356. Pataskar A, Jung J, Smialowski P, et al. NeuroD1 reprograms chromatin and transcription factor landscapes to induce the neuronal program [Internet]. *EMBO J.* 2016;35(1):24–45.[cited 2023 Nov 29] Available from: <https://pubmed.ncbi.nlm.nih.gov/26516211/>
 357. Flaig R, Greschik H, Peluso-Iltis C, Moras D. Structural basis for the cell-specific activities of the NGFI-B and the Nurr1 ligand-binding domain [Internet]. *J. Biol. Chem.* 2005;280(19):19250–19258.[cited 2023 Nov 29] Available from: <https://pubmed.ncbi.nlm.nih.gov/15716272/>
 358. Jesús S, Hinarejos I, Carrillo F, et al. NR4A2 Mutations Can Cause Intellectual Disability and Language Impairment With Persistent Dystonia-Parkinsonism [Internet]. *Neurol. Genet.* 2021;7(1):543.[cited 2023 Nov 29] Available from: </pmc/articles/PMC7879338/>
 359. von Scheibler ENMM, van Eeghen AM, de Koning TJ, et al. Parkinsonism in Genetic Neurodevelopmental Disorders: A Systematic Review [Internet]. *Mov. Disord. Clin.*

- Pract. 2022;10(1):17–31.[cited 2023 Nov 29] Available from:
<https://pubmed.ncbi.nlm.nih.gov/36699000/>
360. Le W dong, Xu P, Jankovic J, et al. Mutations in NR4A2 associated with familial Parkinson disease [Internet]. *Nat. Genet.* 2003;33(1):85–89.[cited 2024 Apr 4] Available from: <https://pubmed.ncbi.nlm.nih.gov/12496759/>
 361. Jiang C, Wan X, He Y, et al. Age-dependent dopaminergic dysfunction in Nurr1 knockout mice [Internet]. *Exp. Neurol.* 2005;191(1):154–162.[cited 2024 Apr 4] Available from: <https://pubmed.ncbi.nlm.nih.gov/15589522/>
 362. Zhai H, Zheng Y, He Y, et al. A case report of infantile parkinsonism-dystonia-2 caused by homozygous mutation in the SLC18A2 gene [Internet]. *Int. J. Neurosci.* 2023;133(5):574–577.[cited 2023 Nov 29] Available from: <https://pubmed.ncbi.nlm.nih.gov/34078222/>
 363. Osumi N. The role of Pax6 in brain patterning [Internet]. *Tohoku J. Exp. Med.* 2001;193(3):163–174.[cited 2024 Jan 17] Available from: <https://pubmed.ncbi.nlm.nih.gov/11315763/>
 364. Ian Simpson T, Price DJ. Pax6; a pleiotropic player in development [Internet]. *Bioessays* 2002;24(11):1041–1051.[cited 2024 Jan 17] Available from: <https://pubmed.ncbi.nlm.nih.gov/12386935/>
 365. Sansom SN, Griffiths DS, Faedo A, et al. The level of the transcription factor Pax6 is essential for controlling the balance between neural stem cell self-renewal and neurogenesis [Internet]. *PLoS Genet.* 2009;5(6)[cited 2024 Jan 17] Available from: <https://pubmed.ncbi.nlm.nih.gov/19521500/>
 366. Ninkovic J, Steiner-Mezzadri A, Jawerka M, et al. The BAF complex interacts with Pax6 in adult neural progenitors to establish a neurogenic cross-regulatory transcriptional network [Internet]. *Cell Stem Cell* 2013;13(4):403–418.[cited 2024 Jan 19] Available from: <https://pubmed.ncbi.nlm.nih.gov/23933087/>
 367. Stoykova A, Gruss P. Roles of Pax-genes in developing and adult brain as suggested by expression patterns [Internet]. *J. Neurosci.* 1994;14(3 Pt 2):1395–1412.[cited 2024 Jan 17] Available from: <https://pubmed.ncbi.nlm.nih.gov/8126546/>
 368. Kohwi M, Osumi N, Rubenstein JLR, Alvarez-Buylla A. Pax6 is required for making specific subpopulations of granule and periglomerular neurons in the olfactory bulb [Internet]. *J. Neurosci.* 2005;25(30):6997–7003.[cited 2024 Jan 19] Available from: <https://pubmed.ncbi.nlm.nih.gov/16049175/>
 369. Hack MA, Saghatelian A, De Chevigny A, et al. Neuronal fate determinants of adult olfactory bulb neurogenesis [Internet]. *Nat. Neurosci.* 2005;8(7):865–872.[cited 2024 Jan 19] Available from: <https://pubmed.ncbi.nlm.nih.gov/15951811/>
 370. G. Thomas M, Welch C, Stone L, et al. PAX6 expression may be protective against dopaminergic cell loss in Parkinson’s disease [Internet]. *CNS Neurol. Disord. Drug Targets* 2016;15(1):73–79.[cited 2024 Jan 17] Available from: <https://pubmed.ncbi.nlm.nih.gov/26295830/>
 371. Schulte D. Meis: New friends of Pax [Internet]. *Neurogenes.* (Austin, Tex.) 2014;1(1):e976014.[cited 2024 Jan 19] Available from: <https://pubmed.ncbi.nlm.nih.gov/27502016/>
 372. Ghanem N, Yu M, Poitras L, et al. Characterization of a distinct subpopulation of striatal projection neurons expressing the *Dlx* genes in the basal ganglia through the activity of the *I56ii* enhancer [Internet]. *Dev. Biol.* 2008;322(2):415–424.[cited 2024 Jan 21] Available from: <https://pubmed.ncbi.nlm.nih.gov/18706405/>
 373. Marcos S, González-Lázaro M, Beccari L, et al. *Meis1* coordinates a network of genes implicated in eye development and microphthalmia [Internet]. *Development* 2015;142(17):3009–3020.[cited 2024 Feb 11] Available from: <https://pubmed.ncbi.nlm.nih.gov/26253404/>

374. Isogai E, Okumura K, Saito M, et al. Meis1 plays roles in cortical development through regulation of cellular proliferative capacity in the embryonic cerebrum [Internet]. *Biomed. Res.* 2022;43(3):91–97.[cited 2024 Jan 21] Available from: <https://pubmed.ncbi.nlm.nih.gov/35718449/>
375. Sakamoto M, Hirata H, Ohtsuka T, et al. The basic helix-loop-helix genes *Hesr1/Hey1* and *Hesr2/Hey2* regulate maintenance of neural precursor cells in the brain [Internet]. *J. Biol. Chem.* 2003;278(45):44808–44815.[cited 2024 Jan 19] Available from: <https://pubmed.ncbi.nlm.nih.gov/12947105/>
376. Tutukova S, Tarabykin V, Hernandez-Miranda LR. The Role of Neurod Genes in Brain Development, Function, and Disease [Internet]. *Front. Mol. Neurosci.* 2021;14[cited 2024 Feb 11] Available from: <https://pubmed.ncbi.nlm.nih.gov/34177462/>
377. Boutin C, Hardt O, De Chevigny A, et al. NeuroD1 induces terminal neuronal differentiation in olfactory neurogenesis [Internet]. *Proc. Natl. Acad. Sci. U. S. A.* 2010;107(3):1201–1206.[cited 2024 Jan 20] Available from: <https://pubmed.ncbi.nlm.nih.gov/20080708/>
378. Kuwabara T, Hsieh J, Muotri A, et al. Wnt-mediated activation of NeuroD1 and retro-elements during adult neurogenesis [Internet]. *Nat. Neurosci.* 2009;12(9):1097–1105.[cited 2024 Feb 11] Available from: <https://pubmed.ncbi.nlm.nih.gov/19701198/>
379. Zhang J, Tam WL, Tong GQ, et al. *Sall4* modulates embryonic stem cell pluripotency and early embryonic development by the transcriptional regulation of *Pou5f1* [Internet]. *Nat. Cell Biol.* 2006;8(10):1114–1123.[cited 2024 Jan 21] Available from: <https://pubmed.ncbi.nlm.nih.gov/16980957/>
380. Ferland RJ, Cherry TJ, Preware PO, et al. Characterization of *Foxp2* and *Foxp1* mRNA and protein in the developing and mature brain [Internet]. *J. Comp. Neurol.* 2003;460(2):266–279.[cited 2024 Jan 18] Available from: <https://pubmed.ncbi.nlm.nih.gov/12687690/>
381. Li X, Xiao J, Fröhlich H, et al. *Foxp1* regulates cortical radial migration and neuronal morphogenesis in developing cerebral cortex [Internet]. *PLoS One* 2015;10(5)[cited 2024 Jan 18] Available from: <https://pubmed.ncbi.nlm.nih.gov/26010426/>
382. Araujo DJ, Anderson AG, Berto S, et al. *FoxP1* orchestration of ASD-relevant signaling pathways in the striatum [Internet]. *Genes Dev.* 2015;29(20):2081–2096.[cited 2024 Jan 18] Available from: <https://pubmed.ncbi.nlm.nih.gov/26494785/>
383. Bacon C, Schneider M, Le Magueresse C, et al. Brain-specific *Foxp1* deletion impairs neuronal development and causes autistic-like behaviour [Internet]. *Mol. Psychiatry* 2015;20(5):632–639.[cited 2024 Jan 17] Available from: <https://pubmed.ncbi.nlm.nih.gov/25266127/>
384. Le Fevre AK, Taylor S, Malek NH, et al. *FOXP1* mutations cause intellectual disability and a recognizable phenotype [Internet]. *Am. J. Med. Genet. A* 2013;161A(12):3166–3175.[cited 2024 Jan 18] Available from: <https://pubmed.ncbi.nlm.nih.gov/24214399/>
385. Konstantoulas CJ, Parmar M, Li M. *FoxP1* promotes midbrain identity in embryonic stem cell-derived dopamine neurons by regulating *Pitx3* [Internet]. *J. Neurochem.* 2010;113(4):836–847.[cited 2024 Jan 17] Available from: <https://pubmed.ncbi.nlm.nih.gov/20175877/>
386. Moparthy L, Koch S. FOX transcription factors are common regulators of Wnt/ β -catenin-dependent gene transcription [Internet]. *J. Biol. Chem.* 2023;299(5)[cited 2024 Jan 18] Available from: <https://pubmed.ncbi.nlm.nih.gov/37011861/>
387. Braccioli L, Vervoort SJ, Adolfs Y, et al. *FOXP1* Promotes Embryonic Neural Stem Cell Differentiation by Repressing *Jagged1* Expression [Internet]. *Stem cell reports* 2017;9(5):1530–1545.[cited 2024 Jan 18] Available from: <https://pubmed.ncbi.nlm.nih.gov/29141232/>
388. Hruska M, Dalva MB. Ephrin regulation of synapse formation, function and plasticity

- [Internet]. *Mol. Cell. Neurosci.* 2012;50(1):35–44.[cited 2024 Feb 11] Available from: <https://pubmed.ncbi.nlm.nih.gov/22449939/>
389. Das G, Yu Q, Hui R, et al. EphA5 and EphA6: regulation of neuronal and spine morphology [Internet]. *Cell Biosci.* 2016;6(1)[cited 2024 Feb 11] Available from: <https://pubmed.ncbi.nlm.nih.gov/27489614/>
 390. Halladay AK, Tessarollo L, Zhou R, Wagner GC. Neurochemical and behavioral deficits consequent to expression of a dominant negative EphA5 receptor [Internet]. *Mol. Brain Res.* 2004;123(1–2):104–111.[cited 2024 Feb 11] Available from: <https://pubmed.ncbi.nlm.nih.gov/15046871/>
 391. Ulc A, Gottschling C, Schäfer I, et al. Involvement of the guanine nucleotide exchange factor Vav3 in central nervous system development and plasticity [Internet]. *Biol. Chem.* 2017;398(5–6):663–675.[cited 2024 Jan 21] Available from: <https://pubmed.ncbi.nlm.nih.gov/28214347/>
 392. Hale CF, Dietz KC, Varela JA, et al. Essential role for vav Guanine nucleotide exchange factors in brain-derived neurotrophic factor-induced dendritic spine growth and synapse plasticity [Internet]. *J. Neurosci.* 2011;31(35):12426–12436.[cited 2024 Jan 22] Available from: <https://pubmed.ncbi.nlm.nih.gov/21880903/>
 393. Cowan CW, Shao YR, Sahin M, et al. Vav family GEFs link activated Ephs to endocytosis and axon guidance [Internet]. *Neuron* 2005;46(2):205–217.[cited 2024 Jan 21] Available from: <https://pubmed.ncbi.nlm.nih.gov/15848800/>
 394. Whitford KL, Marillat V, Stein E, et al. Regulation of cortical dendrite development by Slit-Robo interactions [Internet]. *Neuron* 2002;33(1):47–61.[cited 2024 Jan 24] Available from: <https://pubmed.ncbi.nlm.nih.gov/11779479/>
 395. Bagri A, Marín O, Plump AS, et al. Slit proteins prevent midline crossing and determine the dorsoventral position of major axonal pathways in the mammalian forebrain [Internet]. *Neuron* 2002;33(2):233–248.[cited 2024 Jan 15] Available from: <https://pubmed.ncbi.nlm.nih.gov/11804571/>
 396. Kiryushko D, Berezin V, Bock E. Regulators of neurite outgrowth: role of cell adhesion molecules [Internet]. *Ann. N. Y. Acad. Sci.* 2004;1014:140–154.[cited 2024 Jan 11] Available from: <https://pubmed.ncbi.nlm.nih.gov/15153429/>
 397. Yoshida J, Kubo T, Yamashita T. Inhibition of branching and spine maturation by repulsive guidance molecule in cultured cortical neurons [Internet]. *Biochem. Biophys. Res. Commun.* 2008;372(4):725–729.[cited 2023 Nov 29] Available from: <https://pubmed.ncbi.nlm.nih.gov/18519029/>
 398. Tang J, Zeng X, Li H, et al. Repulsive Guidance Molecule-a and Central Nervous System Diseases [Internet]. *Biomed Res. Int.* 2021;2021[cited 2023 Nov 29] Available from: [/pmc/articles/PMC8112912/](https://pubmed.ncbi.nlm.nih.gov/33589594/)
 399. Oda W, Fujita Y, Baba K, et al. Inhibition of repulsive guidance molecule-a protects dopaminergic neurons in a mouse model of Parkinson’s disease [Internet]. *Cell Death Dis.* 2021;12(2)[cited 2024 Jan 15] Available from: <https://pubmed.ncbi.nlm.nih.gov/33589594/>
 400. Herman GE, El-Hodiri HM. The role of ZIC3 in vertebrate development [Internet]. *Cytogenet. Genome Res.* 2002;99(1–4):229–235.[cited 2024 Jan 22] Available from: <https://pubmed.ncbi.nlm.nih.gov/12900569/>
 401. Ahmed JN, Ali RG, Warr N, et al. A murine Zic3 transcript with a premature termination codon evades nonsense-mediated decay during axis formation [Internet]. *Dis. Model. Mech.* 2013;6(3):755–767.[cited 2024 Jan 22] Available from: <https://pubmed.ncbi.nlm.nih.gov/23471918/>
 402. Lim LS, Hong FH, Kunarso G, Stanton LW. The pluripotency regulator Zic3 is a direct activator of the Nanog promoter in ESCs [Internet]. *Stem Cells* 2010;28(11):1961–1969.[cited 2024 Jan 22] Available from: <https://pubmed.ncbi.nlm.nih.gov/20872845/>

403. Wong ROL, Ghosh A. Activity-dependent regulation of dendritic growth and patterning [Internet]. *Nat. Rev. Neurosci.* 2002;3(10):803–812.[cited 2024 Jan 22] Available from: <https://pubmed.ncbi.nlm.nih.gov/12360324/>
404. Puram S V., Riccio A, Koirala S, et al. A TRPC5-regulated calcium signaling pathway controls dendrite patterning in the mammalian brain [Internet]. *Genes Dev.* 2011;25(24):2659–2673.[cited 2024 Jan 22] Available from: <https://pubmed.ncbi.nlm.nih.gov/22135323/>
405. Lin L, Lesnick TG, Maraganore DM, Isacson O. Axon guidance and synaptic maintenance: preclinical markers for neurodegenerative disease and therapeutics [Internet]. *Trends Neurosci.* 2009;32(3):142–149.[cited 2023 Dec 2] Available from: <https://pubmed.ncbi.nlm.nih.gov/19162339/>
406. Lesnick TG, Papapetropoulos S, Mash DC, et al. A genomic pathway approach to a complex disease: axon guidance and Parkinson disease [Internet]. *PLoS Genet.* 2007;3(6):0984–0995.[cited 2023 Dec 2] Available from: <https://pubmed.ncbi.nlm.nih.gov/17571925/>
407. Rong Y, Wei P, Parris J, et al. Comparison of Cbln1 and Cbln2 Functions using Transgenic and Knockout Mice [Internet]. *J. Neurochem.* 2012;120(4):528.[cited 2023 Dec 2] Available from: [/pmc/articles/PMC3259274/](https://pubmed.ncbi.nlm.nih.gov/22135323/)
408. Seigneur E, Südhof TC. Genetic Ablation of All Cerebellins Reveals Synapse Organizer Functions in Multiple Regions Throughout the Brain [Internet]. *J. Neurosci.* 2018;38(20):4774–4790.[cited 2023 Dec 3] Available from: <https://pubmed.ncbi.nlm.nih.gov/29691328/>
409. Sando R, Jiang X, Südhof TC. Latrophilin GPCRs direct synapse specificity by coincident binding of FLRTs and teneurins [Internet]. *Science* 2019;363(6429)[cited 2023 Dec 3] Available from: <https://pubmed.ncbi.nlm.nih.gov/30792275/>
410. Bänziger C, Soldini D, Schütt C, et al. Wntless, a conserved membrane protein dedicated to the secretion of Wnt proteins from signaling cells [Internet]. *Cell* 2006;125(3):509–522.[cited 2023 Dec 3] Available from: <https://pubmed.ncbi.nlm.nih.gov/16678095/>
411. Martínez A, Alcántara S, Borrell V, et al. TrkB and TrkC signaling are required for maturation and synaptogenesis of hippocampal connections [Internet]. *J. Neurosci.* 1998;18(18):7336–7350.[cited 2023 Dec 3] Available from: <https://pubmed.ncbi.nlm.nih.gov/9736654/>
412. Aimi T, Matsuda K, Yuzaki M. C1ql1-Bai3 signaling is necessary for climbing fiber synapse formation in mature Purkinje cells in coordination with neuronal activity [Internet]. *Mol. Brain* 2023;16(1):1–17.[cited 2023 Dec 3] Available from: <https://molecularbrain.biomedcentral.com/articles/10.1186/s13041-023-01048-4>
413. Sigoillot SM, Iyer K, Binda F, et al. The Secreted Protein C1QL1 and Its Receptor BAI3 Control the Synaptic Connectivity of Excitatory Inputs Converging on Cerebellar Purkinje Cells [Internet]. *Cell Rep.* 2015;10(5):820–832.[cited 2023 Dec 3] Available from: <https://pubmed.ncbi.nlm.nih.gov/25660030/>
414. Reid KM, Steel D, Nair S, et al. Loss-of-Function Variants in DRD1 in Infantile Parkinsonism-Dystonia [Internet]. *Cells* 2023;12(7):1046.[cited 2024 May 2] Available from: <https://pubmed.ncbi.nlm.nih.gov/37048120/>
415. Martier R, Konstantinova P. Gene Therapy for Neurodegenerative Diseases: Slowing Down the Ticking Clock [Internet]. *Front. Neurosci.* 2020;14[cited 2023 Jun 11] Available from: <https://pubmed.ncbi.nlm.nih.gov/33071748/>
416. Mendell JR, Al-Zaidy S, Shell R, et al. Single-Dose Gene-Replacement Therapy for Spinal Muscular Atrophy [Internet]. *N. Engl. J. Med.* 2017;377(18):1713–1722.[cited 2023 Sep 4] Available from: <https://pubmed.ncbi.nlm.nih.gov/29091557/>
417. Fumagalli F, Calbi V, Natali Sora MG, et al. Lentiviral haematopoietic stem-cell gene

- therapy for early-onset metachromatic leukodystrophy: long-term results from a non-randomised, open-label, phase 1/2 trial and expanded access [Internet]. *Lancet* (London, England) 2022;399(10322):372–383.[cited 2024 Jan 31] Available from: <https://pubmed.ncbi.nlm.nih.gov/35065785/>
418. Flotte TR, Cataltepe O, Puri A, et al. AAV gene therapy for Tay-Sachs disease [Internet]. *Nat. Med.* 2022;28(2):251–259.[cited 2022 Sep 25] Available from: <https://pubmed.ncbi.nlm.nih.gov/35145305/>
 419. Eichler F, Duncan C, Musolino PL, et al. Hematopoietic Stem-Cell Gene Therapy for Cerebral Adrenoleukodystrophy [Internet]. *N. Engl. J. Med.* 2017;377(17):1630–1638.[cited 2024 Jan 31] Available from: <https://pubmed.ncbi.nlm.nih.gov/28976817/>
 420. Boespflug-Tanguy O, Sevin C, Pigué F. Gene therapy for neurodegenerative disorders in children: dreams and realities [Internet]. *Arch. Pediatr.* 2023;30(8S1):8S32–8S40.[cited 2024 Apr 29] Available from: <https://pubmed.ncbi.nlm.nih.gov/38043981/>
 421. Bulcha JT, Wang Y, Ma H, et al. Viral vector platforms within the gene therapy landscape [Internet]. *Signal Transduct. Target. Ther.* 2021;6(1)[cited 2024 May 2] Available from: [/pmc/articles/PMC7868676/](https://pmc/articles/PMC7868676/)
 422. Kurian MA, Abela L. DNAJC6 Parkinson Disease [Internet]. In: *GeneReviews®*. 1993[cited 2024 Apr 27] Available from: <http://www.ncbi.nlm.nih.gov/pubmed/33983693>
 423. Grskovic M, Javaherian A, Strulovici B, Daley GQ. Induced pluripotent stem cells--opportunities for disease modelling and drug discovery [Internet]. *Nat. Rev. Drug Discov.* 2011;10(12):915–929.[cited 2024 Jan 3] Available from: <https://pubmed.ncbi.nlm.nih.gov/22076509/>
 424. Wegener G, Rujescu D. The current development of CNS drug research [Internet]. *Int. J. Neuropsychopharmacol.* 2013;16(7):1687–1693.[cited 2024 Feb 2] Available from: <https://pubmed.ncbi.nlm.nih.gov/23651558/>
 425. Sguazzi GP, Muto V, Tartaglia M, et al. Induced Pluripotent Stem Cells (iPSCs) and Gene Therapy: A New Era for the Treatment of Neurological Diseases [Internet]. *Int. J. Mol. Sci.* 2021;22(24)[cited 2024 Feb 3] Available from: <https://pubmed.ncbi.nlm.nih.gov/34948465/>
 426. Simmnacher K, Lanfer J, Rizo T, et al. Modeling Cell-Cell Interactions in Parkinson's Disease Using Human Stem Cell-Based Models [Internet]. *Front. Cell. Neurosci.* 2020;13[cited 2024 Jan 3] Available from: <https://pubmed.ncbi.nlm.nih.gov/32009903/>
 427. Cederquist GY, Tchieu J, Callahan SJ, et al. A Multiplex Human Pluripotent Stem Cell Platform Defines Molecular and Functional Subclasses of Autism-Related Genes [Internet]. *Cell Stem Cell* 2020;27(1):35-49.e6.[cited 2024 Feb 3] Available from: <https://pubmed.ncbi.nlm.nih.gov/32619517/>
 428. Smullen M, Olson MN, Reichert JM, et al. Reliable multiplex generation of pooled induced pluripotent stem cells [Internet]. *Cell reports methods* 2023;3(9)[cited 2024 Feb 3] Available from: <https://pubmed.ncbi.nlm.nih.gov/37751688/>
 429. Incardona JP, Lee JH, Robertson CP, et al. Receptor-mediated endocytosis of soluble and membrane-tethered Sonic hedgehog by Patched-1 [Internet]. *Proc. Natl. Acad. Sci. U. S. A.* 2000;97(22):12044–12049.[cited 2024 Apr 27] Available from: <https://pubmed.ncbi.nlm.nih.gov/11027307/>
 430. Rizzoli SO, Betz WJ. Synaptic vesicle pools [Internet]. 2005;6(1):57–69.[cited 2017 Nov 27] Available from: <http://www.ncbi.nlm.nih.gov/pubmed/15611727>
 431. Murthy VN, Sejnowski TJ, Stevens CF. Heterogeneous release properties of visualized individual hippocampal synapses [Internet]. *Neuron* 1997;18(4):599–612.[cited 2024 Apr 27] Available from: <https://pubmed.ncbi.nlm.nih.gov/9136769/>
 432. Kyung JW, Kim JM, Lee W, et al. DJ-1 deficiency impairs synaptic vesicle

- endocytosis and reavailability at nerve terminals [Internet]. *Proc. Natl. Acad. Sci. U. S. A.* 2018;115(7):1629–1634.[cited 2024 Apr 27] Available from: <https://pubmed.ncbi.nlm.nih.gov/29386384/>
433. Usami Y, Hatano T, Imai S, et al. DJ-1 associates with synaptic membranes [Internet]. *Neurobiol. Dis.* 2011;43(3):651–662.[cited 2024 Apr 27] Available from: <https://pubmed.ncbi.nlm.nih.gov/21645620/>
 434. Scott D, Roy S. α -Synuclein inhibits intersynaptic vesicle mobility and maintains recycling-pool homeostasis [Internet]. *J. Neurosci.* 2012;32(30):10129–10135.[cited 2024 Apr 27] Available from: <https://pubmed.ncbi.nlm.nih.gov/22836248/>
 435. Haucke V, Neher E, Sigrist SJ. Protein scaffolds in the coupling of synaptic exocytosis and endocytosis [Internet]. *Nat. Rev. Neurosci.* 2011;12(3):127–138.[cited 2024 Jan 8] Available from: <https://pubmed.ncbi.nlm.nih.gov/21304549/>
 436. Stern S, Lau S, Manole A, et al. Reduced synaptic activity and dysregulated extracellular matrix pathways in midbrain neurons from Parkinson's disease patients [Internet]. *NPJ Park. Dis.* 2022;8(1)[cited 2024 Apr 27] Available from: <https://pubmed.ncbi.nlm.nih.gov/35948563/>
 437. Yan CH, Levesque M, Claxton S, et al. *Lmx1a* and *Lmx1b* function cooperatively to regulate proliferation, specification, and differentiation of midbrain dopaminergic progenitors [Internet]. *J. Neurosci.* 2011;31(35):12413–12425.[cited 2024 Jan 7] Available from: <https://pubmed.ncbi.nlm.nih.gov/21880902/>
 438. Schwamborn JC. Is Parkinson's Disease a Neurodevelopmental Disorder and Will Brain Organoids Help Us to Understand It? [Internet]. *Stem Cells Dev.* 2018;27(14):968–975.[cited 2024 Apr 27] Available from: <https://pubmed.ncbi.nlm.nih.gov/29415619/>
 439. Endo Y, Rubin JS. Wnt signaling and neurite outgrowth: insights and questions [Internet]. *Cancer Sci.* 2007;98(9):1311–1317.[cited 2024 Jan 11] Available from: <https://pubmed.ncbi.nlm.nih.gov/17627619/>
 440. Brunt L, Scholpp S. The function of endocytosis in Wnt signaling [Internet]. *Cell. Mol. Life Sci.* 2018;75(5):785–795.[cited 2024 Jan 25] Available from: <https://pubmed.ncbi.nlm.nih.gov/28913633/>
 441. Pitulescu ME, Adams RH. Eph/ephrin molecules--a hub for signaling and endocytosis [Internet]. *Genes Dev.* 2010;24(22):2480–2492.[cited 2024 Jan 25] Available from: <https://pubmed.ncbi.nlm.nih.gov/21078817/>
 442. Bonifati V. Genetics of Parkinson's disease – state of the art, 2013 [Internet]. *Parkinsonism Relat. Disord.* 2014;20:S23–S28.[cited 2017 Nov 28] Available from: <http://www.ncbi.nlm.nih.gov/pubmed/24262182>
 443. Sarnat HB, Nochlin D, Born DE. Neuronal nuclear antigen (NeuN): A marker of neuronal maturation in the early human fetal nervous system [Internet]. *Brain Dev.* 1998;20(2):88–94.[cited 2024 Jan 11] Available from: <https://pubmed.ncbi.nlm.nih.gov/9545178/>
 444. Honig LS, Herrmann K, Shatz CJ. Developmental changes revealed by immunohistochemical markers in human cerebral cortex [Internet]. *Cereb. Cortex* 1996;6(6):794–806.[cited 2024 Jan 11] Available from: <https://pubmed.ncbi.nlm.nih.gov/8922336/>
 445. Sann S, Wang Z, Brown H, Jin Y. Roles of endosomal trafficking in neurite outgrowth and guidance [Internet]. *Trends Cell Biol.* 2009;19(7):317–324.[cited 2024 Jan 11] Available from: <https://pubmed.ncbi.nlm.nih.gov/19540123/>
 446. Cosker KE, Segal RA. Neuronal signaling through endocytosis. [Internet]. *Cold Spring Harb. Perspect. Biol.* 2014;6(2):a020669–a020669.[cited 2018 Jun 27] Available from: <http://cshperspectives.cshlp.org/lookup/doi/10.1101/cshperspect.a020669>
 447. Wang D, Chan CC, Cherry S, Hiesinger PR. Membrane trafficking in neuronal

- maintenance and degeneration [Internet]. *Cell. Mol. Life Sci.* 2013;70(16):2919–2934.[cited 2024 Jan 12] Available from: <https://pubmed.ncbi.nlm.nih.gov/23132096/>
448. Fantuzzo JA, De Filippis L, McGowan H, et al. μ Neurocircuitry: Establishing in vitro models of neurocircuits with human neurons [Internet]. *Technology* 2017;5(2):87–97.[cited 2024 Apr 28] Available from: <https://pubmed.ncbi.nlm.nih.gov/28781993/>
 449. Sun J, Roy S. Gene-based therapies for neurodegenerative diseases [Internet]. *Nat. Neurosci.* 2021;24(3):297–311.[cited 2024 Apr 29] Available from: <https://pubmed.ncbi.nlm.nih.gov/33526943/>
 450. Drago D, Foss-Campbell B, Wonnacott K, et al. Global regulatory progress in delivering on the promise of gene therapies for unmet medical needs [Internet]. *Mol. Ther. Methods Clin. Dev.* 2021;21:524–529.[cited 2024 Apr 29] Available from: <https://pubmed.ncbi.nlm.nih.gov/33997101/>
 451. L’Heureux A, Grolinger K, Elyamany HF, Capretz MAM. Machine Learning with Big Data: Challenges and Approaches. *IEEE Access* 2017;5:7776–7797.
 452. Perakakis N, Yazdani A, Karniadakis GE, Mantzoros C. Omics, big data and machine learning as tools to propel understanding of biological mechanisms and to discover novel diagnostics and therapeutics. *Metabolism* 2018;87:A1–A9.
 453. Wu F, Yao PJ. Clathrin-mediated endocytosis and Alzheimer’s disease: an update [Internet]. *Ageing Res. Rev.* 2009;8(3):147–149.[cited 2022 Jun 3] Available from: <https://pubmed.ncbi.nlm.nih.gov/19491039/>
 454. Krach F, Bogionko ME, Winner B. Decoding Parkinson’s disease – iPSC-derived models in the OMICs era. *Mol. Cell. Neurosci.* 2020;106:103501.